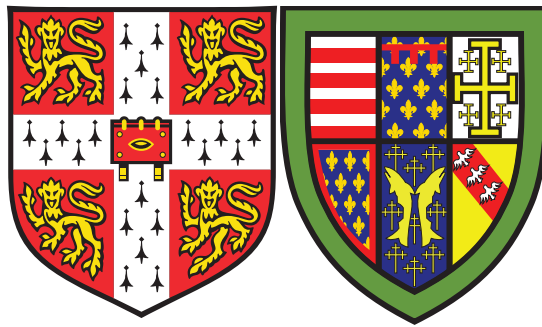


Development of an optogenetic toolkit for the interrogation of T cell signalling dynamics

Michael James Harris



Queens' College
University of Cambridge

November 2017

This dissertation is submitted to Cambridge University for the degree of
Doctor of Philosophy

“All men dream: but not equally. Those who dream by night in the dusty recesses of their minds wake up in the day to find it was vanity, but the dreamers of the day are dangerous men, for they may act their dreams with open eyes, to make it possible. This I did” – T E Lawrence

Declaration

This dissertation is the result of my own work and includes nothing which is the outcome of work done in collaboration except as declared in the Preface and specified in the text. It is not substantially the same as any that I have submitted, or, is being concurrently submitted for a degree or diploma or other qualification at the University of Cambridge or any other University or similar institution except as declared in the Preface and specified in the text. I further state that no substantial part of my dissertation has already been submitted, or, is being concurrently submitted for any such degree, diploma or other qualification at the University of Cambridge or any other University or similar institution except as declared in the Preface and specified in the text. It does not exceed the prescribed word limit for the relevant Degree Committee.

Michael J Harris

October 2017

Acknowledgements

First and foremost, I would like to thank John for his excellent mentorship and keen insight into my various projects. I am truly grateful to have worked under his guidance over the past four years. Even when things got tough, John was always able to put a positive spin on things and I cannot understate how much of a difference that made to my perspective on the work I was doing. I can only hope that my rather liberal use of his open-door policy did not cause too much disruption over my time in his lab.

I would also like to take this opportunity to acknowledge my parents for their continued support throughout my whole life. Thank you for encouraging me on every step of my journey. Our family's continual globe-trotting motivated me to stay curious about everything and to always keep an open mind. And to my teachers over the years, particularly Mr Ferguson, thank you for inspiring in me a love of learning and a love of science. You have all shaped me into the person that I am today.

Thank you to the members of the James lab: Ardi, Lewis, and Andrei. Working (and drinking) with you over the course of my PhD has been great. I honestly could not have hoped for a better group of lab mates. Thank you for fielding my 'potentially stupid' questions and for your continued support during my time in the lab. Thanks as well to Ben, Ed and Philip.

Thank you to my good friends Jon and Eric. Jon, for encouraging me to apply for this PhD and Eric, for reminding me never to take it *too* seriously. Thank you both for being there through the highs and the lows.

I would like to also acknowledge the fantastic support of the core facilities at the LMB. To the guys in the LMB Mechanical and Electronics Workshops and to Maria and the rest of the flow cytometry core, thank you for your help with everything over my time at the LMB. I could not have made it this far without your help.

To everyone on the I&I (&I) programme (and CIMR programme): Tom, Lisa, Sam, Jane, Alex, Niko, Guy, and especially Charlotte, thank you all. I have enjoyed getting to know you all over the past few years and wish you all every success in your future careers. Hopefully our paths will cross again in the future. Charlotte, thank you for always keeping me grounded during my time in Cambridge, for being there for me after long days in the lab, and for cheering me on during my ridiculous sports endeavours. You being there has made all the difference.

Contents

Declaration.....	3
Acknowledgements.....	4
List of tables	12
List of figures	13
List of abbreviations	16
Chapter 1 – Introduction	19
1.1 Overview of immunity	19
1.2 The innate immune response.....	19
1.2.1 Non-cellular constituents of innate immunity	19
1.2.2 Innate immune receptors	20
1.2.3 Innate Immune lymphocytes	23
1.2.4 Dendritic cells translate innate immunity to adaptive immunity	24
1.2 The adaptive Immune response	26
1.3.1 Overview of adaptive immunity	26
1.3.2 B cell development.....	26
1.3.3 T cell development.....	27
1.3.4 Immunological memory response	30
1.4 The T cell antigen receptor and signalling complex	31
1.5 Chemical and optical manipulations of cellular signalling pathways.....	33
1.5.1 Chemically-inducible dimerization.....	33
1.5.2 Overview of optogenetics.....	34
1.5.3 The mechanistic underpinnings of cellular optogenetics	36
1.5.4 Multiplexing optogenetics with the molecular biology toolkit	38
1.6 Overview of results	40
Chapter 2: General Methods & Materials.....	41
2.1 Stock solutions and buffers	41

2.2 Mammalian Cell Culture	42
2.2.1 Suspension cell lines.....	42
2.2.2 Adherent cell lines	42
2.2.3 Cell line cold storage.....	42
2.2.4 Mycoplasma testing.....	43
2.3 Polymerase Chain Reaction Conditions & DNA purification	43
2.3.1 Primer design and in silico PCR.....	43
2.3.2 KOD HotStart Polymerase Conditions	43
2.3.3 Q5 Polymerase Conditions.....	45
2.3.4 MyTaq Colony Screen Polymerase Chain Reaction.....	45
2.3.5 Gel electrophoresis.....	46
2.3.6 Gel Extraction	46
2.3.7 PCR purification	46
3.4 Bacterial Cloning.....	47
3.4.1 Preparation of Competent Bacterial.....	47
3.4.2 Cloning by Restriction Digest.....	47
2.4.3 DNA Ligation	49
2.4.4 Heat-shock Transformation of Competent Bacteria.....	49
2.4.5 Plasmid Purification	50
2.5 DNA transfection and Transduction.....	50
2.5.1 Transient transfection.....	50
2.5.2 Lentiviral Transduction	50
2.5.3 Lentiviral concentration	51
2.6 Confocal Microscopy.....	51
2.6.1 Sample preparation and image acquisition.....	51
2.6.2 Image Processing.....	52
2.7 Flow Cytometry	54
2.7.1 Sample preparation and surface staining.....	54

2.7.2 Intracellular FACS staining.....	56
2.7.3 Ratiometric calcium flux assay	56
2.7.4 FlowJo v10.1r5	57
2.7.5 Fluorophore panel selection.....	57
2.8 Immunoblot Assay	57
2.9 Enzyme-linked immunosorbent assays (ELISA).....	58
2.10 Analysis Software.....	58
2.10.1 Microsoft Excel 2013	58
2.10.2 Matlab R2016b	58
Chapter 3 – Development of an optogenetic toolkit.....	59
3.1 Introduction.....	59
3.1.1 Optogenetic tool development.....	59
3.1.2 Mechanistic overview of the LOV2 domain	59
3.1.3 Designing LOV2-based optogenetic switches	61
3.1.4 Repurposing the TULIPs system for T cell signalling	62
3.1.5 Repurposing the LOVTRAP system for T cell signalling.....	63
3.1.6 Development of CRY2-based signalling systems.....	63
3.1.8 Aims.....	64
3.2 Materials & Methods.....	65
3.2.1 Microscopy.....	65
3.3 Results	66
3.3.1 Design of two opposing LAT-based optogenetic systems	66
3.3.2 Point mutation-based tuning of the LOV2 domain	66
3.3.3 Light-inducible recruitment of LAT using the TULIPs system.....	71
3.3.4 Light-inducible dissociation of LAT using LOVTRAP system	74
3.4 Discussion	80
Chapter 4 – Investigating early T cell signalling dynamics using LAT-based optogenetic switches	84

4.1 Introduction	84
4.1.1 TCR microclusters and immunological synapse maturation	84
4.1.2 Formation of TCR Microclusters	87
4.1.3 LAT is essential for T cell development, function, and immune homeostasis.....	88
4.1.4 LAT localisation and function	91
4.1.5 Molecular interaction partners link LAT to downstream effectors	91
4.1.6 Negative regulation of LAT	94
4.1.7 LAT as the basis for an optogenetic switch	94
4.2 Materials & Methods.....	94
4.2.1 Cas9-mediated gene knockout.....	94
4.2.2 Design of Specialised DNA fragments.....	96
4.3 Results	96
4.3.1 Chronic LAT depletion prevents phenotypic rescue of JCam2.5 cell line	96
4.3.2 Development of a LAT-specific knockout Jurkat E6.1 cell line.....	98
4.3.3 Optogenetic systems partially rescue LAT knockout phenotype	105
4.3.4 Calcium fluxing is invariant to LAT expression above threshold	110
4.3.5 Serial viral transduction improves TULIPs and LOVTRAP expression in J-LKO cell line.....	115
4.3.6 LOVTRAP-LAT optogenetic system reconstitutes TCR signalling pathway	115
4.3.7 Limited LAT population necessary for TCR signal initiation	118
4.3.8 Sustained calcium fluxing requires large pool of LAT	118
4.3.9 LOVTRAP-LAT system fails to sustain downstream signalling	122
4.3.10 TULIPs system partially reconstitutes calcium fluxing.....	122
4.3.11 Intrinsic dissociation rate of TULIPs interaction inhibits sustained calcium fluxing	125
4.3.12 CRY2-CIBN optogenetic system fails to rescue LAT knockout phenotype.....	130
4.3.13 J-LKO cells highly express CD6.....	133
4.4 Discussion	133

Chapter 5 – Investigating T-cell signal integration with a light-controllable chimeric antigen receptor.....	138
5.1 Introduction.....	138
5.1.1 The immune system and collective decision making.....	138
5.1.2 T cell-mediated responses to infection	138
5.1.3 Translating primary infection to adaptive immunity	139
5.1.4 T cell activation and temporally encoded signals	141
5.1.5 Immediate early gene expression and signal integration.....	142
5.1.6 Secondary signals regulate T cell activation.....	143
5.1.7 An engineering approach to cell biology.....	144
5.2 Materials & methods.....	145
5.2.1 Cell-cell conjugate calcium flux	145
5.2.2 Light Plate Apparatus	146
5.2.3 Data Analysis	147
5.3 Results	147
5.3.1 Stable expression of light- and drug-controllable chimeric antigen receptor in Jurkat T cells.....	147
5.3.2 OptoCARs recapitulate early T cell activation.....	154
5.3.3 T cells exhibit tight negative regulation of early signalling events	159
5.3.4 OptoCARs recapitulate late T cell activation	168
5.3.5 TCR signals sharply decay following withdrawal of input signals	174
5.4 Discussion	183
5.4.1 A physiologically-relevant system for studying T cell activation	183
5.4.2 A ‘temporal roadmap’ for T-cell activation	184
5.4.3 Co-stimulatory/-inhibitory receptors in TCR signal transduction.....	187
5.4.4 Conclusions.....	188
Chapter 6 – Structural features of T cell-dependent bispecific antibody epitope affect T-cell activation and therapeutic potential.....	189

6.1 Introduction.....	189
6.1.1 Multiple Myeloma.....	189
6.1.2 FcRH5 as a clinical target	189
6.1.2 Immunotherapy and T cell-dependent bispecific antibodies.....	190
6.1.3 The kinetic segregation model of T-cell activation.....	191
6.2 Materials & Methods.....	191
6.2.1 TDB labelling	191
6.2.2 Transient transfection.....	191
6.2.3 Confocal microscopy	192
6.2.4 Image Analysis.....	192
6.3 Results	192
6.3.1 TDBs activate T cells through the kinetic segregation of CD45	192
6.3.2 Membrane proximity of TDB epitope enhances T-cell activation and target killing.	194
6.4 Discussion	201
6.4.1 Epitope structural features affect therapeutic potential of bsAbs.....	201
6.4.2 Combination Immunotherapy.....	201
6.4.3 Stratification of patient populations	202
Chapter 7 – Final Discussion	203
7.1 Overview of Results	203
7.2 Defining the limitations of the LOV2 optogenetic system	204
7.3 Learning from past LOVs.....	205
7.4 Future directions for the optoCAR system.....	205
7.5 Fine-scale adjustment of TCR signalling	207
7.6 Reapplying the optogenetic signalling approach to other immune receptors	207
Bibliography of References	208
Appendix A.....	230
Appendix B.....	233
Appendix C.....	237

Appendix D	239
Appendix E.....	245
Appendix F	251
Appendix G	252
Appendix H	253
Appendix I	254
Appendix J	255
Appendix K	256
Appendix L	257
Appendix M.....	258
Appendix N	259

List of tables

Table 1.1: Human TLRs and their targets	21
Table 1.2: Human FcR receptors.....	22
Table 1.3: T cell effector subsets	29
Table 1.4: Chemically-Inducible dimerization systems.....	33
Table 1.5: Commonly used optogenetic systems	35
Table 2.1: Stock buffers	41
Table 2.2: List of Antibodies	55
Table 3.1: AsLOV2 mutant photocycle kinetics	71
Table 3.2: AtCRY2PHR mutant photocycle kinetics.....	77
Table 3.3: Rate of CRY2 construct cytoplasmic depletion.....	80
Table 4.1: LAT, CRISPR gRNA oligos.....	95
Table 5.1: Overview of OptoCAR variants.....	149

List of figures

Figure 1.1 Overview of Immunity.....	25
Figure 1.2 Overview of the T cell antigen receptor.....	32
Figure 1.3 Mechanisms of optogenetic systems	37
Figure 2.1 Example pHR IRES plasmid.....	48
Figure 2.2 ImageJ Workflow	53
Figure 3.1 LAT-TM-LOV2 constructs engineered according to LAT structure	67
Figure 3.2 Schematic overview of TULIPs-based system	68
Figure 3.3 Schematic overview of LOVTRAP-based system	69
Figure 3.4 LOV2 domain photocycle kinetics are tunable via point mutation	70
Figure 3.5 Constitutively active LOVpep shows membrane recruitment of PDZ-LAT ^{int}	72
Figure 3.6 Light-inducible recruitment of the TULIPs-LAT constructs	73
Figure 3.7 Control variants of the Zdk system.....	75
Figure 3.8 Light-inducible dissociation of Zdk-LAT ^{int} -Ruby.....	76
Figure 3.9 Schematic overview of CRY2-based optogenetic system	78
Figure 3.10 CRY2PHR-LAT constructs show light-inducible membrane recruitment.....	79
Figure 3.11 Light-inducible recruitment of second generation CRY2 constructs	81
Figure 4.1 Characterising the TULIPs and LOVTRAP system in JCaM2.5 cells	97
Figure 4.2 Chronic depletion of LAT results in decreased TCR surface expression.....	99
Figure 4.3 Characterisation of a LAT-specific knockout Jurkat E6.1 cell line.....	100
Figure 4.4 Confirmation of LAT knockout at the protein and genetic level.....	102
Figure 4.5 LAT frameshift mutations lead to truncated LAT protein.....	103
Figure 4.6 Generating a CRISPR-proof LAT variant	104
Figure 4.7 Expression of the LAT IRES constructs in J-LKO cells.....	106
Figure 4.8 Reconstitution with full-length LAT rescues J-LKO phenotype	107
Figure 4.9 Reconstitution of J-LKO cells with LOVTRAP IRES system partially rescues calcium flux phenotype	108
Figure 4.10 LAT-TULIPs IRES system partially rescues J-LKO calcium flux phenotype.....	109
Figure 4.11 IRES constructs yield low expression of LOV 2 domain	111
Figure 4.12 Jurkat E6.1 cells show low level of endogenous LAT expression	112
Figure 4.13 Independent transduction of the LAT-TM constructs into J-LKO cells improves expression	113
Figure 4.14 Serial transduction of the LAT ^{int} domain improves expression of optogenetic constructs	114

Figure 4.15 LOVTRAP system rescues calcium flux phenotype	116
Figure 4.16 light-inducible modulation of calcium fluxing with the LOVTRAP system	117
Figure 4.17 Fluxing in calcium-free media attenuates sustain flux profile	119
Figure 4.18 Depletion of extracellular calcium causes delay but not ablation of ER calcium release under light stimulation in the LOVTRAP system	120
Figure 4.19 Titration of Zdk-LAT ^{int} -Ruby	121
Figure 4.20 LOVTRAP calcium flux titration	123
Figure 4.21 CD69 upregulation assay	124
Figure 4.22 Light-inducible initiation of signalling using the TULIPs system	126
Figure 4.23 Overview of LAT-TMpep and fused PDZ construct	127
Figure 4.24 Membrane recruitment of the truncated TULIPs system.....	128
Figure 4.25 Truncated LAT-TMpep variant does not rescue calcium flux phenotype, but fusion protein does	129
Figure 4.26 Expression of the CRY2PHR constructs in J-LKO cells	131
Figure 4.27 Calcium fluxing in LAT-CRY2PHR expressing cells	132
Figure 4.28 J-LKO cells show limited fluxing and increased CD6 expression.....	134
Figure 5.1 Optogenetic chimeric antigen receptor	148
Figure 5.2 Expression of the optoCAR systems in JNFAT cells.....	151
Figure 5.3 FRB-ex, BFP expression.....	152
Figure 5.4 Expression of TCR co-stimulatory receptors	153
Figure 5.5 Overview of conjugate flux experiment.....	155
Figure 5.6 Potent calcium fluxing in optoCAR photo-nonresponsive cells	156
Figure 5.7 Majority of optoCAR photo-nonresponsive cells triggered on addition of rapalog..	157
Figure 5.8 OptoCAR _{OPEN} cells do not flux calcium	158
Figure 5.9 Wildtype optoCAR cells show light-controllable calcium fluxing.....	161
Figure 5.10 Wildtype optoCAR cells show variation in number of responding cells.....	162
Figure 5.11 OptoCAR _{FAST} cells (V416T) show light-controllable calcium fluxing, but some background signalling	164
Figure 5.12 OptoCAR _{FAST} cells (V416T) yield low fraction of responding cells	165
Figure 5.13 OptoCAR _{SLOW} cells (V416L) show light-controllable calcium fluxing.....	166
Figure 5.14 OptoCAR _{SLOW} cells (V416L) show delayed return to signalling following blue light exposure	167
Figure 5.15 Light inactivation and drug washout comparison.....	170

Figure 5.16 OptoCAR-expressing cells upregulate NFAT-driven GFP expression following 3 hours of continuous signalling	171
Figure 5.17 OptoCAR-expressing cells upregulate CD69 expression following 3 hours of continuous signalling.....	172
Figure 5.18 IL-2 expression delayed relative to NFAT reporter GFP and CD69	173
Figure 5.19 Assaying signal integration through pulsed activity.....	175
Figure 5.20 TCR signalling is not additive.....	177
Figure 5.21 NFAT-driven GFP expression and S^{OFF} are inversely correlated	179
Figure 5.22 NFAT-driven GFP signal exhibits rapid decay.....	180
Figure 5.23 CD69 is rapidly expressed on optoCAR stimulation	181
Figure 5.24 CD69 signal exhibits rapid decay.....	182
Figure 5.25 T cells as a black box system	185
Figure 6.1 Anti-FcRH5/CD3 TDB conjugated cells mimic pMHC/TCR cell-cell junction	193
Figure 6.2 FcRH5 clustering and CD45 exclusion at cell-cell interface	195
Figure 6.3 Membrane-proximity of TDB FcRH5 epitope drives increased CD45 segregation..	196
Figure 6.4 Increased phosphorylation of downstream signalling proteins with membrane proximal epitope	198
Figure 6.5 Membrane proximal epitope facilitates target cell killing.....	199
Figure 6.6 Truncation of FcRH5 improves CD8 ⁺ killing efficiency	200

List of abbreviations

Abbreviation	Full name/meaning
(<i>Ai</i>)LOV2	(<i>Avena sativa</i>) Light-oxygen-voltage 2
AID	Activation Induced Demaniase
AIRE	Autoimmune regulatory element
AP-1	Activator protein-1
BATF	Basic leucine zipper transcription factor ATF-like
BCR	B cell receptor
BiTE	Bispecific T cell-engager
bsAb	Bispecific antibody
C1	Complement 1
C3	Complement 3
CAR	Chimeric antigen receptor
CCL19/21	Chemokine (C-C) Ligand 19/21
CCR7	Chemokine receptor type 7
CD	Cluster of differentiation
CD4 ⁺	T cell expressing the CD4 coreceptor
CD8 ⁺	T cell expressing the CD8 coreceptor
ChR2	Channel Rhodopsin 2
CID	Chemically-inducible dimerisation
COP1	Constitutively photomorphoc 1
CRISPR	Clustered, regularly interspersed palindromic repeats
CRY2/CIBN	Cryptochrome 2/ Chryptochrome-interacting basic helix-loop-helix protein
CXCR4	C-X-C Chemokine receptor type 4
DAG	Diacylglycerol
DC	Dendritic cell
DMEM	Dulbecco's Modified Eagles Media
DMSO	Dimethylsufaoxide
dsRNA	Double-stranded Ribonuclei acid
EL222	A baceterial LOV domain
ELISA	Enzyme-linked immunosorbent assay
EpCAM	Epithelial cell adhesion molecule
FACS	Fluorescence-activated cell sorting
FAD	Flavin-adenine dinucleotide
FcR	Fc Receptors
FcRH5	FcR homology 5
FKF1	Flavin-binding, Kelch repeat, F-box 1
FMN	Flavin mononucleotide

FN3	Fibronectin type III
Gads	GRB-2 related adaptor downstream of shc
GC	Germinal Centre
GEF	Guanine exchange factor
Grb2	Growth-factor-receptor-bound protein 2
HEK293T	Human embryonic kidney 293T cells
ICAM-1	Intercellular adhesion molecule-1
IFN- γ	Interferon- γ
IgG	Immunoglobulin G
IL	Interleukin
IP3R	Inositol 1,4,5-phosphate receptor
IRAK	Interleukin-1 Receptor-associated kinase
IRF4	Interferon regulatory factor 4
IS	Immunological synapse
ITAM	Immunoreceptor tyrosine-associated activation motif
ITIM	Interleukin 2-inducible T cell kinase
ITK	Interleukin-2-inducible T-cell kinase
J-LKO	Jurkat LAT knockout cell line
JNK	c-Jun N-terminal kinases
K_d	Dissociation constant
KIR	Killer cell immunoglobulin receptor
KOD	<i>Thermococcus kodakarensis</i>
LAT	Linker of activation for T cells
LED	Light-emitting diode
LFA-1	Lymphocyte functional antigen-1
LMB	Laboratory of Molecular Biology
LOVDAD	LOV2 fused to the autoinhibitory DAD domain of mDia2
LOVTRAP	LOV2 trap and release of proteins
LPS	Lipopolysaccharides
LUT	Look-up tables
MAPK	Mitogen-activated protein kinase
MHC I/II (pMH)	Major histocompatibility complex class I/II (peptide-bound MHC)
MKK4	Mitogen-activated protein kinase kinase 4
MM	Multiple Myeloma
MyD88	Myeloid differentiation primary response 88
NFAT	Nuclear factor of activated T cells
NK cell	Natural Killer cell
NKT cell	Natural killer T cell
NOD	Nucleotide binding oligomerisation domain
OptoCAR	Optogenetic chimeric antigen receptor

PAMP	Pathogen-associated molecular pattern
PA-RAC	Photoactivatable Rac1
PAS	PER-ARNT-SIM
PCR	Polymerase chain reaction
PDZ	Post-synaptic density protein, <i>Drosophila</i> disc large tumour suppressor, and zonula occludens-1 protien
PhyB/PIF	Phytochrome B/ Phytochrome-interacting factor
PI3K	Phosphoinositide-3 Kinase
PI-Src	Photoinhibitable Src
PKC θ	Protein Kinase C theta
PLC- γ 1	Phospholipase C- γ 1
POI	Protein of interest
PRR	Pattern recognition receptor
RAG 1/2	Recombinase-activating gene 1 and 2
RasGRP1	Ras guanyl-releasing protein 1
RIG-I	Retinoic acid-induced I
RPMI	Roswell Park Memorial Institute (Media)
SFM	Serum-free media
SH2	Src-homology
SLP76	SH2 domain-containing leukocyte protein of 76 KDa
(c/p/d)SMAC	(central/peripheral/distal) supramolecular activation cluster
SOS1	Son-of-sevenless
ssRNA	Single-stranded RNA
TALENs	Transcription activator-like effector nuclease
TCR	T cell antigen receptor
TDB	T cell-dependent bispecific antibody
TdT	Terminal deoxynucleotidyl transferase
T _{FH}	T follicular helper
TLR	Toll-like receptor
TM	transmembrane
TNF-R	Tumour necrosis factor receptor
T _{reg}	Regulatory T cell
TRIF	TIR-domain-containing adapter-inducing interferon- β
TULIPs	Tunable, Light-controlled interacting protein tags
UVR8	UVB resistance 8
VCA	Verprolin homology central acidic
V(D)J	Variable-to-diversity-to-joining recombination
WAS	Wiskott Aldrich Syndrome
ZAP70	Zeta-associated protein of 70 KDa

Chapter 1 – Introduction

1.1 Overview of immunity

We live in a world predominated by microorganisms. Some of these microbes can cause disease. In order to maintain a healthy constitution, we have evolved an immune system to prevent or counteract the onset of infection. In higher vertebrates, including humans, this system is comprised of a complex network of cells, tissues, and biological processes aimed at fighting pathogenic invaders. It can be broadly divided into two branches: the innate immune system, which relies on germline encoded mechanisms of pathogen detection, and the adaptive immune system, which develops somatically and is specific toward individual pathogens.

1.2 The innate immune response

1.2.1 Non-cellular constituents of innate immunity

The innate immune response is rapid and hard-coded within the genome, responding broadly to almost all classes of pathogenic invaders and microorganism. At its most basic, epithelial cells in the skin, gastrointestinal tract, urogenital tract and respiratory system form tight intercellular junctions sealing the body from the external environment. Epithelial barriers within the body are mucosal membranes. Cells along these surfaces secrete antimicrobial compounds such as lysozyme or phospholipase A₂, which non-specifically kill microbial cells. Cells along epithelial linings are also continually sloughed off, a mechanism particularly important against helminth infection. It has been termed the ‘weep-and-sweep’ mechanism of defence (Anthony et al. 2007).

In the event that this barrier is disrupted, as occurs during burning, wounding or pathogenic breaching, invading microorganisms are immediately confronted with the body’s second line of defence. The complement system is a collection of 30 soluble proteins found in the blood and other bodily fluids. The complement system acts as a network of different pathways, different combinations of which drive direct cell killing or opsonise targets for destruction by innate immune cells (Holers 2014). Many of the components of the complement system are proteases or cytolytic factors and thus are secreted as pro-enzymes, zymogens, to avoid off-target effects.

The complement system can become activated by three main pathways, all three of which rely on C3 (Sarma and Ward 2011). The classic complement pathway is triggered when the C1-

complex binds to either IgM or IgG1 engaged with an antigen. The alternative pathway relies on spontaneous hydrolysis of C3. If this occurs on the surface of a pathogen, C3 becomes covalently bound to the pathogen, blocking it from H-mediated inactivation (Conrad, Carlos, and Ruddy 1978). The final pathway of activation is similar to the classic pathway, but relies on binding of mannose-binding lectin, opsonin, or ficolins, rather than the C1-complex. As mentioned the complement system is tightly regulated and host cells do not accumulate C3 due to the expression of cell surface molecules such as cluster of differentiation 35 (CD35), CD46, CD55 and CD59, which work to inhibit the complement system (Holers 2014).

As well as the complement system, many organism including vertebrates, invertebrates and plants secrete small cysteine-rich polypeptides called defensins (Ganz 2003). Defensins target bacterial, fungal and viral cells for phagocytosis and embed themselves in the microbial cell membrane. Here they form pores in the membrane that cause efflux of the pathogen's cytosol (Ganz 2003).

1.2.2 Innate immune receptors

Key to the activity of the innate immune system are a number of genetically pre-encoded receptors. These receptors are termed pattern recognition receptors (PRRs) as they recognise key chemical or structural motifs specific to pathogenic organisms but not host cells. These pathogen associated molecular patterns (PAMPs) are highly conserved molecules necessary for pathogen survival and include targets like bacterial lipopolysaccharides (LPS), flagellin, and viral-associated nucleic acids, for example double-stranded RNA (dsRNA).

One class of innate immune receptors is the toll-like receptors (TLRs). TLRs derive their name from their similarities to the *Drosophila* developmental receptors (Medzhitov, Preston-Hurlburt, and Janeway 1997). TLRs recognise a variety of different pathogenic molecules summarised in Table 1.1. All TLRs are membrane associated, but TLR3, 7, 8, and 9 are located within intracellular compartments (Kollmann et al. 2012).

All TLRs with the exception of TLR3, and in some situations TLR4, function through the MyD88 adaptor protein. MyD88 recruits IRAK kinases that trigger a signalling cascade culminating in the translocation of NF- κ B to the nucleus and transcriptional activation of genes associated with the induction of an inflammatory response (Akira and Takeda 2004). TLR3, and TLR4 in a MyD88-independent fashion, function through the adaptor protein TRIF (Akira and Takeda 2004).

Receptor	Target(s)
TLR1	Bacterial lipoproteins
TLR2 (heterodimerises with TLR 1 and TLR6)	Lipoproteins/lipopeptides Reptidoglycan Lipoteichonic acid Zymosan
TLR3	Viral dsRNA
TLR4	Taxal LPS RS virus F protein Tamm-Horsfall glycoproteins Damage-associated molecular patterns (DAMPs) Allergens
TLR5	Bacterial Flagellin
TLR6	Mycoplasma lipopeptides Zymosan
TLR7	ssRNA viral RNA
TLR8	ssRNA viral RNA
TLR9	CpG DNA Hemozoin Viral DNA
TLR10	Target unknown

Table 1.1: Human TLRs and their targets

Some innate immune receptors are located within the cytosol to detect intracellular pathogens. Nucleotide-binding oligomerisation domain (NOD) receptors detect peptidoglycan within the cytoplasm of infected cells and signal through NF- κ B to induce an inflammatory response (Philpott et al. 2013). Also expressed intracellularly, are the retinoic acid-inducible gene I (RIG-I)-like receptors. Three of these receptors exist: RIG-I, MDA5, and LGP2. The RIG-I-like receptors bind ssRNA and dsRNA and trigger type I interferon production (Yoneyama et al. 2004; Yoneyama and Fujita 2007).

Another important class of immune receptors is Fc receptors (FcRs). FcRs are found on the surface of a number of different immune cell-types including dendritic cells (DCs), mononuclear phagocytes, and granulocytes (Table 1.2) (Shi, McIntosh, and Pleass 2006) and are so named because they recognise the fragment, crystallisable region of antibodies bound to pathogens. Importantly, FcRs can be associated with either immunoreceptor tyrosine-associated activation motifs (ITAMs) or immunoreceptor tyrosine-associated inhibitory motifs (ITIMs), and

Receptor	Signal motif	Cell type
FcγRI	ITAM	Mast cells Basophils Monocytes Langerhans cells Neutrophils
FcεRII	C-type lectin	B cells T cells NK cells DCs Eosinophils Macrophages
FcRγRI	ITAM Peiplakin	Monocytes Macrophages Neutrophils Eosinophils
FcγRIIa	ITAM	Monocytes Macrophages Neutrophils Langerhans cells Platelets
FcγRIIb	ITIM	Monocytes Macrophages B cells
FcγRIIc	ITAM	Monocytes Macrophages Neutrophils B cells
FcγRIIIa	ITAM	Macrophages NK cells γδ T cells Monocytes
FcγRIIIa	GPI	Neutrophils Eosinophils
FcαRI	ITAM (can inhibit)	Monocytes Macrophages NK cells Neutrophils Eosinophils Kupffer cells DCs
FcRH1-6	ITAM/ITIM	B cells

Table 1.2: Human FcR receptors

regulate the activation state of the host cell. This can either have a dampening or activatory effect on the overall activation state of the target cell. FcR receptors have varying affinities for the Fc region of antibodies and compete with each other for ligand binding (Smith and Clatworthy 2010). Availability of ligand and concentration of the receptors on the cell surface influences the cellular response (Smith and Clatworthy 2010). The final class of innate immune receptors is the C-type lectin receptors. As with FcRs, the C-type lectin receptors are associated with ITAMs, which mediate their activation. C-type lectins drive the expression of reactive oxygen species and inflammatory cytokines in response to specific carbohydrate motifs. They are well reviewed by Osorio and Reis e Sousa (Osorio and Reis e Sousa 2011).

1.2.3 Innate Immune lymphocytes

Operating at the interface of innate and adaptive immunity are several subsets of lymphocytes. Natural killer (NK) cells are cytolytic lymphocytes involved in the immune response to virally infected cells and tumour cells. Critical to NK cell function is inhibitory, killer-cell immunoglobulin-like receptors (KIRs) that recognise MHC I (Parham 2005). This is important because tumour cells are reported to downregulate Major Histocompatibility Complex class I (MHC I) as an immune evasion mechanism (Nouroz et al. 2016; Bubeník 2004). In the absence of this 'self' signal and KIR-derived inhibitory signals (Borrego 2006), NK cells will release cytolytic molecules, such as granzyme B, and inflammatory cytokines, like IFN- γ (Mandal and Viswanathan 2015). NK cells are also activated in response to inflammatory cytokines from other innate immune cells acting at the site of infection.

Another type of lymphocyte operating between innate and adaptive immunity is the Natural Killer T cell (NKT cell). T cells are discussed further in section 1.3.3. NKT cells represent only a small fraction of circulating lymphocytes and are characterised by the expression of an invariant TCR α chain. NKT cells specifically recognise lipid antigens presented on CD1 rather than MHC (Kinjo et al. 2005). NKT cells are important for their rapid release of inflammatory cytokines in response to infection (Barral and Brenner 2007).

Finally, $\gamma\delta$ T cells represent a unique branch of T lymphocytes with innate-like functions. Although $\gamma\delta$ T cells undergo somatic T cell antigen receptor (TCR) rearrangement during development, their TCRs are used as PRRs, much like TLRs. For example, the V γ 9/V δ 2 subset responds rapidly to microbial metabolites during acute infections. $\gamma\delta$ T cells promote the activation of APCs and are proposed to act as APCs themselves (Tyler et al. 2015). Their rapid response to

infection and ability to present antigen means that their function straddles the innate response and the adaptive response to microbes.

1.2.4 Dendritic cells translate innate immunity to adaptive immunity

During acute infection pathogenic antigens are deposited at the site of infection. These antigens are endocytosed either by phagocytosis or pinocytosis by innate immune cells, processed, and presented on MHC II. Although this process can be performed by neutrophils and macrophages, DCs are more specialised in the process of antigen processing and presentation. Dendritic cells act as the sentinels of the immune system. They are resident both in lymphoid and non-lymphoid organs and are usually associated with epithelial cells. Indeed, it was this observation that led to the hypothesis that DCs are important in translating early innate immune responses into adaptive immune responses (Bujdoso et al. 1989) (Figure 1.1). Unlike other immune phagocytes, protein degradation within dendritic cells is slow under steady-state conditions, i.e. in the absence of infection, but switches to become more rapid in the presence of local inflammatory cues (Trombetta et al. 2003). Even in steady-state DCs continually traffic cargo, such as debris from apoptotic cells, from their sites of residence to the draining lymph nodes for presentation to T cells. In the absence of inflammatory signals this process is involved in maintaining peripheral tolerance (Mueller 2010). DCs that are naïve to pathogenic antigen are referred to as immature. On exposure to pathogenic antigen in the presence of inflammatory signals, dendritic cells undergo maturation. During this process antigen uptake is decreased and the DC becomes more migratory, upregulating CXCR4, CCR7, and CCL19/CCL21, which brings mature DCs into proximity with naïve T cells in the lymph nodes (Sallusto et al. 1999; Barrat-Boyes et al. 2000; Yanagihara et al. 1998). DCs, on exposure to pathogenic antigen also upregulate expression of TNF-R, which enhances the expression of the inflammatory cytokine, IL-12. The production of cytokines such as IL-12, IL-6 and type I interferons by DCs is important in driving T cell activation and polarising the T helper immune response. DCs also upregulate T cell costimulatory molecules such as CD86, which is intracellularly clustered with MHC II and remains clustered on the cell surfaces to prime T-cell activation (Turley et al. 2000). These unique features of DCs make them exquisitely specialised for priming the adaptive immune response.

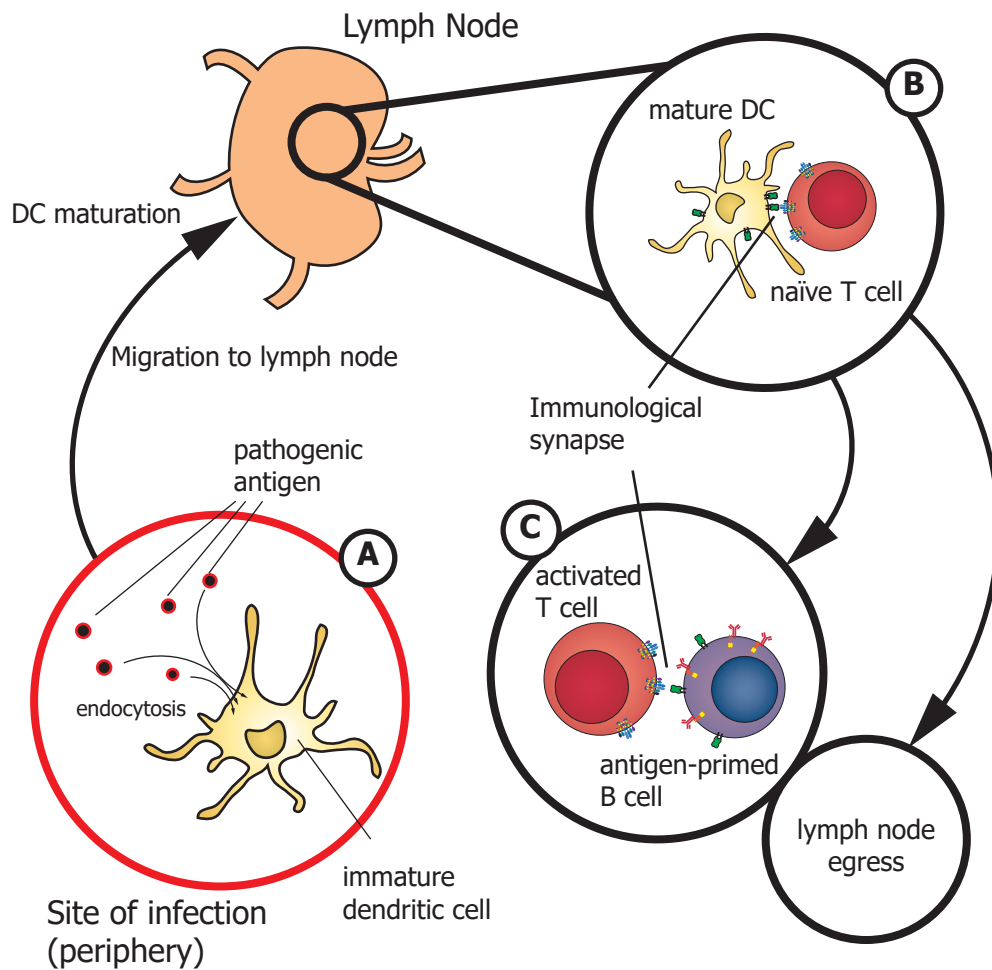


Figure 1.1 Overview of antigen presentation by dendritic cells **(A)** During an infection antigens are deposited in the periphery by pathogens. Tissue resident dendritic cells (DCs) endocytose, process, and present pathogenic antigens. Inflammatory cues from the surrounding tissue activate DCs, which undergo maturation and migrate to tissue draining lymph node. **(B)** Antigen-presenting dendritic cells will cease to migrate once they reach the lymph node and will begin to interact with circulating naïve T cells. Once the cognate TCR is engaged by pMHC on the DC, the T cell will become activated. **(C)** Some subsets of activated T cells will then engage and activate antigen-primed B cells to initiate the process of antibody production. Other subsets will egress from the lymph node to the cite of infection to mediate their effector function.

1.3 The adaptive Immune response

1.3.1 Overview of adaptive immunity

Adaptive immunity differs from innate immunity in that it provides a response to infection that is narrowly specific to each pathogen, rather than broadly specific toward conserved pathogenic motifs. The adaptive arm of the immune response is dependent on B cells and T cells, both of which are derived from common lymphoid progenitor cells in the bone marrow. The fate and function of B and T cells is highly dependent on non-germline encoded antigen receptors, the B cell receptor (BCR) and the TCR, respectively. Both the BCR and TCR are highly diverse in their ligand recognition. This diversity is generated during their development through the process of somatic recombination. Although the actual number of clonal lymphocytes varies from species to species, it is estimated at $\sim 3 \times 10^{11}$ in humans (Hataye et al. 2006; Elhanati et al. 2014). Cross-recognition of antigens allows for recognition of $>10^{15}$ pMHC variants (Regner 2001).

1.3.2 B cell development

Unlike the innate immune system, which relies on germline encoded receptors, the BCR and TCR are assembled through genetic recombination to generate a high degree of diversity amongst different BCRs and TCRs. The BCR is a transmembrane receptor with a unique antigen-binding moiety. On the B cell surface, the BCR forms a complex with the transmembrane proteins CD79a and CD79b, which contain ITAM motifs that mediate BCR-induced signalling (Chu and Arber 2001; Otipoby et al. 2015). B cells (and T cells) express recombinaison activating gene 1 (RAG1) and RAG2 necessary for gene rearrangement, as well as Terminal deoxynucleotidyl transferase (TdT). The BCR is assembled through a process called V(D)J somatic recombination. During the first step of this process, pro-B cells combine one each of the variable (V), diversity (D), and joining (J) gene segments from the immunoglobulin heavy locus (Y. S. Li, Hayakawa, and Hardy 1993; Karasuyama et al. 1997). These combine with a surrogate light chain to form pre-BCRs (Karasuyama et al. 1997; Reth et al. 1985). Cells that successfully complete this process pass to the next stage of development, where they assemble a BCR light-chain via a similar process, but do not include a D segment (Reth et al. 1985). The heavy- and light-chain constructs are then assembled to form a mature BCR. Each B cell that survives development is a unique clone expressing a single variant of the BCR. The error-prone process of non-homologous end joining during V(D)J recombination leads to a high degree of B cell diversity, but frequently results in cells capable of recognising 'self' antigen (Nemazee and Weigert 2000; Wardemann et al. 2003). Autoreactive B cells, recognising self-antigen are eliminated in the bone marrow during their

development and the number of autoreactive B cells decreases through each stage of B cell development.

Once primed with antigens, and activated by T cells, B cells will once again go through somatic mutation of the immunoglobulin region. B cells in germinal centres (GC) express the enzyme AID (Activation Induced Deaminase), which is necessary for further somatic hypermutation and class switching recombination. AID mediates the conversion of cytosine to deoxyuracil, which mimics thymidine when paired with deoxyguanosine, and is acted upon by the DNA repair machinery. Class switching does not change antibody specificity but instead causes a change in the constant region of the heavy chain allowing it to interact with different FcRs (Maul and Gearhart 2010; Maul et al. 2014). In GCs, antigen-primed B cells undergo several rounds of proliferation and hypermutation of the BCR locus. B cell clonal evolution in GCs is driven by affinity-dependent selection in a Darwinian manner to select only B cell clones expressing high affinity BCRs (Maul and Gearhart 2010). Survival is dependent on the ability of B cells to collect and present antigen to local CXCR5⁺, CD4⁺ T-follicular helper cells (T_{FH}) (Figure 1.1) (Kurosaki, Kometani, and Ise 2015).

1.3.3 T cell development

T cells are the second major cell type in the adaptive immune response. Like the BCR, the TCR is also generated through V(D)J somatic recombination. Unlike B cells, T cell progenitors migrate to the thymus to undergo development. During the first stage of development, thymocytes rearrange their TCR β chain, first by D-J rearrangement and then V-DJ joining (Shah and Zuniga-Pflucker 2014). Thymocytes that successfully rearrange TCR β begin to express the pre-TCR along with a surrogate TCR α chain. The developing thymocytes will then undergo V(D)J rearrangement of the TCR α subunit. This process is not allelically exclusive and will use the α subunit from both chromosomes, however T cells expressing two variants of the TCR will have only one variant that signals strongly enough to undergo positive selection (Klein et al. 2014). Thymocytes at this stage of development become double positive for both TCR co-receptors, CD4 and CD8 (Klein et al. 2014).

Once the double-positive thymocyte has successfully rearranged both a TCR β and α chain, it will migrate to the cortex of the thymus for positive selection by MHC I- and MHC II-expressing thymic epithelial cells. Unlike the BCR, which can recognise antigenic structural epitopes, the TCR is restricted to antigens presented on MHC. Therefore, the TCR must be able to recognise self-MHC. Thymocytes unable to recognise MHC undergo 'death by neglect' during positive selection.

Those cells that survive positive selection move to the medulla of the thymus for negative selection. Here, thymocytes are presented with self-antigen by specialised epithelial cells expressing the transcription factor AIRE (autoimmune regulatory element) (Klein et al. 2014). AIRE allows these thymic epithelial cells to express self-antigen from around the body (Anderson 2002). T cells that react too strongly to these self-antigens are triggered to undergo apoptosis, though some are thought to be driven down the T regulatory (T_{reg}) lineage (M. O. Li et al. 2016; A. G. Levine et al. 2014; A. E. Moran et al. 2011). These developmental checkpoints help establish a population of non-autoreactive naïve T cells capable of recognising MHC-restricted antigenic peptide. These immature T cells then exit the thymus into the periphery where they recirculate through secondary lymphatic organs. Here, they are presented with antigen by mature DCs (Figure 1.1).

1.3.4 *T cell effector subsets*

Optimal T-cell activation through the $\alpha\beta$ -TCR, discussed further in Section 1.4 and in Chapter 4, is mediated by either the CD4 or CD8 co-receptor. Developing thymocytes express both the CD4 and CD8 coreceptors, but mature T cells are committed to either a CD4- or CD8-single positive lineage fate. Co-receptor expression is partially determined by the MHC-specificity of the TCR. Thymocytes recognising MHC-II will commit to expression of the CD4 co-receptor and thymocytes that recognise MHC-I will commit to expression of CD8. This process is reviewed by Germain (Germain 2002). Mature T cells can thus be subdivided and classified based on their expression of either the CD4 or CD8 coreceptor. Further subclassifications can be made based on a T cell's effector function within the adaptive immune response (Table 1.3).

Activated $CD8^+$ T cells mediate killing of cells expressing foreign antigen on MHC-I, this includes tumour cells and pathogen-infected host cells. These cytotoxic T lymphocytes (CTLs) rapidly proliferate in the presence of IL-2 and mediate target cell killing through the polarised secretion of perforin and granzymes, as well as through activation of the Fas signalling pathway in target cells.

Naïve $CD4^+$ T cells are driven toward particular effector lineages (Table 1.3) through a combination of TCR-derived activation signals and environmental cues in the form of cytokines. Each subset is defined by a particular cytokine secretion profile. Each lineage helps fulfil a particular function during an immune reaction. T helper 1 (T_H1) cells, which are characterised by the expression of transcription factor Tbet (Kanhere et al. 2012), differentiate following stimulation by IFN- γ and IL-12 to secrete pro-inflammatory interferons and TNFs, which facilitate immunity against intracellular pathogens. Activated T cells expressing IL-4, IL-5 and IL-13 belong

to the T_H2 subset and mediate immunity against extracellular parasites (Kanhare et al. 2012). Also involved in the host response to parasites is the T_H9 subset, which is characterised by the expression of IL-9 and the anti-inflammatory cytokine, IL-10 (Kaplan 2013). T helper cells expressing IL-17, IL-21, IL-22, and IL-26 are involved in host defences against extracellular bacterial infections and fungal pathogens. These T cells belong to the T_H17 lineage (Tesmer et al. 2008). The T_H22 lineage is particularly associated with mucosal immunity, secreting IL-22 (Eyerich et al. 2009). Follicular helper T cells (T_{FH}) are characterised by expression of the transcription factor Bcl-6 and the surface receptor CXCR5, which allows them to home to the B cell follicles of secondary lymphoid organs. They secrete the cytokine IL-21 and are intrinsically tied to the survival and selection of germinal centre B cells (Fazilleau et al. 2009). T_{FH} cells may display a cytokine profile similar to that of the previously mentioned T helper cell subsets.

$CD4^+$ T cells can also be directed toward a regulatory lineage (Treg). Regulatory T cells are characterised by the expression of the FoxP3 transcription factor and secrete the anti-inflammatory cytokines IL-10 and TGF- β (Hori et al. 2009). It is thought that developing thymocytes are driven toward a regulatory phenotype by strong recognition of self-MHC (M. O. Li and Rudensky 2016). Tregs are involved in the suppression of other effector T cell subsets.

T cell subset	Activating cytokines	Cytokine Expression profile
$CD8^+$ cytotoxic T cell	IL-2	-
$CD4^+ T_H1$	IL-12, IFN- γ	INF- γ , TNF, IL-2
$CD4^+ T_H2$	IL-4, IL-33	IL-4, IL-5, IL-13, IL-10
$CD4^+ T_H9$	IL-4, TGF- β	IL-9, IL-10
$CD4^+ T_H17$	IL-1, IL-6, IL-21, IL-23, TGF- β	IL-17, IL-21, IL-22, IL-25, IL-26
$CD4^+ T_H22$	IL-6, TNF	IL-22
$CD4^+ T_{FH}$	IL-6, IL-21	IL-21
$CD4^+ T_{reg}$	IL-2, TGF- β	IL-10, IL-33, TGF- β

Table 1.3: T cell effector subsets

1.3.5 Immunological memory response

The general paradigm in immunology is that the adaptive immune response is responsible for the generation of immunological memory. This is perhaps somewhat simplistic as recent findings have suggested that epigenetic changes to innate immune cells may allow for a different type of immunological memory (Netea et al. 2015). However, classic immunological memory is restricted to B and T lymphocytes. The T cell immune response is characterised by three phases: expansion, contraction, and maintenance. Following activation by an APC (Figure 1.1), both CD4⁺ T helper cells and CD8⁺ cytotoxic T cells undergo a phase of rapid proliferation. This proliferative phase lasts approximately 2 weeks and allows the T cells to exert their effector function. This is followed by a phase of decline during which most activated T cells undergo apoptosis. However, some T cells are selected to undergo memory lineage commitment through a process that is not fully understood (W. Huang et al. 2017). CD8⁺ memory T cells are retained almost indefinitely and CD4⁺ memory T cells have a half-life of ~15 years (Hammarlund et al. 2003). Memory T cells are found in both lymphoid and non-lymphoid organs, known as T central memory (T_{CM}) and T effector memory (T_{EM}), respectively. Tissue specific signals derived from DCs drive the homing capacity of T_{EM} cells (Shin and Iwasaki 2013; Bouneaud et al. 2005; X. Zhou et al. 2010; Speiser et al. 2014). On re-infection, pathogen-specific memory T cells are able to rapidly mount an inflammatory response against the invader. Memory T cells are sustained through a process termed homeostatic proliferation, where the population occasionally turns over (Boyman et al. 2009). This is in contrast to naïve T cells, which are maintained in interphase (Surh and Sprent 2000).

B cells can also undergo commitment to a memory lineage. Once activated, T cells will migrate to the B cell-zone of the secondary lymphoid organs where they interact with B cells that have internalised, processed, and presented the cognate antigen on MHC II (Figure 1.1) (De Silva and Klein 2015). Following activation in the presence of T_{FH} cells, B cells undergo proliferation in the germinal centre. Most clones will become antibody-producing plasma cells, but some are directed down a memory B cell lineage. B cells that undergo memory formation tend to be those that have undergone somatic hypermutation and have been affinity selected to produce high-affinity BCRs (De Silva and Klein 2015). Like the T cell memory response, B cell memory allows for the rapid onset of antibody-mediated immunity on re-infection by a previously encountered pathogen.

1.4 The T cell antigen receptor and signalling complex

Decades of research has provided us with a good working understanding of the classic TCR complex. The TCR is comprised of an α and a β subunit, which have the variable regions responsible for the recognition of pMHC (Sancho et al. 1989; Geisler, Kuhlmann, and Rubin 1989). These subunits do not contain any intrinsic signalling capacity themselves but form an obligate multimeric complex with six CD3 subunits – two ζ subunits, two ϵ subunits, and one each of γ and δ (Figure 1.2). Collectively these CD3 subunits have ten ITAMs, which are defined as a pair of YxxI/L amino acid sequences. Although the TCR itself does not have any intrinsic enzymatic activity, the CD3 ITAMs are phosphorylated by the src-family kinase Lck and serve as a docking site for the SH2-domain of the zeta-associated protein-kinase of 70 KDa (ZAP70) (Wange et al. 1993). The immediate downstream substrates of ZAP70 phosphorylation are Linker for Activation of T cells (LAT) and SH2 domain containing leucocyte protein of 76 KDa (SLP76). LAT and SLP76 serve to nucleate other TCR signalling molecules involved in calcium fluxing and downstream kinase signalling cascades (Balagopalan et al. 2010) (Figure 1.2). The TCR signalling machinery and activation process are well reviewed by Smith-Garvin (Smith-Garvin et al. 2009). Although our knowledge of the underlying TCR signalling machinery is reasonably comprehensive, precisely how varying signals through the TCR and costimulatory receptors are internalised and translated into an appropriate output response is still poorly understood. However, new techniques for the manipulation of cell signalling pathways are beginning to yield fresh insights into signalling dynamics. In this thesis I discuss the development of an optogenetic approach to T cell signalling. Mechanisms of TCR signal transduction are discussed further in Chapter 4.

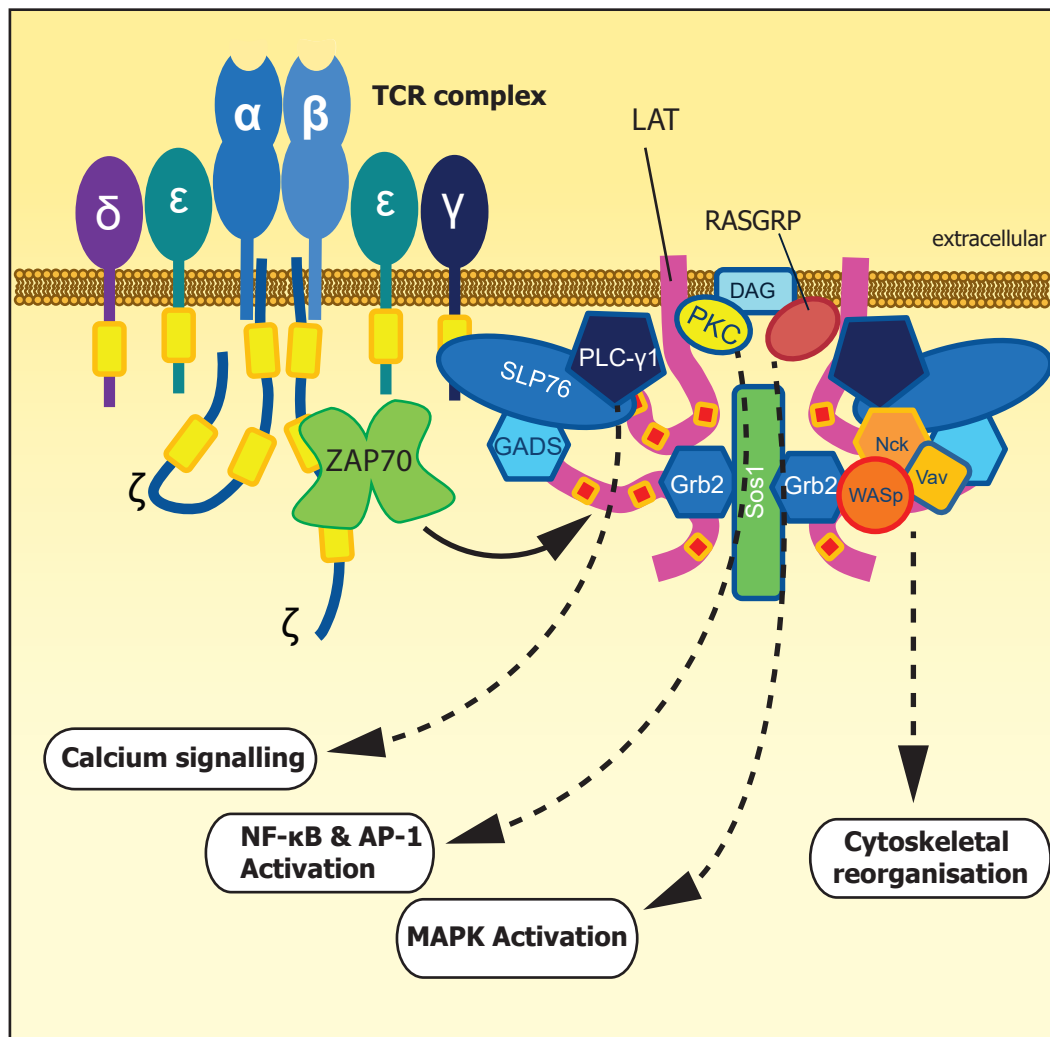


Figure 1.2 Overview of the T cell antigen receptor The TCR complex is comprised of an α and a β subunit, as well as six CD3 subunits. The α and β subunits are assembled through V(D)J recombination and bear the variable region responsible for antigen recognition. The TCR forms an obligate heterodimer with six CD3 subunits; two ε subunits, two ζ subunits, one δ subunit, and one γ subunit. These CD3 subunits each have ITAM motifs (yellow), which once phosphorylated by Lck (not shown), serve as a docking site for ZAP70. Immediately downstream of ZAP70 is the scaffolding protein LAT (pink). LAT has 9 phosphorylatable tyrosine motifs (red), which serve as the docking site for several TCR-associated signalling proteins. Shown in this figure are a limited selection of signalling proteins including, SLP76, the SLP76-adaptor protein GADS, PLC-γ1, PKC, RASGRP, Sos1, the Sos1 adaptor protein Grb2, Nck, Vav, and WASp. Shown as well is the secondary messenger DAG. Together these proteins, among others, serve to regulate downstream T cell activation events including Calcium fluxing, Transcription factor activation, kinase signalling, and cytoskeletal reorganisation.

1.5 Chemical and optical manipulations of cellular signalling pathways

1.5.1 Chemically-inducible dimerization

Cells are dynamic entities, continually responding to spatially- and temporally-encoded environmental signals. A multitude of different cellular receptors act as sensors for these cues and transmit signals accordingly through networks of signalling proteins. Proteins within these signalling networks need to be tightly controlled and many fulfil their function only at specific cellular locations or in complex with other proteins. Although genetic knockout or overexpression studies have traditionally been used to study cell biology, the chronic nature of such manipulations does not reflect the dynamicity of cell biology. Chemically-inducible dimerization (CID), provides a mechanism to more acutely interrogate cellular signalling pathways. Over the past few years a number of different CID systems have been developed (Table 1.3).

Domain	Partner	Dimeriser	Reference
FKBP12	FKBP12	FK1012	(Spencer et al. 1993)
FKBP12	Calcineurin A	FKCsA	(Belshaw et al. 1996)
FKBP12	FRB	Rapalog	(Liberles et al. 1997)
ABI _{CS}	PYL _{CS}	ABA	(Liang, Ho, and Crabtree 2011)
GAI	GID1	GA ₃ -AM	(Miyamoto et al. 2012)
SNAP-tag	HaloTag	MeNV-HaXS	(Erhart et al. 2013)

Table 1.4: Chemically-Inducible dimerization systems

In CID systems, protein-protein interactions can be acutely induced on the addition of a small molecule, most commonly a rapamycin analogue (Bayle et al. 2006; Putyrski and Schultz 2012). CID dimerization has been particularly important in interrogating lipid signalling pathways (DeRose, Miyamoto, and Inoue 2013). In these studies, one CID domain is localised to the plasma membrane, whilst its interaction partner is fused to a protein of interest (POI). Addition of the dimerising drug results in the recruitment of the interaction partner to the plasma membrane typically within seconds to minutes. Here, the POI exerts its effector function. For example, in a study by Varnai et al. (Varnai et al. 2006) the type IV 5-phosphatase domain was fused to the FKBP domain. On the addition of a rapamycin analogue, the FKBP fusion protein was recruited to a membrane-anchored FRB domain. This process resulted in the rapid dephosphorylation of PI(4,5)P₂ at the plasma membrane, ATP-induced calcium influx, and decreased activity of TRPM8

channels (Varnai et al. 2006). In this way CID was used to rapidly trigger a physiological response in the cell.

Among the earlier CID studies is Graef et al.'s (Graef et al. 1997) interrogation of ZAP70's orientation during T cell activation. As mentioned before, ZAP70 is recruited to the TCR complex on phosphorylation, where it exerts its kinase activity. Again, the FKBP-FRB CID system was employed. Using rapamycin analogues that allowed for differing degrees of rotational freedom of a fused ZAP70 kinase, Graef et al. (Graef et al. 1997) determined that simply recruiting ZAP70 to the plasma membrane was not enough to mediate its function. Instead, ZAP70 conformational freedom was necessary to drive downstream signalling, as rapamycin analogues that restricted the movement of ZAP70 did not result in T cell activation (Graef et al. 1997).

Studies such as the two outlined above highlight the utility of CID as a method to interrogate cell signalling. However, they also bring to the fore a major weakness of CID as a technique. Even with the advent of microfluidics technology, it is still currently difficult to precisely spatially administer drugs. It is now becoming clear that cells must respond to highly localised cellular signals, such as Cytotoxic CD8⁺ T cells polarizing their release of cytolytic granules toward an APC (Stinchcombe et al. 2006). New techniques in cell biology are emerging that bypass this limitation. As well as this, CID systems are difficult to reverse and in some cases the dimerisation is irreversible.

1.5.2 Overview of optogenetics

Over time, diverse groups of organism across all phylogenetic kingdoms have evolved mechanisms to sense and respond to various wavelengths of light (380-790nm; UV-Infrared). These light-inducible sensors allow organisms to detect continually varying environmental light conditions and respond appropriately. Molecular cloning and genetic manipulation of the proteins underlying these light response mechanisms has given rise to a new set of techniques in the field of molecular biology known as 'optogenetics' (Häusser 2014). Optogenetics is so named because it relies on genetically-encoded, light-responsive proteins, which distinguishes it from chemical photocaging methods. The fundamental modularity of cell biology has allowed for the rapid expansion of a suite of light-controllable protein tools for the modulation of diverse cell signalling pathways (Lim 2010; Tischer and Weiner 2014). Some of the more commonly used systems are outlined in Table 1.4, adapted from (Repina et al. 2017).

System	$Td_{1/2}$	λ_{ON} (nm)	λ_{OFF} (nm)	Size (aa)	Reference
ChR2	15 ms	~470		737	(Boyden et al. 2005; Nagel et al. 2002)
<i>Ai</i> LOV2	~50 s	~450		143	(Wu et al. 2009)
Phy/PIF	4 s	650	~760	908/100	(Levskaya et al. 2009)
BphP1/PpsR2	15 min	~760	~650	732/465	(Kaberniuk, Shemetov, and Verkhusha 2016)
CRY2/CIBN	~12 min	~450		498/170	(Kennedy et al. 2010)
FKF1/Gigantea	h	~450		619/1173	(Yazawa et al. 2009)
EL222	~50 s	~450		222	(Motta-Mena et al. 2014)
UVR8/COP1	Irreversible	~300		440/675	(Favory et al. 2009)

Table 1.5: Commonly used optogenetic systems

Optogenetics first emerged in the early 2000s for use in neuroscience. Structural and functional similarities between endogenously expressed ion channels in mammalian neurons and bacterial (Boyden et al. 2005) and algal light-gated ion channels (Nagel et al. 2002; Nagel et al. 2003) meant that when these foreign proteins were expressed in mammalian neurons, light could be used to regulate neuronal polarisation. This finding revolutionised the field of neuroscience, heralding the beginning of more precise and regulated neuronal modulation (Fenno, Yizhar, and Deisseroth 2011). Individual neurons or brain regions in free moving mice could be precisely activated or inactivated. As many neuronal signals are temporally encoded by time-varying signals (Gao and Wehr 2015), the ability to precisely modulate individual cells and cell networks has yielding new molecular and behavioural insights in neurobiology.

Following the success of optogenetics in neuroscience, the technique has been adopted more widely in cell biology. The most common systems are outlined in Table 1.4 (Repina et al. 2017). Advances in our understanding of fundamental cell biology over recent decades has underscored that fact that cells are not merely a random assortment of proteins, salts and lipids, but rather are complex and dynamic, anisotropic structures; constantly changing in both space and time in response to varying environmental stimuli. When viewed in this context, the utility of optogenetics becomes immediately apparent. Existing techniques include the genetic manipulation and pharmaceutical obstruction of cellular signalling pathways and individual proteins. Gene knockout and overexpression studies have yielded important insights into cell biology, and new

technologies such as CRISPR-Cas9 (Sander and Joung 2014) and TALENs (Joung and Sander 2012) have made genetic manipulation considerably easier, but ultimately these techniques are a blunt instrument. Genetic manipulations are temporally imprecise and can have broad, unintended consequences beyond the pathway in question; destroying, rather than modulating, the cellular circuitry (Fenno, Yizhar, and Deisseroth 2011). Though there is no doubt that these kinds of consequences can be interesting, this sort of genetic perturbation does not reflect the intrinsic spatial and temporal nuances of cell biology. Pharmaceutical interventions have also been implemented for the interrogation of cellular signalling pathways. Normally, these molecules function as inhibitors rather than activators of signalling pathways. A key feature of pharmaceutical perturbation is that it can be employed on a relatively rapid timescale, compared to genetic manipulations. However, the slow rate of reversibility means that any degree of spatial resolution is lost. Moreover, identifying protein-specific inhibitors can require laborious efforts in chemical engineering (Repina et al. 2017).

Optogenetics holds promise in addressing some of the issues seen with common genetic engineering techniques and pharmaceutical interventions. First, optogenetic tools can be implemented in parallel with the endogenous signalling machinery. This circumvents the problem of pathway subversion or normalisation seen with long-term genetic knockout or knock-in systems. As the effect of the optogenetic system is tightly regulated by exposure to a specific wavelength of light, the effects of modulation are acute and in most cases reversible. Likewise, the kinetic tunability and responsiveness of optogenetic tools mean that they can be engineered for spatial precision. When combined with steerable laser systems and live cell imaging, optogenetics can be administered with a high degree of spatial precision (Repina et al. 2017; Tischler and Weiner 2014). The tunability and intrinsic variety of optogenetic tools making them an intriguing option for the interrogation of cellular dynamics.

1.5.3 The mechanistic underpinnings of cellular optogenetics

Although optogenetic tools in cell biology have so far been implemented in a number of different settings, from cell migration (Kato et al. 2014) and organelle positioning (van Bergeijk et al. 2015; Duan et al. 2015) to protein localisation (Strickland et al. 2012) and developmental signalling (Johnson et al. 2017), they all fundamentally rely on two basic mechanisms (Toettcher et al. 2011): 1) allosteric caging of protein function or 2) the formation (or dissociation) of protein-protein interactions (Figure 1.3). The first method was used by Wu et al. (Wu et al. 2009) to control the activity of Rac1. Photoisomerisation of a Rac1-fused optogenetic domain relieved inhibition of

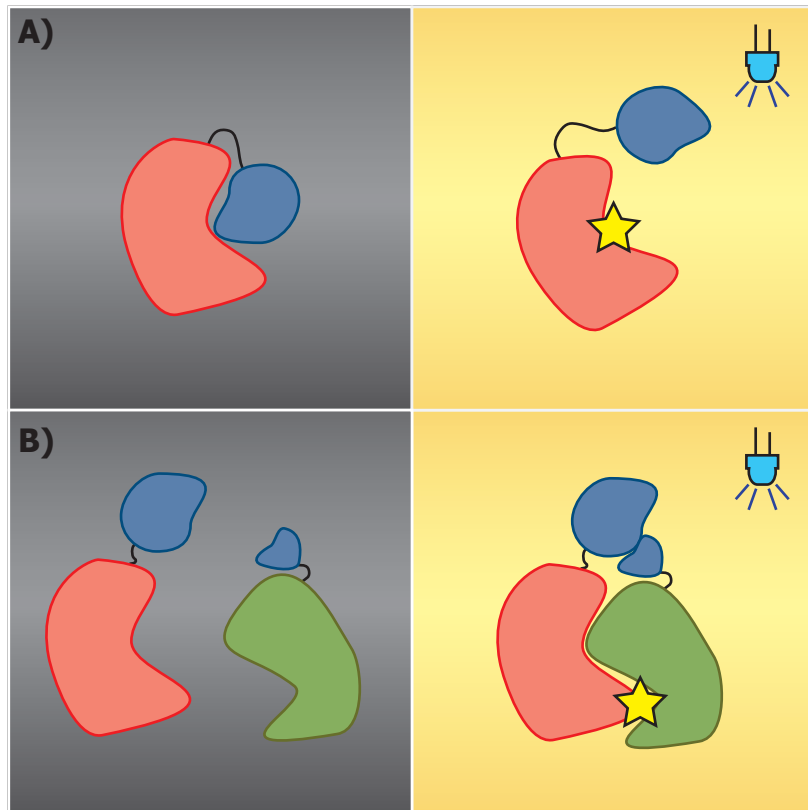


Figure 1.3 Mechanistic overview of optogenetic systems Optogenetic systems can be broadly classed into two main mechanisms of action: **(A)** photocaging and **(B)** light inducible protein interactions. The optogenetic domains are shown here in blue. **(A)** In the first method, the activity of the protein of interest (POI) is caged by the optogenetic domain in the dark state. Treatment with light results in a conformation change in the fused optogenetic domain, allowing the POI to fulfil its function. **(B)** In the second method, the the POI(s) are separate in the dark. On exposure to light the POI(s) are brought into proximity allowing them to fulfil their stated function. Of note, optogenetic systems also allow for the light-inducible dissociation of protein complexes. The symbol in the top, right-hand corner of denotes light and will be used throughout the rest of this thesis.

the constitutively active Rac1 protein allowing it to exert its function within the cell. A similar approach was used to allosterically cage a nuclear localisation sequence (Niopek et al. 2014) and a nuclear export sequence (Niopek et al. 2016), which allowed for light-inducible control of protein recruitment to or from the nucleus. More commonly, optogenetic domains have been used to induce protein-protein interactions, either through heterodimeric interactions (Strickland et al. 2012; Kennedy et al. 2010) or intrinsic homo-oligomerisation (Che et al. 2015; Park et al. 2017). Such techniques have proven successful because proteins often rely on specific interaction partners or specific cellular localisation to exert their function. By precisely controlling these properties, one can exert an effect on the underlying signalling circuitry.

1.5.4 Multiplexing optogenetics with the molecular biology toolkit

In engineering, complex electrical systems can be interrogated by modulating the amplitude and frequency of incoming signals and measuring the output response. Optogenetics now provides researchers with a similar means of interrogating complex cellular signalling modules. By multiplexing optogenetic tools with existing techniques in molecular biology, such as fluorescent protein tags, fluorescent and luminescent gene reporters, immunoblots, and RNAseq (Wilson et al. 2017) among many others; researchers can combine input modulation with quantitative readouts of cellular activity. This type of precise examination can allow researchers to delineate the effect of specific signalling axes from within complex multi-faceted responses. For example Toettcher, Weiner & Lim (Toettcher, Weiner, and Lim 2013) recently used such an approach to investigate the Ras/Erk signalling pathway. By modulating the pulses of Ras signalling activity, they were able to show how modulation of a single signalling pathway can lead to divergent output responses. In this way, it was shown that the Ras-Erk signalling module behaved as a bandpass filter, with signals >1 hr activating STAT3. High-frequency, short duration signals did not activate STAT3. This highlights the fact that cells are able to integrate temporally encoded signals. Chemically-inducible and traditional genetic knockout and knock-in approaches do not provide the spatiotemporal resolution or reversibility to answer these sorts of questions.

1.6 Scientific Aims

Chemical and optical methods of cell manipulation are providing previously unprecedented control over cellular signalling dynamics. I began the work presented in this thesis with the goal of leveraging these newly described tools for the interrogation of immune cell signalling pathways,

with particular focus on signalling downstream of the TCR. I began this project by designing and testing an optogenetic switch based on the T cell scaffolding protein, LAT. In doing this I had hoped to define the duration of membrane proximal signalling necessary for T cells activation. One outstanding question in the field of T cell biology, and indeed this is true for other systems as well, is whether or not sustained signalling is necessary for a specific output response and how a cell is able to interpret the duration of membrane proximal stimulation once a signal has been internalised. Optogenetics provides a precise means for defining time-limited signal pulses.

It is now becoming apparent that cells are able to sense and interpret gradients and directionality of environmental cues. How such signals are interpreted by the cells remains a relative unknown. The formation of an immunological synapse provides T cells with a defined directionality toward a target antigen presenting cell. However, it is not known whether signalling complexes nucleated by the LAT scaffolding protein must remain membrane localised to retain their signalling capacity. I sought to test this hypothesis through the optogenetic relocalisation of the LAT protein.

Actin cytoskeletal remodelling is an integral process in T cell activation. LAT is known to interact indirectly with the actin remodelling protein WASp, but the temporal association of these two proteins remains unknown. Through the use of optogenetics I sought to precisely define the location and temporal initiation of microcluster formation. Although microcluster formation is known to be important in T cell activation, the dynamics of microcluster formation have proven difficult to define with existing tools.

Finally, as I developed the project further, I shifted focus slightly to interrogate the ability of T cells to integrate signals over time. In the periphery, naïve T cells interact with multiple different dendritic cells on their transit through the lymph node, the significance of these sub-threshold activation events in the overall state of T cell activation remains unknown. Furthermore, computer modelling of T cell activation has given the suggestion that sub-threshold activation events may result in the accumulation of unstable signalling intermediates that reduce the duration of signalling necessary for a future activation event. To test this hypothesis I used a LOV2-based chimeric antigen receptor to precisely modulate the duration of incoming activation signals to a Jurkat T cell lines expressing a fluorescent gene reporter system.

1.7 Overview of results

In this thesis, I will discuss the development of an optogenetic toolkit for the interrogation of T cell signalling dynamics. I begin with a chapter focused on tool development, outlining the kinetics and design of the systems used in the subsequent chapters. In Chapter 4, I identify the limitations of a LAT-based optogenetic system for the interrogation of TCR microcluster formation and early T cell signalling. In Chapter 5, I discuss the development of a light-controllable chimeric antigen receptor. Here, I multiplex the FRB-FKBP CID system with the light controllable LOVTRAP system. This was used to investigate T cell signal integration and illustrate the rapid rate of signal decay in the proximal TCR signalling pathway following disengagement of the receptor. This work illustrates that TCR proximal signalling functions under tight negative feedback. I was also able to show that an increase in signal duration caused a decrease in the rate of signal decay. This finding will allow us to build a timeline of TCR-induced signalling events and understand how T cells integrate sub-threshold activation signals over time. Finally, in chapter 6, I illustrate the biophysical mechanism of T-cell triggering by bispecific antibodies.

Chapter 2: General Methods & Materials

2.1 Stock solutions and buffers

A number of common stocks and buffers were used throughout the course of this project. A list of these buffers can be found in Table 2.1.

	Stock Solution/Buffer	Protocol
2.1.1	TE buffer (1X)	10 mM Tris-HCl, 1 mM EDTA. Bring to pH 8.0 with HCl
2.1.2	Orange G loading dye (6X)	10 mM Tris-HCl (pH 7.6), 0.15% Orange G, 60% glycerol, 60 mM EDTA
2.1.3	FACS Wash	0.1% Sodium Azide, 2% FCS in 10 mM PBS pH 7.4
2.1.4	FACS Fix	0.1% Sodium Azide, 2% Glucose, 1.6% PFA in 10 mM PBS pH 7.4
2.1.5	ELISA Wash	0.05% Tween 20 in 10 mM PBS pH 7.4
2.1.6	ELISA Stop Solution	1M P3PO4
2.1.7	NP40 Lysis buffer	250 μ l 10X TBS, 25 μ l NP40, 100 μ M NaVi 25 μ l, 200 μ M PMSF (Thermo Fisher Scientific) 13 μ l, 10X CI tablet (Roche) 250 μ l, ddH ₂ O 1937 μ l
2.1.8	TBS (10X) – 1 L	24g Tris base, 88g NaCl, 900mL ddH ₂ O, pH to 7.6 with HCl (adjust to 1 L with ddH ₂ O)
2.1.9	TBS-T	TBS, 0.1% Tween 20
2.1.10	TBE buffer (10X) – 1 L	108g Tris base, 55 g Boric acid in 900 ml ddH ₂ O, 40 ml of 0.5 M Na ₂ EDTA pH 8.0 (adjust to 1 L with ddH ₂ O)
2.1.11	Filtered (0.22 μ m syringe) TSS buffer (1X)	10 % PEG-3350 (or PEG-8000) 5 % DMSO 50mM MgCl ₂ Prepare in LB broth, pH 6.5

Table 2.1: Stock buffers

2.2 Mammalian Cell Culture

2.2.1 Suspension cell lines

Jurkat E6-1 human T lymphocytes (Weiss et al. 1984), Jurkat-derived JCaM2.5, and Raji human B lymphocytes (Pulvertart 1964; Epstein et al. 1965) cell lines were grown in suspension in RPMI-1640 media (Life Technologies), supplemented with HEPES (1 mM Final concentration), 10% Heat Inactivated Foetal Calf Serum (HI-FCS[Gibco]) and a Penicillin-Streptomycin-Glutamine cocktail (PSG [Gibco]); final concentration 2 mM L-glutamine. Stock cell lines were passaged in T-12.5 flasks (Falcon™) and expanded into larger cultures as necessary. Cell cultures were incubated at 37°C in 5% CO₂. Jurkat cell lines were maintained at a density of 0.2-1.0 x 10⁶ cells/ml and passaged every 2-3 days. The Raji cell line was maintained at a density of 0.4-1.2 x 10⁶ cells/ml and passaged every 2-3 days as necessary.

2.2.2 Adherent cell lines

HEK293T human embryonic kidney cells (DuBridge et al. 1987) and NIH3T3 mouse embryonic fibroblast cells (Green and Meuth 1974) were maintained in a T-75 flask in Dulbecco's Modified Eagle's Medium (DMEM [Life Technologies]) supplemented with 10% HI-FCS and PSG. Cells were incubated at 37°C in 5% CO₂. Cultures were established by seeding ~2 x 10⁶ cells into a fresh T-75 flask in 13 ml of Complete DMEM. Cells were grown to 90% confluency prior to next split (3-4 days).

To split, spent media was removed and discarded and cells were washed once in tissue culture-grade, sterile calcium-free PBS (prepared in house at the LMB). 3 ml of 0.25% Trypsin, phenol red (Gibco) for HEK293T cells or 0.25% Trypsin-EDTA, phenol red (Gibco) for NIH3T3 cells was added and cells were returned to 37°C tissue culture incubator for 5 minutes to allow for dissociation. Trypsin was inactivated by adding 7 ml of complete DMEM and mixing gently to ensure that cells were in single-cell suspension. Cells were counted by eye using a haemocytometer by mixing the suspended cells 1:1 in Trypan Blue (Gibco). 2 x 10⁶ cells were seeded into a fresh T-75 flask and volume was brought to 13 ml with fresh complete DMEM. Cells were split every 3-4 days as necessary.

2.2.3 Cell line cold storage

To maintain consistency between experiments, cell lines were expanded, stored, and periodically thawed and re-expanded. Cells were stored in freezing media, either complete RPMI or complete

DMEM supplemented with 10% DMSO, depending on the cell line. Suspension cells were grown to a density of $\sim 0.8 \times 10^6$ cells/ml and then centrifuged at 1200 rpm for 3 minutes and media discarded. Cell pellet was resuspended in the residual volume of media and brought to a density of 2×10^6 cells/ml in freezing media. Cell suspension was divided into 1 ml aliquots into 1.8 ml CryoTube Vials® (Thermo Fisher Scientific), which were placed in a Mr. Frosty™ (Nalgene) container with 100% isopropyl alcohol and allowed to cool overnight to -70°C. Once frozen, cells were transferred from the -70°C freezer to vapour-phase liquid Nitrogen storage at -180°C. Similarly, adherent cells were prepared for storage via the same protocol, but were first washed in PBS and dissociated into single cell suspension using the trypsinisation protocol described in 2.2.2.

2.2.4 *Mycoplasma testing*

Mycoplasma testing was performed using a MycoAlert™ Mycoplasma Detection Kit (Lonza). Positive and negative controls were kindly provided by Yvonne Vallis.

2.3 *Polymerase Chain Reaction Conditions & DNA purification*

2.3.1 *Primer design and in silico PCR*

Prior to *in vitro* DNA replication, restriction cloning or In-Fusion cloning, reactions were designed and tested *in silico* using SnapGene® Version 4.0.1. SnapGene® software was used to predict expected band sizes following PCR reactions and annealing temperatures for all primers (Appendix A). Where necessary, RevComp was used to identify reverse-complement from DNA FASTA sequence for reverse primer design. The IDT® OligoAnalyzer 3.1 Tool¹ was used to test the propensity of primers to form hairpins and homo- or hetero-dimers. All subsequent Polymerase Chain Reactions were performed using a G-Storm (GS-1) Thermocycler.

2.3.2 *KOD HotStart Polymerase Conditions*

KOD Master Mix, containing MgCl₂ and dNTPs (71086-3, Millipore) was prepared according to manufacturer's protocol and distributed into 150 µl aliquots in 500 µl microcentrifuge tubes (Eppendorf). Aliquots were stored at -20°C and thawed to room temperature prior to use.

¹ <http://www.idtdna.com/calc/analyzer>

Lyophilized primers were diluted in TE buffer to a stock concentration of 100 mM. Prior to reaction, primers were diluted 1:10 in MilliQ water to prepare 10 mM stocks. Standard PCR reaction mixture is as follows:

<i>Reagent</i>	<i>Volume (μl)</i>
Template DNA (100 ng)	0.5
Forward primer (10 mM)	2.0
Reverse primer (10 mM)	2.0
KOD polymerase	0.5
KOD master mix	13.0
(DMSO*)	(2.5)
dH ₂ O	Adjust to 50

* DMSO was added to a final concentration of 5% when template GC >65%.

In the case of overlap extension PCR (‘stitch PCR’) reactions were prepared as follows:

<i>Reagent</i>	<i>Volume (μl)</i>
Template DNA 1 (50 ng)	5.0
Template DNA 2 (50 ng)	5.0
Forward primer (10 mM)	2.0
Reverse primer (10 mM)	2.0
KOD polymerase	0.5
KOD master mix	13.0
(DMSO)	(2.5)
dH ₂ O	Adjust to 50

DNA fragments were amplified under the following thermocycler conditions:

	32 cycles				
95°C for 2 min	95°C for 20 s	Lowest Primer T _m °C 10s	70°C for 15s/kb	70°C for 2 min	hold at 10°C

2.3.3 Q5 Polymerase Conditions

Q5 PCR conditions were established according to manufacturer's protocol (M0491S, NEB). Standard reaction mix is as follows:

<i>Reagent</i>	<i>Volume (μl)</i>
Template DNA 1 (100 ng)	5.0
Forward primer (10 mM)	1.25
Reverse primer (10 mM)	1.25
Q5 polymerase	0.25
Q5 Reaction Buffer (5x)	5.0
(Q5 high GC enhancer*)	(5.0)
dNTPs (10 mM)	0.5
dH ₂ O	Adjust to 25.0

* GC Enhancer was added to a final concentration of 5% when template GC >65%.

Thermocycler conditions for the above reaction are as follows:

	32 cycles				
98°C for 30 s	98°C for 10 s	Lowest Primer T _m °C 15 s	72°C for 30s/kb	72°C for 2 min	hold at 10°C

2.3.4 MyTaq Colony Screen Polymerase Chain Reaction

In order to check success of bacterial cloning (outlined **Section 3.4**), colony screen PCR was performed using MyTaq (Bioline) colony screen PCR reagent according to manufacturer's protocol. A master mix was prepared for each set of reaction conditions – primer pairs were determined by the vector being screened and confirmed *in silico* using SnapGene® – with 15 colonies screened per condition. Reaction mixture was divided into 15 μl aliquots in individual PCR tubes. Each colony was gently sampled using a fresh, sterile p10 tip, leaving that majority of the colony still intact. Each sample was then transferred to a PCR tube and immersed in pre-prepared reaction mix containing primers. The tip was gently spun in the mixture to dissociate the bacterial cells. The reaction mixture is outlined as follows:

<i>Reagent</i>	<i>Volume (μl)</i>
Forward primer (10 mM)	0.6
Reverse primer (10 mM)	0.6
MyTaq Mix	7.5
dH ₂ O	6.3

Thermocycler conditions for the MyTaq reactions were as follows:

	32 cycles			
95°C for 1min	95°C for 15 s	Lowest Primer T _m °C 15 s	72°C for 30s/kb	hold at 10°C

2.3.5 Gel electrophoresis

Agarose gel was prepared by dissolving agarose powder (Eurogentec) in TBE buffer to a final concentration of 1%, for DNA fragments of an expected size of >500bp. For DNA fragments of an expected size of <500bp but >250bp, a final concentration of 1.5% was used. For DNA fragments of an expected size <250bp, a final concentration of 2% was used. Gels were run in TE buffer in electrophoresis unit (GeneFlow) at 130V for 25 minutes. Run time and voltage were adjusted where necessary to improve band separation. Samples were prepared by adding 6X Orange G loading dye at a dilution of 1:6.

2.3.6 Gel Extraction

DNA fragments were isolated from agarose gel post-electrophoresis by cutting out desired bands. Agarose gel fragments were transferred to a 1.5 ml microcentrifuge tube (Eppendorf) and DNA was extracted using Gel Purification Kit as per manufacturer's protocol (Qiagen). Samples were eluted into 50 μl of elution buffer. Once eluted, samples were screened for DNA concentration using Nano-photometer (GeneFlow).

2.3.7 PCR purification

For non-restriction digested DNA fragments, PCR products were purified directly from PCR reaction using a PCR purification kit (Qiagen). DNA concentration was screened using a Nano-

photometer. Band size was confirmed by performing gel electrophoresis using 4 µl of eluted sample.

2.4 Bacterial Cloning

2.4.1 Preparation of Competent Bacteria

Competent bacterial cells were prepared in house. A starter culture was established by thawing a 50 µl aliquot of DH5α *E. coli* and adding it to 4 ml of sterile LB buffer (prepared in house at the MRC-LMB). Starter culture was incubated overnight in shaking incubator at 37°C. Overnight culture was used to inoculate 20 ml of fresh LB buffer in a non-vented T75 bacterial culture flask (Falcon). Flask was returned to shaker and incubated at 37°C until OD₆₀₀ reached 0.4-0.6. OD₆₀₀ measurement was acquired using a spectrophotometer (Eppendorf). Once the specified optical density was achieved, cells were centrifuged at 3000 rpm for 10 minutes in a benchtop centrifuge (Thermo Fisher Scientific). Media was discarded and pellet was resuspended in residual volume by gentle flicking. Cells were resuspended in 2.5 ml of chilled TSS buffer and mixture was incubated on ice for 30 minutes. Following incubation cells were gently mixed and distributed into 50 µl aliquots in 500 µl microcentrifuge tubes. Aliquots were frozen at -70°C and stored until use.

2.4.2 Cloning by Restriction Digest

Restriction digestions were prepared and performed according to manufacturer's protocol (NEB). Digest buffers were determined using the NEB Double Digest Finder Tools². A schematic of the standard vector is shown in Figure 2.1. Digestions were performed at 37°C in water bath for 1 hour. The reaction mixture is as follows:

<i>Reagent</i>	<i>Volume (µl)</i>
DNA vector (300 ng)	15.0
Restriction Enzyme 1	2.5
(Restriction Enzyme 2*)	2.5
Digest Buffer**	5.0
dH ₂ O	Adjust to 50

*Second restriction was used in double digest reactions, **Digest buffers were selected according to NEB Double Digest Finder

² <https://www.neb.com/tools-and-resources/interactive-tools/double-digest-finder>

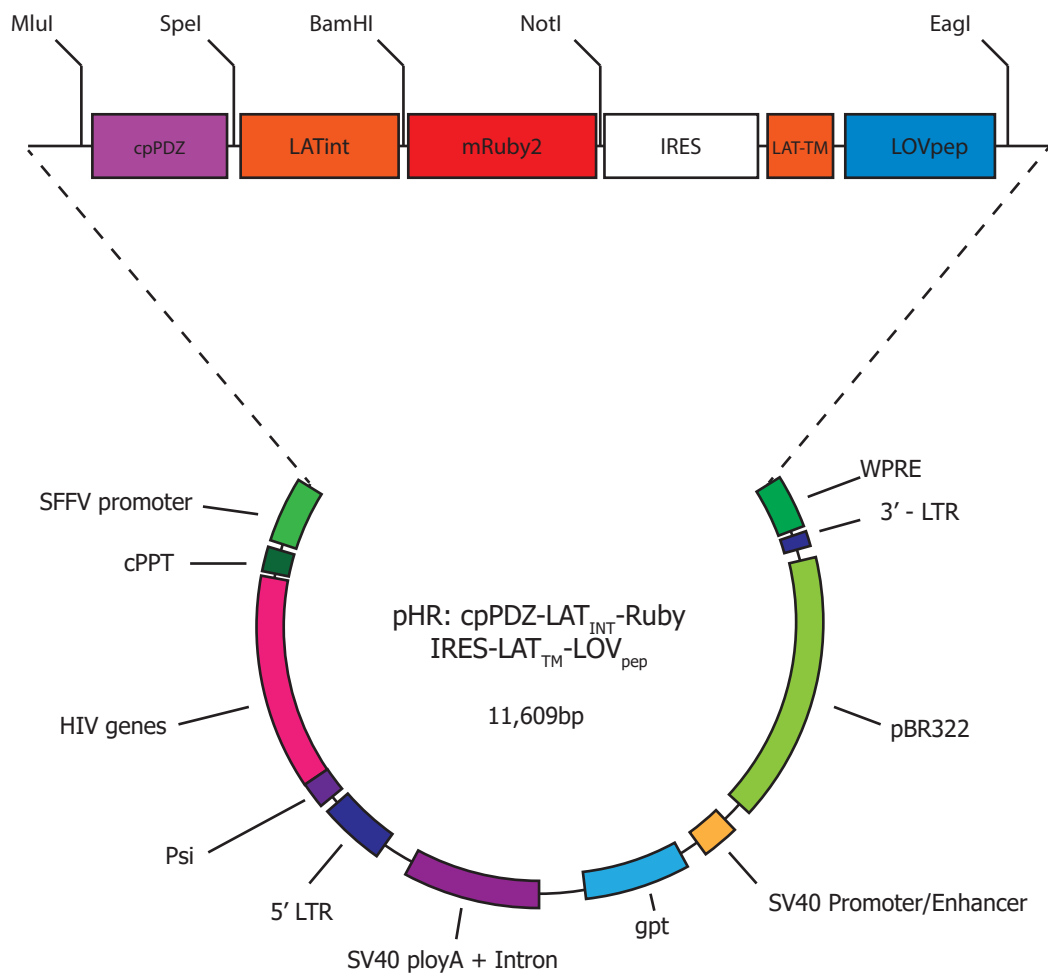


Figure 2.1 Example pHR IRES plasmid Plasmids were designed to be easily interchangeable by restriction cloning. Shown here is the low affinity TULIPs construct. The PDZ binding domain is interchangeable by MluI/SpeI subcloning from non-IRES vectors. The LOVTRAP constructs were designed in the same way. Both components of the system were expressed on the same vector.

To improve the efficiency at which fragments were inserted in the correct orientation during NotI single digest and EagI cloning reactions, 6 µl of AP buffer and 2 µl of Antarctic phosphatase (NEB) were added directly to completed digestion mixture. Total volume was brought to 60 µl with dH₂O. Sample was transferred to thermocycler and incubated at 37°C for 30 minutes and then brought to 80°C for 2 minutes to heat inactive. Linearised vector was then used directly in ligation reactions.

2.4.3 DNA Ligation

DNA ligation was performed using T4 ligation buffer and T4 ligase (NEB) at room temperature for 2 hours (or overnight at 16°C). Serial dilution reactions were performed as follows:

<i>Reagent</i>	<i>Volume (µl)</i>
Purified vector	5.0
Purified insert	0.0, 1.0, 10.0
T4 Ligase buffer	2.0
T4 DNA ligase	1.0
dH ₂ O	Adjust to 20

2.4.4 Heat-shock Transformation of Competent Bacteria

DH5α competent cells were thawed on ice for 15 minutes and 5 µl of ligation mixture was added to cells. Cells were gently flicked to mix. Transformation mixture was incubated on ice for 1 hour and then heat shocked at 37°C for 5 minutes and returned to ice for 2 minutes. 200 µl of pre-warmed, 37°C SOB media was added to the tubes and samples were returned to water bath to recover for 1 hour at 37°C.

Following 37°C incubation, samples were spread on an Agar plate for overnight incubation on plate with appropriate antibiotic resistance. Agar plates were prepared in house at the MRC-LMB. As the pHR vector uses Ampicillin resistance, I predominantly used Agar plates with Ampicillin (100 µg/ml). Plates were allowed to dry briefly at room temperature for 15 minutes before transferring to 37°C bacterial incubator (SciQuip) for overnight incubation.

2.4.5 Plasmid Purification

Following overnight incubation, DH5 α colonies were screened using the MyTaq Colony Screen PCR protocol (Section 2.2.4). Positive colonies were harvested using a clean, sterile p10 Tip and transferred to a 15 ml Falcon tube containing 4 ml of LB broth supplemented with 100 μ g/ml Ampicillin. Cultures were incubated overnight at 37°C in shaking incubator.

Once the DH5 α cultures were expanded, p10 tips were removed from 15 ml falcon tubes and cells were harvested by centrifugation at 3000 rpm for 10 minutes at 4°C. Media was decanted from the samples and plasmids were purified according to Plasmid Purification Mini-prep Kit protocol (Qiagen). Purified plasmids were eluted into 80 μ l of TE elution buffer and DNA concentration was determined using Nano-photometer. Samples were adjusted to 200 ng/ μ l with TE buffer. Plasmids were stored at -20°C until use.

2.5 DNA transfection and Transduction

2.5.1 Transient transfection

HEK293T cells were seeded at a density of 0.2×10^6 cells per well in a single well Cell View™ 35 mm glass bottom, Advanced Tissue culture, No. 1.5 dishes. Cells were allowed to settle and expand overnight at 37°C and 5% CO₂. The following day, cells were transfected with 1-1.5 μ g of DNA and GeneJuice reagent (Millipore). 3 μ l of GeneJuice reagent were used per 1 μ g of DNA. A master mix of transfection reagent was made by adding 3 μ l of gene juice to 100 μ l of serum free DMEM (SFM) and incubating the mixture for 5 minutes at room temperature prior to adding the DNA. After adding DNA, tubes were flicked gently to mix and left to incubate at room temperature for 25 minutes. Following incubation, DNA mixture was added dropwise to the imaging dishes and the plates were gently rocked and swirled to evening distribute the transfection reagent across the dish. Plates were incubated overnight again and then processed for imaging or flow cytometry.

2.5.2 Lentiviral Transduction

HEK293T cells were seeded at a density of 1×10^6 cells per well in a 6-well plate (Greiner bio-one) and allowed to settle and expand overnight at 37°C and 5% CO₂. The following day, HEK293T cells were at a confluency of ~60-80% and transfection reagent was prepared by adding 4.5 μ l of GeneJuice to 100 μ l of SFM. Mixture was incubated for 5 minutes prior to adding DNA. DNA lentiviral transduction mixture was prepared using 3 μ l of pMD2.G expressing the VSV-G

envelope at 100 ng/ μ l stock concentration; 3 μ l of p8.91, expressing the HIV-1 packaging genes Gag, pol, rev, and tat, at 200 ng/ μ l stock concentration; and 3 μ l of the vector to be transduced, also at a stock concentration of 200 ng/ μ l. The total amount of DNA in each transduction reaction was 1.5 μ g. DNA mixture was added to the pre-prepared SFM with GeneJuice reagent and allowed to incubate for 25 minutes at room temperature. Following the incubation, DNA transduction mixture was added dropwise to HEK293T cells and incubated for 48 hours at 37°C and 5% CO₂.

After 48 hours, viral media was harvested by carefully removing media from HEK293T cells and transferring to a 2 ml screw-top tube (StarLab) and centrifuging at 8K rpm in benchtop microcentrifuge for 3 minutes. The viral media was then stored at 4°C for up to one week prior to use or used immediately for transductions. In transducing suspension cells, such as Jurkat E6-1 cells, 500 μ l of cells at a density of $\sim 0.8 \times 10^6$ were transferred to each well of a 6-well plate. Viral media was carefully removed from the 2 ml tube so as not to disrupt the pellet and added directly to the suspension cells in the 6-well plate. Cells were then incubated in viral media at 37°C and 5% CO₂. After 24 hours, a further 2 ml of fresh, complete RPMI was added to the transduced cells. In transducing adherent cells, the cells were plated at a density of 0.5×10^6 cells per well in a 6-well plate the night before. The media was then removed and replaced with viral media. After 24 hours, the viral media was removed and replaced with fresh, complete DMEM. Two days after viral transduction, cells were passaged again as normal using 0.25% trypsin or trypsin-EDTA.

2.5.3 Lentiviral concentration

In cases where construct expression was low, we increased the viral titre using Lenti-X concentrator (Takara). This was done according to the manufacturer's protocol. Following the overnight incubation at 4°C and subsequent centrifugation, the Lenti-X concentrated virus was resuspended in 250 μ l of fresh complete RPMI. This was added 1:1 to 250 μ l of Jurkats at 1×10^6 cells/ml in a 24-well dish and incubated overnight at 37°C in 5% CO₂. The following day, the transduced cells were transferred to 1.5 ml of fresh RPMI in a 6-well plate. Two days after lentiviral transduction the transduced cells were passaged again as normal.

2.6 Confocal Microscopy

2.6.1 Sample preparation and image acquisition

Optogenetic relocation assays were performed using live cell, multi-channel confocal microscopy. Imaging was carried out on an Eclipse Ti Spinning Disk confocal microscope (Nikon)

equipped with an Okolab incubation chamber. Chamber was equipped to provide 5% CO₂ and 37°C. Blue light illumination was supplied via an overhead condenser fitted with a white light LED source and 450nm condenser filter. To ensure that our blue light illumination protocols were directed at a small subset of cell for any given time course, the condenser was narrowly focused using the field aperture in the correct plane at 10X magnification prior to running microscopy imaging protocols. Fluorophore excitation was provided by a set of Andor lasers: 405 nm, 488 nm, 561 nm, and 640 nm. Images were acquired at 60X or 100X magnification.

HEK293T cells were prepared for imaging through the transient transfection protocol outline in section 2.5.1. Just before imaging, spent DMEM was removed from cells and replaced with DPBS with Ca²⁺ and Mg²⁺ (Gibco).

To standardise and automate our imaging protocol we wrote a script using the BeanShell programming language, which was executed using the MicroManager 1.4 software package (ImageJ). This script allowed for standardisation of the channel settings across multiple images with regards to laser colour, filter, and exposure time. When conducting time course images the duration of the time course and the blue LED exposure time were programmed using our script. LED intensity and laser intensity were controlled manually and adjusted where necessary on a cell-cell basis. The annotated BeanShell imaging script can be found in Appendix C.

2.6.2 Image Processing

All image processing was carried out using Fiji (ImageJ) open source image analysis software. To avoid inconsistencies in analysis between samples I generated a standardised image analysis workflow (Figure 2.2). Briefly, multichannel images were separated into single channel images and then Look Up Tables (LUTs) were converted to greyscale. Time series images were corrected for photo-bleaching using the exponential fit method. Background was subtracted in each channel using a 100 pixel rolling ball background subtraction method. A 100 pixel radius was selected to avoid loss of signal in time course images where cytoplasmic fluorophore intensity was low. Contrast was then enhanced by histogram normalisation so that images were comparable between channels. RGB colour images were prepared by merging the channels and single colour images were saved in grayscale.

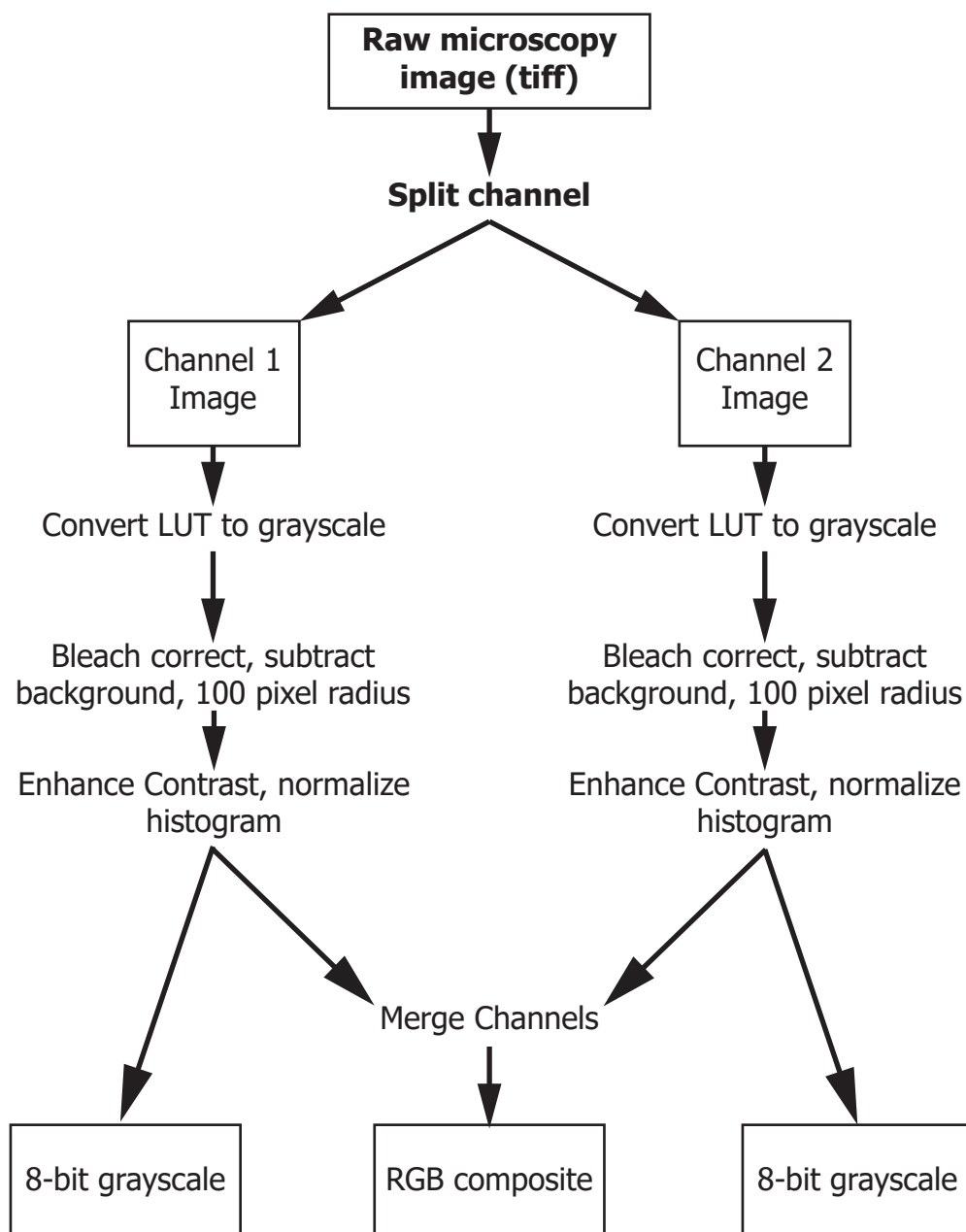


Figure 2.2 Overview of ImageJ workflow All images were processed using a standardized image analysis protocol. Multichannel images were split into single channel image stacks. Single channel images were converted to grayscale, photobleach corrected using the exponential fitting method and background was subtracted using the rolling ball subtraction method. Contrast was enhanced by normalizing the histogram and then channels were merged and converted to RGB composite images for colour images, or to 8-bit grayscale images as single channel images.

2.7 Flow Cytometry

2.7.1 Sample preparation and surface staining

In preparing samples for flow cytometry, $\sim 0.75 \times 10^6$ cells were centrifuged at 1.2K rpm for 3 minutes in a FACS tube (Falcon™). Media was discarded and samples were resuspended by gentle agitation in the residual media. For each sample antibodies were prepared in 100 μ l FACS wash buffer (Table 2.1, 2.1.3) 10 μ g/ml final concentration. Complete list of antibodies can be found in Table 2.2. Cells were transferred to 4°C fridge and incubated for 25 minutes with occasional agitation. Cells were then washed once in 3 ml of FACS wash buffer by centrifugation at 1.2K rpm for 3 minutes. Wash buffer was discarded and cells were resuspended by flicking in the residual volume. In cases where secondary antibodies were used, 100 μ l of FACS wash buffer containing secondary conjugated antibody at a final concentration of 2.5 μ g/ml was added to the cells and incubated at 4°C for a further 25 minutes and washed once more. Cells were fixed in FACS fix buffer and either analysed immediately by flow cytometry or stored at 4°C until analysis could be performed.

When staining for co-receptors CD80 and CD86 on Raji cells Fc Receptor Blocking Solution (Human TruStain FcX, Biolegend) was used prior to staining with antibodies. 5 μ l of FcX was added directly to cells and incubated at room temperature for 10 minutes. Cells were then stained as normal.

All data were collected using an LSRII Flow cytometer (Becton Dickinson [BD]) or a Fortessa flow cytometer (BD). All machines were installed with FACSDiva acquisition software (BD). Data were stored and imported as .fcs files.

<i>Antigen</i>	<i>Isotype</i>	<i>Species</i>	<i>Fluorophore</i>	<i>Clone</i>	<i>Notes</i>
CD54	IgG1, κ	Mouse	Alexa Fluor 488	HCD54	ICAM-1
CD11a	IgG1, κ	Mouse	Unconjugated	HI111	α Chain subunit of LFA-1
LAT	IgG1	Mouse	Unconjugated	1111	Used to check intracellular expression of LAT
TCR α/β (human)	IgG1, κ	Mouse	Alexa Fluor 647	IP26	Used to check T cell receptor expression

CD3ε (human)	IgG2a, κ	Mouse	Alexa Fluor 647	Hit3a	Used to check T cell receptor expression
CD3ε (human)	IgG2a, κ	Mouse	Unconjugated	Hit3a	Calcium Flux assay, primary unconjugated antibody
CD3ε (human)	IgG2a, κ	Mouse	Unconjugated	OKT3	Primary unconjugated and plate bound activation assays
CD6	IgG1, κ	Mouse	PE	BL-CD6	Screen co-receptor expression in T cells
CD28 (human)	IgG1, κ	Mouse	Unconjugated	CD28.2	Primary unconjugated and soluble antibody in plate-bound activation assays. Used to check co-receptor expression in T cells
CD69 (human)	IgG1, κ	Mouse	Alexa Fluor 647	FN50	Early activation marker of T cells
CD80 (human)	IgG1, κ	Mouse	Alexa Fluor 647	2D10	Co-receptor expressed on B cells
CD86 (human)	IgG2b, κ	Mouse	Alexa Fluor 647 Brilliant violet 421 Brilliant violet 605	IT2.2	Used to check Synthetic Antigen receptor Expression and B-cell CD86 expression
IgG1 (mouse)	IgG	Goat	Alexa Fluor 647	Polyclonal	Secondary Antibody
Isotype control	IgG1, κ	Mouse	Alexa Fluor 647	MOPC-21	
ZAP70	IgG	Rabbit	Unconjugated	3165	T cell immunoblot input control

Table 2.2: List of Antibodies

2.7.2 Intracellular FACS staining

When assaying for the ablation of LAT in the knockout cell lines it was necessary to perform intracellular FACS staining. Staining was performed according to manufacturer's protocol using Nuclear Factor Fixation and Permeabilisation buffer set (BioLegend). Briefly, Approximately 1×10^6 cells were centrifuged at 1200 rpm for 3 minutes, media was decanted and cells were resuspended by vortex in the residual volume. Cells were fixed for 20 minutes at room temperature using nuclear factor fixation buffer (BioLegend) and washed in permeabilisation buffer (BioLegend). Cells were immune-labelled in 100 μ l permeabilisation buffer with α LAT (1111) at a final concentration of 2.5 μ g/ml. Cells were washed again in permeabilisation buffer and stained with 5 μ g/ml of α IgG1-AF647 antibody. Cells were then washed once more in permeabilisation buffer to remove excess unbound antibody, then in standard FACS wash buffer, and finally resuspended in FACS fix solution.

2.7.3 Ratiometric calcium flux assay

Indo-1 AM leak resistant (Grynkiewicz, Poenie, and Tsien 1985) (TEFlabs) stock solution was prepared by resuspending 50 μ g of lyophilized Indo-1 with 50 μ l of DMSO, final concentration of 1 mg/ml. 500 μ l of indo-1 staining solution was prepared per calcium flux sample in SFM to a final concentration of 5 μ g/ml. 30% pluronic acid was also added to the SFM in a 1:1 ratio with the volume of Indo-1 stock solution added. Jurkat E6.1 T cells ($\sim 0.5 \times 10^6$ /sample) were centrifuged at 1200 rpm for 3 minutes in FACS tubes, media was discarded and cells were resuspended in residual volume by flicking. Cells were resuspended in 500 μ l of SFM with Indo-1 and pluronic, lids were sealed, and samples were incubated in 37°C water bath for 30 minutes with occasional agitation.

Cells were washed by centrifugation in 3 ml of DPBS with Ca^{2+} and Mg^{2+} to remove any excess Indo-1. Media was discarded and cells were resuspended by gentle agitation in the residual volume. In the meantime, a stock solution of α CD3, clone Hit3a (BioLegend) antibody was prepared at 1 μ g/ml in Complete RPMI. 500 μ l of antibody-containing RPMI was added to the resuspended cells and samples were incubated at room temperature for 15 minutes. All further steps were performed at room temperature. Following incubation, cells were washed in 3 ml of complete RPMI, media was discarded and cells were resuspended in 500 μ l of Complete RPMI for calcium flux analysis. Cells were rested at room temperature for 15 minutes prior to the start of the experiment.

The Indo-1 calcium indicator dye has an excitation of 375 nm and undergoes a peak shift in emission from 475 nm in calcium-free state to 400 nm in the presence of calcium. Calcium flux can be measured ratiometrically on a cell-cell basis using a flow cytometer equipped with an ultraviolet laser (355 nm). Calcium flux was calculated as the calcium-bound signal divided by the calcium un-bound signal. Our Assay was performed on a Becton Dickinson (BD) Biosciences Fortessa Flow Cytometer. Cells were run for 30 seconds to establish baseline reading and 10 µl of anti-IgG polyclonal antibody was added to activate Jurkat E6.1 T cells. Samples were run for an addition 5 minutes and Indo-1 ratiometric data were collected.

2.7.4 FlowJo v10.1r5

All initial data analysis of flow cytometry samples was performed using the FlowJo v10.1r5 software. This software provides a robust tool for data analysis and allows for sample gating and limited statistical processing. Processed data were exported as .csv files and opened with Microsoft Excel 2013 or Matlab 2016b for further statistical analysis and graphing.

2.7.5 Fluorophore panel selection

When performing flow cytometry analysis, we attempted to minimise spectral overlap between our fluorophores. Fluorophore panels were selected using the SearchLight Spectra Viewer (Semrock) and Spectrum Viewer (BD).

2.8 Immunoblot Assay

We conducted Immunoblot assays to confirm expression or ablation of LAT. Jurkat LAT Knockout or Jurkat wildtype cells (2×10^6) were lysed for each sample. Lysis was performed on ice in NP-40-based lysis buffer for 1 hour with occasional agitation. Once lysed samples were centrifuged at max speed for 10 minutes at 4°C to remove cell debris. NuPAGE-LDS loading dye (15 µl; Thermo Fisher Scientific) supplemented with 100 µM DTT was added per 50 µl of sample and samples were boiled in thermocycler at 90°C for 5 minutes to denature proteins. Samples were cooled and frozen at -20°C until use or cooled and run on 4-12% Bis-Tris NuPAGE, 1.5 mm Protein Gel (Thermo Fisher Scientific). Per lane, 10 µl of each sample was run at 200V for 1 hour. Run duration was adjusted where necessary according to protein size.

Blot was transferred using iBlot (Thermo Fisher Scientific) P0 – 20 V for 1 minute, 23 V for 4 minutes, 25 V for 2 minutes – onto a PVDF membrane and blocked for 30 minutes in 2.5% Milk TBS. Membrane was carefully cut in half with the lower half blotted with 5 μ l of α LAT (1111) antibody was diluted in 10 ml of 2.5% Milk TBS-T to a final concentration of 250 ng/ml and the upper half blotted with α ZAP70 (D1C10E, Cell Signalling) as input control. PVDF Membrane was incubated overnight at 4°C with rocking.

The following day, membrane was washed 3 x 5 minutes in 2.5% TBS-T. DyLight 800 (Thermo Fisher Scientific) secondary antibody was diluted 1:20,000 in 2.5% Milk TBS-T and incubated with membranes for 15 minutes at room temperature. Membranes were washed 3 x 5 minutes in TBS-T and imaged using Licor Odyssey. Western Blot Images were prepared using Fiji ImageJ.

2.9 Enzyme-linked immunosorbent assays (ELISA)

For long term activation assays, IL-2 expression was used as a late-stage marker of T-cell activation. This was assayed in spent media from 24-hour time course experiments (details in chapter 5). ELISAs were performed using Life Tech kit according to manufacturer's protocol. Media was harvested in 24-well plates following time course assays and stored at -70°C until use. Samples were diluted 1:5 in ELISA dilution buffer and run in triplicate. Plate was read using ELISTAR plate reader and data were exported as .txt files for analysis in Excel 2013 (Microsoft) and Matlab 2016b.

2.10 Analysis Software

2.10.1 Microsoft Excel 2013

Raw data were compiled and analysed using Microsoft Excel 2013; including data from FlowJo, ELISTAR, and ImageJ.

2.10.2 Matlab R2016b

Matlab was used for statistical analysis of data compiled using Excel. Annotated Matlab Analysis scripts are included in Appendices D & E. Details on Matlab analysis can be found in specific chapter methods sections.

Chapter 3 – Development of an optogenetic toolkit

3.1 Introduction

3.1.1 Optogenetic tool development

Individual cells are highly ordered and dynamic structures, constantly changing in both space and time in response to varying stimuli. Genetic manipulations of signalling networks can have broad off-target effects and are temporally imprecise. Pharmaceutical perturbations, although much more temporally precise, lack spatial resolution and are also susceptible to off-target effects. Although both types of approach have been extremely important in shaping our understanding of basic cell biology, neither truly reflects the underlying complexity of cellular signalling dynamics. Optogenetics provides a means for spatially and temporally interrogating the underlying circuitry of the cell.

In this chapter, I outline the development of an optogenetic toolkit for the interrogation of immune cell signalling. Although our understanding of the cellular machinery underlying the TCR signalling network is comprehensive (Smith-Garvin, 2009; Malissen & Bongrand, 2015), the spatiotemporal dynamics of T cell activation remains to be fully explained, particularly those events in early activation. It is also not understood how small variations in early signalling are internalised by the T cell and translated into an appropriate downstream response (Mayya and Dustin 2016). It was reasoned, that by developing a system to precisely regulate T cell activation, we would be able to investigate both early activation events and signal integration. Although a number of optogenetics systems exist – reviewed by Tischer & Weiner (Tischer and Weiner 2014) and Schmidt & Cho (Schmidt and Cho 2015) – I focused primarily on the development of several Light-Oxygen-Voltage 2 (LOV2) domain-based systems. The most commonly implemented optogenetic LOV2 domain is derived from *Avena sativa*, the common oat (Peter, Dick, and Baeurle 2010; Lungu et al. 2012).

3.1.2 Mechanistic overview of the LOV2 domain

Plants, although sessile, must still respond to changes in environmental conditions. They are particularly responsive to changes in temperature and light exposure, which influence such processes as leaf movement, flowering time, stomatal opening and hypocotyl elongation (C. Lin 2002). Several families of photoreceptor are involved in regulating these responses, in higher plants: phototropins, cryptochromes, and phytochromes. The LOV2 domain is derived from

phototropin 1. Phototropins are blue light-activated serine/threonine kinases and were identified in screens for *Arabidopsis thaliana* mutants lacking the chloroplast avoidance response (Christie et al. 1999; Harper, Neil, and Gardner 2003). LOV2 forms part of a tandem domain structure with LOV1, which is located at the N-terminus of the phototropin protein (Briggs and Christie 2002). This tandem LOV domain structure is unique among the 5 subsets of LOV-domain containing proteins, as all of the other groups contain only a single LOV domain. Although structurally and mechanistically related, LOV1 and LOV2 display quantitatively different photocycle kinetics (Christie et al. 1999; Crosson, Rajagopal, and Moffat 2003; Kawano et al. 2013). Studies of LOV domain proteins from different species have shown that LOV1 and LOV2 are quantitatively more different when derived from phototropin 1 than from phototropin 2, with LOV2 displaying a marked slower rate of dark recovery than LOV1 (Christie et al. 1999; Briggs and Christie 2002).

Work published by Crosson & Moffat (Crosson and Moffat 2001) has given us insight into the structure and mechanism of light-mediated signal transduction in the LOV2 domain (Peter, Dick, and Baeurle 2010; Crosson and Moffat 2001; Salomon et al. 2001). LOV domains belong to the PER-ARNT-SIM (PAS) superfamily of protein domains. PAS domain-containing proteins have been described in plants, animals, and prokaryotes with roles in sensing and responding to environmental and developmental signals (McIntosh, Hogenesch, and Bradfield 2010; Vogt and Schippers 2015). The LOV2 domain has several structural motifs that help mediate the domain's function in phototropin 1. Two mobile helical motifs exist in the LOV2 domain, a short α 'A helix at the N-terminus and a longer J α -helix at the C-terminus. The second feature has been utilised in the design of several optogenetics tools. Key to the function of the LOV2 domain is a single cysteine residue located approximately 4Å from the Flavin mononucleotide (FMN) atom C (4a). FMN is the natural chromophore necessary for LOV2 domain function (Zayner and Sosnick 2014; Crosson, Rajagopal, and Moffat 2003; Peter, Dick, and Baeurle 2010). In the dark-state, the FMN is non-covalently associated with the LOV2 domain. However, on blue light irradiation, a covalent cysteinyl-C(4a) adduct is formed with the FMN, resulting in a conformational change to the cysteine residue that is transmitted through the core of the protein. This structural change results in unwinding and undocking of the two helix motifs from the PAS core of the domain (Peter, Dick, and Baeurle 2010). Mutation of the FMN-proximal cysteine residue renders the domain photo-nonresponsive (Zayner, Antoniou, and Sosnick 2012; Zayner et al. 2013; Zayner and Sosnick 2014).

3.1.3 Designing LOV2-based optogenetic switches

As was discussed in chapter 1, optogenetic tools rely primarily on two mechanisms: 1) allosteric caging and 2) inducible protein-protein association (or dissociation). In terms of the LOV2 domain, all existing optogenetic systems rely on conformational changes to the J α -helix to drive the photo-switchability of the system. Discussed in this subsection are a few prominent examples.

Work by Di Ventura and colleagues has shown that the LOV2 domain can be used to allosterically cage a protein localisation sequence. Niopek et al., (Niopek et al. 2014) sterically caged a nuclear localisation sequence (NLS) within the J α -helix. On exposure to blue light and undocking of the helical domains, the NLS became exposed allowing for recruitment of the protein of interest to the nucleus. The same principle was applied again by Niopek et al. (Niopek et al. 2016) with a nuclear export sequence. These experiments highlight how optogenetics can be used to precisely control the relocalisation of particular proteins. It should be noted that as optogenetics is still relatively in its infancy, some degree of optimisation is still required in the implementation of these tools. Lungu et al. (2012) report that in engineering caged peptide sequences, a high degree of sequence homology is necessary between the sequence of interest and the J α -helix, at least until peptide I539. Peptide sequences caged within the N-terminus or middle of the J α -helix are reported to function only weakly (Lungu et al. 2012).

Less commonly, the LOV2 domain has been used to allosterically inhibit entire proteins. Some examples featuring LOV2 fusion proteins are Baarlink et al.'s (2013) photoactivatable RAC1 (PA-RAC) and Wu et al.'s (2009) LOV-DAD. PA-RAC features the LOV2 fused to a constitutively active mutant of the small GTPase Rac1. Photoisomerisation of the LOV2 domain sterically uncages the constitutively active Rac1 mutant allowing it to exert its downstream effect (Baarlink, Wang, and Grosse 2013). LOV-DAD is comprised of a LOV2 fusion to the autoinhibitory DAD domain of the actin nucleation and elongation factor formin mDia2 (Wu et al. 2009). Photoisomerisation of the LOV2 domain has also been used to inhibit protein activity. Dagliyan et al. (2017) engineered a light-inactivated Src kinase (PI-Src) by replacing a non-conserved loop in a constitutively active Src kinase (Y535F) with the LOV2 domain. In the ground state the kinase was active, but on irradiation by blue light conformational changes to the LOV2 domain were transmitted through the kinase, sterically disrupting the active site (Dagliyan et al. 2016).

Although the methods described above could be implemented in interesting ways with regards to the T cell signalling pathway, particularly with regards to kinase activation or inactivation in proximal signalling, our tools rely instead on light inducible protein-protein association and dissociation. We have repurposed two LOV2-based systems for use in T cells. The first, 'tunable,

light-controlled interacting protein tags for cell biology (TULIPs)' method described by Strickland et al. (2012), relies on the blue light-inducible interaction between an engineered LOV2 domain and an engineered PDZ domain (Ferrer et al. 2005; Strickland et al. 2012). The second variant is based on the LOV2 trap and release of protein (LOVTRAP) system. In the LOVTRAP system an engineered binding partner interacts specifically with the dark state of LOV2, but conformation changes result in a greatly reduced binding affinity and dissociation of the engineered interaction partner from the LOV2 domain (H. Wang et al. 2016).

3.1.4 Repurposing the TULIPs system for T cell signalling

Strickland et al. (2012) originally designed the TULIPs system for the interrogation of MAPK signalling downstream of the peptide hormone G-protein Couple Receptor in yeast. By inducing light-specific recruitment of the Ste5N scaffolding protein Strickland et al. were able to define the polarised secretion of yeast mating hormone. The role of Ste5N can be considered analogous to that of LAT in T cells. LAT acts as a scaffolding protein to nucleate signalling molecules downstream of the TCR (Figure 1.1). Thus, it was reasoned that a similar approach to signal interrogation might provide useful insight to T cell activation. This is discussed in detail in Chapter 4.

The TULIPs system itself is comprised of two components: an engineer Erbin PDZ domain (J. Huang et al. 2008; Reina et al. 2002) and its binding target an engineered LOV2 domain, 'LOVpep' (Strickland et al. 2012; Möglich and Moffat 2010). LOVpep features a truncation of the J α -helix and a fusion of the –SSADTWV-COOH peptide sequence, which shares some amino acid sequence homology to the wildtype domain but is bound by the engineered PDZ (ePDZ) domain, whereas the wildtype LOV2 sequence is not (Strickland et al. 2012). Strickland et al., (2012) tested three variants of the PDZ domain, which display binding affinities of >10 μ M (K_d) to ~0.5 nM (K_d). The lowest affinity variant, cpPDZ (Low), features a single PDZ domain. The higher affinity variants, ePDZb (Mid) and ePDZb1 (High), have been engineered into clamp-like protein structures featuring a FN3 domain fused to the PDZ domain (Jin Huang, Makabe, et al. 2009; Jin Huang, Nagy, et al. 2009). In the dark the LOVpep binding sequence is caged within the core of the LOV2 domain but on blue light irradiation, unwinding of the J α -helix exposes the peptide sequence for binding by the PDZ domains.

In establishing a TULIPs-based system for use in T cells I focused my initial efforts on the membrane scaffolding protein LAT (Sommers, Samelson, and Love 2004). The role of LAT in T cell activation is discussed in more detail in chapter 4. LAT has no intrinsic enzymatic activity and

relies on its binding partners and membrane positioning to exert its function (Balagopalan et al. 2010). Following Strickland et al.'s suggested workflow, I created a membrane anchored LOVpep domain and a cytosolic truncation of LAT fused to the C terminal of the ePDZ domains. The truncated LAT still had all of its signalling motifs intact. The LOVpep domain was localised at the plasma membrane by fusion to the C-terminal of the transmembrane domain of LAT.

3.1.5 Repurposing the LOVTRAP system for T cell signalling

Using a similar approach to the TULIPs system I developed a LOVTRAP version of the LAT-based optogenetic tool. This system was adapted further in Chapter 5 for use with CD3 ζ to interrogate TCR signal integration. The LOVTRAP system provides an interesting alternative to the TULIPs system as it provides a mechanism for light-inducible dissociation of LAT from the plasma membrane. The LOVTRAP system was established by a large scale mutation screen of the Z subunit of the Staphylococcal immunoglobulin binding protein A (H. Wang et al. 2016). The Z protein variants were screened for binding of the dark state of LOV2 and domains with a high affinity for the dark state, but low affinity for the light state were selected for further screening. I used the highest binding affinity variant, Zdk1, which shows 26.2 nM (K_d) affinity in the dark but $>4 \mu\text{M}$ (K_d) affinity for the light-state of LOV2. Two other variants of the Zdk domain have also been described with different binding site and affinities (H. Wang et al. 2016). The Zdk1 binding site is located at the C-terminus of the LOV2 domain, overlapping the J α -helix (H. Wang et al. 2016). The kinetics of this interaction are tunable via mutations to the LOV2 domain. Faster or slower cycling variants affect the rate at which the Zdk domain can re-associate with LOV2 following the cessation of blue light irradiation. I also tested the fast cycling V416T variant and slow cycling V416L variant, which have been shown to have $t_{1/2}$ of 5 seconds and 496 seconds³, respectively (H. Wang et al. 2016; Zayner and Sosnick 2014; Zayner, Antoniou, and Sosnick 2012). As our LOVTRAP system used only the Zdk1 variant, it will herein be referred to a Zdk for the sake of simplicity.

3.1.6 Development of CRY2-based signalling systems

Given the unpredictability of optogenetic engineering, I did not limit my approach solely to the development of LOV2-based tools. An alternative optogenetic system that has been widely used in cell biology is the *Arabidopsis thaliana*-derived CRY2 (Cryptochrome 2) domain. CRY2 is one

³ Half-life time taken for the LOV2 domain to thermally revert from the lit state to the ground state

of five cryptochrome proteins found in *Arabidopsis*. These proteins are involved in blue-light entrainment of the circadian central oscillator (Devlin and Kay 2000; X. Yu et al. 2010). CRY2 operates endogenously via two main mechanisms. First, CRY2 has the capacity to interact with transcription factors and direct gene expression indirectly. Second, CRY2 can bind chromatin independently of other proteins to directly modulate transcription (Liu et al. 2008; Pedmale et al. 2016). On blue light exposure, the CRY2 domain undergoes a conformational change allowing it to interact with its binding partner CIB1 (Liu et al. 2008). Mechanistic details of the conformational change and protein-protein interaction remain to be fully described. Like the LOV2 domain, the CRY2 domain is similarly dependent on an mammalian cell endogenously expressed Flavin cofactor, Flavin adenine dinucleotide (FAD) (C. Lin and Todo 2005), thus preventing the need for exogenous supplementation of the tissue culture media or further genetic alteration of the host cell line. However, at 593 residues in length, the (*At*)CRY2⁴ domain is structurally much larger than the (*As*)LOV2⁵ domain (Pathak et al. 2014). Likewise, the CIB1 binding partner is also a large domain, at 191 residues. Work done by Taslimi et al. (2014) has provided the optogenetics community with a set of second generation truncated CRY2 variants with altered binding kinetics; as well as truncated variants of the CIB1 binding partner, CIBN (residues 1-170) and CIB81 (residues 1-81). Although CIB81 showed light-dependent recruitment of CRY2, the interaction was reportedly substantially weaker than when combined with CIBN or CIB1 (Taslimi et al. 2016; Taslimi et al. 2014). For this reason, I elected to conduct my experiments using the CIBN variant.

As with the LOV2 domain, the CRY2 domain is also tunable by point mutations. Taslimi et al. (2016) reported the development of both a fast cycling and slow cycling variant, bearing the point mutations W349R and L348F, respectively. The fast cycling mutant was stated to have a $t_{1/2}$ of 2.5 minutes, whereas the slow cycling mutant was reported to interact with CIBN with a $t_{1/2}$ of 24 minutes. The tunability of these optogenetic domains can allow for signal interrogation at varying time scales with minimal light exposure. Light toward the UV end of the spectrum in particular can be toxic to cells (Stockley et al. 2017).

3.1.8 Aims

In this chapter I will outline the steps taken to develop the LAT-based optogenetic tools employed in chapter 4. The approaches described herein were performed in HEK293T cells for the purposes

⁴ Specifically the CRY2 domain from *Arabidopsis thaliana*

⁵ Specifically the LOV2 domain from *Avena sativa* as LOV domains from other organisms have also been applied to optogenetics

of system optimisation and visualisation. The limited cytoplasmic volume of T cells meant that Jurkat T cells did not provide an adequate system for investigating LOV2 and CRY2 variants with regards to LAT recruitment. Once a functional set of optogenetic tools was developed, these were then transduced into T cells for the interrogation of T cell activation.

3.2 Materials & Methods

3.2.1 Microscopy

To measure recruitment and dissociation of the optogenetic LAT constructs to and from the plasma membrane and other intracellular locations I developed a time course imaging script written in the BeanShell programming language and executed on Micromanager 1.4. As described in the general methods section, this script allowed us to automate and standardize the imaging procedure across different optogenetic systems.

In testing the individual LOVTRAP and TULIPs constructs I wanted to measure localisation and dissociation in the light and dark states. I adapted the imaging script to take images in two channels every second for 1 minute. For the first 5 seconds images were taken in the dark state to establish a baseline of localisation. Constructs were designed with yellow-green- (561 nm) and red-excited (640 nm) fluorophores, mRuby2 and IFP2, to avoid unintended activation of the LOV2 domains (<475 nm). After 5 seconds, the script was programmed to illuminate the cells with 450 nm light using the overhead condenser for 20 seconds, while still taking images in the 561 Ex/607 Em and 640 Ex/708 Em channels once per second. After 20 seconds of blue light irradiation, the script was programmed to switch off the condenser and continue imaging in both channels every second for a further 35 seconds, so that the rate of return to the dark state could be observed. The BeanShell Script can be found in Appendix C.

Similarly, I tested the two-component (TULIPs-LOVTRAP multiplexed) optogenetic “knock-sideways” (Robinson, Sahlender, and Foster 2010; Haruki, Nishikawa, and Laemmli 2008) system using a time course protocol programmed in Beanshell for Micromanager. However, my imaging script was adapted to image over 80 seconds. Cells were illuminated from 5-35 seconds during the time course and then allowed to recover to the dark state.

3.3 Results

3.3.1 Design of two opposing LAT-based optogenetic systems

The main T cell membrane scaffolding protein LAT, is reported to be intrinsically disordered (van der Lee et al. 2014). This lack of 3D structure and LAT's relatively small size (36 KDa) means that phosphorylation events have a large impact on LAT's binding properties, promoting high avidity interactions between multiple binding partners (Balagopalan et al. 2010; Flock et al. 2014). Post-translational modifications drive contortions of LAT resulting in overlapping binding moieties allowing for the rapid exchange of binding partners and the nucleation of multiple competing signalling molecules (Van Roey and Davey 2015). The first ~30 amino acids of LAT are predicted to be comprised of a short extracellular domain and transmembrane (TM) domain (Figure 3.1). Experimental evidence has shown that a CxxC motif at the C-terminal end of the TM domain is a palmitoylation site (W Zhang et al. 1999), which facilitates LAT's insertion into the plasma membrane. We designed our optogenetic constructs with the LOV2 domain anchored at the plasma membrane via the TM domain of LAT (Figure 3.2 & Figure 3.3). The C-terminal J α -helix is thus exposed to the cytoplasm on blue light irradiation. The second half of the TULIPs- and LOVTRAP-LAT systems is comprised of the LOV2 domain interaction partner fused to the intracellular domain of LAT; that is, either ePDZ or Zdk, respectively. Thus the TULIPs system allows for light-inducible recruitment of LAT to the plasma membrane and the LOVTRAP system allows for light-inducible dissociation from the plasma membrane (Figure 3.2 & Figure 3.3).

In chapter 5, the LOVTRAP system was redesigned for use with CD3 ζ . In this system the LOV2 domain was still bound at the plasma membrane, but we used a myristoylated variant of Zdk fused to the ITAM motifs of CD3 ζ . The kinetics of the interaction between Zdk and mutants of the LOV2 domain itself are assumed to be comparable between the systems. The second system is discussed in detail in chapter 5.

3.3.2 Point mutation-based tuning of the LOV2 domain

A number of mutations have been reported to alter the photocycle kinetics of the LOV2 domain (Figure 3.4). The mutations affect the rate at which the LOV2 domain decays back to the dark state, but do not alter the rate at which it structurally changes to the light state (Harper, Neil, and Gardner 2003; Christie et al. 1999). In accordance with Strickland et al.'s development workflow we tested a number of different variants of the LOV2 domain including constitutively active and inactive variants (Table 3.1).

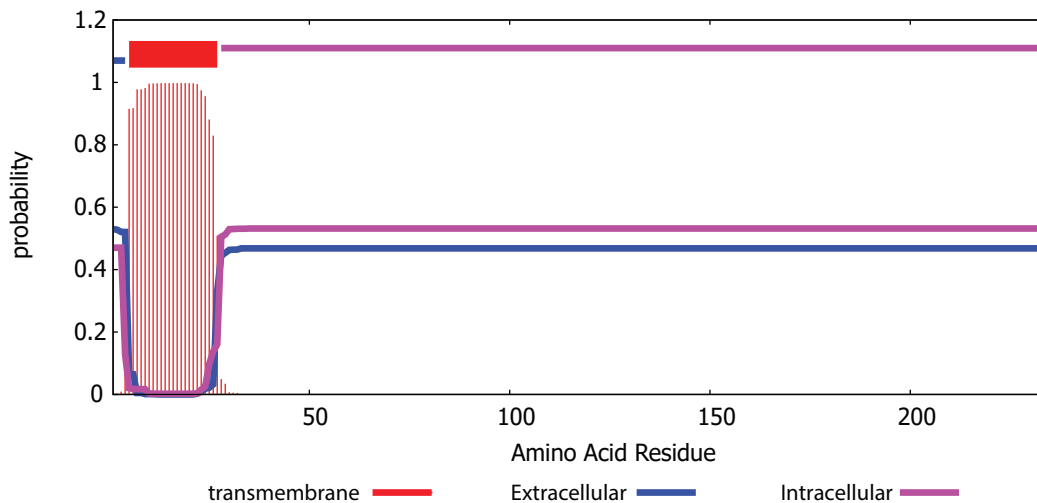


Figure 3.1 LAT-TM-LOV2 constructs engineered according to structural properties of LAT The DTU Bioinformatics SignalP 1.4 Server was used to predict the transmembrane motif of LAT. The single amino acid sequence was entered into the predictive software and the results shown here give the probability that a particular amino acid falls within the intracellular, extracellular, or transmembrane region of LAT. It is known that LAT has a short extracellular domain and thus it can be inferred that the N-terminal amino acids to the left of the graph represent the extracellular domain of the protein.

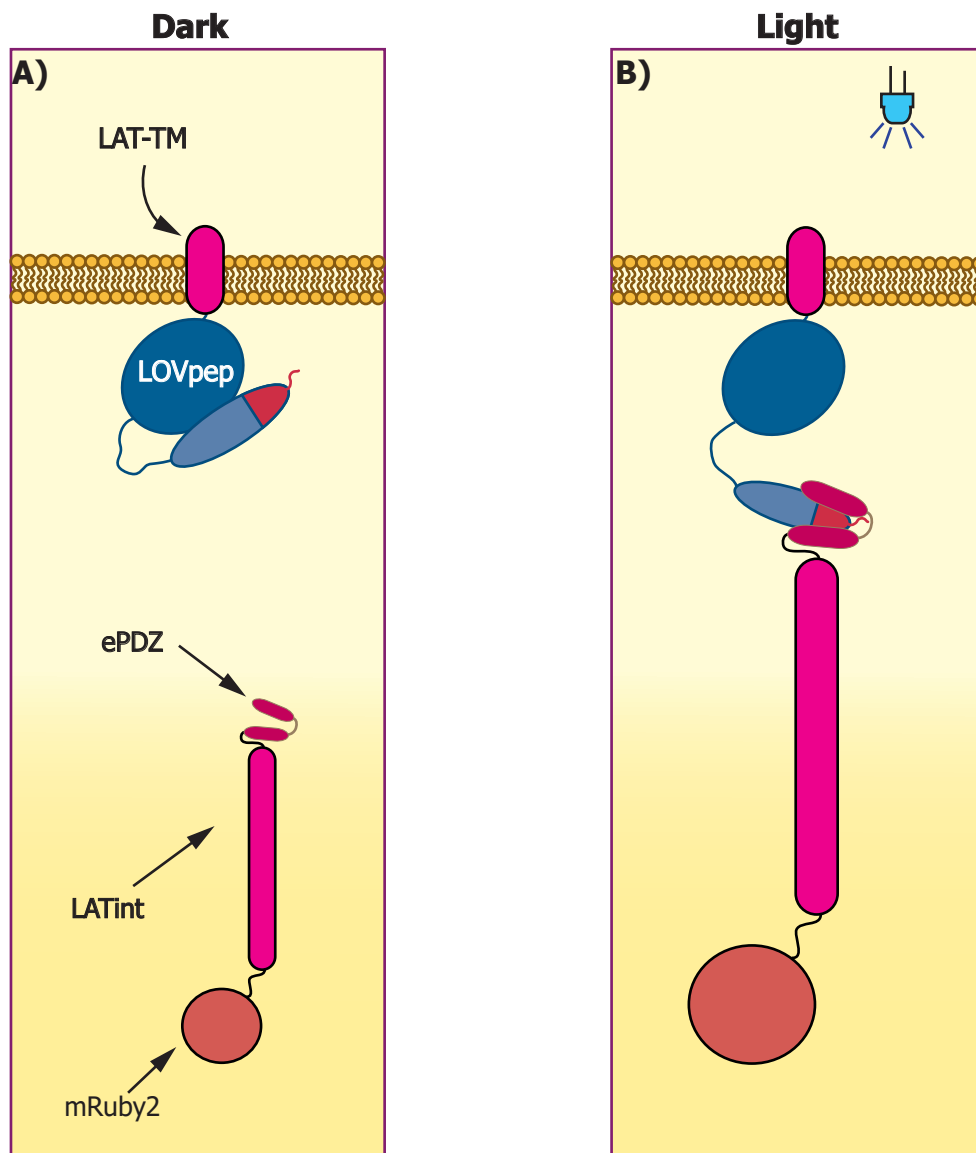


Figure 3.2 Schematic overview of the TULIPs-based system (A) In the dark state, the peptide binding sequence (red) of the engineered LOVpep domain is caged within the J α -helix and ePDZ-LATint-Ruby is localised to the cytoplasm. **(B)** Under 450nm illumination, the J α -helix of LOVpep unwinds and undocks from the PAS domain core, uncaging the peptide for binding by the PDZ domain. The intracellular domain of LAT is then localised to the plasma membrane. On Cessastion of blue light stimulation LOVpep reverts to its dark-state conformation causing dissociation of PDZ-LATint-Ruby back to the cytoplasm.

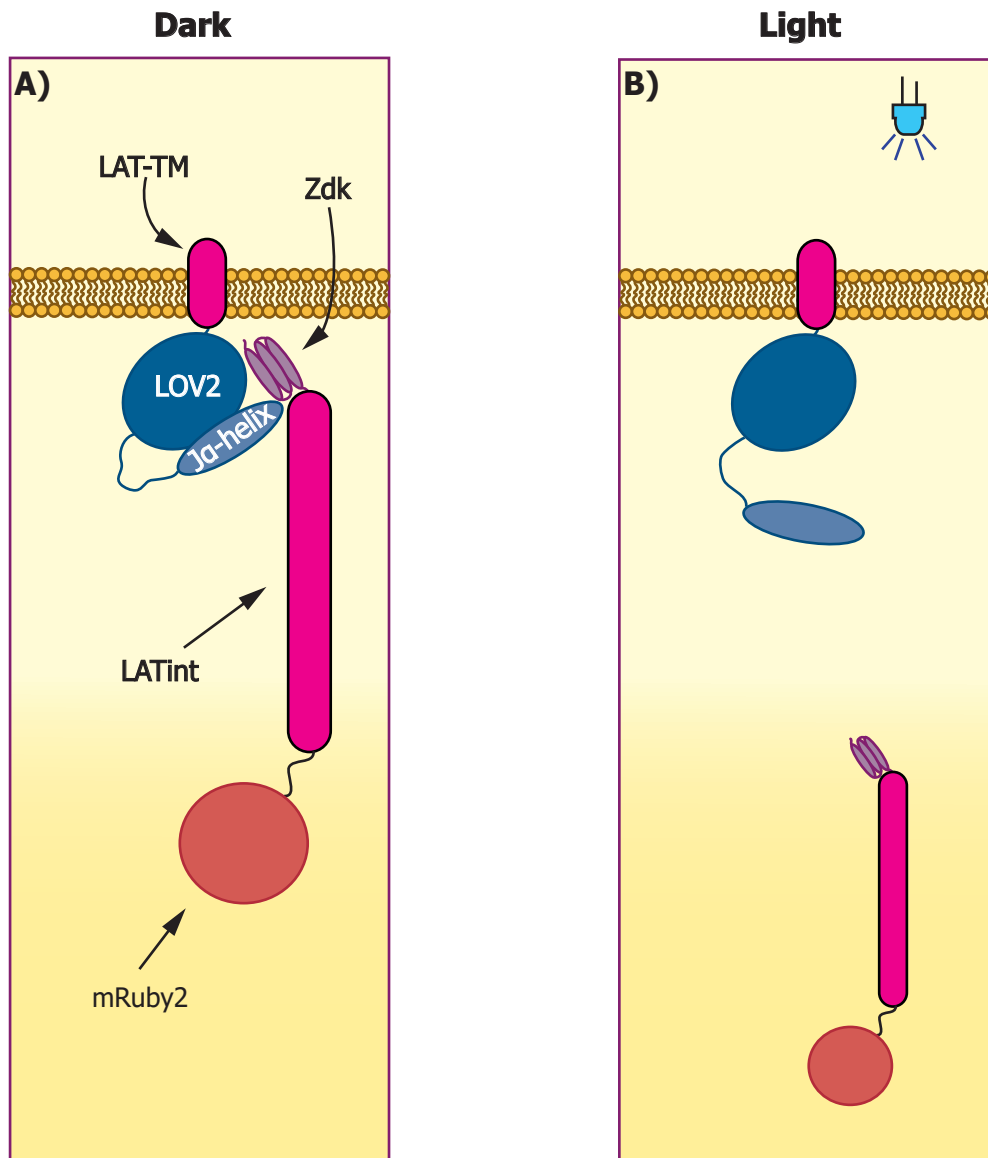


Figure 3.3 Schematic overview of the LOVTRAP-based system (A) In the dark state, Zdk-LATint-Ruby is anchored at the plasma membrane by its interaction partner, LAT-TM-LOV2. **(B)** Under ~ 475 nm illumination, the J α -helix of the LOV2 domain unwinds and undocks from the PAS domain core resulting in the passive dissociation of Zdk-LATint-Ruby into the cytoplasm. On cessation of blue light stimulation, the LOV2 domain reverts to the dark state allowing Zdk-LATint-Ruby to return to the plasma membrane. This process is repeatable.

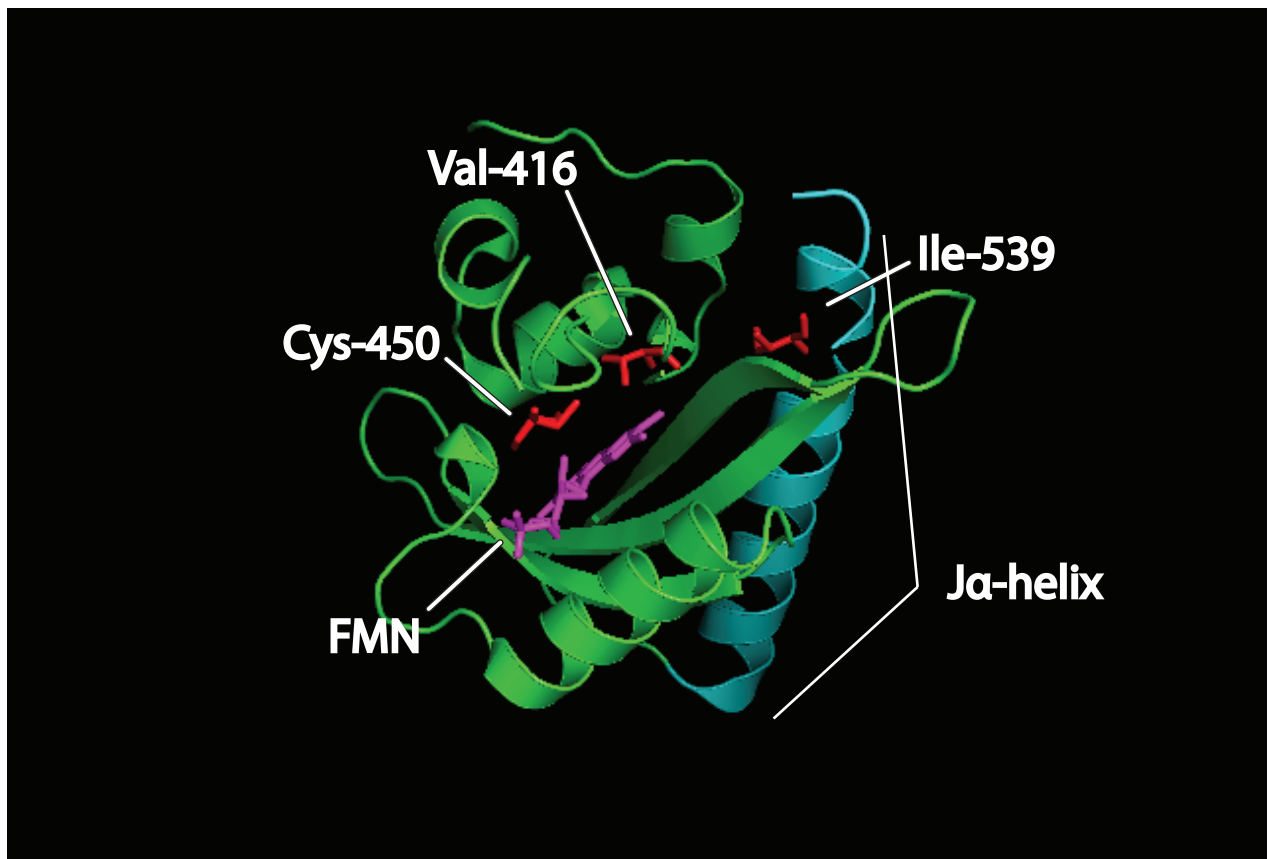


Figure 3.4 LOV2 domain photocycle kinetics are tunable via point mutations mutable residues Val-416, Cys-450, and Ile-539 are shown here in red. The FMN co-factor is shown in magenta. The Ja-helix is shown in cyan. The following point mutations were generated via overlap extension PCR: V416T (fast cycling), V416L (slow cycling), I539E (constitutively active), C450G (constitutively inactive), and C450S (constitutively inactive).

Mutation	$t_{1/2}$ (s)	Reference
Wildtype	80	(Zayner and Sosnick 2014)
C450G	Constitutively Inactive	(Zayner and Sosnick 2014)
V416T	2.6	(Kawano et al. 2013)
V416L	495	(H. Wang et al. 2016)
I539E	Constitutively Active	(Zayner, Antoniou, and Sosnick 2012)
LOVpep ^{CA}	Constitutively Active	(Strickland et al. 2012)

Table 3.1: AsLOV2 mutant photocycle kinetics

I performed site directed mutagenesis PCR to generate the mutants outline in Table 3.1. The products were confirmed by sequencing. The complete list of constructs and primers can be found in the Appendices A & B.

3.3.3 Light-inducible recruitment of LAT using the TULIPs system.

LAT's lack of significant tertiary structure makes it a good candidate for our optogenetic systems, as it is unlikely to sterically hinder the interaction of the ePDZ (or Zdk) domain with the LOV2 domain. To test the functionality of the TULIP-LAT system, I transiently expressed the LAT-TM-LOVpep domain and ePDZ-LATint fusion proteins in HEK293T cells. The LATint constructs were tagged with a C-terminal mRuby2 fluorophore (Kredel et al. 2009) for real-time visualisation of LAT recruitment and dissociation from the plasma membrane. By first expressing the constitutively-active variant of LOVpep (Strickland et al. 2012) I was able to confirm that the LATint fusion protein was indeed able to bind the lit-state of LOV2. The pattern of localisation was identical to that of full length, Ruby-tagged LAT (Figure 3.5). The same pattern of expression was observed in Jurkat cell lines (Appendix F). HEK293T cells expressing the the LATint-Ruby constructs in the absence of their LOV2 binding partners show distinct cytoplasmic localisation (Appendix O).

Having confirmed that the LATint fusion protein was capable of binding the LOVpep domain I next sought to confirm light-inducible localisation of LAT. I focused my analysis on the high (ePDZb1) and low (cpPDZ) affinity variants of the ePDZ domain. By measuring depletion of the LATint construct from the cytoplasm we were able to infer plasma membrane recruitment

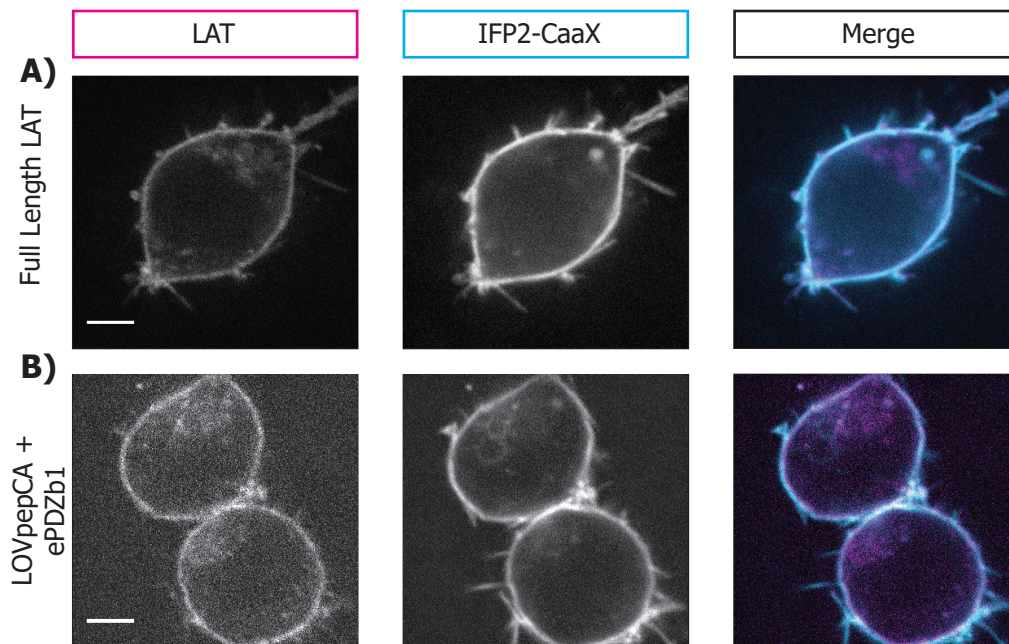


Figure 3.5 Constitutively active LOVpep shows membrane recruitment of PDZ-LATint construct (A) HEK293T cells expressing Full length LAT tagged with an mRuby2 fluorophore and IFP2 anchored at the membrane via a CaaX motif. Both markers show clear colocalisation at the plasma membrane. Cells were transiently transfected with the pHR-full-length LAT and pHR-IFP2-CaaX **(B)** The constitutively active LOVpep variant recruits the high affinity (ePDZb1) variant of the TULIPs system to the plasma membrane. Images are taken at 100X magnification, scale bar 5 μ m. Cells were transfected with pHR-ePDZb1-LATint-Ruby, pHR-LOVpep(CA), and pHR-IFP2-CaaX

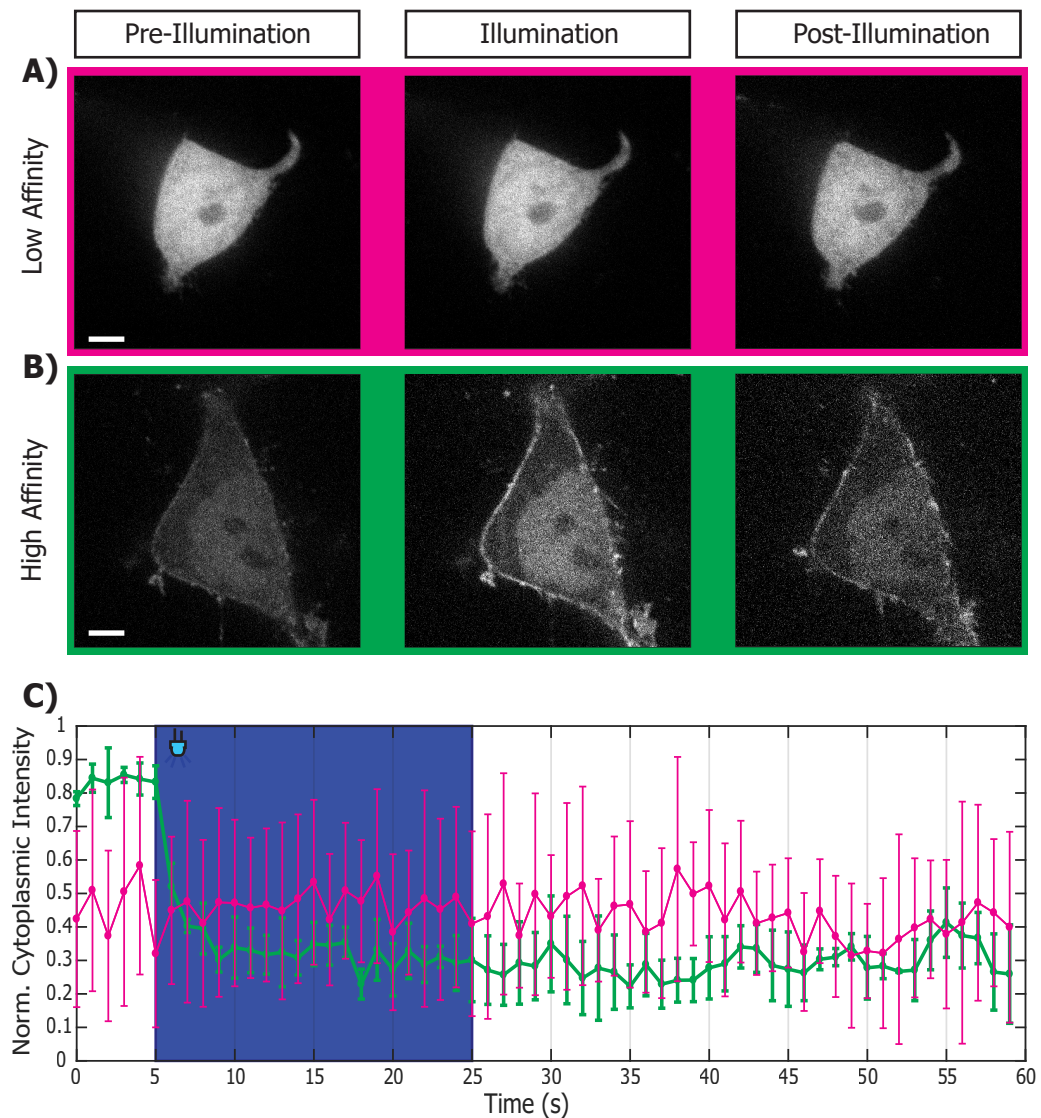


Figure 3.6 Light-inducible recruitment of the TULIPs-LAT constructs Pre-illumination images are taken a 1 s, illumination images are taken at 7 s, and post-illumination images are taken at 50 s. Images were taken at 100X magnification. Scale bar 5 μ m. **(A, C)** The low affinity PDZ (cpPDZ) variant (magenta) of the TULIPs system shows no quantifiable recruitment to the plasma membrane-bound LOVpep binding partner under blue light illumination (1 mW/cm²). Cells were transfected with pHR-cpPDZ-LATint-Ruby and pHR-LAT-TM-LOVpep. **(B, C)** The high affinity PDZ variant of that LATint construct (ePDZb1) shows rapid membrane recruitment on blue light irradiation. Cells were transfected with pHR-ePDZb1-LATint-Ruby and pHR-LAT-TM-LOVpep **(C)** Cytoplasmic mRuby2 intensity shows depletion kinetics of TULIPs constructs. Line colours are given by the background colours **(A-B)**. Blue area denotes illumination. Error given as SD, n=3 (Biological replicates). Samples were normalised to the baseline cytoplasmic intensity (t= 1-5 seconds) after correcting for photobleaching.

(Figure 3.6). Under the conditions tested, I was unable to detect recruitment of the low affinity variant to the plasma membrane (Figure 3.6A, C), however I was able detect membrane recruitment of the high affinity variant (Figure 3.6B, C). There was no observable return of the high affinity variant to the cytoplasm on the time scale measured (Figure 3.6B, C). This finding is in agreement with previously published work (Strickland et al., 2012).

3.3.4 Light-inducible dissociation of LAT using LOVTRAP system

In parallel with the TULIPs system I also designed and tested different variants of the LOVTRAP construct (H. Wang et al. 2016). In accordance with the recommended workflow, I first tested the constitutively active and photo-nonresponsive variants of the LOV2 domain to establish whether the Zdk-LAT fusion protein was able to interact with the LOV2 domain and would correctly dissociate under illumination. As expected, the LOV2(C450G) photo-nonresponsive mutant resulted in recruitment of the Zdk-LAT^{tint} fusion protein to the plasma membrane (Figure 3.7A). In the presence of the LOV2(I539E) constitutively open variant, no recruitment was observed and the Zdk-LAT^{tint} fusion protein was permanently localised to the cytoplasm (Figure 3.7B). As expected localisation of LAT with both the photo-nonresponsive LOV2 mutant and the constitutively active LOV2 mutant was unaffected by blue light irradiation (Figure 3.7).

Once it had been confirmed that the Zdk-LAT^{tint} fusion protein was capable of interacting with the dark state of the LOV2 domain and incapable of interacting with the lit state of the LOV2 domain, I tested LAT^{tint} dissociation and recruitment with three variants of the LOV2 domain showing different photocycle kinetics (Figure 3.8A-C) (Table 3.1) (Zayner and Sosnick 2014; H. Wang et al. 2016). With all three variants there was a sharp increase in cytoplasmic mRuby2 intensity following blue light irradiation (Figure 3.8D). This reflects the fact that the rate at which the LOV2 domain photoisomerises from the dark state to the lit state is unaffected by photocycle-altering point mutations. There was little measureable difference in the rate of return to the plasma membrane between the fast-cycling and wildtype variants, however, on the timescale measured, there was no observable change in cytoplasmic Ruby intensity following cessation of blue light irradiation when using slow-cycling variant of the system (Figure 3.8D). These results are in accordance with previously published work (Wang et al., 2016). With regards to the fast-cycling variant and the wildtype variant, these results suggest that the rate of return of the LAT^{tint} construct to the plasma membrane is at least partially limited by its rate of diffusion in the cytoplasm. Given the smaller cytoplasmic volume of Jurkats when compared to HEK293T cells it

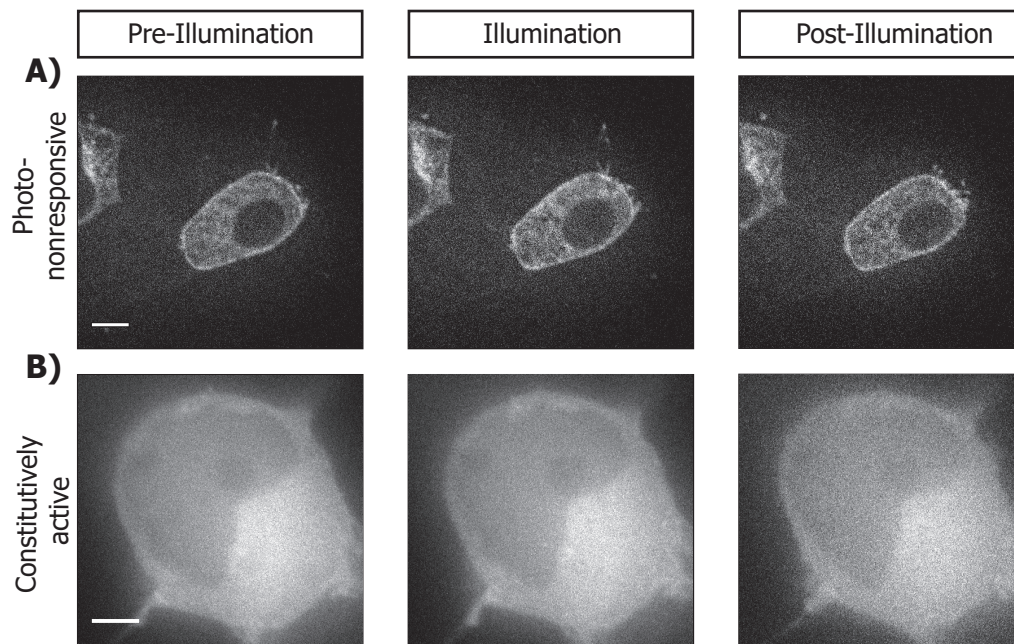


Figure 3.7 Control variants of the Zdk system (A) The photo non-responsive (C450G) mutant of the LOV2 domain allows for constitutive recruitment of Zdk-LATint-Ruby to the plasma membrane. HEK293T cells were transfected with pHR-Zdk-LATint-Ruby and pHR-LAT-TM-LOV2(C450G). **(B)** The constitutively active (I539E) mutant of the LOV2 domain prevents the LOV2-Zdk interaction. HEK293T cells were transfected with pHR-Zdk-LATint-Ruby and pHR-LAT-TM-LOV2(I539E). Images taken at 100X magnification, scale bar 5 μ m.

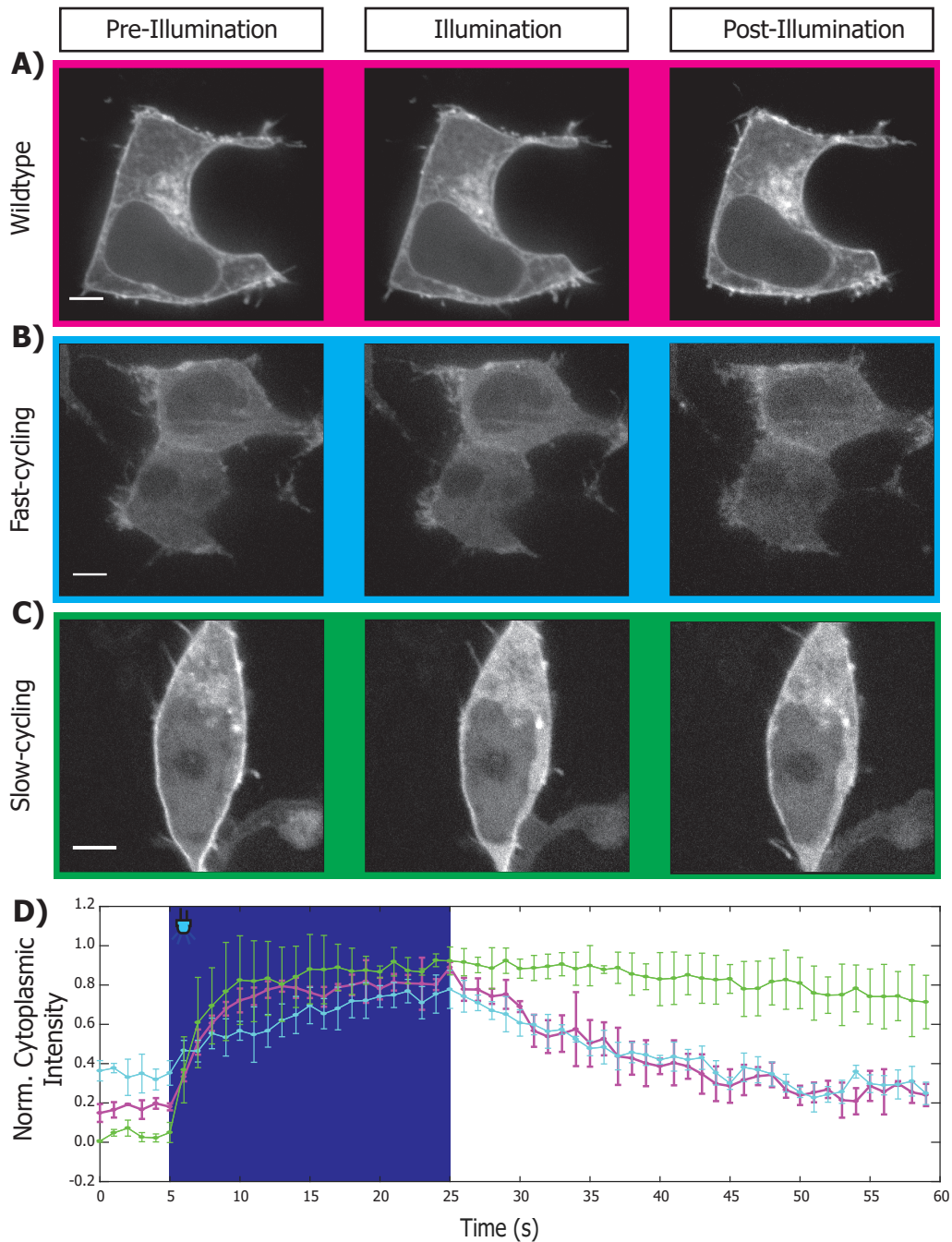


Figure 3.8 Light-inducible dissociation of Zdk-LATint-Ruby Pre-illumination images are taken at 1 s, illumination images are taken at 7 s, and post illumination images are taken at 50 s. **(A,D)** In the dark, Zdk-LATint-Ruby is anchored at the plasma membrane via the Zdk-LOV2 interaction (magenta). Low intensity ($\sim 1\text{mW}/\text{cm}^2$) 450 nm illumination results in the rapid dissociation of the LATint construct to the cytosol. On cessation of blue light irradiation the Zdk-LOV2 interaction can re-initiate. **(B)** The fast cycling LOV2 (V416T) variant (cyan) shows kinetics comparable to the wildtype **(A)** version of the domain. **(C)** The Slow cycling LOV2 (V416L) variant shows a slower rate of return to the plasma membrane on cessation of blue light irradiation (green). **(D)** Normalised cytoplasmic mRuby2 intensity. Colours are given by the background colours **(A-C)**. The blue area denotes blue light irradiation. Images taken at 100X magnification in HEK293T cells. Scale bar 5 μm . Error given as SD, $n=3$ (Biological Replicates).

would be expected that the rate of return would be somewhat faster with the fast-cycling variant when compared with the wildtype variant assuming protein expression levels were comparable.

3.3.5 Light-inducible recruitment of LAT using CRY2

In establishing an optogenetic LAT-based system for T cell signalling, I focused primarily on LOV2 systems because of its small size, endogenously expressed cofactor, and high degree of tunability. However, I also tested the feasibility of a CRY2-based system. Like the TULIPs system, CRY2 has also been used to induce protein-protein interactions on blue light irradiation (Taslimi et al. 2016; Taslimi et al. 2014; Spiltoir et al. 2016). Recent work by Taslimi et al. (2016) has also provided a set of second generation CRY2 constructs with altered photocycle kinetics and smaller molecular sizes. I tested the truncated CRY2PHR variant with the fast- and slow-cycling mutations (Taslimi et al. 2016).

Mutation	$t_{1/2}$ (min)	Reference
Wildtype	5.5	(Taslimi et al. 2016)
L348F	24	(Taslimi et al. 2016)
W349R	2.5	(Taslimi et al. 2016)

Table 3.2: AtCRY2PHR mutant photocycle kinetics

As with the previously described LOVTRAP and TULIPs constructs, the CRY2 domain was fused at the N-terminus of LATint via a short linker sequence. To test recruitment of CRY2-LATint to the plasma membrane under blue light irradiation we used the previously described pmGFP-CIBN construct (Tucker, Vrana, and Kennedy 2014), which is anchored at the plasma membrane via a prenylation (CaaX) motif and features a GFP marker and the CRY2 interaction partner, CIBN (Taslimi et al. 2016; Kennedy et al. 2010) (Figure 3.9). When expressed in HEK293T cells, it was found that both the wildtype CRY2PHR construct and the fast-cycling CRY2PHR construct (W349R) constructs behaved as expected (Figure 3.10A, B, D). The rate of depletion from the cytoplasm was comparable between the two variants, again suggesting that this was limited by cytoplasmic diffusion of the construct. A gradual increase in cytoplasmic Ruby intensity was observed in the fast-cycling variant ~5 seconds after the cessation of blue light stimulation. This was in contrast to the wildtype CRY2PHR variant, where an increase in cytoplasmic ruby intensity could not be observe during the 35 second recovery period. The slow-cycling CRY2PHR (L348F)

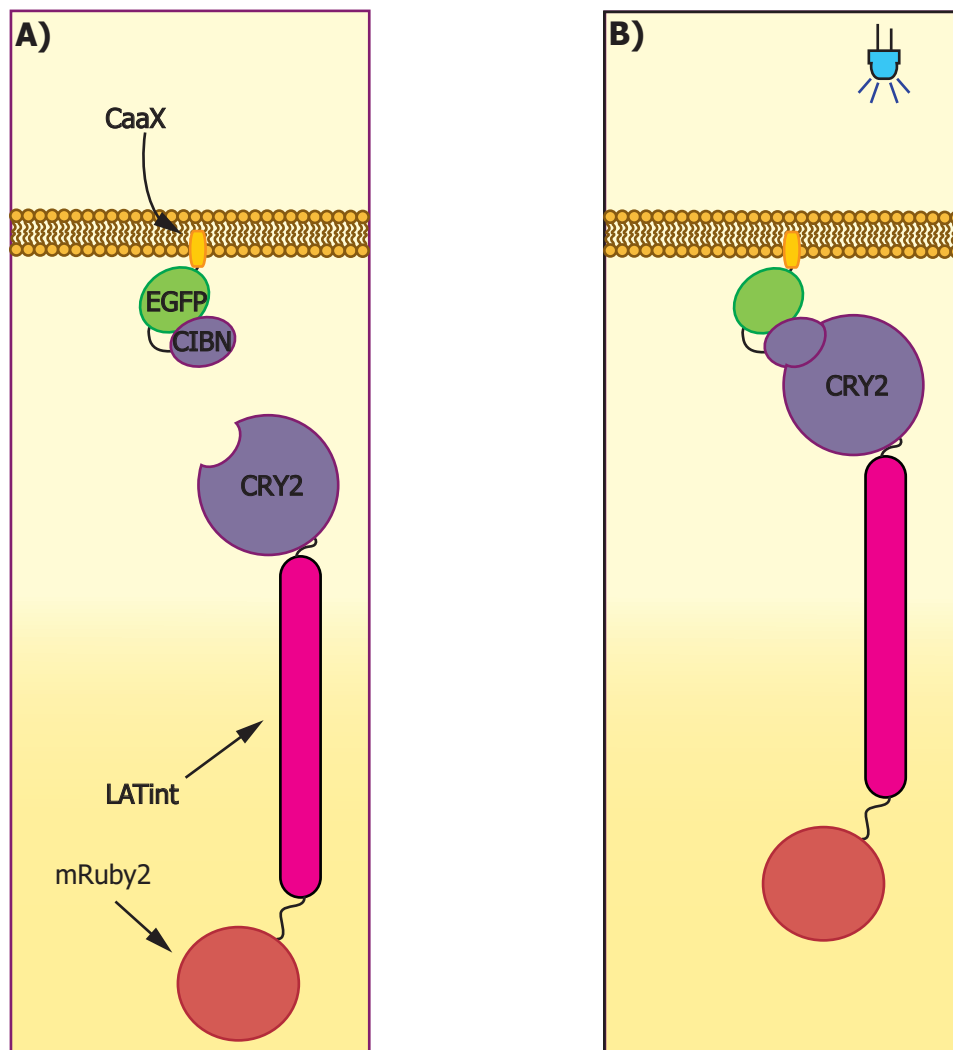


Figure 3.9 Schematic overview of the CRY2-based optogenetic system
(A) In the dark state, CRY2-LATint-Ruby is localised to the cytoplasm. **(B)** photoisomerisation of the CRY3 domain allows it to interact with its binding partner, CIBN, which is anchored at the plasma membrane via a CaaX motif. CIBN is tagged with a GFP marker to visualise protein expression.

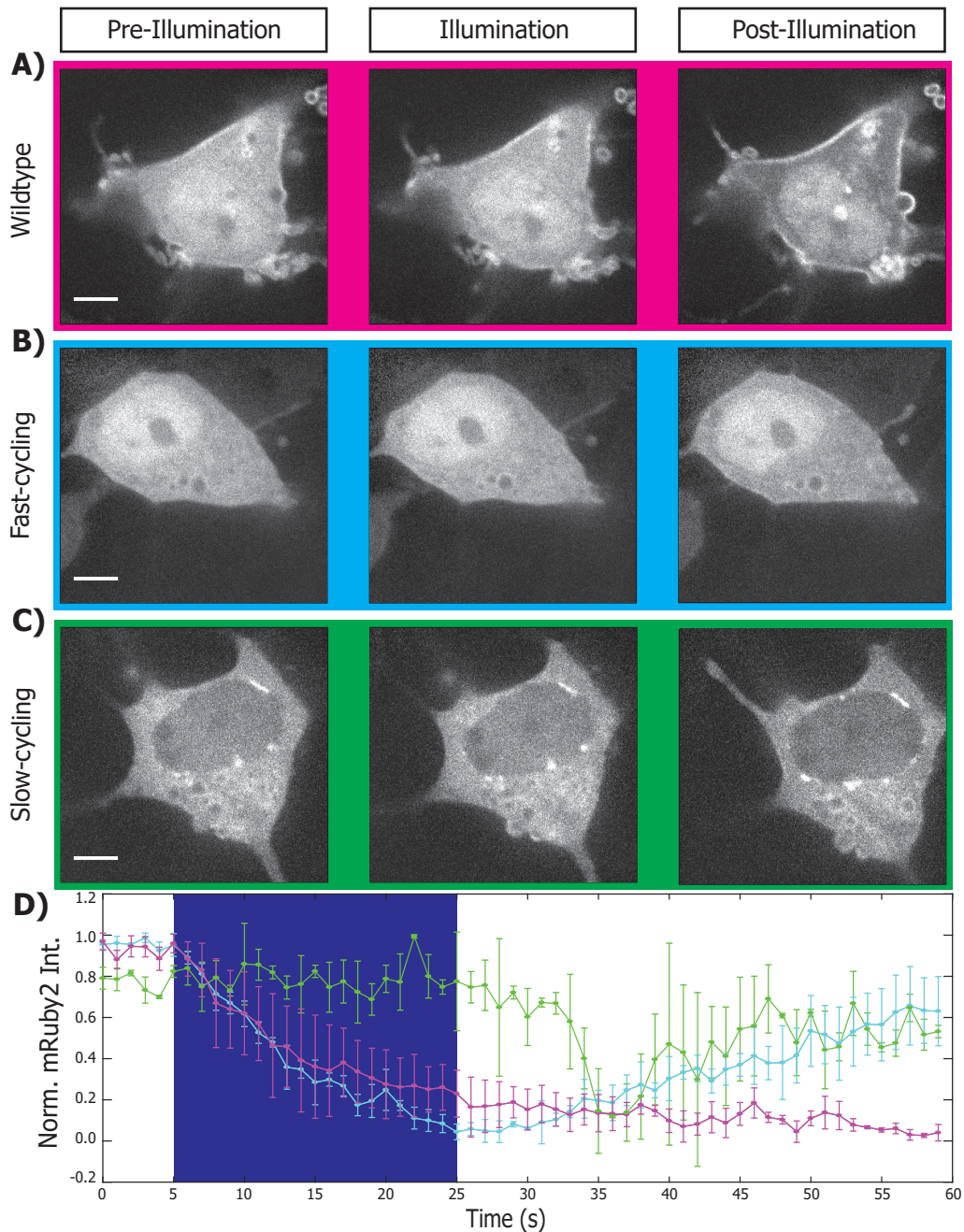


Figure 3.10 CRY2PHR-LAT constructs show light-inducible membrane recruitment HEK293T cells expressing CIBNpm-GFP and variants of the CRY2PHR construct were illuminated with 450 nm light ($\sim 1 \text{ mW/cm}^2$). Pre-illumination images are taken at 1 s, illumination images were taken at 7 s, and post illumination images were taken at 50 s. All images were taken at 100X magnification. **(A, D)** Wildtype CRY2PHR shows rapid, and sustained membrane recruitment on blue light irradiation (magenta). **(B, D)** The fast-cycling (W349R) variant shows cytoplasmic depletion comparable to the wildtype variant, but a more rapid return to the cytoplasm (cyan). **(C, D)** No plasma membrane recruitment was detectable with the slow-cycling (L348F) CRY2PHR variant (green). **(D)** The kinetics of cytoplasmic depletion of CRY2PHR-LATint-Ruby presented as normalised MFI. The blue area denotes illumination. The line colours are representative of the background colours **(A-C)**. Images at 100X magnification, scale bar 5 μm . Error given as SD, n=3.

variant, although expressed, did not behave as expected (Figure 3.10C, D). No recruitment of LAT^{int} to the plasma membrane was detectable.

I tested two other truncations of the CRY2 system, CRY2(535) and CRY2(515), described in detail by Taslimi et al. (2016). These were found to recruit LAT in a manner identical to the CRY2PHR variant (Figure 3.11). A complete list of the CRY2 constructs can be found in Appendix B. Using the Matlab curve fitting function I was able to calculate the rate of cytoplasmic depletion for each of the CRY2 variants (Table 3.3). All were found to be comparable suggesting that the rate of recruitment is dependent on cytoplasmic diffusion. As with the LOV2-based systems, it would therefore be expected that this would occur somewhat faster in Jurkat T cells because of their low cytoplasmic volume.

Mutation	Rate Constant
CRY2PHR	-7.8×10^{-2}
CRY2(515)	-9.8×10^{-2}
CRY2(535)	-9.5×10^{-2}
CRY2PHR(W349R)	-5.1×10^{-2}

Table 3.3: Rate of CRY2 construct cytoplasmic depletion

3.4 Discussion

Here, I have shown the feasibility of several LAT-based optogenetic constructs for the interrogation of T cell signalling dynamics. Optimisation of these systems was performed in HEK293T cells prior to using them in T cells. HEK293T cells represent a good model system because they are an easily-manipulable human cell line and unlike Jurkat T cells they have a large cytoplasmic volume relative to the nucleus. This made observing and quantifying LAT recruitment considerably easier than in Jurkat T cells.

As optogenetics is still a relatively new field, some degree of optimisation is necessary for the development of new tools. Here, I adapted the TULIPs system for use with the T cell scaffolding protein LAT. As such I was able to show rapid, light-driven association of the LAT^{int} construct with the plasma membrane. This process occurred immediately on exposure to blue light. However, there was no quantifiable recruitment detected with the low affinity (cpPDZ) version of the system. This may indicate that the interaction between cpPDZ and LOVpep has a short half-life and may simply have a high turnover rate, even when the system is in the lit state.

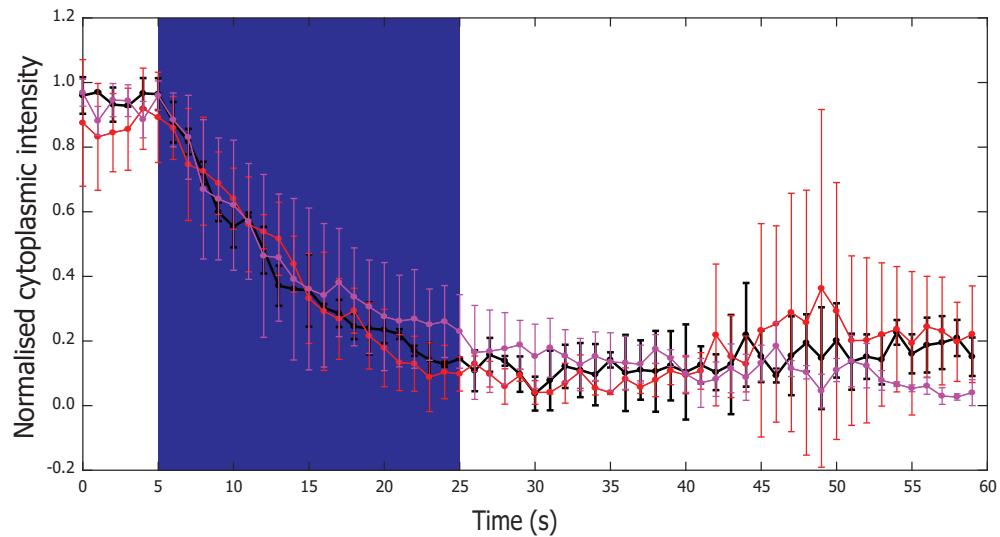


Figure 3.11 Light-inducible recruitment of second generation CRY2 constructs
Immediately on blue light stimulation (blue area) the CRY2 LATint constructs show depletion from the cytoplasm and recruitment to the plasma membrane. The kinetics of recruitment were identical between the wildtype CRY2 system (black), the CRY2(535) truncated variant (magenta), and the CRY2(515) truncated variant (red). Error given as SD, n=3.

Although I was not able to detect cytoplasmic depletion using the low affinity version, this may still be occurring allowing LAT to mediate downstream signalling functions in T cells. Importantly, the addition of the high affinity PDZ (ePDZb1) domain to the C-terminus of the intracellular domain of LAT did not seem to sterically hinder the PDZ domain and quantifiable recruitment of LAT^{int} was detectable. This is significant given that others have reported steric hindrance of proteins when fused to the LOV2 domain (Lungu et al. 2012). This TULIPs-LAT tool provides a unique mechanism for light-driven T-cell activation. Previous groups have tried this with chemically-caged antigens (Huse et al. 2007), but this approach results in irreversible activation of the T cell. The TULIPs-LAT system is reversible with tunable kinetics allowing for more precise interrogation of the T-cell signalling pathway.

Similarly, I also adapted the LOVTRAP system for use with LAT. It was shown that while using the LOVTRAP system, LAT was anchored at the plasma membrane and dissociated on blue light stimulation. Wildtype, full length LAT is normally anchored at the plasma membrane, therefore the dark-state of the LOVTRAP system closely mimics the endogenous signalling pathway. Previous work has reported that T cells require chronic low level TCR signalling to maintain cellular homeostasis (Štefanová et al. 2003). This process is referred to as 'tonic signalling'. It has been shown that in the absence of tonic signalling through the TCR, T cells gradually begin to downregulate TCR expression and eventually apoptose (Polic et al. 2001). By closely mirroring the endogenous signalling machinery, it might be expected that T cells expressing the LOVTRAP-LAT system would be less susceptible to changes in the downstream signalling pathway.

I also confirmed that the kinetics of LAT recruitment were tunable via point mutations in the LOVTRAP system, meaning that this approach may be useful not only for proximal signalling events, but also for more distal signalling events. It was noted however that the rate of return to the baseline dark-state was at least partially dependent on the rate of LAT diffusion in the cytoplasm. It would therefore be expected that the photocycle kinetics of the LOV2 domain may have a more pronounced impact when employed in a T cell signalling context because the cytoplasmic volume in Jurkat T cells is lower than that of HEK293T cells.

In this chapter I also optimised an alternative approach to LAT recruitment, by testing several variants of the CRY2 system. The CRY2 system provides a good alternative to the TULIPs system, because both are blue light responsive and reliant on endogenously expressed Flavin cofactors. Thus, there is no need for extensive adaptation of the experimental equipment or exogenous supplementation of the culture media, as would be the case with the red-light

responsive Phytochrome system. Like the TULIPs version of the LAT system, I was able to show light-inducible recruitment of LAT to the plasma membrane using the CRY2 domain and plasma membrane-anchored CIBN. The rate of return to the ground state, in which LAT^{int} was localised to the cytoplasm, was tunable via point mutations. These results indicate that the CRY2 system is a good alternative to the LOV2 based systems.

Other variants of the LOV2 domain have also been reported. Kawano et al. (2015) developed a pair of light-switchable proteins from a fungal photoreceptor, Vivid (VVD). These domains were engineered in parallel to express complementary electrostatic interaction sites, which were caged in the dark state. This system was reported to have low background binding due to the engineered electrostatic interactions and was tunable via point mutations to have an interaction $t_{1/2}$ of between 25 seconds and ~2 hours (Kawano et al. 2015). Although this system in theory provides a good alternative to the TULIPs system, I was unable to express the complementary VVD domains in HEK293T cells when combined with the LAT system. This, however, does not appear to be unique to LAT, as our collaborator Ralitsa Madsen was also unable to detect expression of an optogenetic PI3K system using the same constructs acquired independently (Personal Communication).

Although other groups have successfully used the red/far red-responsive PhyB domain (Stratiievska and Gordon 2016; Toettcher et al. 2011), I did not test this system for use with LAT. The PhyB system requires exogenous supplementation of the cofactor and re-engineering of the hardware necessary to control light stimulation and so is not a good alternative to the LOV2 domain.

Taken together, the findings presented in this chapter indicate that LOVTRAP, TULIPs and CRY2 all provide feasible mechanisms for controlling LAT recruitment and localisation. All three systems are tunable and thus provide flexibility to interrogate signalling events across varying time scales.

Chapter 4 – Investigating early T cell signalling dynamics using LAT-based optogenetic switches

4.1 Introduction

4.1.1 TCR microclusters and immunological synapse maturation

The Immunological synapse (IS) or Supramolecular Activating Cluster (SMAC) forms at the interface between a T cell and an APC and is an important step in the process of T cell activation. The classical, Kupfer-type immunological synapse is comprised of a series of concentric rings that form a bullseye pattern on the surface of the T cell. Each ring is enriched for different sets of signalling molecules associated with the TCR signalling network. At the centre of the structure (cSMAC) there is an enrichment for the TCR, Protein Kinase C Theta (PKC θ), and the co-receptor CD28 (Sanchez-Lockhart, Graf, and Miller 2008). It has been proposed that these molecules are partitioned within the cSMAC and function somewhat independently in signal propagation, implying that signalling from the two receptors is integrated downstream from the plasma membrane (Saito, Yokosuka, and Hashimoto-Tane 2010; Sanchez-Lockhart and Miller 2006). Immediately outside of the cSMAC is the peripheral SMAC (pSMAC). The pSMAC is enriched for integrin signalling molecules such as LFA-1 (Lymphocyte function-associated antigen 1) and its associated factor Talin. LFA-1 interacts with its APC-expressed counterpart ICAM-1 (Intercellular Adhesion Molecule 1) to form a tight adhesion between the T cell and the APC (Graf, Bushnell, and Miller 2007). The interaction of integrins on the surfaces of the T cell and the APC bring their membranes within ~40nm of one another. The pSMAC is also characterised by a dense F-actin network, whereas the cSMAC is cleared of actin and is reported to be a site for exocytosis of cytokines and cytolytic proteins and endocytosis of the TCR (Bunnell et al. 2001; Comrie, Babich, and Burkhardt 2015; Comrie et al. 2015). The cell-cell junctions formed by the interactions of pMHC and the TCR (~15nm) and the integrins serve to sterically exclude phosphatases; including the main TCR phosphatase, CD45, in a process of T cell triggering referred to as kinetic segregation (S. J. Davis and van der Merwe 2006; James and Vale 2012; Cordoba et al. 2013). This ring of exclusion around the pSMAC is referred to as the distal SMAC (dSMAC). CD45 is passively driven to the dSMAC because of its large, rigid extracellular domain (Chang et al. 2016). This structural feature also precludes CD45 from entering smaller microclusters (Varma et al. 2006). Truncations of the CD45 extracellular domain result in abrogated TCR activation due to increased dephosphorylation of key signalling molecules such as

CD3 and ZAP70 (James and Vale 2012). It should be noted, however, that dephosphorylation by CD45 is necessary to relieve the inhibition of the co-receptor associated kinase Lck and trigger the downstream signalling cascade.

Since the initial description of the immunological synapse by Monks et al. (Monks et al. 1998) as a site for sustained TCR signalling, our understanding of the precise role of the IS in TCR activation has been adapted and improved. As the cSMAC is enriched for TCR signalling molecules and the co-receptor CD28, the IS was initially proposed as a site for enhanced T cell activation signals. This paradigm has been shifted with the discovery of TCR microclusters, which are the smallest detectable unit of TCR-induced signalling (Varma et al. 2006; Saito and Yokosuka 2006; Yokosuka et al. 2005). Although the precise composition of TCR microclusters is somewhat loosely defined, it is generally agreed that these signalling platforms contain the TCR complex, including the CD3 chains; LAT; SLP76; ZAP70 and, at least transiently, Lck (Varma et al. 2006; Yokosuka et al. 2005; Hashimoto-Tane et al. 2010). These microclusters form continuously in the dSMAC during T cell activation and are trafficked to the centre of the IS where the signals are terminated and the TCR is endocytosed (Griffiths, Tsun, and Stinchcombe 2010; Čemerski et al. 2008). Even this view is somewhat simplistic as it has been reported that not all T cell-APC interactions result in the formation of an IS. Brossard et al. (2005) report that conjugates between splenic DCs and splenic T cells formed multifocal adhesions between the two cell types, but on conjugation with macrophages or B cells the same T cells formed a more classic bullseye structure (Brossard et al. 2005). As activating signals seem to be driven by microclusters rather than the IS, this could provide a mechanism for enhanced T cell activation. Moreover it has been reported that in the presence of weak signals – low concentrations of antigenic peptide or low affinity peptide – the IS does indeed act as a signal booster, concentrating TCR activating signals within the cSMAC (Čemerski et al. 2008). If correct, this means that T cells are able to rapidly gauge signal strength and regulate their morphology accordingly to titrate incoming TCR signals. Given that the response seems to be at least partly cell type dependent, this also suggests that differences in secondary, co-stimulatory or co-inhibitory signals may play a role in shaping IS formation.

Reports that microclusters are trafficked toward the cSMAC from the dSMAC have led to the conclusion that interactions between the cytoskeleton and TCR microclusters must be important for the overall formation of the IS. During the formation of the IS, the TCR, co-stimulatory receptors, and LAT are swept toward the cSMAC via retrograde actin flow (Yi et al. 2012; Comrie, Babich, and Burkhardt 2015; Beemiller and Krummel 2010; Beemiller, Jacobelli, and Krummel 2012). Although TCR microclusters are trafficked toward the cSMAC by retrograde actin flow they are reported to travel at a slower rate than the flow of actin (DeMond et al. 2008).

This was shown by deflection of the TCR's trajectory of motion by micro-patterned surfaces. The TCR would move parallel to the micro-patterning, whereas the underlying retrograde actin flow remained unchanged. Work performed by C. Yu et al. (2010) in Jurkat T cells confirms this 'slippage model' of actin association. It is therefore assumed that interactions between the actin cytoskeleton and TCR microclusters are transient and dynamic, with microclusters being shunted along F-actin tracks at a slower rate than the flow of actin. This occurs in a frictional manner (Y. Yu, Smoligovets, and Groves 2013). Furthermore, it has been shown that the actin motor protein, myosin IIA, is important in the formation of the IS and trafficking of the microclusters toward the cSMAC (Kumari et al. 2012). This finding lends further credence to the involvement of the actin cytoskeleton in the formation and trafficking of microclusters toward the immunological synapse.

Work by Kumari *et al.*, showed that F-actin reorganisation is important in the early formation and trafficking of microclusters, but during late synapse formation and trafficking within the cSMAC this role seems to be taken over by interactions of microclusters with microtubules. Evidence for this comes from work performed by Varma et al. (2006). Inhibition of F-actin polymerization with Latrunculin A slowed the trafficking of existing TCR-microclusters toward the cSMAC, but did not affect the size of existing microclusters or the stability of the cSMAC itself. Blocking F-actin polymerization inhibited the formation of new microclusters resulting in the termination of T cell signalling. Signalling, as measured by calcium influx, terminated as the existing clusters completed their transit toward the cSMAC. This finding indicates not only the involvement of actin polymerization in microcluster formation, but supports the idea that TCR signalling is initiated and sustained by the formation of new microclusters and not in the concentration of TCR microclusters at the cSMAC (Varma et al. 2006; Yokosuka et al. 2005). Conversely, siRNA downregulation or pharmaceutical inhibition of the microtubule motor protein dynein also inhibited trafficking of microclusters to the cSMAC but increased T cell activation through the stabilization of microclusters in the actin-rich pSMAC (Hashimoto-Tane et al. 2011). Dynein-inhibited cells showed increased phosphorylation of LAT and Src family kinases, as well as enhanced IL-2 production (Hashimoto-Tane et al. 2011). Taken together these results indicated a strong link between TCR signalling microclusters and the T cell cytoskeletal network. Different components of the cytoskeleton show temporally distinct roles in the mediation of TCR signalling (Billadeau, Nolz, and Gomez 2007).

4.1.2 Formation of TCR Microclusters

Despite more than a decade of work into the immunological synapse, surprisingly little is known about the early events in synapse formation. In particular, the events leading to the generation of microclusters have been difficult to observe and quantify.

It is well established that a signalling cascade beginning with CD3 ITAM phosphorylation by co-receptor-bound Lck is responsible for initiating TCR signal transduction. This signal is transmitted along the pathway by phosphorylation and activation of ZAP70 and subsequent phosphorylation of the downstream signalling components. However, it is not understood how signals transduced through the interaction of the TCR and pMHC induce the formation of TCR microclusters. A recent study by Taylor et al. (2017) indicated that the dwell time of the TCR-pMHC interaction promotes the formation of clusters. This was shown using DNA-based chimeric antigen receptors with different interaction affinities. Those with higher affinities promoted more receptor clustering. This research also supports the hypothesis that receptor clustering plays a role in ligand discrimination (Taylor et al. 2017). Others have reported somewhat different mechanisms of cluster formation.

It has been proposed that pre-existing microclusters containing the molecules necessary for downstream signalling are already present on naïve T cells (Crites et al. 2014). These pre-existing clusters were described in both naïve and activated murine T cells and were shown to contain the signalling machinery necessary for T cell activation. The formation of such clusters was not dependent on ligand binding as T cells stimulated with non-activating pMHC or MHC-negative surfaces still had pre-existing microclusters on their cell surfaces. This is consistent with work by Schamel et al. (W. W. A. Schamel 2007; W. W. A. Schamel and Alarcón 2013), which suggests that the TCR exists in pre-clustered oligomers on the cell surface. Work done by Paeon et al. (2016) also confirmed the existence of these nanoscale TCR-complex structures, but further advocated for a functional role for these clusters in signal transduction. Pre-clustering of the TCR into functional oligomers on the cell surface with the signal transduction proteins LAT, Lck, and ZAP70 could provide a mechanism for the transduction of signals from rare antigenic peptides on the surface of APCs (Castro et al. 2014). This hypothesis fits nicely with the experimental data shown by Taylor et al. (2017), but does not provide mechanistic insight into nanocluster or microcluster formation. Small platforms of pre-clustered TCR and downstream signalling molecules would increase the probability of a productive re-binding event with low frequency pMHCs. The density of clusters was higher in activated cells suggesting the recruitment of more

molecules and larger complexes were also more likely to include phosphorylated molecules. These nanoclusters aggregate on activation to form signal-transducing microclusters (Pagoon et al. 2016).

Pre-existing microclusters containing the scaffolding protein LAT were also shown by Williamson et al. (Williamson et al. 2011), but in their analysis, it was determined that these pre-existing microclusters did not fulfil a role in signal transduction. Instead, they proposed that the supply of LAT on the plasma membrane was instead supplemented by a vesicular supply of LAT that was responsible for signal transduction. This hypothesis is somewhat difficult to explain, and would need to involve an as-yet-undetermined membrane anchor for the recruitment of vesicular LAT. CD6 may be able to fulfil this role but that remains to be determined (Malissen and Marguet 2011; Bounab et al. 2013). In 2013, the claim that LAT clusters on the plasma membrane did not participate in signalling was directly refuted by Balagopalan et al. Using a chimeric version of LAT that could be tracked from the cell surface, Balagopalan et al. (Balagopalan et al. 2013) were able to show that LAT on the plasma membrane does indeed play a role in TCR-induced signalling and particularly in early signalling. It may be that recruitment of vesicular LAT is instead important in sustaining TCR signalling.

Work by Lillemeier *et al.* seems to indicate a different mechanism of microcluster formation, with the partitioning of different signalling components into separate and non-interacting membrane protein islands. Again, their work suggested the formation of pre-existing protein clusters on the surface of T cells with enhanced clustering on activation. What was striking was that electron microscopy of activated T cells seemed to suggest that LAT and the TCR exist on separate protein islands and that even during activation the interaction of these separate protein islands was only transient (Lillemeier et al. 2010). This work does not seem to agree well with the more recent studies discussed earlier, which suggest a more prolonged interaction between LAT and other microcluster signalling components. It is possible that the dissociation of LAT from the TCR is a mechanism of attenuating input signals and regulating the downstream signalling response. Although there is some contention among groups regarding the exact mechanism of T cell activation these findings point to the key involvement of LAT in microcluster formation and TCR signalling. Cytoskeletal involvement also appears to be critical for complete T cell activation.

4.1.3 LAT is essential for T cell development, function, and immune homeostasis

Membrane bound scaffolding proteins play an integral role in a number of cell surface receptor signalling pathways in a variety of different cell types (Horejsí et al. 2004). They serve as docking hubs for the nucleation and propagation of downstream signalling responses. The role of

LAT as a scaffolding protein in the TCR-induced signalling pathway has been well studied since its initial discovery in 1998 by Zhang *et al.* and by Weber *et al.* (W. Zhang et al. 1998; Weber et al. 1998).

Evidence for LAT as critical in both the positive and negative regulation of T cell signalling can be seen from studies of LAT knockout mice and the recent identification of two highly consanguineous families with allelic variations in LAT resulting in partial or complete loss of protein expression. Studies of LAT knockout mice by Zhang et al. (1999) showed that LAT is important for linking the pre-TCR to the intracellular signalling network. Although these mice appeared relatively healthy – in contrast to other mouse lines deficient in another T cell scaffolding protein SLP76 or the tyrosine kinase Syk, which are characterised by bleeding disorders and platelet deficiencies (Judd et al. 2002; Cornall et al. 2000) – it was shown that the loss of LAT affected primarily T cell development. Specifically both $\alpha\beta$ - and $\gamma\delta$ -T cells were observed to be absent and thymic T cell development was arrested in the CD4/CD8 double negative stage (W Zhang et al. 1999). This phenotype is comparable to mouse TCR knockout lines, which fail to undergo the process of RAG recombination and mature T cell development (Mombaerts et al. 1992). Ultimately, the loss of LAT in early development was responsible for severe immunodeficiency.

Several studies in the early 2000s determined that the role for LAT in maintaining T cell-mediated immune homeostasis was not clear-cut and that LAT is essential for both positive and negative regulation of T cell signalling and activation, as well as differentiation toward particular effector lineages. In 2002, a set of back-to-back studies by Aguado et al. (2002) and Sommers et al. (2002) looked at a mutant variant of LAT in which tyrosine residue 136, which is the binding site for PLC γ 1, was mutated to phenylalanine (Y136F). Using knock-in mouse models bearing the mutant tyrosine motif both groups observed that T cell development was severely inhibited, but not completely blocked. Of note, the negative regulator of T cell activation, CD5, was down regulated during thymic development and upregulated in the periphery (Sommers et al. 2002). This points to the tunability of T cell signalling and the dynamic nature of cell biology. Similar findings have been reported using a mutant of the T cell kinase ZAP70, in which the SKG mutation resulted in a reduced T cell activation threshold and the development of an autoreactive immune response (Sakaguchi et al. 2003; Siggs et al. 2007). Moreover, it was observed that the Y136F mutation resulted in increased T cell infiltration to the liver and spleen as well as lymphopenia, eosinophilia, and an enhanced B cell response (Sommers et al. 2002; Aguado et al. 2002). These results are somewhat surprising and are accounted for by the enhanced T_H2 profile seen in the homozygous mutant mice. These results indicate that LAT is involved in both the positive and negative regulation of the T cell activation process. These findings were later confirmed using a Cre-

inducible LAT knockout system (Shen et al. 2009). In these experiments mice heterozygous for LAT Y136F and a wildtype LAT flanked by *loxP* were treated with a Cre-recombinase via lentiviral transduction resulting in normal thymic T cell development, but mature T cells in which signalling competent LAT had been ablated. When transferred back into T cell deficient mice the LAT Y136F cells caused splenomegaly and lymphadenopathy, and were characterised by a potent T_H2 effector profile. Again, these results suggest that LAT also mediates an important negative regulatory role in T cell activation.

Work by Nuñez-cruz *et al.*, (2003) looked at the role of the 3 C-terminal tyrosine residues in T cell development. Mutation of tyrosines 175, 195, and 235 in mice resulted in the complete block of $\alpha\beta$ T cell development and a partial block in $\gamma\delta$ T cell development. Interestingly the $\gamma\delta$ T cells that did develop had a phenotype skewed toward T_H2, which resulted in increased IgG1 and IgE production with splenomegaly and enlarged lymph nodes (Nuñez-Cruz et al. 2003). These results further validate the role of LAT in immune regulation and homeostasis.

The significance of LAT as important in T cell activation is further confirmed by the identification of two consanguineous families with separate LAT frameshift mutations. The first case presented with three siblings homozygous for a 2-bp deletion in LAT resulting in a truncated version of the protein, but with intact extracellular and transmembrane domain. The mutation resulted in the loss of Y132, Y171, Y191, and Y226, but seemed to retain enough signalling capacity through the other tyrosines to induce T cell development. The three siblings presented with chronic infection and autoimmunity characterised by hepatosplenomegaly, lymphadenopathy and red oedematous nodules on the forearms (Keller et al. 2016). These findings were not unlike those seen in the mouse models of LAT. The second mutation was caused by a 1bp insertion in exon 1 of the LAT gene. The 5 members of the consanguineous family homozygous for this mutation presented with complete loss of LAT and severe immunodeficiency. The patients had extremely low T cell numbers, but B cell and NK cell development was apparently unaffected (Bacchelli et al. 2017) highlighting the role of LAT specifically in the development of T cells.

Conversely, upregulation of LAT expression has also been linked to severe pathologies. Patients with Severe Aplastic Anaemia (SAA) have been reported to show increased total LAT and phosphorylated LAT, as well as increased ZAP70 activation (Sheng et al. 2014). The upregulation of LAT was linked to increased perforin and granzyme B expression in CD8⁺ T cells. Moreover the immune polarization of SAA patients is skewed toward a T_H1 response with enhanced IL-2 and IFN- γ expression.

Taken together, the mouse and human studies of LAT indicate the critical role that this scaffolding protein plays in mediating T cell development, function and immune polarisation. Although the dynamic nature of cell signalling is able to compensate for mutations in LAT to a certain extent, it would appear that the necessity for LAT to fulfil varying roles during T cell development and in the periphery mean that mutations resulting in loss of wildtype LAT function diminishes the capacity of T cells to fulfil their roles appropriately. Dysregulation of LAT can result in both autoimmunity and immunodeficiency.

4.1.4 LAT localisation and function

LAT is a type III membrane protein, which are similar to Type I membrane proteins in that they have a cytosolic c-terminus. However, unlike type I membrane proteins, type III membrane proteins lack a signal peptide sequence and instead have a palmitoylation sequence that allows for lipidation and anchoring of the protein at the plasma membrane (W Zhang, Tribble, and Samelson 1998). In LAT, this lipidation site is comprised of a pair of N-terminal cysteine residues. Substitution of the palmitoylation site for other membrane anchoring motifs has been shown not to affect LAT's function (M. Hundt et al. 2006; Zhu et al. 2005; M. Hundt et al. 2009), but preventing LAT from associating with the plasma membrane through mutation of the two cysteine residues (C26 and C29) in the palmytolaytion motif results in a complete block of LAT-mediated signalling activity (J. Lin et al. 1999). Loss of these palmitoylation sites has also been shown to make LAT more susceptible to degradation (Gringhuis et al. 2000). Thus we reasoned that by controlling the intracellular position of LAT we would be able to modulate the LAT-mediated signalling pathway.

4.1.5 Molecular interaction partners link LAT to downstream effectors

LAT is a critical component of TCR microclusters and regulates the nucleation of downstream TCR signal-associated molecules. LAT-deficient T cell lines were shown to have abrogated signalling along the MAPK axis, defective calcium mobilisation and failure to upregulate markers of T cell activation (Finco et al. 1998; Pasquet et al. 1999; Bunnell et al. 2002). These processes are linked to LAT via a diverse array of signalling cascades and protein-protein interactions. Super-resolution microscopy of T cells on activating surfaces indicate that LAT is recruited to signalling clusters within seconds (Bunnell et al. 2002).

At the molecular level LAT has been shown to interact directly or indirectly with an expansive network of signalling proteins in T cells. LAT contains 233 amino acids and is predicted to have no intrinsic enzymatic function. Its role in T cell activation is mediated by nine phosphorylatable tyrosine motifs that allow for interaction with SH2 domain-containing proteins (Wonerow and Watson 2001; Roncagalli et al. 2014). LAT is phosphorylated immediately downstream of the TCR-associated kinase ZAP70 (Paz et al. 2001). Affinity Purification Mass Spectroscopy (AP-MS) analysis of the LAT and SLP76 'signalosome' identified dozens of diverse protein interactions in a network formed by protein and lipid kinases, phosphatases, Guanine nucleotide Exchange Factors (GEFs), E3 ubiquitin ligases and phospholipases (Salek et al. 2013; Roncagalli et al. 2014). The TCR signalling network showed significant enrichment for proteins containing SH2, SH3 and pleckstrin-homology domains. Below are described some of the more well-characterised LAT signalling partners.

One important mediator of T cell activation is the multi-domain protein, phospholipase C- γ 1 (PLC- γ 1). This protein has been shown to interact directly with LAT, but it is thought that multivalent interactions with SLP76 and Vav1 are responsible for positioning PLC- γ 1 in the correct orientation for optimal function (Knyazhitsky et al. 2012). PLC- γ 1 hydrolyses phosphatidylinositol 4,5-bisphosphate (PIP₂) to form 1,4,5-triphosphate (IP₃) and diacylglycerol (DAG) (Fu et al. 2010). The formation of IP₃ is detected by IP₃ Receptors (IP3Rs) on the endoplasmic reticulum, promoting the release of intracellular calcium stores (Nagaleekar et al. 2008). Once intracellular stores of calcium are depleted, extracellular calcium influx is triggered through the Orai1-STIM pathway (Y. Zhou et al. 2010). This sustained calcium signal is necessary for the activation of the NFAT (Nuclear Factor of Activated T Cells) transcription factor, which is necessary for regulating the expression of genes associate with T cell activation (Oh-hora 2009).

In parallel to the IP₃ signals, DAG also serves as a secondary messenger to activate Ras guanyl-releasing protein 1 (RasGrp1) and PKC θ signal transduction (J. P. Roose et al. 2005). RasGrp1 and SOS1, which associates with LAT via Grb2 (Growth-factor-receptor-bound protein 2), function together in a positive feedback system to increase Ras activation and subsequent MAP kinase pathway signalling (J. P. Roose et al. 2007). Of note, the interaction between SOS1, Grb2, and LAT has been proposed as a mechanisms of LAT oligomerization as SOS1 interacts with 2 Grb2 molecules and thus bridges the interaction of two LAT molecules (Houtman et al. 2006). SOS1 and Grb2 constitutively interact with one another and are recruited to LAT simultaneously (Buday et al. 1994). Grb2 is also thought to recruit the signal titrating molecule, Themis into the LAT signalosome (Paster et al. 2013).

Activation of PKC θ signalling is also indispensable for productive T cell activation. Cellular depletion or pharmacological inhibition of PKC θ results in the inhibition of T cell activation (Altman and Villalba 2002). It has been shown that PKC θ exerts its function on T cell activation through the activation of JNK and subsequent downstream signalling to the AP-1 transcription factor (Ohtsuka, Kaziro, and Satoh 1996). AP-1 is involved in the transcription of genes involved in T cell activation, for example interaction between AP-1 and NFAT drive *IL2* gene expression.

LAT also interacts with another member of the Grb2 family, Gads (Grb2-related protein downstream of src). Gads is structurally similar to Grb2, but has a unique glutamine- and proline-rich domain (O. Moran et al. 2008). Gads bridges the interaction between LAT and SLP76 (Harkiolaki et al. 2003), another scaffolding protein whose presence is essential for T cell activation (Yoder et al. 2001). SLP76 interacts with Vav1, Nck, and ITK and is involved in mediating and regulate further downstream signalling via Rap1 and PLC γ 1 (Zeng et al. 2003).

SLP76 is a particularly important protein in the TCR signalling network because it provides a link to the actin cytoskeleton. The interaction between Nck, Vav1, Cdc42 and SLP76 recruits the actin reorganising protein WASp (Wiskott Aldrich syndrome Protein) (Zeng et al. 2003; Barda-Saad et al. 2005). Wiskott Aldrich syndrome (WAS) is an X-linked genetic condition with a strong immune phenotype. Loss of WASp results in an increased risk of eczema and inflammatory disease as well as susceptibility to infection (Notarangelo, Miao, and Ochs 2008). Mouse knockout models seem to accurately recapitulate the WAS phenotype and give rise to T cells with impaired migratory capacity that fail to form a polarising immunological synapse (Cotta-de-Almeida et al. 2007). WASp activates the Arp2/3 complex via its verprolin homology, central acidic (VCA) domain to facilitate actin reorganisation at the immunological synapse a process reviewed in detail by Millard, Sharp, and Machesky (2004). More recently, Vav1 was reported to participate in this protein complex in a scaffolding capacity, as GEF activity-deficient Vav1 is still recruited to the multiprotein complex and still facilitates T cell activation (Miletic et al. 2009). WASp has also been proposed to form de novo actin foci that help regulate the activity of PLC γ 1 (Kumari et al. 2015) and thus plays an important role not only in actin remodelling, but also TCR-induced signalling.

Finally, in a 12-component cell-free reconstitution system, Su and Ditlev showed that induction of CD3 phosphorylation results in the spontaneous formation of downstream signalling components into clusters (Su et al. 2016). This finding is interesting as it indicates that the formation of clusters within the TCR signalling network appears to be an intrinsic property of the system. Although this result indicates that the cytoskeleton and LAT seems to have an important role in the formation of TCR signalling microclusters *in vitro*, it does not fully explain the formation

of such signalling platforms *in vivo*. In this study, multimeric protein complexes were also found to exclude CD45.

4.1.6 Negative regulation of LAT

Ubiquitination is an important process in cell homeostasis and protein degradation and LAT is also subject to this process. Ubiquitination of LAT has been proposed to occur on two lysine residues, K52 and K204 (Balagopalan et al. 2011). The ubiquitination of LAT has been proposed as a mechanism of TCR internalisation and signal termination (Brignatz et al. 2005). Cells in which these residues were mutated showed an enhanced propensity for signalling and prolonged activation (Kunii et al. 2012; Balagopalan et al. 2011). The ubiquitination of LAT appears to be dependent on its association with c-Cbl, an E3-ubiquitin ligase. Grb2 mediates the LAT-c-Cbl, but this complex may be stabilized through interactions with PI3K and Nck (Balagopalan et al. 2007).

4.1.7 LAT as the basis for an optogenetic switch

In an attempt to explain the early events and signalling dynamics involved in early T cell activation I developed and tested a number of LAT based optogenetic tools (Chapter 3). LAT was selected as a good candidate for our optogenetic systems because of its lack of intrinsic enzymatic activity and requisite membrane proximity to fulfil its scaffolding function. LAT is also unstructured and the results presented in Chapter 3 indicate that when combined with the LOVTRAP, TULIPs, or CRY2 optogenetics systems it is correctly localised on blue light irradiation and can be controlled with tunable interactions kinetics. LAT is also reported to be phosphorylated early during TCR-induced signalling and is an important component of signalling microclusters, thus controlling the cellular position of LAT provides a means of controlling the TCR signalling process early in activation (Huse et al. 2007).

4.2 Materials & Methods

4.2.1 Cas9-mediated gene knockout

Two sets of Cas9 guide RNAs were designed against the transmembrane region of LAT using the Zhang lab CRISPR design tool (Cong et al. 2013). The guide sets are as follows:

Pair	Name	Sequence
1	LAT-CRISPR1_Forward	5'-caccgatcctgggtcccctgcgtgct-3'
1	LAT-CRISPR1_Reverse	5'-aaacagcacgcaggggaccaggatc-3'
2	LAT-CRISPR2_Forward	5'-caccgatctgaggatgtgctctcgt-3'
2	LAT-CRISPR2_Reverse	5'-aaacacgacagcacatcctcagatc-3'

Table 4.1: LAT, CRISPR gRNA oligos

The pHR-Cas9-GFP vector (Appendix B) was linearised according to the manufacturer's protocol (NEB) using the following reaction:

Reagent	Volume (μl)
BsmBI (NEB)	1.5
Buffer 3.1 (NEB)	5.0
Cas9 Vector (200ng/μl)	15.0
dH ₂ O	28.5

Plasmid was incubated with BsmBI restriction enzyme at 55°C for 1 hour and gel purified as outline in Chapter 2. Guide oligo pairs were prepared according to the following reaction:

Reagent	Volume (μl)
Forward oligo (100 μM)	1.0
Reverse oligo (100 μM)	1.0
T4 Ligation buffer	1.0
dH ₂ O	7.0

Guide oligos were annealed in the thermocycler at 37°C for 30 minutes, followed by 5 minutes at 95 °C. The temperature was then reduced to 25°C at a rate of 5°C/min. Annealed primers were diluted 1:100 in dH₂O for use in cloning reaction. The complete cloning and transformation procedure can be found in Chapter 3.1 'Bacterial Cloning'. Cas9 plasmids were screened for gRNA oligo insertion by sequencing (primer JJ2187):

5'-ctcgagcggccggcccccttcaccgagggcctatcttcccatgattcc-3'

Jurkat E6.1 cells were serially transduced through two rounds of lentiviral transduction with pHCr-[LAT]-GFP vectors according to the protocol outline in Chapter 2.5 'DNA

transfection and 'Transduction'. Transduced Jurkat E6.1 cells were single cell sorted into a 1:1 mixture of fresh complete RPMI and spent, filtered complete RPMI using a Sony iCyt Synergy Dual Channel, High Speed Cell sorter. Spent RPMI was prepared by centrifuging 12.5 ml of wildtype Jurkat-containing RPMI two days after split to remove the majority of cells. The cell pellet was discarded and media was passed into a fresh 50 ml Falcon tube through a 0.45 μ m syringe filter to remove any remaining suspension cells. Spent media was then mixed with fresh complete RPMI and 50 μ l was transferred into each well of two 96-well plates (Gibco). Transduced Jurkats were single cell sorted according to GFP expression. The top 15% of GFP-expressing cells were sorted and the rest discarded. Following sorting, 96-well plate was centrifuged at 1200 rpm for 3 minutes to settle cells.

Cas9-mediated LAT knockout Jurkat clone cell lines were selected on their inability to flux calcium and on TCR expression. Protocols for these procedures are outline in Chapter 2.7 'Flow Cytometry'. Cells unable to flux calcium, but with parental levels of TCR expression were again single cell sorted and expanded to create a single LAT-specific knockout Jurkat clone line. Immediately following expansion, liquid nitrogen stocks of the Jurkat LAT-specific knockout cell lines were prepared to preserve their phenotypes.

4.2.2 Design of Specialised DNA fragments

Signalling incompetent LAT was designed with the flanking primer binding sequences for the primer oligos JJ1166 and JJ1167 (Appendix A). The construct was also designed with a 5' SpeI cut site and a 3' BamHI cut site as well as point mutations to avoid targeting by Cas9.

4.3 Results

4.3.1 Chronic LAT depletion prevents phenotypic rescue of JCam2.5 cell line

In chapter 3 a number of LAT-based optogenetic tools are outlined. These tools were designed based on two existing systems, the LOVTRAP system and the TULIPs system. In both systems the LOV domain is anchored to the cytoplasmic side of the plasma membrane via the transmembrane domain of LAT. The cytoplasmic domain of LAT, with its nine phosphorylatable tyrosines, is fused to the C-terminus of either the Zdk domain or the ePDZ domain. To test the capacity for these systems to reconstitute downstream signalling in T cells I initially used the previously described JCam2.5 cell line (W. Zhang et al. 1999). These cells are derived

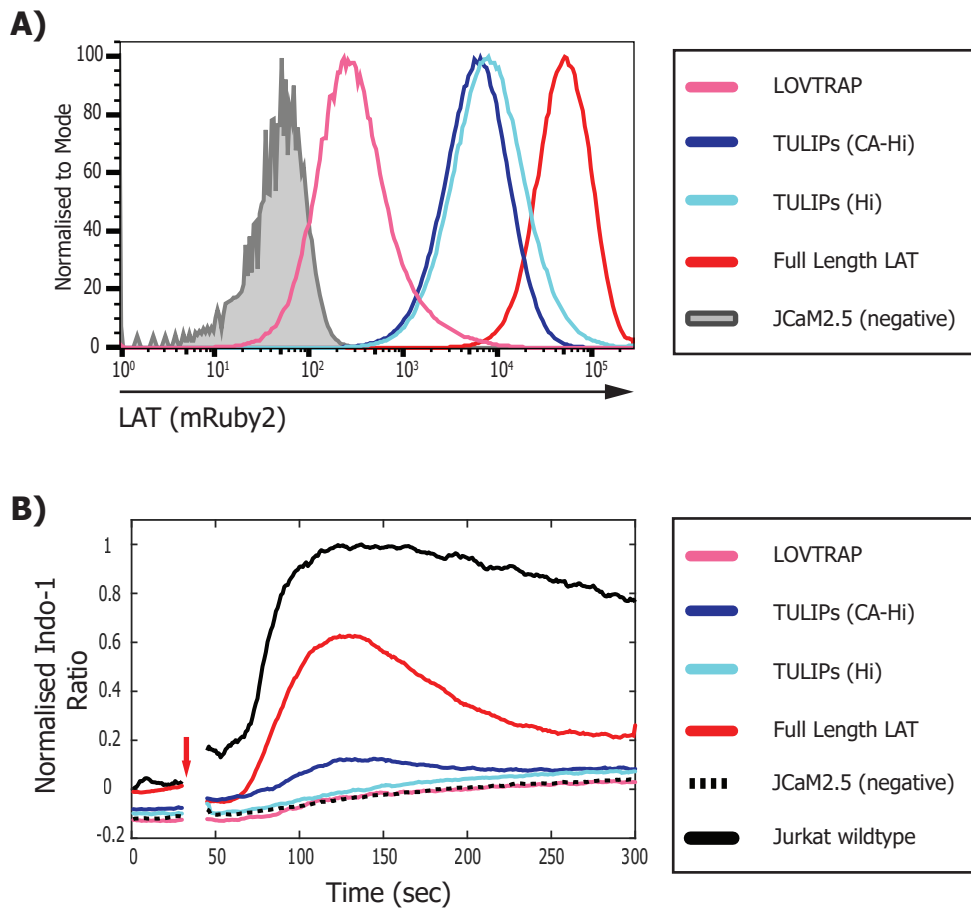


Figure 4.1 Characterising the TULIPs and LOVTRAP system in JCaM2.5 cells

(A) JCaM2.5 LAT-deficient Jurkat E6.1 cells were transduced with IRES vectors with either the LOVTRAP or TULIPs systems. To validate the system I first tested the constitutively active version of the TULIPs system with the high affinity PDZ domain (CA-Hi). I also tested the wildtype version of the construct (LOVpep) with the high affinity PDZ domain (Hi). As a positive control I transduced the JCaM2.5 cell line with the wildtype full-length version of LAT. Each of the LAT constructs was tagged with an N-terminal mRuby2 fluorescent tag. **(B)** Once transduced with the LAT constructs, calcium flux was measured ratiometrically using Indo-1 dye. JCaM2.5 cells were labelled with anti-CD3 antibodies and a baseline reading was established for 30 seconds. A polyclonal IgG crosslinking antibody was added at 30 seconds (red arrow) to trigger the cells. Flux profiles are representative of $n=3$ (technical replicates).

from the commonly used model T cell system, Jurkat E6.1, and were generated through random chemical mutagenesis. JCaM2.5 cells are LAT-deficient and fail to initiate signalling on TCR ligation.

Reconstitution of JCaM2.5 cells with the optogenetic LAT constructs and full length LAT resulted in highly variable LAT expression (Figure 4.1A). Once expression of the constructs had been confirmed, I wanted to test if the optogenetic LAT systems could reconstitute downstream signalling. The JCaM2.5 cell line was initially characterised by its inability to flux calcium and it has been reported that reconstitution of JCaM2.5 cells with LAT rescues this phenotype (W. Zhang et al. 1999). This was found not to be the case. Reconstitution of JCaM2.5 cells with full length LAT only partially rescued the calcium flux phenotype (Figure 4.1B). Moreover, I was unable to detect calcium fluxing in both the high affinity, constitutively active version of the TULIPs system and the LOVTRAP system in the dark state.

It has previously been reported that chronic depletion of LAT results in a drop in TCR surface expression (Myers, Zikherman, and Roose 2017). I confirmed this to be the case in our JCaM2.5 cell line (Figure 4.2). In an attempt to isolate a population of JCaM2.5 cells with high TCR surface expression I sorted cells on their surface CD3 ϵ expression by flow cytometry. The TCR α and β subunits form an obligate heterodimer with the CD3 and thus it can be used as a direct readout of TCR expression. The top 10% highest expressing cells were isolate. Despite gating on those cells expressing relatively high amounts of the TCR complex, I found that by the time I had re-expanded the population TCR surface expression had again diminished. To confirm that TCR deficiency was cell line-specific, the Acuto lab kindly provided us with a vial of JCaM2.5 cells from their own stock. The results presented in Figure 4.2 confirm a ~10-fold drop in TCR expression in the JCaM2.5 cell line relative to the Jurkat parental cell line. This finding helps explain why the JCaM2.5 cells do not signal as expected when expressing the full length LAT construct.

4.3.2 Development of a LAT-specific knockout Jurkat E6.1 cell line

Given its obvious problems as a model system, I abandoned the JCaM2.5 cell line and returned to the Jurkat parental cell line. Using CRISPR-Cas9 technology I created a LAT-specific knockout cell line. Two sets of gRNAs were designed against the first and second exons of LAT, which comprise the transmembrane motif of LAT. The Cas9 plasmid jointly expresses the selection marker GFP via a viral P2A sequence. Thus, following serial transduction of the Jurkat cell line with Cas9 and guides, I was able to single cell sort based on GFP expression to create

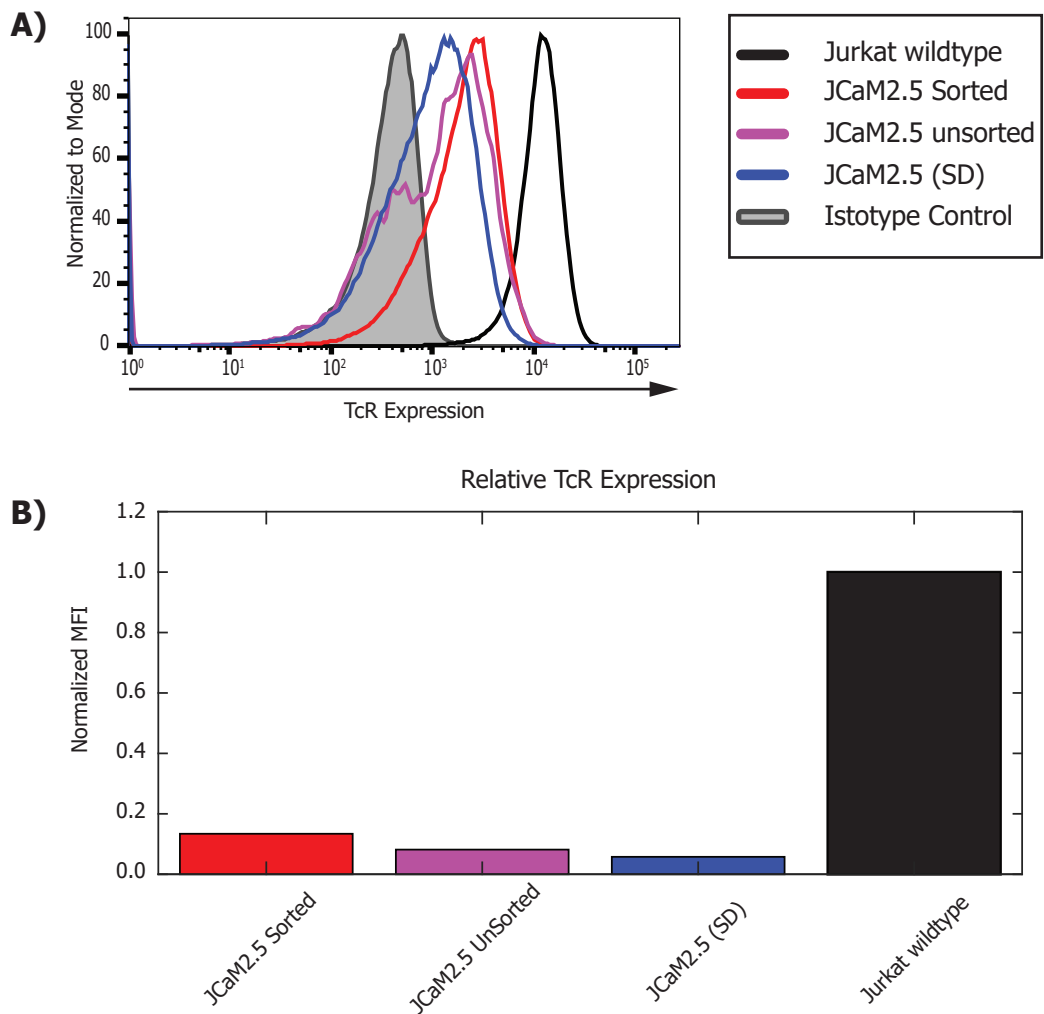


Figure 4.2 Chronic depletion of LAT results in decreased TCR surface expression (A) The TCR complex was labelled with anti-CD3, AF647-conjugated antibodies. JCaM2.5 cells from two separate lines both showed decreased TCR surface expression. When sorted on high TCR expression, the JCaM2.5 cells rapidly returned to baseline. **(B)** TCR expression relative to the Jurkat E6.1 cell line shows that the JCaM2.5 cells express considerably less TCR on their cell surface. FACS plots are representative of at least 3 separate experiments.

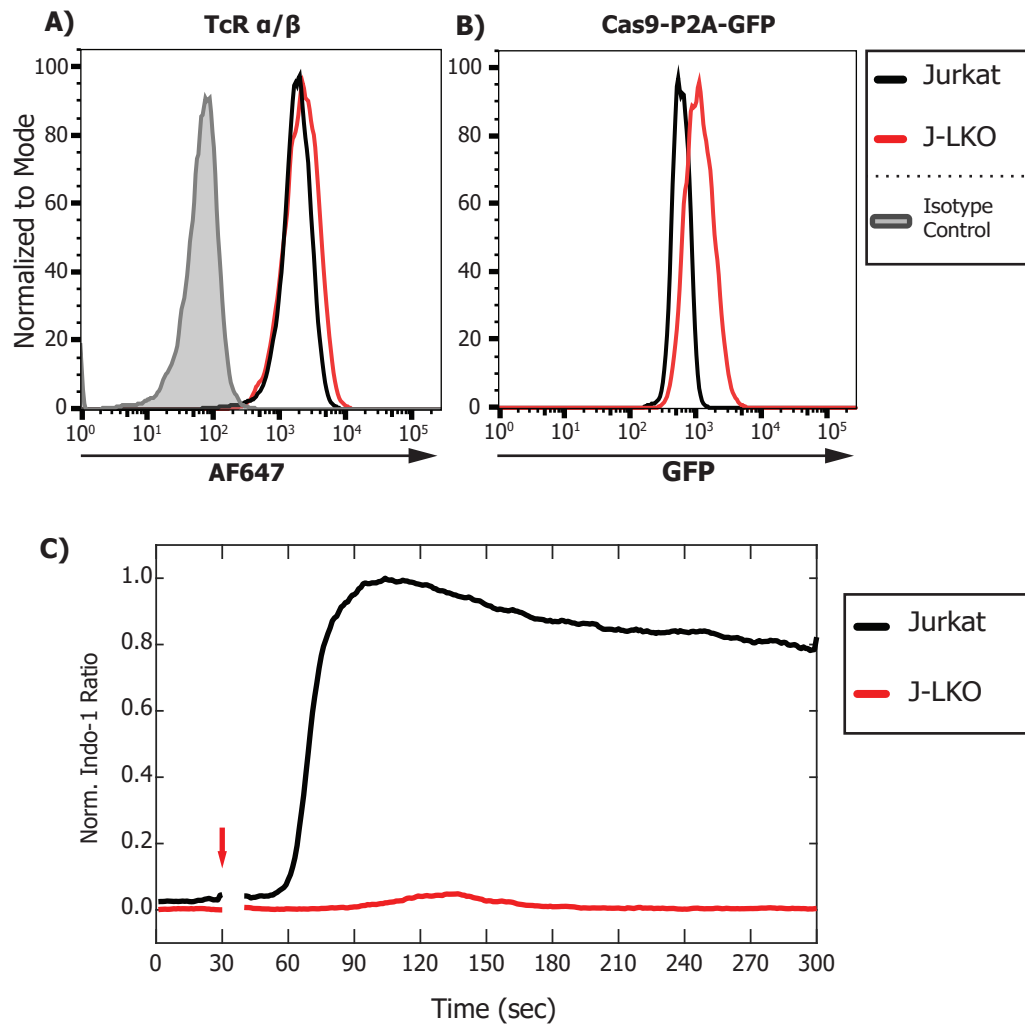


Figure 4.3 Characterisation of a LAT-specific Knockout Jurkat E6.1 cell line (A) CRISPR-Cas9 technology was used to specifically disrupt LAT in the Jurkat E6.1 T cell line. TCR surface express remained unchanged relative to the parental cell line as measure using AF647-conjugated, anti-CD3 antibodies. **(B)** The Cas9 vector coexpressed GFP as a marker. GFP expression was found to be low relative to the parental line. **(C)** Calcium fluxing was measured ratiometrically using Indo-1 dye. Polyclonal crosslinking antibody was added at 30 seconds to initiate fluxing (red arrow). The LAT knockout cell line (J-LKO) does not flux calcium (red).

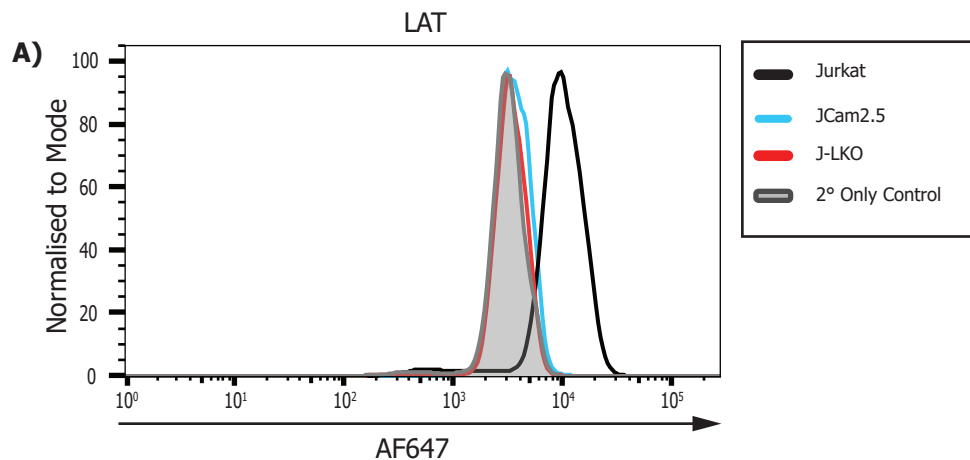
a library of LAT knockout CRISPR clones (Appendix G). Given that absence of LAT has previously been described to attenuate calcium fluxing, I screened the library of CRISPR LAT knockout Jurkat cells ability to flux calcium and on surface TCR expression. After two rounds of single cell cloning I was able to identify one clone that was both unable to flux calcium and retained wildtype levels of surface TCR expression (Figure 4.3). This cell line will herein be referred to as J-LKO (Jurkat E6.1-LAT Knockout).

To confirm that the calcium flux phenotype that I observed in the J-LKO clone was caused by loss of LAT I performed flow cytometry with intracellular staining for LAT. The results presented in Figure 4.4A show that the J-LKO cells overlay with the secondary-only control and the previously described LAT knockout cell line, JCaM2.5. I also attempted to confirm ablation of LAT by immunoblot assay, but was unable to obtain a signal. This was most likely due to the relatively low expression of LAT and use of a monoclonal antibody for immunoblotting (Appendix H). Genomic sequencing of the indel sites confirmed with a high degree of certainty ($P = 0.968$) that the Jurkat parental cells are homozygous for LAT, at least within the first two exons, and that the J-LKO cell line had a frameshift mutation in each of the LAT alleles, each resulting in a premature stop codon and truncation of LAT (Figure 4.4B). Allele 1 was predicted to generate a 41 amino acid protein fragment and Allele 2, a 45 amino acid protein fragment. Transmembrane prediction software⁶ further confirmed that the two truncated LAT variants, if expressed, would be unlikely to localise to the plasma membrane (Figure 4.5).

It is worth noting that while TCR surface expression was initially high in the J-LKO cells I did observe a gradual decrease in expression over time (Appendix I). This suggests that chronic absence of LAT is responsible for the drop in TCR expression and confirms the phenotype seen in the JCaM2.5 cell line. This result also suggests that tonic signals through the TCR are necessary to drive TCR surface expression in a positive feedback loop.

This result represents the first LAT-specific Knockout Jurkat E6.1 cell line. The original JCaM2.5 cell line shows decreased TCR expression due to the loss of LAT. Interestingly, transduction of the JCaM2.5 cells with full length LAT only partially rescued their flux phenotype. This may suggest that the amplitude of the downstream calcium signal and ability to sustain signalling is proportional to TCR expression. The presence of chronic mutations outside of the LAT locus process may offer an alternative explanation for the observed phenotype of the JCaM2.5 cell line.

⁶ <http://www.cbs.dtu.dk/services/TMHMM/>



B)

Exon 1

WT: 5' - ATCCTGGTCCCCTGCGT-GC----TG-3'

I L V P C V L

J-LKO Allele 1: 5' - ATCCTGGTCCCCTGCGT**C**GC----TG-3'

I L V P C V R

J-LKO Allele 2: 5' - ATCCTGGTCCCCTGCGT-GC**GTG**CTG-3'

I L V P C V R A

Exon 2

WT: 5' - TACG-----ACAGCACATCCTCAGAT-3'

Y D S T S S D

G10F2 Allele 1: 5' - TAC-----AGCACATCCTCAGAT-3'

L G H I L R

G10F2 Allele 2: 5' - TACG**GAATCC**ACAGCACATCCTCAGAT-3'

L R N P Q H I L R

Figure 4.4 Confirmation of LAT knockout at the protein and genetic level (A)

To confirm the absence of LAT I used intracellular FACS staining with a primary, unconjugated anti-LAT antibody and an AF647 conjugated secondary antibody. The known LAT-deficient Jurkat cell line, JCam2.5 was used as a positive control (cyan). **(B)**

Sequencing of the CRISPR indel site confirmed that both allele of LAT had a frame shift mutation, which disrupts the LAT coding sequence. Shown here are the DNA basepair sequences and corresponding single letter amino acid codes.

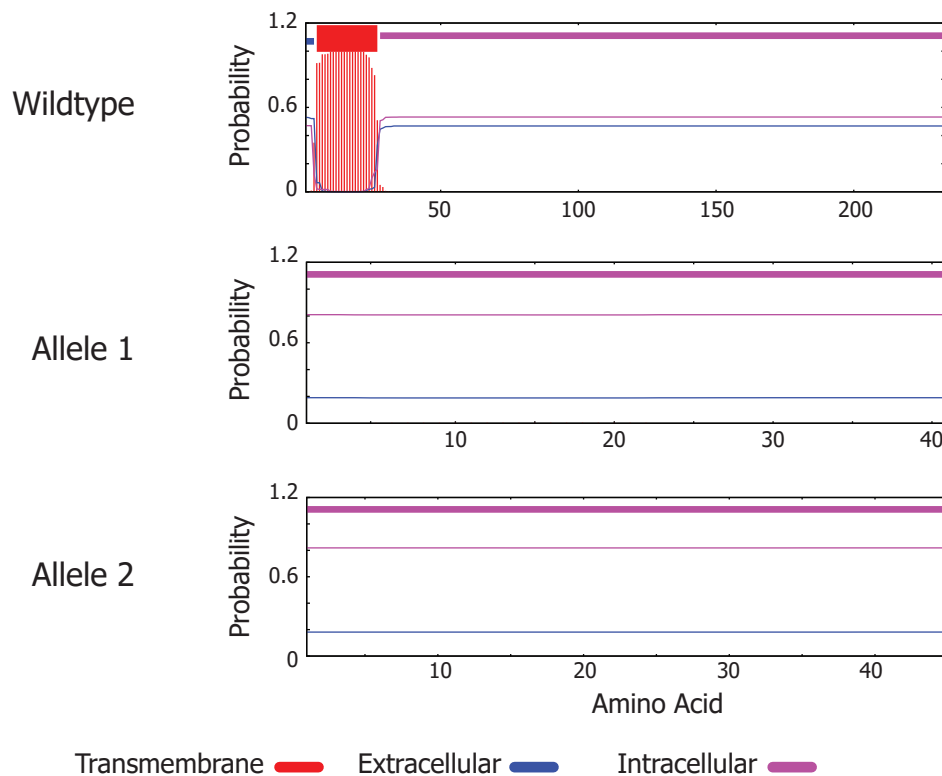
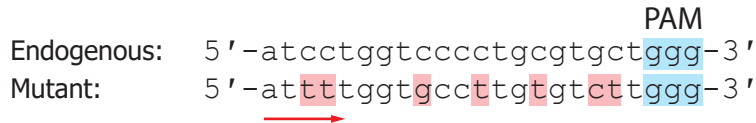


Figure 4.5 LAT frameshift mutations lead to truncated LAT protein The DTU Bioinformatics SignalP 1.4 Server software was run on the predicted single amino acid sequences of the Cas9-altered LAT alleles. The wildtype LAT sequence is shown above for reference. Both Cas9-mediated frameshift mutations resulted in LAT truncations, both of which are expected to give rise to polypeptides lacking a transmembrane motif.

CRISPR target sequence 1:

Endogenous: 5'-atcctggtccccctgcgtgctggg-3' PAM
Mutant: 5'-at^{ttt}ggt^{gcct}gtgt^{ctt}ggg-3'



CRISPR target sequence 2:

Endogenous: 5'-^{tcc}tacgacagcacatcctcagat-3' PAM
Mutant: 5'-^{agt}tacgacagcacatcctcagat-3'

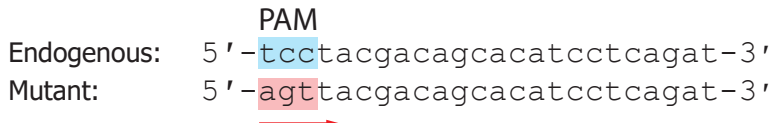


Figure 4.6 Generating a CRISPR-proof LAT variant as the J-LKO cell line constitutively expresses Cas9 I made a series of point mutations to the PAM site and gRNA binding site of both of the LAT-CRISPR binding sites. The PAM sites are show in blue, the synonymous point mutations are highlighted in red.

4.3.3 Optogenetic systems partially rescue LAT knockout phenotype

Before the J-LKO cell line could be reconstituted with LAT, I made a series of point mutations to prevent the constructs from being targeted by the Cas9 enzyme. Cas9 is restricted in its activity by the necessity for a flanking protospacer adjacent motif (PAM), most commonly 5'-NGG-3' (Kleinstiver et al. 2015). Mutations that alter the PAM site prevent Cas9 activity. I was able to identify a synonymous mutation in the second CRISPR target site which would knock out the PAM site, but the first target site could not be modified in this way. Instead, I made synonymous point mutations in 7 of the 20 base pairs along the gRNA binding sequence (Figure 4.6).

Once the J-LKO cell line had been fully characterised for the absence of LAT, the cells were lentivirally transduced with the optogenetic constructs. As discussed in the Chapter 2 Materials & Methods the two component optogenetic systems were jointly expressed on the same vector using an IRES sequence. The LATint components were labelled with a C-terminal mRuby2 fluorescent tag. Expression of different variants of the TULIPs system yielded comparable levels of protein expression, however expression of the LOVTRAP system was considerably lower (Figure 4.7).

Unlike the JCaM2.5 cell line, reconstitution with the full length wildtype LAT protein was sufficient to rescue the LAT knockout phenotype of the J-LKO cells (Figure 4.8). To test the capacity for the LOVTRAP system to reconstitute downstream signalling I measured calcium fluxing under continuous dark conditions. In this state, it would be expected that the LATint construct would be present at the plasma membrane. Engagement of the TCR by antibody crosslinking was sufficient to trigger a small but detectable calcium flux. Interestingly, the calcium flux profile was improved in cells that had been serially transduced twice with the LOVTRAP-IRES system (Figure 4.9). However, neither singly nor doubly transduced cells showed a flux profile comparable to the parental Jurkat cell line.

As described by Strickland et al. (2012), I tested the TULIPs optogenetics system using a constitutively active version of LOVpep with the high affinity variant of the ePDZ domain, ePDZb1. It was reasoned that this would be most likely to recapitulate TCR-induced signalling. As with the LOVTRAP system, a small but detectable calcium flux was detectable using the constitutively active TULIPs system. As would be expected, no flux was detected with the light-inducible variant under the continuous dark conditions tested (Figure 4.10).

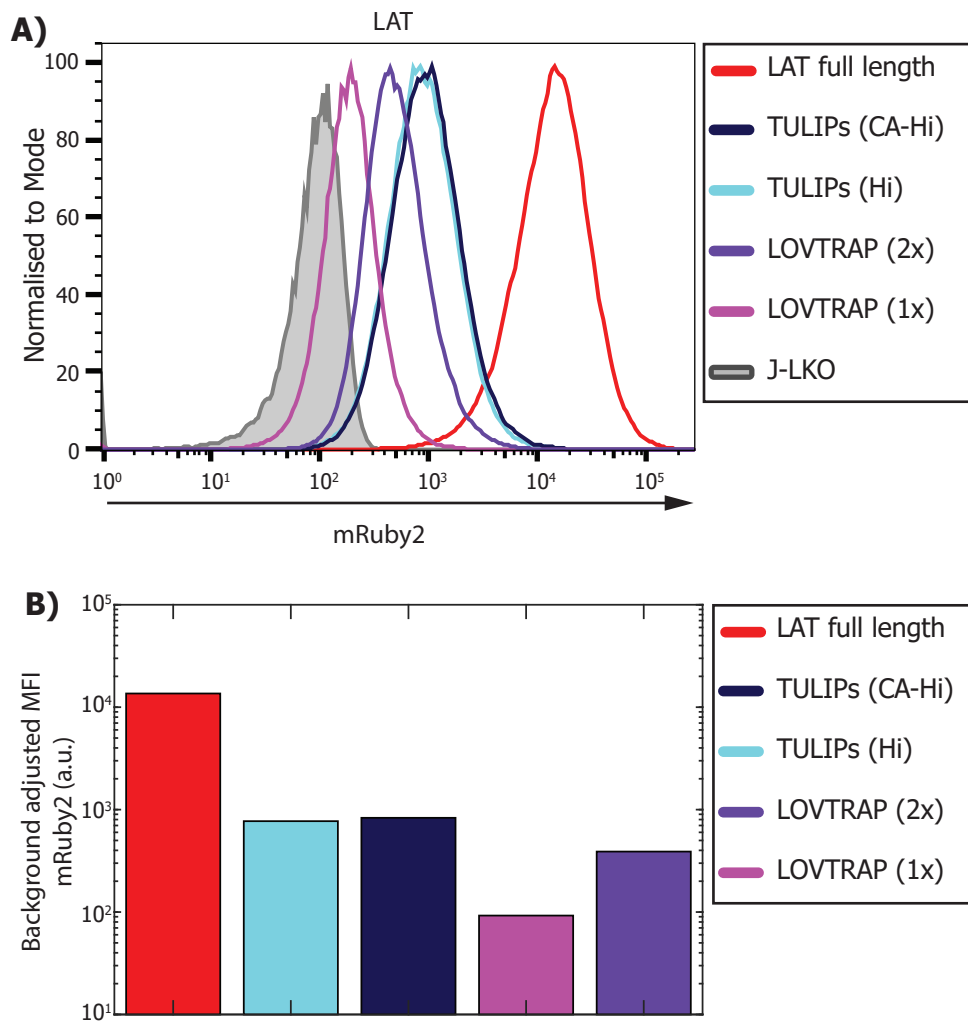


Figure 4.7 Expression of the LAT IRES constructs in J-LKO cells (A) J-LKO cells were transduced with the IRES variants of the TULIPs and LOVTRAP constructs. To first evaluate the system, the cells were transduced with the constitutively active version of the TULIPs construct and high affinity PDZ domain (CA-Hi). Likewise, I also transduced the cells with the LOVpep high affinity version of the system. As expression of the LOVTRAP system was low, I serially transduced the J-LKO cells twice with the LOVTRAP construct. Expression levels were quantified by expression of the mRuby2, fluorescent tag. (B) Here, mRuby2 expression is represented as a bar chart to highlight the differences in expression between the various constructs. Full-length LAT was used as a control. FACS plots are representative of at least 3 separate experiments.

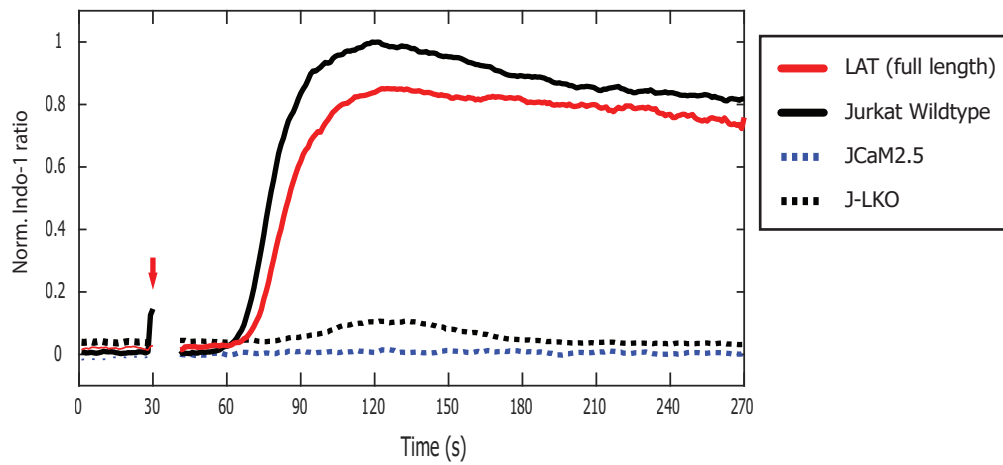


Figure 4.8 Reconstitution with full-length LAT rescues J-LKO phenotype Reconstitution of the J-LKO cell line with full-length, CRISPR-proof LAT rescued the calcium flux phenotype (red). Calcium flux was measured ratiometrically with indo-1 dye and normalised to the Jurkat E6.1 parental control. Calcium fluxing was triggered by antibody crosslinking at 30 seconds (red arrow). Flux profiles are representative of $n = 5$ (biological replicates). The LAT-rescued J-LKO cells consistently retained their flux capacity, even following cryopreservation and thawing.

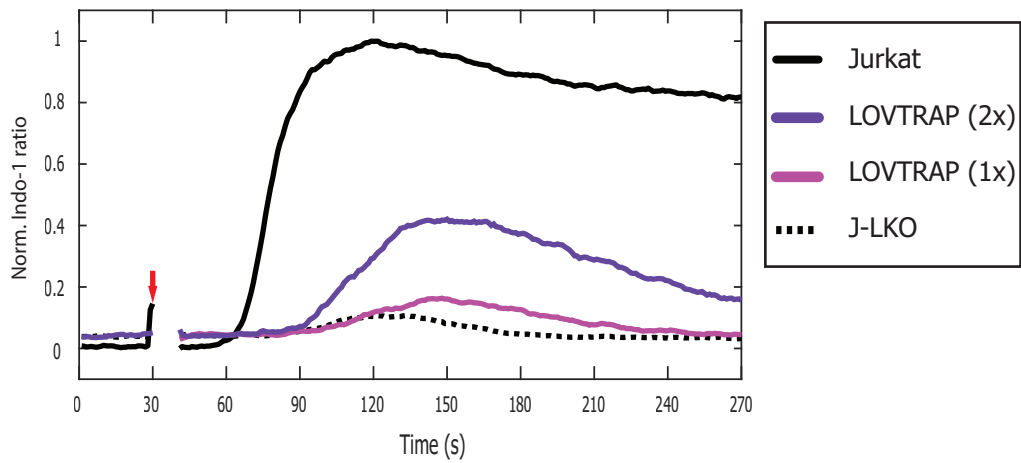


Figure 4.9 reconstitution of J-LKO cells with LOVTRAP IRES system partially rescues calcium flux phenotype J-LKO cells transduced with the CRISPR-proof LOVTRAP-LAT system were tested for their ability to flux calcium. Calcium fluxing was measured ratiometrically using indo-1 dye and normalised to the Jurkat E6.1 positive control. J-LKO cells were transduced either one or twice with the IRES version of the LOVTRAP system. Antibody crosslinking was used to trigger calcium fluxing at 30 seconds (red arrow).

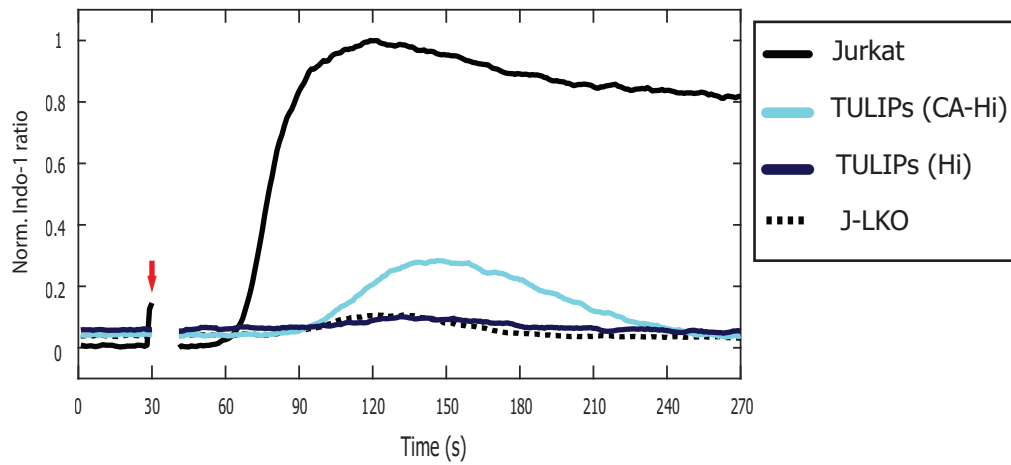


Figure 4.10 LAT-TULIPs IRES system partially rescues J-LKO calcium flux phenotype J-LKO cells were transduced with either the LOVpep or the constitutively active version of the TULIPs system, both with the high affinity version of the PDZ domain (ePDZb1). Calcium fluxing was measured ratiometrically with indo-1 dye and normalised to the Jurkat parental control cell line. Polyclonal antibody crosslinking was used to trigger calcium fluxing at 30 seconds (red arrow).

It was shown that reconstitution with full length LAT was able to reconstitute wildtype levels of calcium fluxing in the J-LKO cell line. However, reconstitution with both the LOVTRAP and TULIPs optogenetics system was only partially able to restore TCR downstream signalling. Given the differences in expression it was reasoned that not enough LAT was present at the plasma membrane to produce a robust calcium flux response. The dark state of LOV2 is reported to have peak emission at 498nm and 522nm due to the FMN cofactor (Kawano et al. 2013). This signal can be measured by flow cytometry and can be used to approximately gauge LOV2 expression. No emission could be detected from the IRES expression vector indicating low LOV2 expression in both the TULIPs- and LOVTRAP-expressing cell lines (Figure 4.11). Wang et al. (2016) reported that in the case of the LOVTRAP system, the LOV2 domain should be in excess of the Zdk component of the system to maximise viability of the system. I therefore sought to quantify the amount of LAT necessary for downstream signalling in the Jurkat E6.1 cell line to see if this could explain the lack of activity in my constructs.

4.3.4 Calcium fluxing is invariant to LAT expression above threshold

Serially transducing the J-LKO cells twice with the LOVTRAP system improved the ability of those cells to flux calcium. It was therefore reasoned that LAT expression levels may influence the amplitude and duration of the calcium flux response. I performed a titration assay to investigate the level of LAT expression required to drive and sustain downstream signalling. Three variants of the full-length LAT vector were established, each with a different promoter to provide varying levels of protein expression. The highest expressing variant was under control of the SFFV promoter, mid-levels of expression were driven by the Δ SV40 promoter, and low expression levels were driven by the inducible mHSP promoter, which is inducible but shows leaky expression (John James, personal communication). Although no LAT expression was detectable from the low-level expression construct (Figure 4.12A), it was found that endogenous LAT expression in the Jurkat E6.1 cell line was still lower than both the SFFV or Δ SV40 promoters (Figure 4.12B). The calcium flux profiles of J-LKO cells transduced with either the high- or mid-level expression systems were indistinguishable from the wildtype Jurkat cells (Figure 4.12C). These results suggest that only a small amount of LAT is necessary to drive sustained downstream signalling and a robust calcium flux response. As we did not detect a shift in 530 nm emission in cells transduced with the optogenetic systems as part of an IRES construct, it is conceivable that these cells simply were not expressing enough LOV2 at the plasma membrane to recruit a sufficient amount of LAT to generate wildtype levels of calcium signalling. With this in mind, I decided to alter my transduction

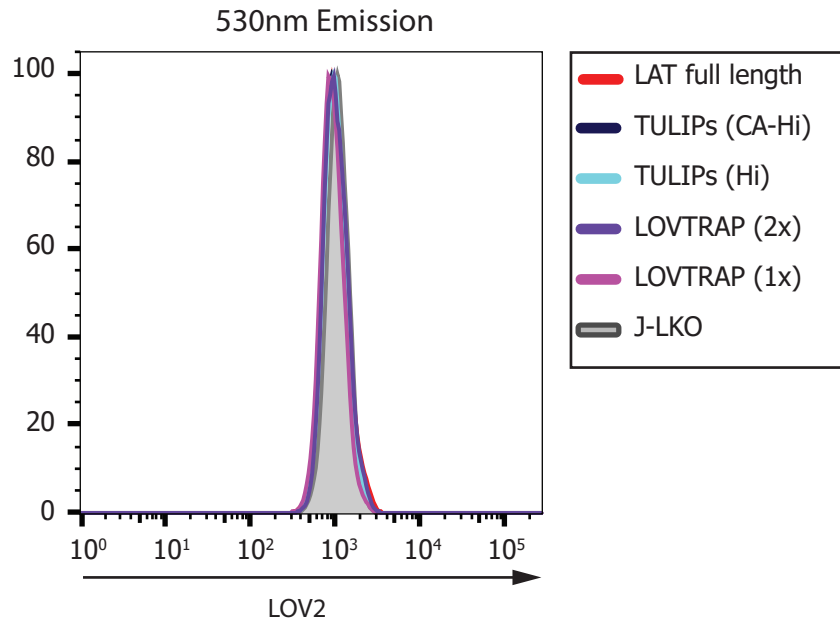


Figure 4.11 IRES constructs yield low expression of LOV2 domain expression of the LOV2 domain can be measured by its ground-state emission (530 nm). J-LKO cells expressing the IRES versions of the LOVTRAP and TULIPs constructs show low levels of LOV2 expression.

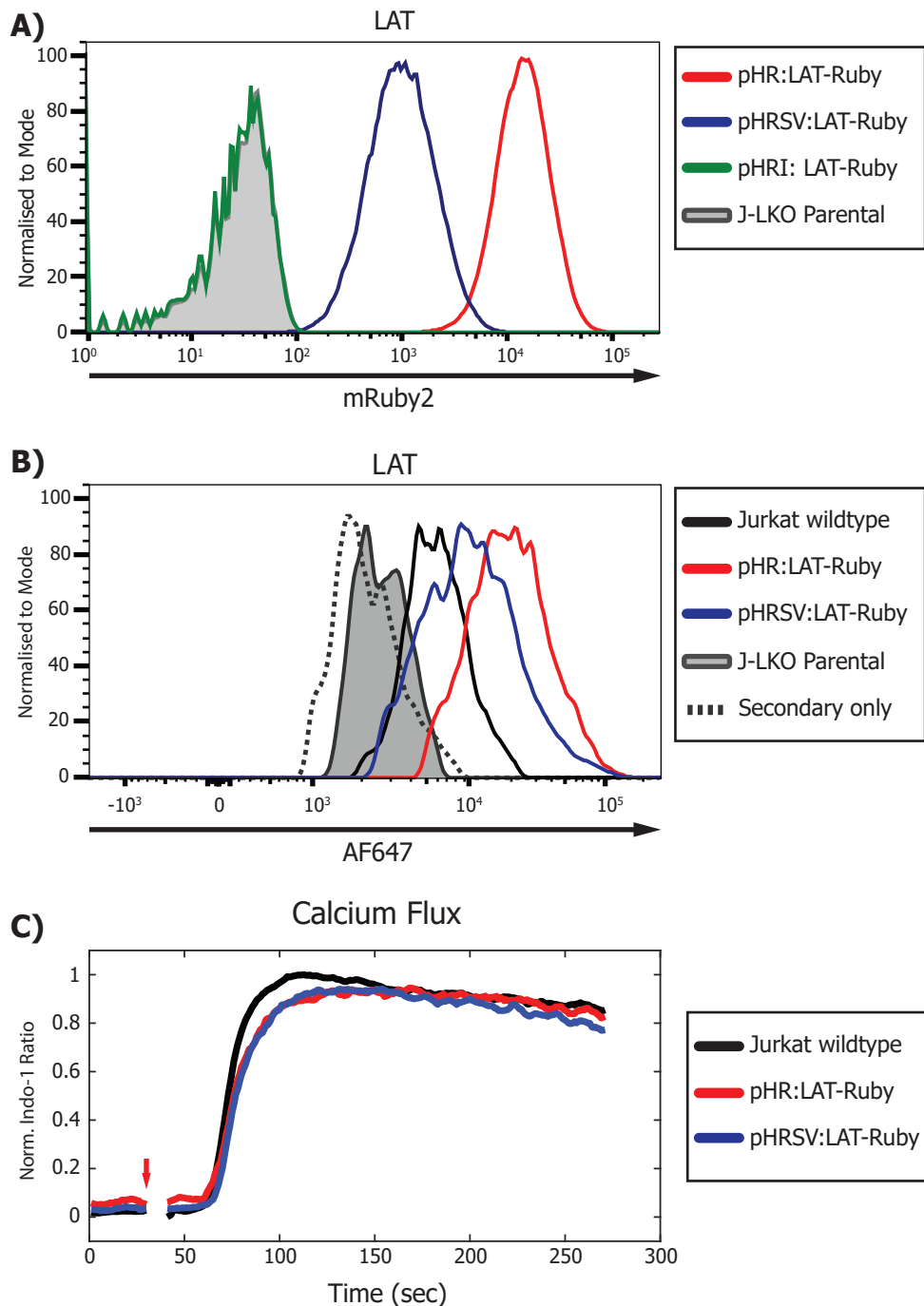


Figure 4.12 Jurkat E6.1 Cells show a low level of endogenous LAT expression
(A) J-LKO cells were transduced with mRuby2-tagged LAT under the control of three different promoters: pHR (High), pHRSV (Mid), pHRI (Low). The Low level expression construct could not be detected. **(B)** Staining for intracellular LAT by FACS showed that endogenous LAT shows lower expression than the pHRSV construct. **(C)** Calcium fluxing showed that both the pHRSV and pHR versions of the LAT construct were able to rescue the J-LKO phenotype, indicating that only a limited amount of LAT is necessary for the cells to undergo calcium fluxing. Calcium flux was measured ratiometrically using indo-1 dye and triggered by the addition of polyclonal crosslinking antibodies at 30 seconds (red arrow). The flux profiles **(C)** are representative of n=2 (biological replicates).

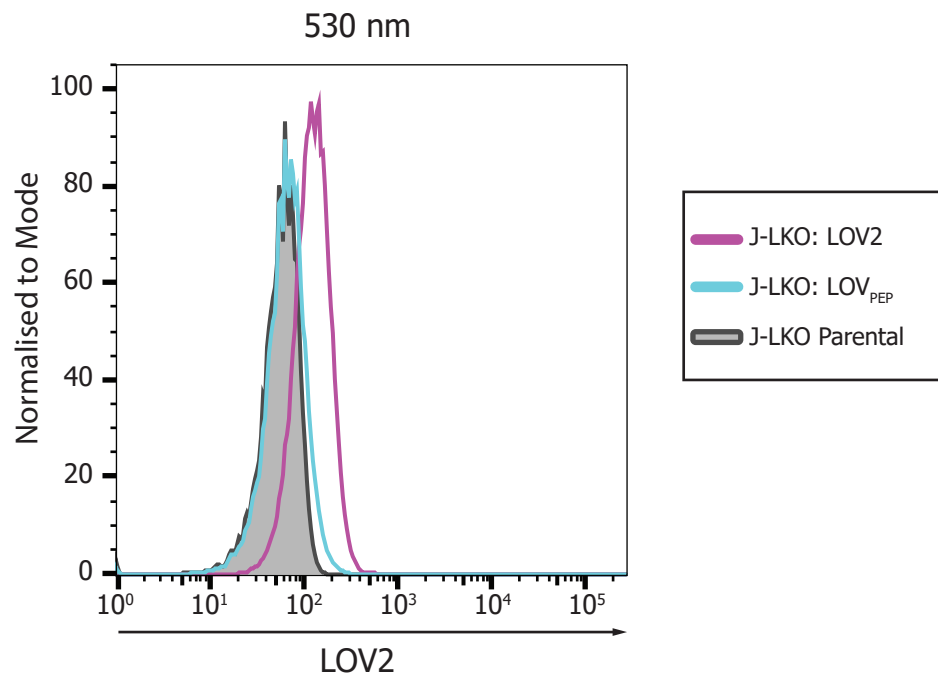


Figure 4.13 Independent transduction of the LAT-TM construct into J-LKO cells improves expression By first transducing the J-LKO cells with the LAT-TM-LOV_{PEP} and LAT-TM-LOV2 membrane anchors, expression of the membrane-anchored optogenetic domains was improved.

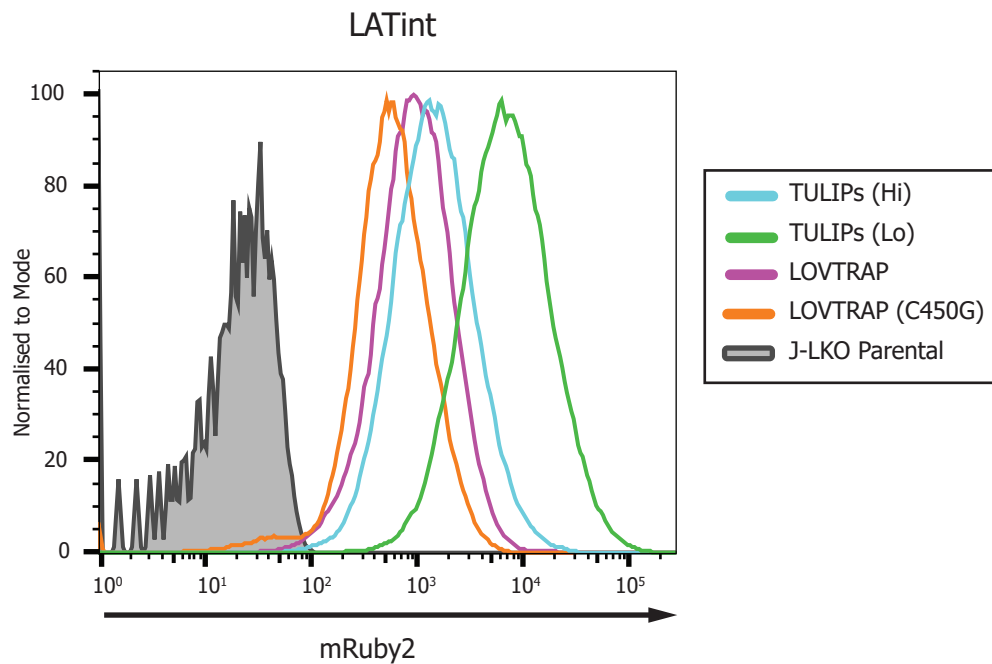


Figure 4.14 Serial transduction of the LATint domain improves expression of optogenetic constructs J-LKO cells transduced with the LOV2 domain membrane anchors were serially transduced with their complementary LATint-tagged binding partners. Transduction first with the LAT-TM-LOV domains and then with the LATint domain was able to improve expression of the LOVTRAP and TULIPs system components.

strategy by serially transducing the J-LKO cells with each component of the optogenetic systems separately.

4.3.5 Serial viral transduction improves TULIPs and LOVTRAP expression in J-LKO cell line

To reduce variability between different optogenetic cell lines I first transduced the J-LKO cell line with either LAT-TM-LOV2 or LAT-TM-LOVpep. LAT^{int} constructs were then transduced into cell lines expressing the correct counterpart. This strategy was particularly relevant for the ePDZ variants of LAT^{int} as it allows for reduced variability between the different versions of the TULIPs system. Using this approach I was able to detect a considerable shift in 530 nm emission in cells expressing LAT-TM-LOV2 and a slight shift in 530 nm emission in J-LKO cells expressing LAT-TM-LOVpep, relative to a J-LKO parental control. (Figure 4.13).

By serially transducing the J-LKO cells first with the membrane-anchored LOV2 domain and then with its intracellular interacting partner, I was able to improve expression of the optogenetic systems (Figure 4.14). Of note, the Zdk-fused LAT^{int} construct in the LOVTRAP system still produced lower levels of expression than the equivalent PDZ-tagged construct in the TULIPs system, suggesting possible protein misfolding caused by the presence of the Zdk domain.

4.3.6 LOVTRAP-LAT optogenetic system reconstitutes TCR signalling pathway

Once expression of the LOVTRAP system had been improved, especially with regards to the LOV2 membrane ‘sink’, I next sought to test the ability of the LOVTRAP-LAT system to reconstitute downstream TCR signalling. Intriguingly, it was found that when triggered under continuous dark conditions, the LOVTRAP system now closely mirrored the Jurkat E6.1 cell line. However, triggering under continuous light conditions only slightly delayed the onset of calcium fluxing and caused only a slight decrease in the peak amplitude of the calcium flux (Figure 4.15). This was somewhat surprising, as under blue-light irradiation it would be expected that the LOVTRAP-LAT system would not be active. The constitutively active variant of the LOVTRAP system also recapitulated TCR signalling, but had a reduced calcium flux capacity (Figure 4.15). This can be explained by the reduced level of LAT^{int} expression (Figure 4.14).

More surprisingly, although I was unable to ablate signalling under continuous light exposure, I was able to completely attenuate signalling in LOVTRAP-expressing cells using short pulses of light after calcium fluxing had been initiated. This process was repeatable and

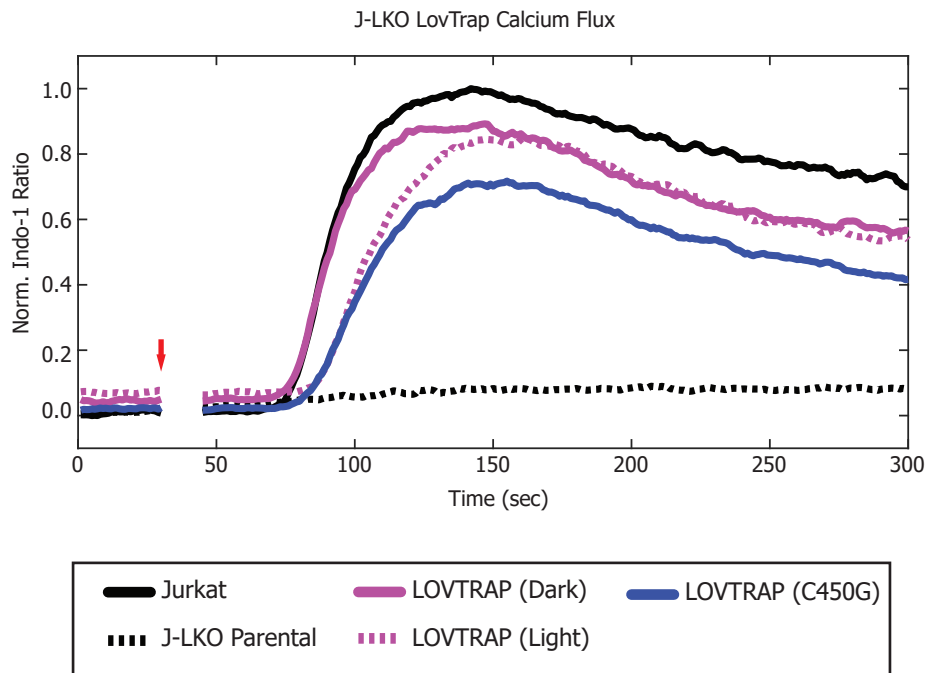


Figure 4.15 LOVTRAP system rescues calcium flux phenotype J-LKO cells expressing the LOVTRAP-LAT optogenetic system were tested for their capacity to flux calcium. Calcium fluxing was induced at 30 s following the addition of polyclonal antibody crosslinker (red arrow). The wildtype system is shown in magenta, the photo non-responsive control system is shown in blue. Samples were normalised to the Jurkat E6.1 parental control line (black).

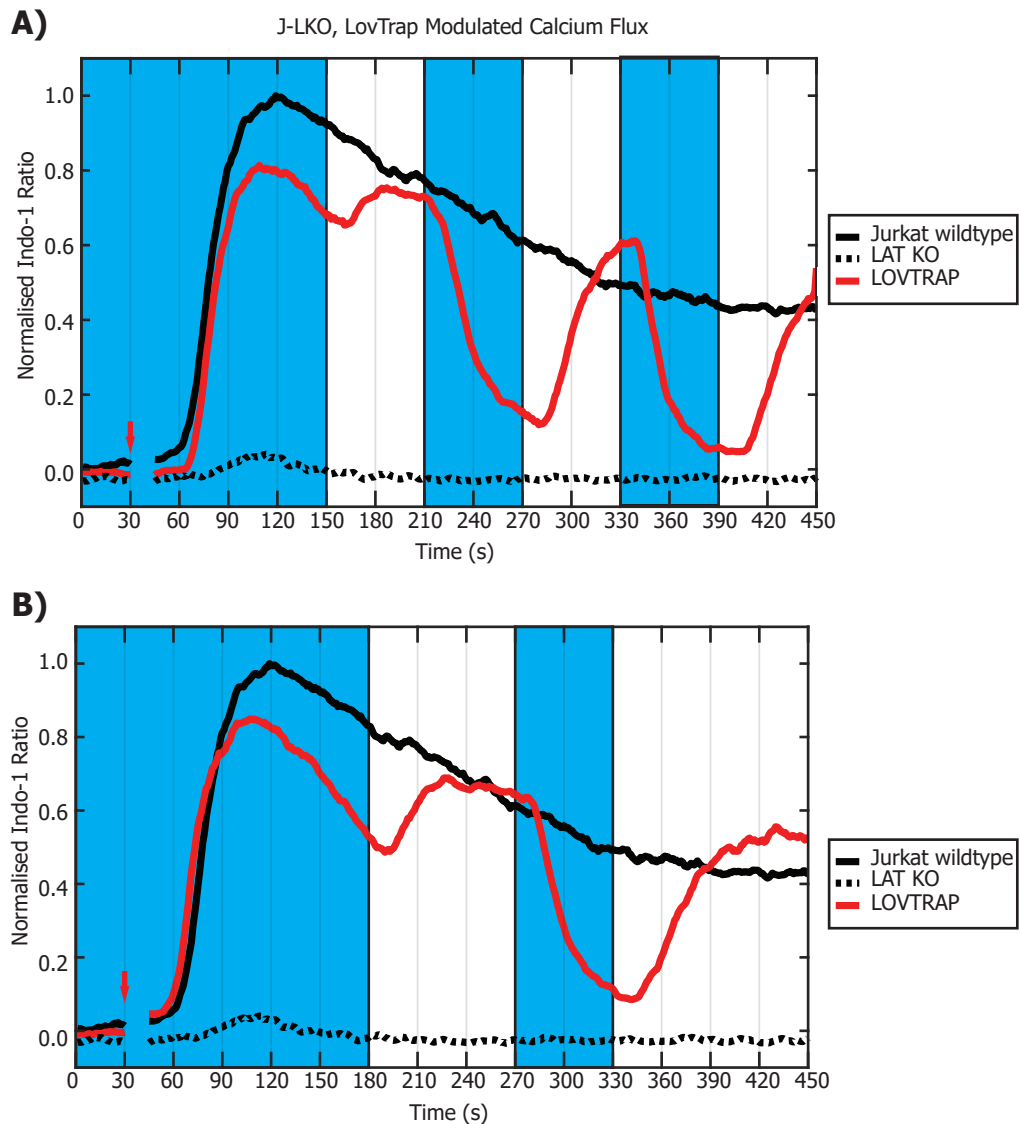


Figure 4.16 light-inducible modulation of calcium fluxing with the LOVTRAP system Blue light irradiation is able to rapidly terminate calcium fluxing in the LOVTRAP system. This is caused by dissociation of the Zdk-LATint construct into the cytoplasm. **(A)** J-LKO cells expressing the LOVTRAP system were pre-illuminated for 1 minute prior to beginning the experiment. Blue light irradiation was terminated at 150 s and re-initiated at 210 s. Light was pulsed for 1 minute (from 270 s) and then terminated. Light was re-initiated at 330 s and pulsed for 1 minute before again terminating. **(B)** An alternative pattern of illumination. Cells were again pre-illuminated for 1 minute prior to the start of the experiment. Blue light irradiation was terminated at 180 s and then re-initiated for 1 minute at 270 s. Calcium fluxing was initiated at 30 s in both samples by the addition of polyclonal crosslinking antibodies (red arrow). Calcium flux was normalised to the Jurkat E6.1 control (black). Each condition here is representative of n=1 (biological replicates).

reversible (Figure 4.16). Signal decay was immediate following blue light irradiation suggesting tight negative regulation of the TCR signalling pathway. Calcium fluxing was again initiated following a short delay after cessation of blue light irradiation. Wang et al. (2016) report that the LOVTRAP system is susceptible to background binding of the Zdk domain. As the early peak in calcium fluxing was unaffected by blue light irradiation background binding would imply that only a small pool of LAT is necessary to initiate downstream signalling, but that sustained signalling requires the recruitment of a larger pool of LAT.

4.3.7 Limited LAT population necessary for TCR signal initiation

To test the hypothesis that sustained calcium signalling is dependent on the recruitment of a larger LAT pool I sought to delineate extracellular calcium influx from the release of intracellular calcium stores. To do this, the calcium flux assay was performed in calcium free media using LOVTRAP-expressing J-LKO cells. On antibody engagement of the TCR, it was found that calcium fluxing rapidly peaked and then declined as intracellular stores were depleted. Returning calcium to the media triggered the re-initiation of calcium fluxing (Figure 4.17). This result indicates that T cells rapidly switch from utilising intracellular calcium to utilising extracellular calcium. Again, differences in peak amplitude of the flux are likely due to differences in expression level between different variants of the LOVTRAP system (Figure 4.14).

By controlling both light conditions and calcium concentration in the media, it was observed that even under continuous light conditions release of intracellular calcium stores could not be ablated by light, only slightly delayed (Figure 4.18). This finding indicates that background binding of the LOVTRAP system is responsible for the release of intracellular calcium. It also suggests that a limited pool of LAT is necessary to trigger IP₃ signalling to IP₃Rs on the endoplasmic reticulum. However, to sustain calcium signalling a larger pool of LAT is required.

4.3.8 Sustained calcium fluxing requires large pool of LAT

To try and address the background signalling in the LOVTRAP system I titrated expression of the LAT^{int} construct. As with the full length LAT construct, Zdk-LAT^{int}-Ruby expression was controlled using different strength promoters: SFFV (high), ΔSV40 (mid), and mHSP (low) (Figure 4.19). As the LAT^{int} constructs were expressed independently from the LAT-TM-LOV2 construct, the transmembrane component of the system was expressed equally in all three LOVTRAP cell lines. As before, the high expression system showed almost identical flux profiles

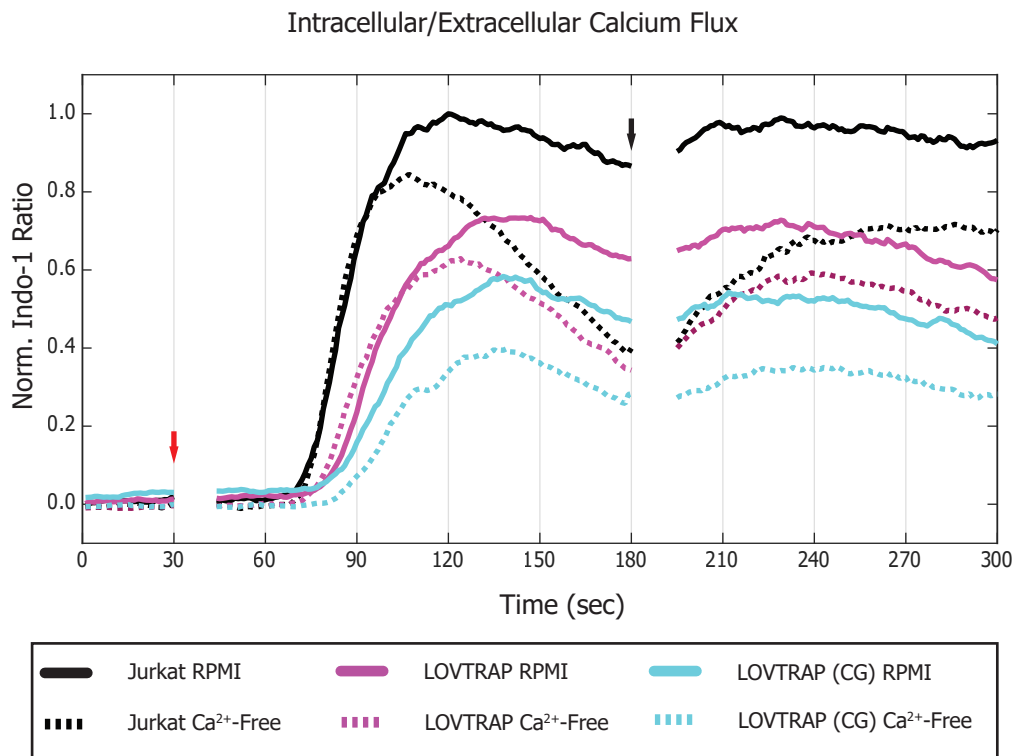


Figure 4.17 Fluxing in calcium-free media attenuates sustained flux profile To delineate the release of intracellular calcium stores from extracellular calcium influx, calcium fluxing was performed in a calcium free media (dotted lines). Parental Jurkat E6.1 cells (black) were compared to J-LKO cells the wildtype (magenta) and photo-non-responsive (cyan) variants of the LOVTRAP system. Polyclonal antibodies were added at 30 s to trigger calcium fluxing (red arrow) Calcium was returned to the media at 180 s (black arrow) to a final calcium concentration of 1 mM.

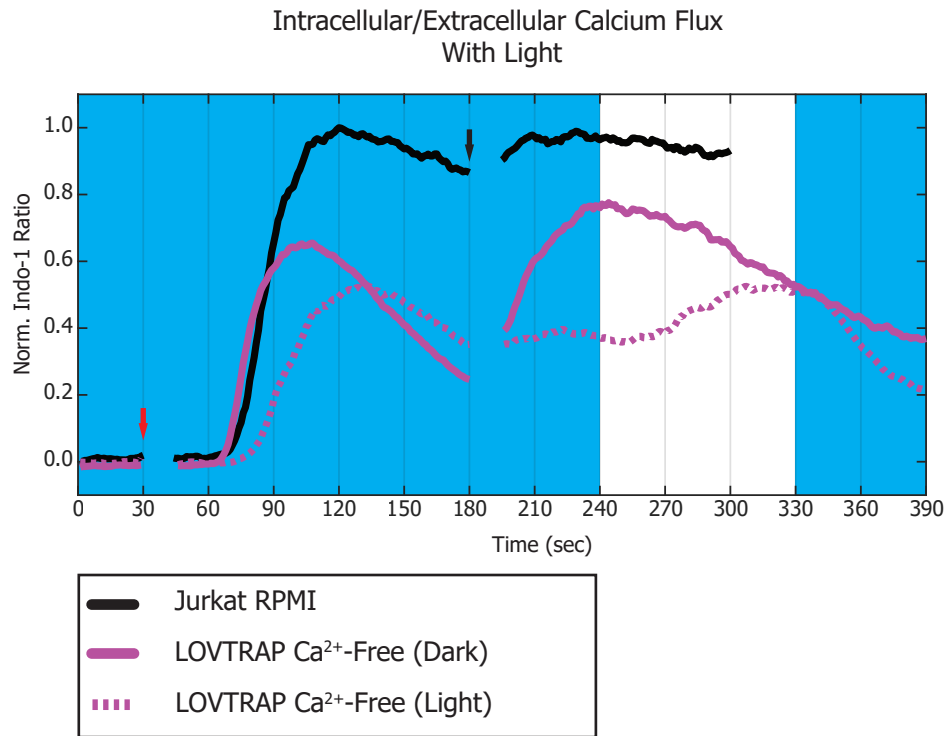


Figure 4.18 Depletion of extracellular calcium causes delay but not ablation of ER calcium release under light stimulation in LOVTRAP system To overcome the background release of intracellular calcium LOVTRAP cells were triggered under blue light conditions in the absence of calcium (magenta, dotted). These were compared to control cells triggered under continuous dark (magenta, solid). Light pulses are shown in blue. Cells were pre-illuminated for 1 minute prior to the start of the experiment. Indo-1 values were normalised to the Jurkat E6.1 control (black). Calcium fluxing was triggered by the addition of polyclonal crosslinking antibodies at 30 s (red arrow). Calcium was returned to the media to a final concentration of 1 mM at 180 s (black arrow).

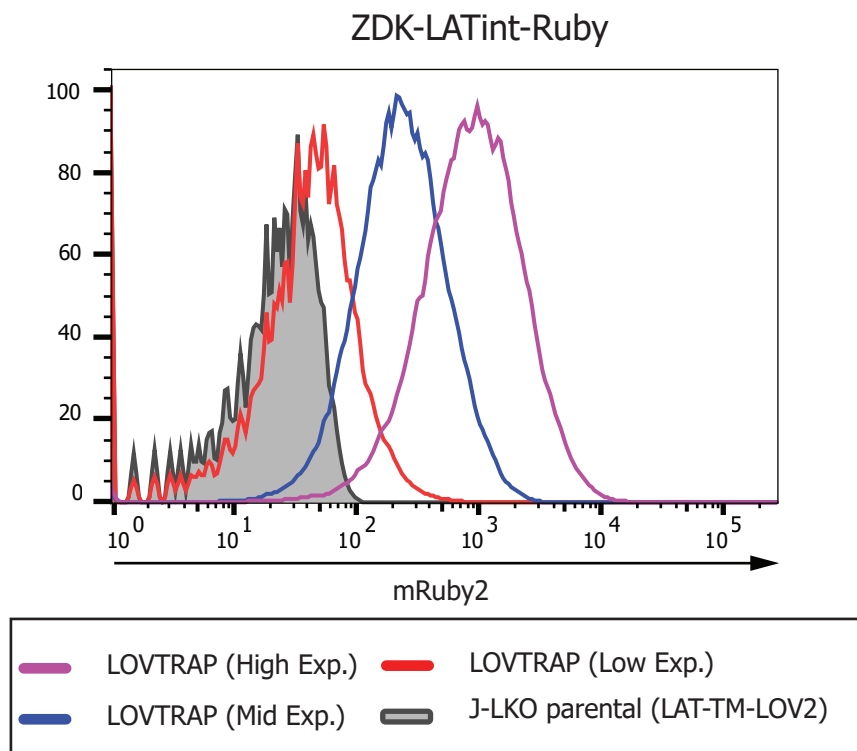


Figure 4.19 Titration of Zdk-LATintRuby Expression of the ZDK-LATint-Ruby construct under three different promoters SFFV (High, magenta), Δ SV40 (Mid, blue), and mHSP (Low, red).

under continuous light or continuous dark (Figure 4.20A, D). The mid-level expression system showed a pronounced flux in the dark that rapidly diminished over time. However, fluxing under continuous light almost completely inhibited calcium fluxing (Figure 4.20B, D). In the low-level expression system this was more pronounced. Fluxing rapidly peaked and then diminished even under the dark state and fluxing was entirely ablated under continuous light (Figure 4.20C, D). This finding is consistent with the results from the calcium-free fluxing assay (Figure 4.17-4.18) that only a small population of LAT is necessary to initiate fluxing, but a sustained calcium signalling requires the recruitment of a larger pool of LAT.

4.3.9 LOVTRAP-LAT system fails to sustain downstream signalling

Once it had been established that the LOVTRAP-LAT system was able to rescue early TCR signalling events in the J-LKO cell line, I next investigated whether the system could reconstitute complete T-cell activation. Surface expression of the C-type lectin protein CD69 is upregulated within hours of T cell activation (Llera et al., 2001). J-LKO cells expressing the LOVTRAP-LAT system were mixed with dynabeads conjugated to α CD3/ α CD28 antibodies. CD69 upregulation was measured over a 7 hour time course. As expected Wildtype Jurkats began to express CD69 within 3 hours of activation. This steadily increased over the next 4 hours (Figure 4.21). Parental J-LKO cells showed no upregulation of CD69 (Figure 4.21). Likewise, no upregulation of CD69 was observed in the LOVTRAP-expressing cells (Figure 4.21). This finding, when taken in the context of the Zdk-LAT_{int} titration experiment (Figure 4.20) suggests that the interaction between LOV2 and Zdk may not occur sufficiently long enough to sustain downstream signalling. This effect is mitigated in early signalling in the high expression system (Figure 4.20A), but can be observed in the mid- and low-expression systems (Figure 4.20B, C).

4.3.10 TULIPs system partially reconstitutes calcium fluxing

In parallel with the LOVTRAP-LAT system, I also sought to improve the TULIPs-LAT system. As with the LOVTRAP system, I first transduced the parental J-LKO cell line with LAT-TM-LOV_{pep} to reduced variability between cell lines (Figure 4.13). The expression of LAT-TM-LOV_{pep} was somewhat lower than the expression of LOV2 in the LOVTRAP parental cell line. J-LKO cells expressing LAT-TM-LOV_{pep} were then transduced with either the high affinity (ePDZb1) or low affinity (cpPDZ) variants of the LAT_{int} construct. There is almost a two orders of magnitude difference in the binding affinity of these two domains for the LOV_{PEP} domain (Strickland et al., 2012). Expression of the low affinity version of LAT_{int} was considerably higher

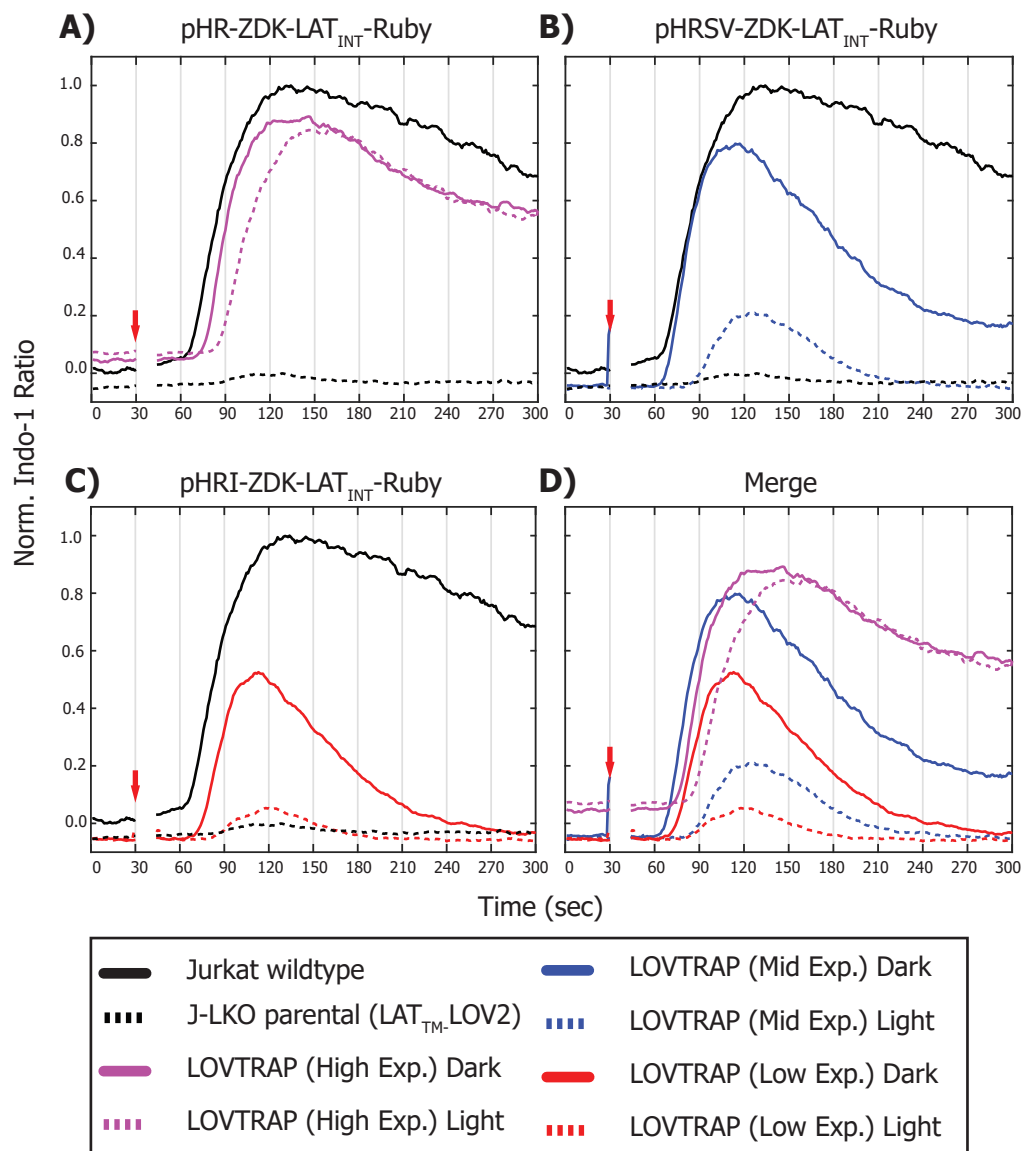


Figure 4.20 LOVTRAP calcium flux titration Calcium fluxing was triggered by the addition of polyclonal crosslinker at 30 s (red arrow) and flux was measured ratiometrically with indo-1 dye. Samples are normalised to the Jurkat E6.1 control (black). **(A)** calcium flux profile of the high expression SFFV promoter LOVTRAP system. **(B)** Calcium flux profile of the mid-level expression system, Δ SV40 promoter. **(C)** Calcium flux profile of the Low expression system, mHSP promoter. **(D)** comparison of all three variants of the LOVTRAP system. All three expression vectors were transduced into j-LKO cells expressing the LAT-TM-LOV2 construct, thus expression of the membrane recruiter is comparable across all samples.

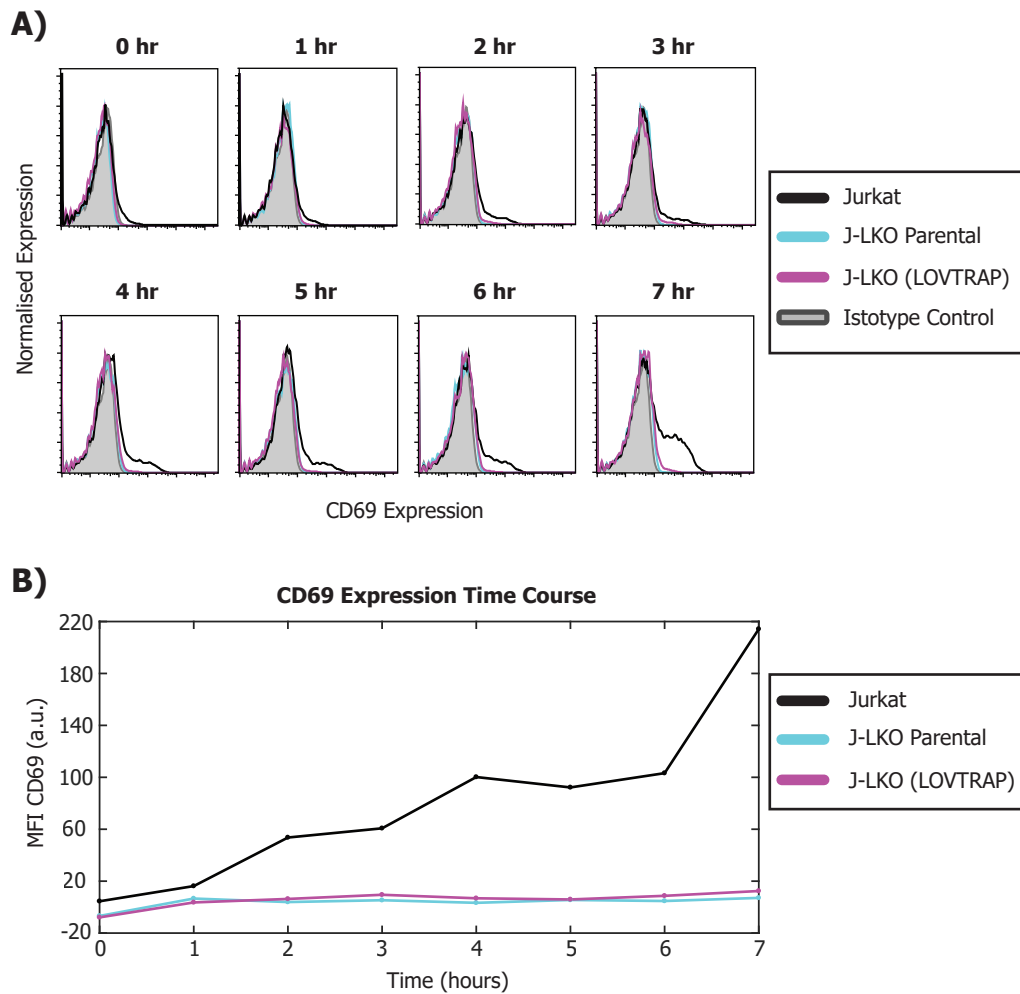


Figure 4.21 CD69 upregulation assay (A) J-LKO parental, Jurkat E6.1, and J-LKO LOVTRAP (high expression) cells were conjugated with dynabeads linked to CD28 and CD3 antibodies to stimulate T-cell activation. The duration of activation is presented above each of the FACS blots showing CD69 expression. CD69 was detected using a primary conjugated antibody (AF647) **(B)** The mean fluorescent intensity of CD69 expression across the population shows a gradual increase in CD69 expression, n=2 (technical replicates of each time point).

than the high affinity variant (Figure 4.14). To determine if the TULIPs-LAT optogenetic systems were able to reconstitute TCR signalling, I conducted calcium fluxing assays under continuous blue light or continuous dark conditions (Figure 4.22). It was found that with the high affinity domain both light and dark conditions resulted in an early peak in calcium fluxing reminiscent of the high expression LOVTRAP system (Figure 4.22). The amplitude of this peak was similar between both datasets, but signalling returned to baseline more rapidly in the dark-state cells. Of note, even under continuous blue light irradiation there was a gradual decay in calcium flux signal in the high affinity variant of the TULIPs system (Figure 4.22). Next, using the low affinity TULIPs variant it was observed that calcium fluxing was present under blue light illumination, but almost entirely absent when fluxing was performed in the dark (Figure 4.22). Taken together with previous results this seems to suggest that there is high background binding particularly in the high affinity TULIPs system and that low levels of LAT are needed to initiate intracellular calcium signalling. However, the intrinsic K_d of the LOVpep/ePDZ interaction is unable to sustain downstream signalling.

4.3.11 *Intrinsic dissociation rate of TULIPs interaction inhibits sustained calcium fluxing*

The interaction between LAT, SLP76 and Vav1 has been proposed to position PLC γ 1 in an optimal orientation to initiate the calcium signalling cascade (Knyazhitsky et al. 2012). Although the LOV2 domain is small relative to other optogenetic domains, it is possible that positioning a structured domain between the intracellular signalling domains of LAT and the plasma membrane creates a steric inhibitory effect and diminishes signalling capacity. To test this hypothesis I generated a truncated version of the LOVpep system, missing the entire LOV2 domain, but retaining the PDZ peptide binding sequence, 'LAT-TM-pep' (Figure 4.23A). I also generated a variant in which the ePDZb1 domain was tagged directly to the C-terminus of the transmembrane domain of LAT with a short glycine/serine linker and fused to the binding domain was the intracellular domain of LAT, thus creating a single continuous construct (Figure 4.23B). The LAT-TM-pep construct has no intrinsic marker and thus it was expressed as part of a joint IRES expression vector with ePDZb1-LAT_{int}-Ruby. Microscopy of HEK293T cells expressing the LAT-TM-pep construct (Figure 4.24A) or the constitutively active LOVpep variant (Figure 4.24B), LAT-TM-LOVpep(CA), showed identical recruitment of ePDZb1-LAT_{int}-Ruby to the plasma membrane. Importantly both of the two component systems showed identical calcium flux profiles (Figure 4.25A), whereas the LAT_{TM}-ePDZb1-LAT_{INT}-Ruby chimeric fusion proteins showed a flux profile identical to that of full length LAT (Figure 4.20B). Thus, the inability to

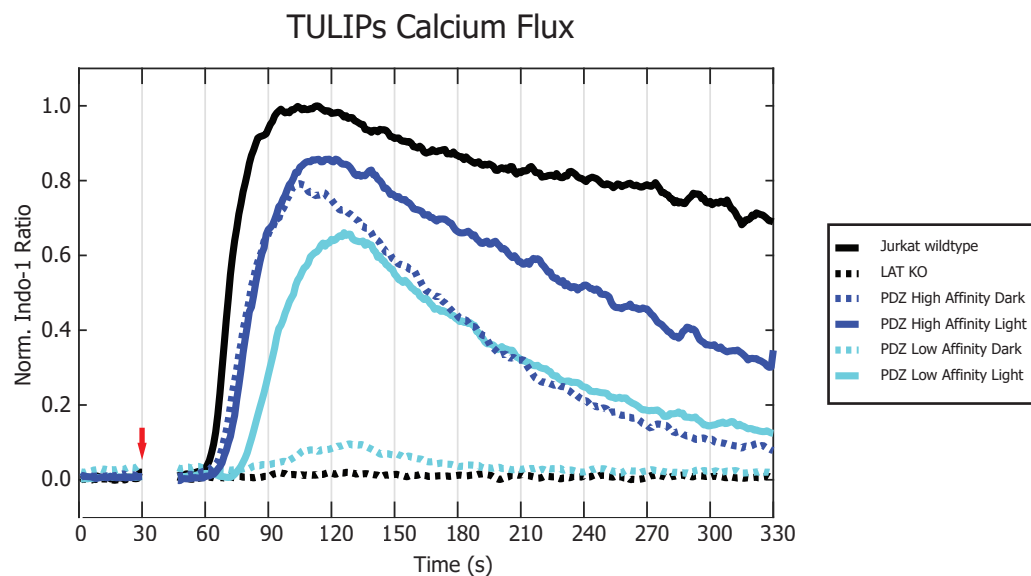


Figure 4.22 Light-inducible initiation of signalling using the TULIPs system
Blue light irradiation can be used to induce the interaction of the PDZ domain with the LOVpep domain. The low affinity PDZ (cpPDZ) domain shows minimal calcium fluxing in the dark (cyan, dotted) and high calcium fluxing in the light (cyan, solid). The high affinity PDZ (ePDZb1) shows some fluxing in the dark (blue, dotted) and more sustained fluxing in the light (blue, solid). Samples were normalised to the Jurkat E6.1 control (black). Calcium fluxing was triggered by the addition of polyclonal crosslinking antibodies at 30 s (red arrow).

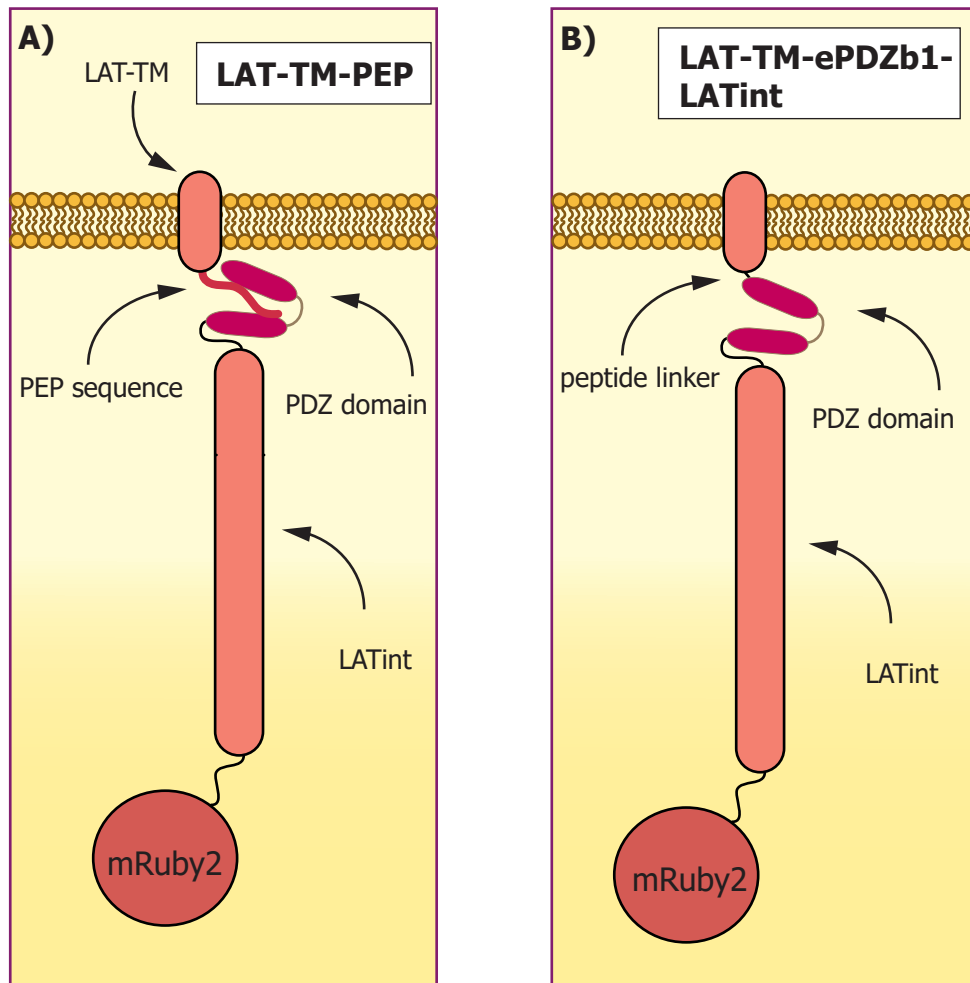


Figure 4.23 Overview of LAT-TM_{pep} and fused PDZ construct (A) Truncated version of the TULIPs system with the pep binding sequence fused directly to LAT-TM. **(B)** LAT-TM-ePDZb1-LATint-Ruby fusion protein. The high affinity PDZ domain is fused within the LAT construct with two short linkers.

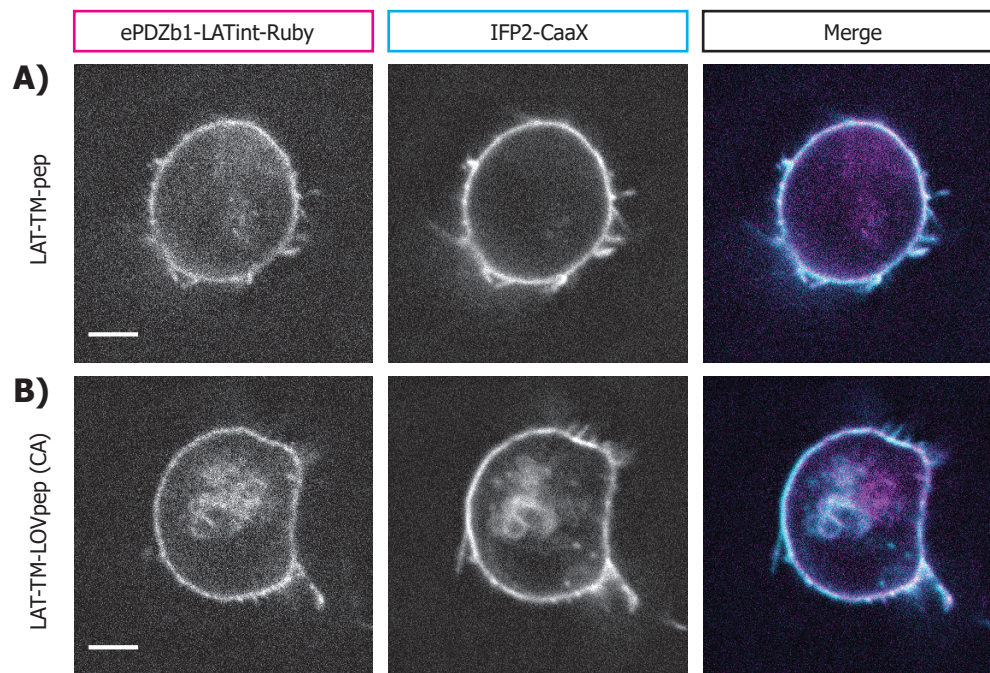


Figure 4.24 Membrane recruitment of the truncated TULIPs system **(A)** the LAT-TM-pep truncated variant shows membrane recruitment identical to **(B)** the constitutively active variant of the LOVpep domain. **(A)** HEK293T cells were transfected with pHR-LAT-TM-pep, pHR-ePDZb1-LATintRuby, and pHR-IFP2-CaaX. **(B)** HEK293T cells were transfected with pHR-LAT-TM-LOVpep(CA), pHR-ePDZb1-LATint-Ruby, and pHR-IFP2-CaaX.

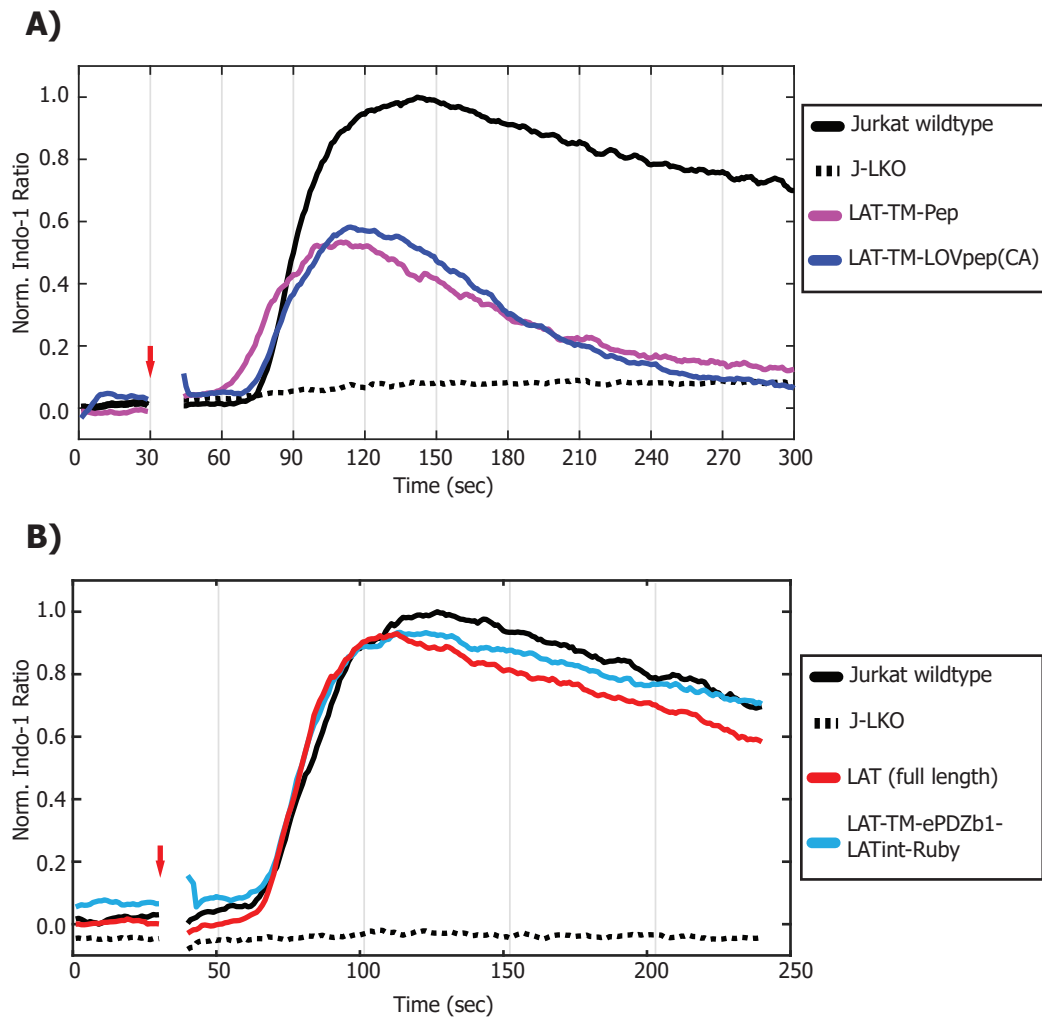


Figure 4.25 truncated LAT-TMpep variant does not rescue calcium flux phenotype, but fusion protein does (A) J-LKO cells expressin the LAT-TM-pep (magenta) and LAT-TM-LOVpepCA (blue) constructs with the high affinity PDZ domain show identical calcium flux profiles. **(B)** The LAT-TM-ePDZb1-LATint fusion (cyan) protein shows an identical flux profile to full-length LAT (red). Calcium fluxing was triggered at 30 s with the addition of polyclonal crosslinker and indo-1 ratios were normalised to the Jurkat E6.1 parental control.

sustain calcium fluxing was due to the intrinsic dissociation rate of the PDZ domain from its binding sequence rather than a steric effect caused by the presence of the PDZ domain or oscillation of the LOV2 domain between the light and dark state.

Although I was able to modulate calcium fluxing with light using the TULIPs system, I determined that the inability of these J-LKO TULIPs cells to sustain proximal signalling and the high degree of background in the high affinity versions of the system made TULIPs unsuitable for the analysis of proximal TCR signalling events.

4.3.12 CRY2-CIBN optogenetic system fails to rescue LAT knockout phenotype

As discussed in chapter 3, I also attempted to establish a CRY2-based version of the LAT optogenetic system. CRY2 functions in a manner analogous to the TULIPs system and provides a mechanism for light-inducible membrane recruitment of LAT (Figure 3.10-11). CRY2 also represents a particularly attractive alternative to the LOV2 systems because it is blue light-inducible and relies on an endogenously expressed cofactor, FAD.

I constructed a number of CRY2-LAT^{int} fusion proteins using the second generation CRY2 systems described by Taslimi et al. (2016) (Appendix B). As with the TULIPs and LOVTRAP systems, I first transduced the J-LKO cells with the membrane recruiter component of the system, in this case the pmGFP-CIBN construct (Figure 4.26). The LAT^{int} component of the system was virally transduced into the cells once stable expression of the CIBN construct had been confirmed (Figure 4.26). Although the J-LKO cells were positive for both the membrane CIBN anchor and the LAT^{int} constructs, no calcium flux could be detected (Figure 4.27). Importantly, we tested the CRY2 W347A mutant, which is reported to be constitutively active (X. Li et al. 2011). In this variant of the CRY2 system, LAT^{int} is constitutively anchored at the plasma membrane by the CIBN interaction partner. It would be expected to behave similarly to the constitutively active variant of the TULIPs system, but instead no calcium flux was detectable following TCR crosslinking (Figure 4.27). No flux could be detected in the other variants even under blue light irradiation. The CRY2 domain is much larger than the LOV2 domain (Pathak et al. 2014). It is therefore possible that the complete absence of fluxing is due to steric hindrance of LAT-associated proteins.

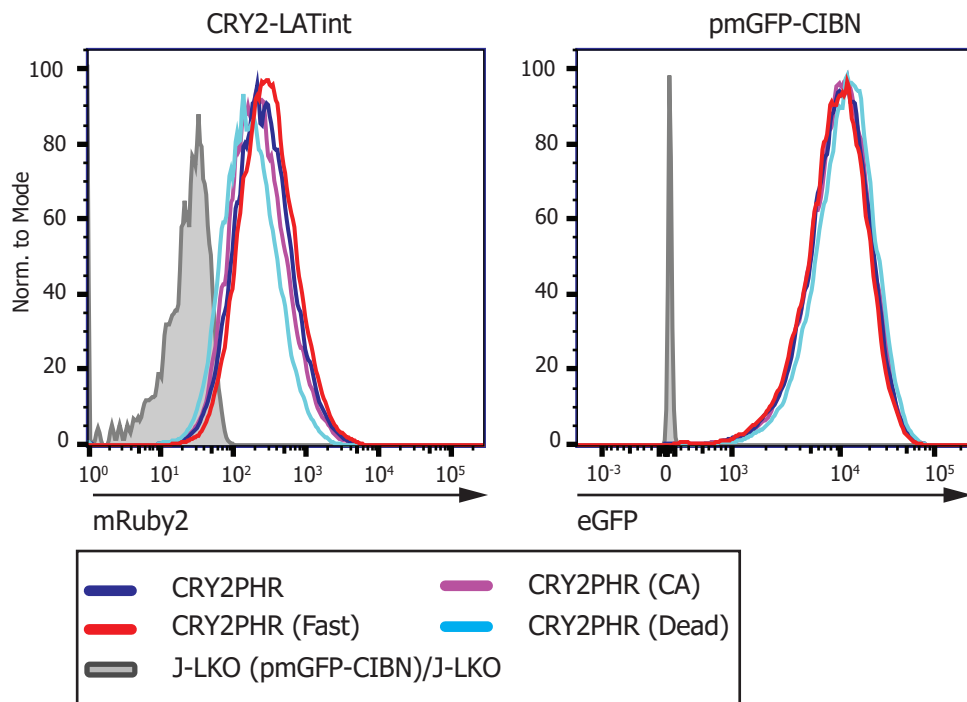


Figure 4.26 Expression of the CRY2PHR constructs in J-LKO cells J-LKO cells were first transduced with the pmGFP-CIBN recruiter and then serially transduced with the variants of CRY2PHR. The four variants tested show similar levels of CRY2PHR-LATint ruby expression.

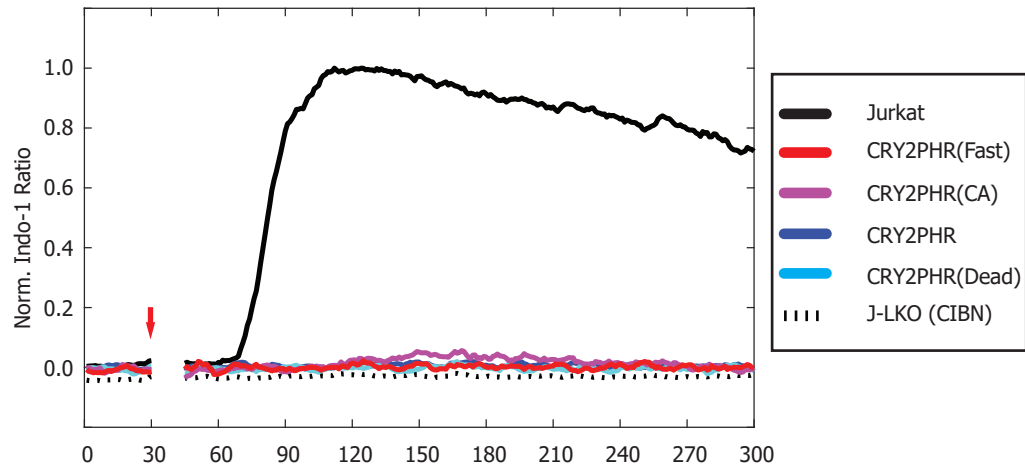


Figure 4.27 Calcium fluxing in LAT-CRY2PHR expressing cells J-LKO cells expressing the variants of the CRY2PHR system and CIBN membrane recruiter were triggered with the addition of polyclonal crosslinker at 30 s (red arrow) and indo-1 ratio was normalised to the Jurkat E6.1 cell line (black). Flux profiles are representative of n=2 (biological replicates).

4.3.13 J-LKO cells highly express CD6

It was noted that although we had knocked out LAT expression by CRISPR-Cas9 the Calcium flux profile of the J-LKO cell line did not precisely match that of the JCaM2.5 cell line (Figure 4.28A). In the J-LKO cell line, TCR ligation resulted in a small but unsustained peak in calcium fluxing. No such peak was observed in the JCaM2.5 cell line. Membrane receptors other than LAT have been proposed to anchor the scaffolding protein SLP-76 at the plasma membrane, providing an alternative mechanism for the nucleation of downstream signalling molecules (Roncagalli et al. 2014; Malissen et al. 2014). I screened the J-LKO cell line and three other LAT knockout clones for surface CD6 expression and found there to be an increase in CD6 expression in three of the four clones tested when compared to the Jurkat parental cell line. No CD6 expression was detectable on the JCaM2.5 cell line (Figure 4.28B). This finding warrants further consideration as the JCaM2.5 cells, which show no calcium flux on TCR ligation and low expression of the TCR complex (Figure 4.1), are negative for CD6 expression (Figure 4.28). The upregulation of CD6 could provide a mechanism for sustained tonic signalling in the absence of LAT (Myers, Zikherman, and Roose 2017).

4.4 Discussion

In this chapter I created and tested three different LAT-based optogenetic tools for the interrogation of T cell signalling. The T cell scaffolding protein LAT has no secondary structural motifs or enzymatic activity, minimising the need for detailed structural analysis in the design and implementation of a LAT-based optogenetic system. Using both the TULIPs and LOVTRAP systems I was able to show real-time modulation of TCR-induced signalling outputs and modulate early T cell activation dynamics.

Huse et al. (2007) implemented a light-based approach to T-cell activation using a photoactivatable TCR agonist in the past. This approach allowed for precise temporal and spatial activation of signalling, but could not be used to modulate the downstream signalling pathway. Our results using the LOVTRAP system indicate that T cell signalling is under tight negative regulation. Although I was unable to ablate intracellular calcium fluxing due to background binding of the Zdk domain, I was able to show almost immediate cessation of extracellular calcium fluxing on blue light irradiation. This indicates that membrane-proximal signals via LAT are required for sustained calcium fluxing on TCR stimulation. Once this membrane-proximal signal is terminated, signalling along the entire downstream pathway ceases. Unfortunately, the LOVTRAP-LAT

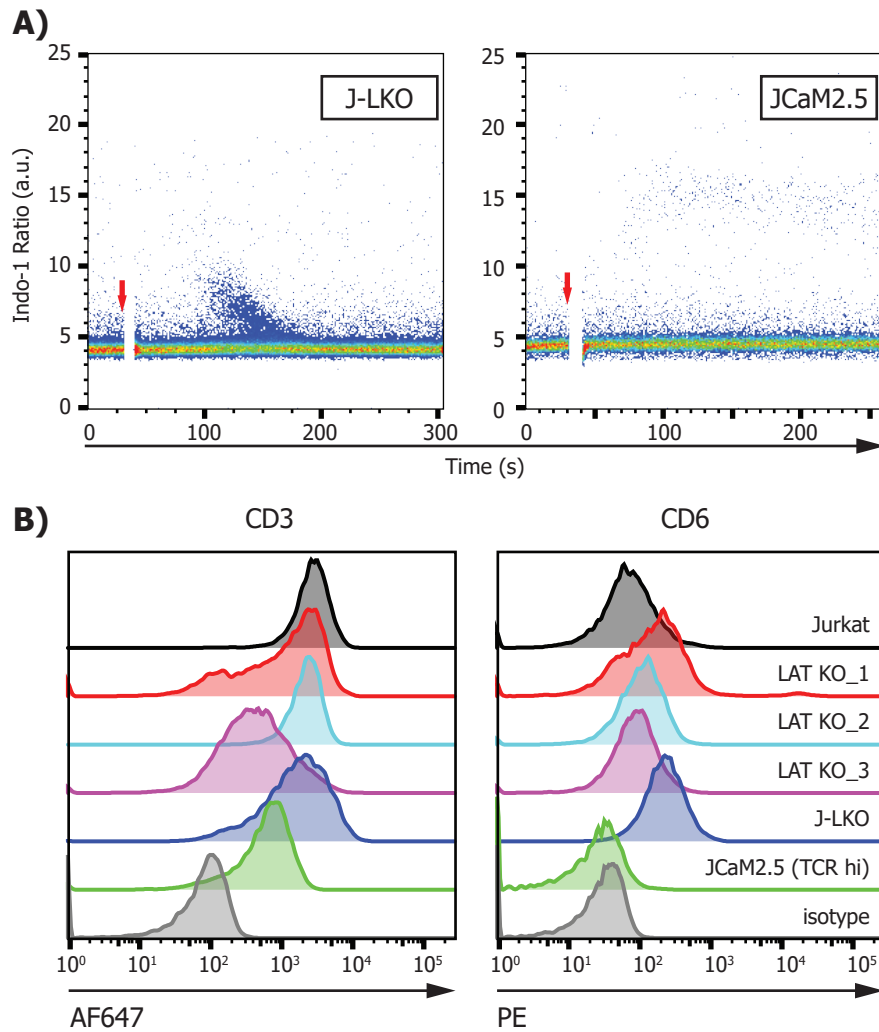


Figure 4.28 J-LKO cells show limited fluxing and increased CD6 expression
(A) scatter plot of calcium flux for the J-LKO cell line and the JCaM2.5 cell line. Polyclonal crosslinker was added at 30 s to trigger calcium fluxing (red arrow). **(B)** CD6 expression and TCR expression in 4 J-LKO clone lines and the JCaM2.5 cell line

system did not completely reconstitute T cell activation, so it was not possible to infer how long these membrane proximal signals were needed to commit T cells to activation. This finding has interesting implications for the physiology of the T cell response. As aberrant T-cell activation can result in autoimmune disease, allergies, or asthma, it follows that T cell activation must be tightly regulated. Here, I have shown that within seconds of signal termination, downstream TCR signalling is completely halted. The delay in signal re-initiation indicates that downstream signalling 'memory' is rapidly lost. This signalling memory is proposed to occur in the form of unstable signalling intermediates, and may include post-translational modifications, like phosphorylation (Lever et al. 2014). The rapid clearance of T cell signalling memory likely provides a mechanism for T cell antigen discrimination. T cells are able to recognise antigens with a high degree of selectivity and specificity, the precise mechanism of this remains to be fully described.

The experiments outlined above have also identified some of the limitations of optogenetics in T cell signalling. Neither the high affinity nor the low affinity variants of the TULIPs system were able to sustain proximal signalling downstream of the TCR. Of note, the rate of signal decay under continuous light conditions in the low affinity variant was more rapid than the rate of signal decay seen under the same conditions for the high affinity TULIPs system. This strongly implicated involvement of the ePDZ domain as the concentration of LOVpep membrane binding partner would be invariant in these systems. Both cell lines were derived from the same parental J-LKO cell line expressing LAT-TM-LOVpep. The same should be true for the intrinsic photocycle kinetics of the LOV2 domain which would be expected to affect both the high affinity and low affinity TULIPs systems identically. Thus, the increased rate of signal decay seen with the low affinity variant is likely due to the increased K_{off} of the interaction between the LOVpep binding sequence and the cpPDZ domain.

We found that the LOVTRAP-LAT system, like the TULIPs-LAT system, had a high degree of background binding in the 'off' state. Although it was found that LOVTRAP was able to reconstitute near wildtype levels of calcium fluxing, this signal was not ablated under continuous light treatment. Downstream analysis of other T cell activation events also suggested limited feasibility of the LOVTRAP-LAT system for investigating T cell signalling dynamics at later time points. It was found that J-LKO cells reconstituted with the LOVTRAP system failed to upregulate CD69 on dynabead stimulation. Again this finding is similar to that in the TULIPs cells in that sustained signalling is necessary to drive T cell activation and that a split LAT construct is unable to sustain these signals. Physiologically this points to the tight regulation of the LAT signalosome during TCR-induced signalling.

These results taken together, suggest that a split LAT system becomes dependent on two equilibrium states of the domains involved in mediating the binding interaction. First, productive signalling is dependent on the photocycle kinetics of the LOV2 domain, which displays equilibrium light state and ground state conformations. Illumination skews the equilibrium toward the light-state and cessation of blue light stimulation skews the equilibrium toward the dark state, however under each condition a proportion of the LOV2 domain is still in either state (Strickland et al. 2010). Intensity of the blue light stimulation also affects this equilibrium. Second, productive signalling is also dependent on the interaction between either the Zdk domain and the LOV2 domain in the LOVTRAP system or the ePDZ domain and the LOVpep domain in the TULIPs system. These effects present themselves at different points in proximal TCR signalling output. The equilibrium state of the LOV domain appears to be dominant immediately following TCR ligation as both LOVTRAP-LAT and TULIPs-LAT. The high affinity variant of the TULIPs system in particular displayed a high degree of background signalling in the “off” state. The binding kinetics of the interaction partners appear to have the dominant effect in sustained signalling. Each protein has an intrinsic off rate and because LAT activation is tightly regulated, once the interaction between the optogenetic binding partners is terminated the TCR downstream signal is rapidly attenuated. These findings confirm those seen by Strickland et al. (2012), that under continuous illumination in a slow cycling mutant of LOVpep the downstream activity and growth cycle arrest corresponded to the affinity of the LOVpep domain. In the future, computational analysis of the point mutations on LOV2 stability may allow for the rational design of a construct with minimal background bind in the off state, but high affinity protein-protein interactions in the on state (Strickland et al. 2010; Lungu et al. 2012; Stein and Alexandrov 2014). This represents a major challenge in the field of optogenetics research and will be critical in adapting these approaches for future uses in cell biology.

I noted as well that on interruption of the *LAT* gene by CRISPR-Cas9 and loss of LAT protein expression there was an apparent increase in the expression of the T cell surface receptor CD6, which appears to have low expression levels on the parental Jurkat E6.1 cell line. CD6 has 3 scavenger receptor cysteine-rich domains and interacts with CD166 on the surface of APCs. Tandem Affinity Mass Spectroscopy has indicated that SLP76 is able to interact with CD6 and thus CD6 may be able to nucleate some of the LAT-associated TCR signalling network molecules (Roncagalli et al. 2014; Breuning and Brown 2017). Upregulation of CD6 may provide a compensatory mechanism to maintain tonic signalling in the absence of the LAT signalosome and could indicate a role for CD6 in the titration of T cell signalling inputs. GWAS analysis of autoimmune diseases such as multiple sclerosis have implicated a role for CD6 in disease aetiology

(Y. Li et al. 2017). Of note, our J-LKO line maintained a minor peak in calcium fluxing on induction by TCR-crosslinking antibodies. This was consistent across other Cas9-mediated LAT knockout cell lines, but not in the JCam2.5 cells, which show no expression of CD6. This finding is interesting and warrants further investigation.

The LAT-specific knockout Jurkat cell line could provide interesting insights into T cell homeostasis and tonic signalling. Furthermore, the CRISPR Cas9 process resulted in the creation of several different T cell lines with varying calcium flux profiles (Appendix G). Future work may provide insights into the mechanisms of signal maintenance by LAT. It should be noted that some of the Cas9 clones displayed a calcium flux phenotype strikingly similar to the TULIPs and LOVTRAP reconstituted cells in which there was an early peak in TCR signalling followed by rapid signal decay. Analysis of the genetic nature of these mutants could provide further insight into the results described below. It is possible that this phenotype in LAT-deficient Jurkat E6.1 cells is caused by haploinsufficiency.

In conclusion, although the LOVTRAP- and TULIPs-based LAT optogenetics systems were not viable for the interrogation of microcluster formation, they did provide valuable insight into the nature of TCR signalling. The results provided in this chapter indicate that the TCR signalling network is tightly regulated. Even signals downstream from the plasma membrane are rapidly attenuated on cessation of TCR signalling. Such tight regulation may provide T cells with a mechanism to discriminate between even closely related antigens.

Chapter 5 – Investigating T-cell signal integration with a light-controllable chimeric antigen receptor

5.1 Introduction

5.1.1 *The immune system and collective decision making*

All living organisms must sense and respond to a diverse array of environmental stimuli. Any given stimulus must be internalised, translated, and interpreted so that the output response is proportional to, and in accordance with the stimulus input. In multicellular organisms, responses to environmental stimuli are highly coordinated, but reflect the collective decision making of individual cells. The immune system represents an important paradigm of this concept. The collective action of a diverse array of cell types is important in regulating steady-state immune homeostasis and the systemic response to pathogens. T cells are important mediators of the overall immune response (B Zheng, Han, and Kelsoe 1996; B Zheng et al. 1996; Qi et al. 2014). Once activated, certain subsets are involved in direct target cell killing, while others release varying arrays of cytokines which serve to activate other immune cell types. Inappropriate T-cell activation, however, can result in autoimmune conditions, asthma, and allergies (Palomares et al. 2014; Chaplin 2010). Furthermore, unchecked T-cell driven inflammation toward an infection can result in systemic level collateral damage to tissues and organs (Dudley 2002). Hence, it is imperative to maintain a balanced immune response. To do this, individual T cells must sense and interpret environmental cues including inflammatory cytokines, signals received through the TCR and co-receptors, and tissue-specific factors (Saleiro and Platanias 2014; Linterman et al. 2014; Campbell and Butcher 2002). Precisely how these signals are integrated on the cellular level has remained an outstanding question for immunologists and cell biologists.

5.1.2 *T cell-mediated responses to infection*

As mentioned above, the activation state of individual T cells in an immune reaction collectively forms a systemic response to infection. Precisely how this response is titrated to the severity of infection remains somewhat unclear. That is, during a severe infection, the T cell response must be appropriately strong, but if the burden of infection is low then the T cell response should be proportionate to the severity of infection to mitigate off-target effects (King et al. 2012). This implies that individual T cells are able to sense signal strength and respond accordingly.

To measure T cell responses in infection several models have been used over the years, but *Listeria monocytogenes* has been a favoured model system by immunologists. *L. monocytogenes* is a gram-positive bacterium responsible for listeriosis and is capable of infecting a murine host (Hamon, Bierne, and Cossart 2006). It is also known that clearance of this infection is T-cell mediated (Szalay, Ladel, and Kaufmann 1995; Lara-Tejero and Pamer 2004). Using a *L. monocytogenes* OVA model of infection, van Heijst, et al. (2009) showed that the magnitude of the T cell response to infection is primarily driven by clonal expansion of activated naïve T cells. This result complements previous findings by Prlic, Hernandez-Hovos & Bevan (2006) and Badovinac, Porter & Harty (2002) suggesting that the magnitude of the T cell response is proportional to the burden of infection and that these signals are transduced via the TCR. Such findings have raised questions as to the nature of T cell activation. Specifically, how are T cells able to tailor their output response to the severity of infection? T cell activation results in T cell proliferation and differentiation, yet this response must be titrated so as to mitigate collateral damage. So how are T cells able to interpret and scale the immune response to best combat infections?

A number of studies have shown that during an infection, the majority of antigen specific T cells become activated (K. E. Tkach et al. 2014; van Heijst et al. 2009). This speaks to the selectivity of the T cell response but also to the efficiency of the overall immune reaction. It also indicates that the response to infection must be self-limiting and able to provide a diverse output. During activation, T cells undergo proliferation and differentiation. Two processes that are synchronous, yet independent (Buchholz, Schumacher, and Busch 2016). Ultimately, the process of activation gives rise to a population of effector and memory T cells with diverse functional specificities; T_H1 , T_H2 , T_{FH} , etc. but with a proliferative capacity proportional to the magnitude of infection. Functional diversity is thought to be explained partially by TCR signal strength, but also by cell-intrinsic differences in protein expression (Cho et al. 2017; Feinerman et al. 2008; Tubo and Jenkins 2014; Tubo et al. 2013). This probabilistic determination of effector cell phenotypes ensures a more balanced response to infection. Availability of antigen and TCR signal strength and duration are thought to be the key variables affecting the T cell proliferative response, with increased antigen availability increasing the amount of contact time between T cells and DCs (C. Kim et al. 2013).

5.1.3 Translating primary infection to adaptive immunity

As discussed in Chapter 1, the immune system can be broadly divided into two major responses, innate and adaptive. The innate immune response is non-specific, relying on pathogen-specific

molecular motifs that distinguish pathogenic organisms from the host (Table 1.1). A series of checkpoints allows the innate immune system to detect and respond to the severity of infection. These checkpoints allow cells to determine whether the pathogenic organism is present (Napolitani et al. 2005), its viability, and the severity of infection (Blander and Sander 2012). These innate immune signals are internalised by DCs (and other cells of the innate immune system), which migrate to lymph nodes and translate these responses to adaptive immunity via T cell activation (Figure 1.1).

The probability of a T cell encountering its cognate pMHC in the periphery is low, thus naïve T cells recirculate through the lymphatic organs, where the probability of them encountering their cognate pMHC is much higher. The architecture of secondary lymphoid organs, including lymph nodes, has evolved in such a way as to maximise the efficiency of adaptive immune response activation. Indeed, studies modelling the T cell response to infection have shown that during an adaptive immune response, effectively all of the cognate T cells become activated (Zehn, Lee, and Bevan 2009). Two-photon microscopy of immune cells within the lymphatics has shown that DCs can interact with as many as 5000 T cells an hour. T cells migrate through the lymph nodes at a rate of $\sim 10 \mu\text{m}$ per minute and are likely to encounter multiple DCs during their journey (Cahalan and Parker 2008; Qi, Kastenmüller, and Germain 2014). On encountering cognate pMHC, T cells down-regulate their cellular migration machinery, such as Rho GTPases, and form stable contacts with an APC (Bousso and Robey 2003; Michael L. Dustin 2004; M L Dustin et al. 1996; Negulescu et al. 1996). The precise duration of T cell-APC interaction necessary to drive T cell proliferation and differentiation is still somewhat contentious and seems to vary between CD8^+ and CD4^+ T cells (Obst 2015), with CD8^+ T cells reportedly requiring only hours of contact to drive activation (Williams and Bevan 2004) and CD4^+ T cells requiring several days (Corbin and Harty 2004). The duration of this interaction likely influences the proliferative, but not the differentiation, capacity of the T cells and is intrinsically influenced by antigen dose, in a ‘dose-to-duration’ manner (Miskov-Zivanov et al. 2013; Obst 2015; Mayya and Dustin 2016; Keck et al. 2014). This seems to be true both for proliferation and the cytokine response to infection (van Panhuys, Klauschen, and Germain 2014; K. E. Tkach et al. 2014; Tschärke et al. 2015). Furthermore it is clear that the manner in which antigen is presented influences the outcome of stimulation, i.e. the presence or absence of co-stimulatory/co-inhibitory receptors and tissue-specific signals (Campbell and Butcher 2002).

5.1.4 T cell activation and temporally encoded signals

In the past two decades we have seen massive progress in our understanding of the process of T-cell activation; particularly events in early activation. Although our knowledge of the signal transduction apparatus has significantly improved, precisely how activatory signals are transduced, translated, and interpreted remains somewhat of a mystery. Advances in microscopy and live cell imaging have highlighted the complexities of T cell-APC interactions. In particular, it has been shown that T cells seem to interact with multiple dendritic cells on their passage through the lymph node (Mempel, Henrickson, and von Andrian 2004; Henrickson et al. 2008). The physiological significance of these interactions remains incompletely understood, but it has been proposed that transient, non-activatory interactions between T cells and APCs may impart the T cell with 'short-term' memory of this interaction (Mayya and Dustin 2016). This feature of T cell activation is separate from immunological memory and occurs during the T cell activation process. The short-term memory hypothesis of T cell activation states that complete T cell activation occurs due to the accumulation of as-yet-undefined signalling intermediates (Locasale 2007). The accumulation of signalling intermediates allows the T cell to accumulate discontinuous periods of signalling into a cumulative output response. In other words, as the T cell interacts with APCs within the lymph node, each transient interaction contributes marginally toward the activation state of that T cell. If this hypothesis were correct, such signals would need to be tightly regulated to avoid off-target activation toward a potentially non-activatory ligand, yet persist long enough to contribute toward a second activatory encounter.

The above hypothesis can be reconciled by the fact that a number of modelling and experimental studies now seem to point to the fact that several TCR-associated enzymatic signalling pathways and transcription factors are controlled in a 'digital' manner. That is, they are either maintained in a state of low activity or a state of high activity. This characteristic is imparted on the TCR signalling network through several feedback and feedforward mechanisms that tightly control the activation state of proteins within the network.

For example, work by Au-Yeung et al. (2014) using a Nur77 GFP reporter system showed that increasing the amount of antigen present within the system did not increase the degree to which the cells became activated, but rather increased the fraction of responding cells. This seems to confirm work by Huang et al. (2013) showing that as little as a single agonistic pMHC is needed to initiate T cell activation. This finding is interesting because it confirms modelling studies suggesting that T cell activation is amplified by feed forward mechanisms that digitise the TCR signalling input (Altan-Bonnet and Germain 2005). In these studies, the T cell discrimination

threshold is set by a negative feedback loop that counteracts the positive one. In accordance with these modelling studies, Das et al. (2009) were able to show that the Ras signalling pathway is under the control of positive feedback mediated by SOS1 and RASGRP. Moreover the authors pointed out that the rapid digitisation of the Ras signalling pathway generates lag between the upstream and downstream signalling modules. This hysteresis could be a mechanism that imparts short-term memory into the signalling network, i.e. if a second signal is received through the TCR before the first signal has completely dissipated then the T cell may be able to sum those signals into a cumulative output response. Other groups have also shown the digital nature of other TCR-associated signalling modules, such as NF- κ B (Kingeter et al. 2010) and NFAT (Podtschaske et al. 2007). All of these findings point to the temporal summation of discontinuous digital signals in T-cell activation, but do not explain how the T cell is able to sum such signals.

5.1.5 Immediate early gene expression and signal integration

To test the TCR signal integration hypothesis, Faraoudi et al. (2003) used the Src kinase inhibitor PP2. In their experiment T cells and B cells were conjugated within a collagen matrix and calcium activity, ERK mobilisation and IFN- γ production was observed. After 30 minutes of activation, the cells were pulsed for 20 minutes with PP2, which was then washed out and the cell were activated for an additional 30 minutes. This pattern was then repeated. It was found that a single, 30-minute pulse of continuous signalling was not enough to drive cytokine production, but several pulses of signalling could drive cytokine production, showing that these signals were cumulative. Computer modelling by Locasale (2007) posited that these signalling events could accumulate through the expression and stabilisation of immediate early genes (IEGs). As their name suggests, these genes are expressed early in the activation process of multiple signalling response pathways and do not require the upregulation of other transcription factors to drive their expression. They are expressed using the ubiquitously present cellular transcription machinery (Bahrami and Drabløs 2016).

Several candidates have been proposed to fulfil the role of signal integrator in T cells, including Interferon regulatory factor 4 (IRF4), basic leucine zipper transcription factor, ATF-like (BATF), Myc, and Fos, among others. IRF4 is reported to accumulate gradually during the first 24-48 hours of T cell activation, providing a graded IRF4 signal corresponding to the duration of TCR signalling (Man et al. 2013; Nayar et al. 2014). IRF4 has also been shown to act as a 'read-write integrator and drive expression of antigen-dependent genes (Man et al. 2013; Krishnamoorthy et al. 2017). IRF4 binds specific promoters regions in an affinity-dependent

manner, with heightened IRF4 expression increasing the probability of promoter occupancy. The resulting altered transcription profile affects T cell fate decision (Krishnamoorthy et al. 2017).

BATF may also be involved in integrating discontinuous TCR signals. BATF reportedly accumulates within the first 72 hours of T cell activation but is dispensable in the later stages of activation (Man et al. 2013; Kurachi et al. 2014). Interestingly, haploinsufficiency of BATF or IRF4 results in decreased proliferative capacity of the activated T cells (Man et al. 2013; Kurachi et al. 2014). It could be that these factors accumulate and then are diluted in response to successive proliferation events, leading to a cell-intrinsic 'stop' signal.

Myc is another early response factor and serves to prime cells for activation. Myc is not unique to T cells, but functions downstream of multiple different signalling pathways (Dang 2013; Guy et al. 2013). Transient engagement of the TCR may activate Myc leading to a change in the genetic regulatory landscape of the T cell. These changes may serve to prime the T cell for further encounters with APCs.

Finally, Fos is another IEG candidate proposed to impart short-term memory on the T cell signalling network. Many IEG products are rapidly degraded, but hyperphosphorylation of the Fos protein may provide enough stability to allow for its accumulation following intermediate pulses of signalling (Locasale 2007). Moreover, Fos forms part of the AP-1 transcription factor, which interacts with NFAT to trigger gene transcription following T-cell activation (Macian 2005).

5.1.6 Secondary signals regulate T cell activation

Prolonged signalling combined with gene transcription creates an intrinsic lag period in the signalling network. In the event of prolonged signalling, as might be expected with T cell activation, this feature of cell biology would be expected to maximise the dynamic range of the signalling output because small differences in the signalling input would be amplified over the duration of the activation signal, with longer signals amplifying these differences more than shorter signals. However, this does not appear to be the case in the TCR signalling network. Although, heterogeneity in protein expression has been suggested to lead to differences in cell fate (Tubo et al. 2013) this process is predictable and remarkably consistent between immune responses in different mice or different infection models (Cho et al. 2017). This suggests that extrinsic signalling factors normalise the T cell response.

It is known that T cell fate outcomes are not completely autonomous, but dependent on external cues, such as cytokine signalling or co-stimulatory receptor signalling (N. Zhang and

Bevan 2011). Experimentally, IL-2 has been shown to actively regulate TCR signalling within the first 12 hours of signal initiation (Voisinne et al. 2015). IL-2 expression has been shown to be self-limiting as expression of IL-2 accelerates expression of the IL-2 receptor (IL-2R) and blocks further IL-2 expression through a feedback mechanism mediated by STAT5 (K. E. Tkach et al. 2014). Increased receptor expression gradually leads to the internalisation and degradation of the extracellular IL-2 supply, thus limiting IL-2 signalling. This time-integrated signal feeds into the T cell activation state to limit proliferation in the absence of proliferative signals. Thus, this IL-2 feedback mechanism serves to dampen the T cell response and reduce heterogeneity in the T cell-mediated immune reaction. Other mechanisms beyond IL-2 likely play a role in tuning the T cell response to infection including IL-12, IL-1 β , IL-6 and IFN α (Starbeck-Miller, Xue, and Harty 2014). Prolonged presence of antigen likely extends the duration of IL-2 expression, delaying the feedback loop (K. Tkach and Altan-Bonnet 2013; K. Tkach et al. 2014).

It should also be noted that these secondary signals occur in concert with self-limiting TCR feedback signals. Prolonged TCR signalling results in TCR internalisation and a reduction in the magnitude of signals received through the TCR (Boyer et al. 1991; Martínez-Martín et al. 2011). This response, together with cytokine receptor feedback and co-stimulatory or –inhibitory signals, serves to regulate the duration of TCR signalling.

5.1.7 An engineering approach to cell biology

As discussed in Chapter 3, optogenetics and CID are providing new ways of interrogating cell signalling dynamics. Indeed, an excellent series of work by Toettcher and colleagues has yielded new insights into the mechanisms of signal transduction through the canonical Erk signalling pathway (Toettcher, Weiner, and Lim 2013; Toettcher et al. 2011; Johnson et al. 2017). Using a light-controllable GEF they were able to exert precise temporal control over MAPK signalling to show how temporal modulation of a single signalling pathway can yield phenotypically distinct outcomes, they were able to show that the Erk signalling module, downstream of the PDGF receptor acts as a bandpass filter to screen out low frequency or short duration signals and allow long duration signals through. It follows that T cells may be able to interpret the same sort of temporally encoded signals through the TCR; as T cells must be able to interpret MHC-restricted signals within a narrow range of affinities it follows that they should be able to distinguish temporally between activating signals and non-activating signals. Moreover, the work outlined above suggests that T cells are also able to interpret temporally discontinuous signals through an incompletely understood mechanism.

Optogenetics is unique in its ability to provide high spatial resolution and precise temporal control to cellular signalling pathways. By coupling input modulation to a quantifiable output response one can begin to assess the underlying mechanisms of a system. To an extent this has been attempted in T cells with the Nur77-GFP reporter system (A. Moran et al. 2011; Zikherman, Parameswaran, and Weiss 2012; Au-Yeung BB et al. 2014) but the limited spatiotemporal resolution of the drug and antigen inducible system limits the extent of information that can be gained from such an approach.

By reducing the system to its minimal components we can begin to understand the basic mechanisms behind a biological process (Lim 2010). Here I use the Jurkat T cells as a model for T cell activation (Bartelt et al. 2009). To address the challenge of signal integration in T cells I have developed a drug-inducible, optogenetic chimeric antigen receptor (CAR), ‘optoCAR’ based on the blue light-responsive LOV2 domain and the LOVTRAP optogenetic system (Wang et al., 2016). The idea behind CARs is relatively straightforward and was conceived in the 1980s (Gross, Waks, and Eshhar 1989). An immunoglobulin domain specific toward a surface-expressed cancer biomarker is fused to the intracellular signalling motifs of CD3 ζ and the CD28 co-receptor (Sadelain, Brentjens, and Rivière 2013). Host T cells are then extracted and genetically modified to express the CAR, endowing them with the ability to recognise cells expressing the target epitope. This technology has successfully been implemented against CD19-expressing myelomas (Posey et al. 2016; B. L. Levine et al. 2017) and HER2-positive breast, lung and ovarian cancers (M. Sun et al. 2014; Globerson-Levin, Waks, and Eshhar 2014). Rather than an extracellular immunoglobulin domain the optogenetic chimeric antigen receptor features a drug-inducible dimerization domain which can be used to engage the complementary binding partner expressed on the surface of a surrogate APC. Like other CARs, the optogenetic CAR relies on the signalling domains of CD3 ζ . Photoisomerisation of the intracellular LOV2 domain leads to dissociation of the CD3 signalling domains from the rest of the receptor and signal termination. In this way I was able to precisely control periods of TCR-like signalling and signal termination.

5.2 *Materials & methods*

5.2.1 *Cell-cell conjugate calcium flux*

The conjugate calcium flux procedure was adapted from the calcium flux protocol outlined in Chapter 2, section 2.7.3. JNFAT T cells were preloaded with Indo-1 AM leak resistant dye (TEFlabs) and washed in DPBS as described previously. OptoCAR-positive, Indo-1-loaded

JNFAT cells were mixed 1:1.5 with Raji B-cells expressing the complementary FRB-Ex receptor in 100 μ l of complete RPMI. The cell mixture was aliquoted into individual PCR tubes, which were sealed and transferred to a 37°C water bath for 30 minutes to allow the cells to sediment and conjugate. Following the incubation the cells were gently resuspended by pipetting and transferred into FACS tubes (Falcon) containing 500 μ l of fresh, room temperature, complete RPMI. The cells were then left for 30 minutes to equilibrate at room temperature with occasional, gentle agitation to prevent clumping.

Calcium flux measurements were acquired using a BD Fortessa flow cytometer equipped with a UV (355 nm) laser. Live cells were gated on forward scatter and side scatter. The JNFAT cells express the fluorescent protein iRFP as a marker and the Raji B cells express TagBFP. Conjugates were determined to be events positive for both iRFP and BFP.

Samples were run for 1 minute prior to triggering to establish a baseline Indo-1 reading. After acquiring a baseline, the FACS tube was removed and the cytometer was left running. To trigger the cells, A/C heterodimeriser (AP21967; Clontech) rapalog was added to a final concentration of 1 μ M. The FACS tube was then returned to the cytometer and ratiometric shift in calcium fluxing was observed as described in chapter 2. Gating was performed in Flowjo v10.1r5.

5.2.2 Light Plate Apparatus

For long-term cell activation assays I used the 24-well light plate apparatus (LPA). Design and implementation are well described by Gerhardt et al. (2016). Our LPA was fitted with forty-eight 5 mm, 475nm LEDs (TEKCORE) and a frosted acrylic diffuser plate, which was designed in-house (Appendix K). Gaskets were cut using a Trotec Speedy 300 laser cutter. The LPA adapter plate was designed for use with a tissue culture-treated, black, glass-bottomed, 24-well plate (4titude). The light conditions in each well were programmed according to protocol described by Gerhardt et al. (2016).

For the 24-hour time course stimulations and pulse width modulation experiments, cells were conjugated together in PCR tubes for 30 minutes in a 37°C water bath in a total volume of 100 μ l of complete RPMI. Cells were conjugated at a ratio of 1:1.5, JNFAT:Raji. Cells were gently resuspended by pipetting and added to each well of a 24-well plate containing 400 μ l of RPMI and A/C heterodimeriser (AP21967), with a final concentration of 1 μ M. The loaded LPA was then returned to incubator at 37°C, 5% CO₂ for 24 hours.

After the time course was completed cells were transferred to individual FACS tubes and centrifuged for 3 minutes at 800 rpm. Media was harvested and immediately frozen for subsequent ELISA analysis of IL-2 secretion as described in chapter 2, section 2.9. ELISA samples were diluted 1:5 in ELISA dilution buffer prior to analysis. Cells were prepared for FACS analysis as described in chapter 2, section 2.7.1.

5.2.3 Data Analysis

Sample gating and compensation were performed using Flowjo v10.1r5. Data was exported as a CSV file for analysis in Matlab R2016b (Appendix D & E). For calcium flux samples, baseline flux was established and percent of activated cells above the baseline were calculated along with the median ratiometric Indo-1 value. A second script was developed to calculate peak separation between positive and negative cells in the 24-hour time course assay. This script was used to calculate the percentage of positive cells for each sample relative to a negative control sample as well as the median fluorescent intensity of the positive fraction of cells.

For generating signal decay curves samples were normalised to the single pulse controls; that is, 6 hours of continuous stimulation as the maximum value or a single pulse stimulus corresponding to the increment of dark time for the minimum value. I tested dark increment times of 5 minutes, 15 minutes, 30 minutes, 60 minutes, 90 minutes, 120 minutes, and 180 minutes. All figures were prepared using Matlab R2016b and Adobe Illustrator.

5.3 Results

5.3.1 Stable expression of light- and drug-controllable chimeric antigen receptor in Jurkat T cells

Existing models of T-cell activation traditionally rely on either plate bound or soluble antibodies to crosslink the TCR, or on mouse-derived T cells with a known antigen specificity. Although these models have been extremely instructive in developing working models of T-cell activation, they are ultimately restricted in their capacity for rapid and tunable modulation of T cell signalling dynamics. I sought to develop a physiologically-relevant, tunable CAR compatible for use in a cell-

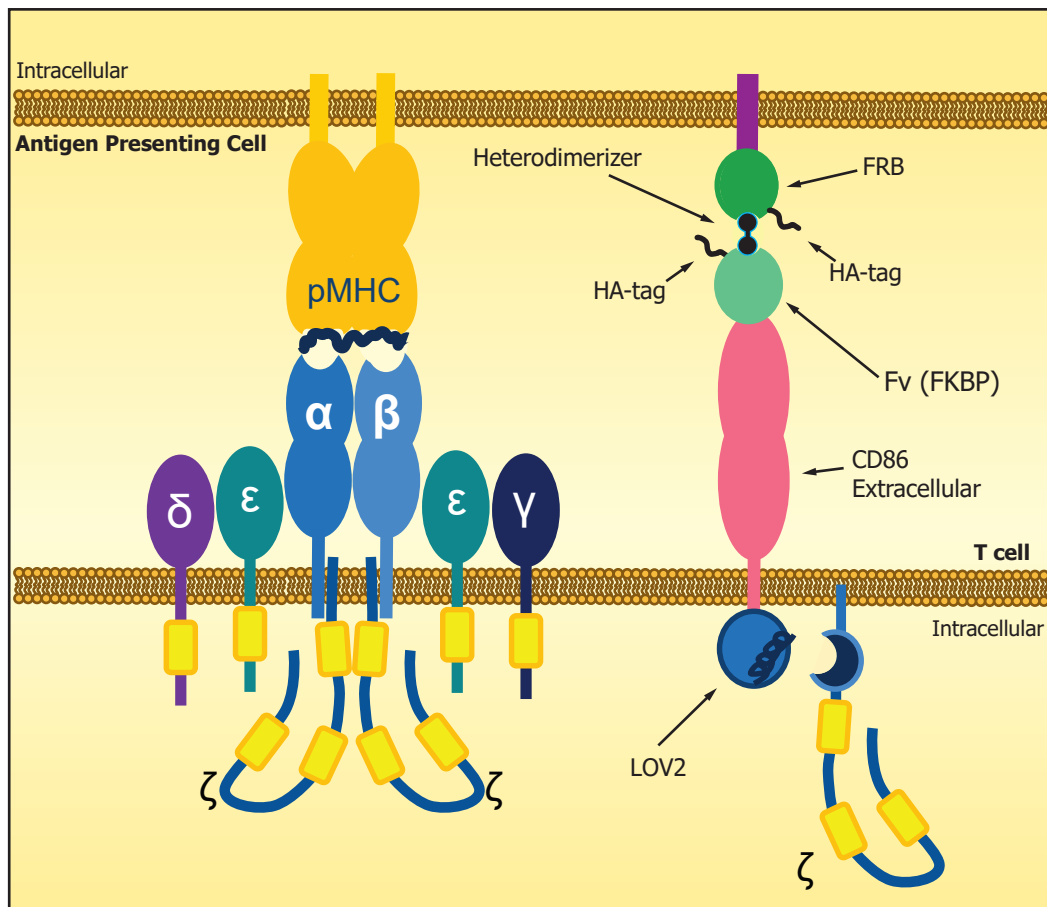


Figure 5.1 Optogenetic chimeric antigen receptor (Right) On engagement with pMHC the ITAM domains of CD3 (yellow) become phosphorylated by LcK. **(Left)** To mimic this interaction a drug-inducible, optogenetic chimeric antigen receptor was designed. Addition of the heterodimerising Rapamycin analog causes the formation of a ternary complex between FRB, expressed on a surrogate APC, and Fv, fused to the extracellular domain of CD86. The LOV2 domain is fused to the cytoplasmic side of the chimeric receptor and allows for light-inducible dissociation of the signalling domain. The CD3 ζ signalling domains of the chimeric antigen receptor are fused to a myristoylated Zdk domain and diffuse laterally across the plasma membrane.

cell system. This optoCAR is drug-inducible via the FRB-FKBP interaction and light-controllable via an intracellular LOV2 domain (Figure 5.1). The receptor was designed around the LOVTRAP optogenetic system and the Rapalog-inducible FRB-FKBP12 system. In this case, the Zdk domain was anchored at the plasma membrane using an N-terminal myristoylation motif and fused via a short linker to the three ITAM motifs of CD3 ζ at the C-terminus of the construct (Figure 5.1, right). The transmembrane component of the optoCAR is comprised of an N-terminal Fv (FKBP12) domain fused with the extracellular and transmembrane domains of CD86. At the C-terminus of the optoCAR on the cytoplasmic side of the plasma membrane is the LOV2 domain (Figure 5.1, right). In the dark, the optoCAR mimics the architecture of the wildtype TCR complex (Figure 5.1, left) with the signalling domains anchored to the intracellular domain of the receptor via the LOV2-Zdk interaction. Under blue light irradiation, photoisomerisation of LOV2 causes the CD3 ζ chain to laterally dissociate across the plasma membrane away from the transmembrane component of the receptor. The transmembrane receptor component and intracellular signalling component would be expected to diffuse at different rates within the plasma membrane, thus allowing for their complete dissociation (Vaz, Goodsaid-Zalduondo, and Jacobson 1984). The optoCAR is activated in the presence of a Rapamycin-analogue ('rapalog'), which induces the formation of a complex between the extracellular, N-terminally expressed Fv domain and its interaction partner, FRB, expressed likewise on the surface of a synthetic APC (Figure 5.1). CID between the FRB and Fv domains forms a high affinity ternary complex ($K_d = \sim 12$ nM) (Banaszynski, Liu, and Wandless 2005) and mimics a high-affinity TCR-pMHC interaction. The extracellular interaction of the optoCAR functions orthogonally to the endogenous TCR and is thus unlikely to interfere with cellular homeostasis.

Mutation	$t_{1/2}$ Reversion (s)	Name
Wildtype	~ 81	OptoCAR
V416T	~ 2.6	OptoCAR _{FAST}
V146L	~ 496	OptoCAR _{SLOW}
C450G	Photo-nonresponsive (Zdk constitutively bound)	OptoCAR _{CLOSED}
I539E	Constitutively active (Zdk constitutively unbound)	OptoCAR _{OPEN}

Table 5.1: Overview of OptoCAR variants

Photocycle kinetics of the LOV2 domain are tunable via a series of point mutations (Table 3.1). These mutations have been well characterised and yield LOV2 variants that revert from the active lit-state to the unstimulated ground-state at rates both faster and slower than the wildtype domain (Zayner and Sosnick 2014; Zayner et al. 2013; Zimmerman, Kuhlman, and Yumerefendi 2016). It was reasoned that different variants of the optoCAR system would be useful for interrogating signalling at different stages of activation. I developed 5 variants of the optoCAR system, which are outlined in Table 5.1.

The optoCARs were stably transduced into the Jurkat-derived, JNFAT cell line. JNFAT cells are a clonal population stably expressing a cytoplasmic iRFP marker as well as GFP under control of the NFAT promoter, which provides a reliable readout of T-cell activation (Clipstone and Crabtree 1992). To minimise variation between optoCAR-expressing cell lines, I transduced the signalling component of the system, myrZdk-CD3 ζ -Ruby, into the JNFAT cells first. As would be expected, expression of the iRFP marker was identical between each cell line (Figure 5.2A). Although most variants of the receptor showed equivalent levels of myrZDK-CD3 ζ -Ruby it was noted that the LOV2_{C450G} (OptoCAR_{CLOSED}) cell line expressed more than the other cell lines (Figure 5.2B). For the case of the C450G mutant which shows constitutive binding with the Zdk domain, the constitutive engagement of the two receptor components may serve to stabilise myrZDK-CD3 ζ -Ruby at the cell surface and prevent its degradation. It was found that the transmembrane component of the optoCARs were not well-expressed and thus I used lentiviral concentration to increase transduction efficiency. This strategy allowed for approximately equivalent levels of expression between all of the receptors (Figure 5.2C). Over a period of weeks, it was found that expression of the optoCAR system had a tendency to drop, thus I periodically returned to frozen stocks to maintain consistency between experiments (Appendix L). Expression of the complementary FRB receptor in a clonal Raji B cell line was observed by concurrent BFP expression (Figure 5.3).

The ‘Two Signal Hypothesis’ states that T-cell activation is directed not only through TCR signalling, but also through signals derived from co-stimulatory (or inhibitory) receptors (Chen and Flies 2013). One well-characterised co-stimulatory receptor is CD28, which is expressed on the surface of T cells (Nunes et al. 1996). We confirmed expression of CD28 on our JNFAT line by flow cytometry (Figure 5.4A). CD28 interacts with CD80 and CD86 expressed on the surface of APCs (Greene et al. 1996). We confirmed expression of these receptors on Raji B cells (Figure 5.4B, i & ii). Previous studies have confirmed that Jurkat T cells also express the integrin receptor LFA-1 (CD11a) (Bartelt et al. 2009) and that Raji B cells express its interaction partner ICAM-1

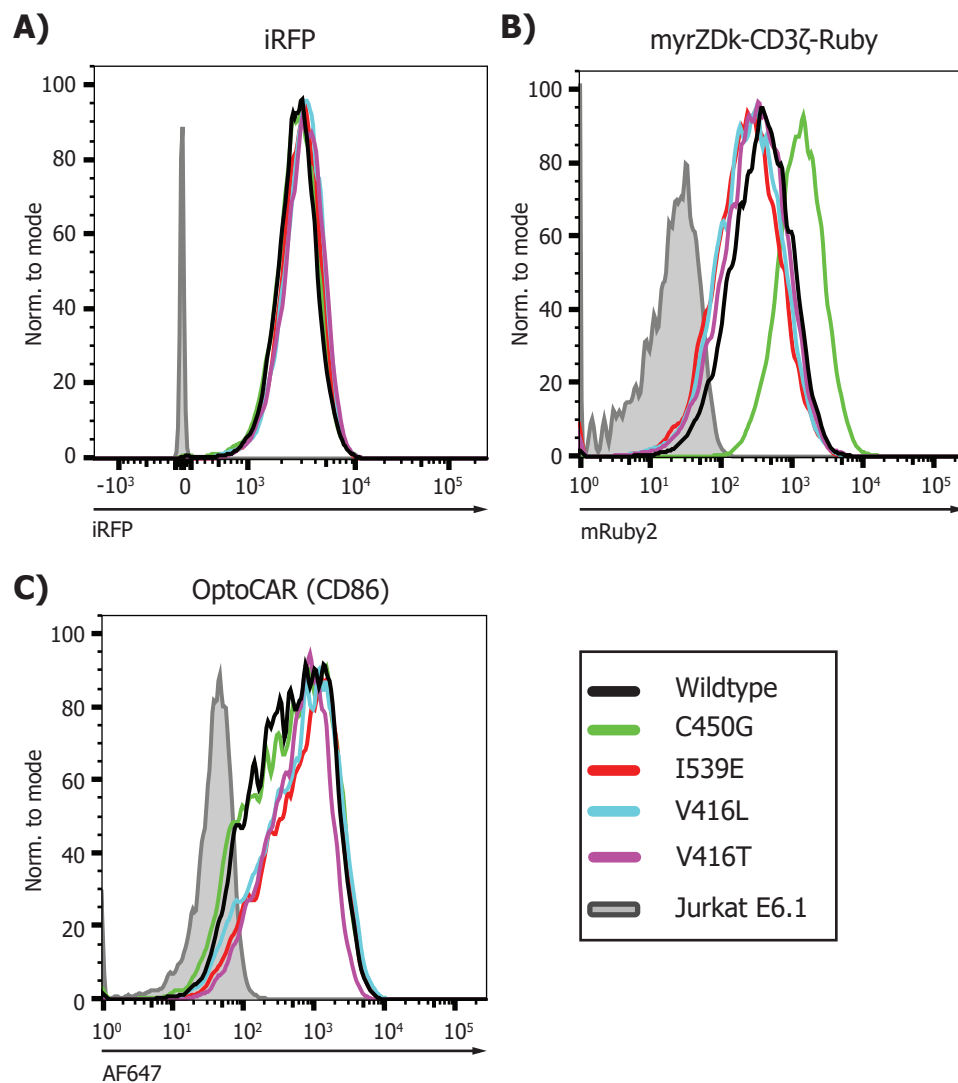


Figure 5.2 Expression of the OptoCAR systems in JNFAT cells (A) JNFAT cells express a cytoplasmic iRFP marker, which remains unperturbed by the addition (B) myrZdk-CD3ζ signalling motifs and (C) transmembrane receptor components of the opto-CAR systems

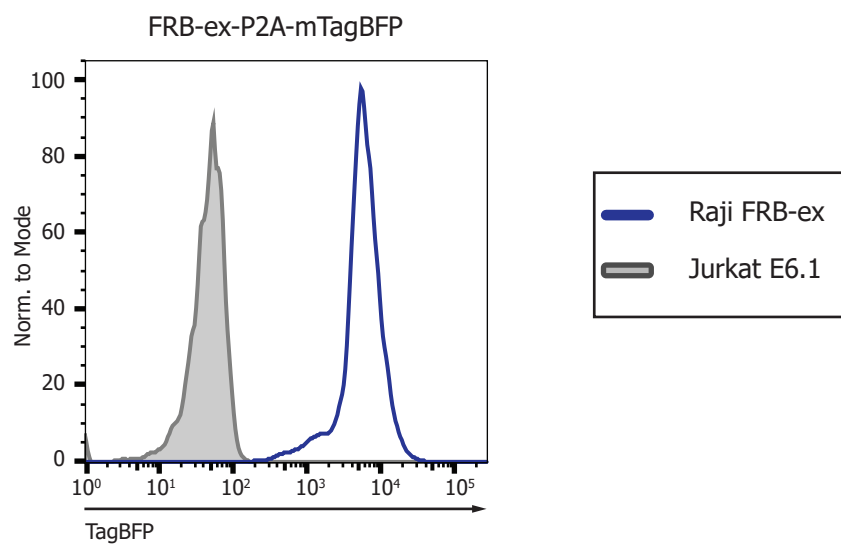


Figure 5.3 FRB-ex, BFP expression The FRB receptor was coexpressed on a vector with the fluorescent marker mTagBFP in Raji B cells

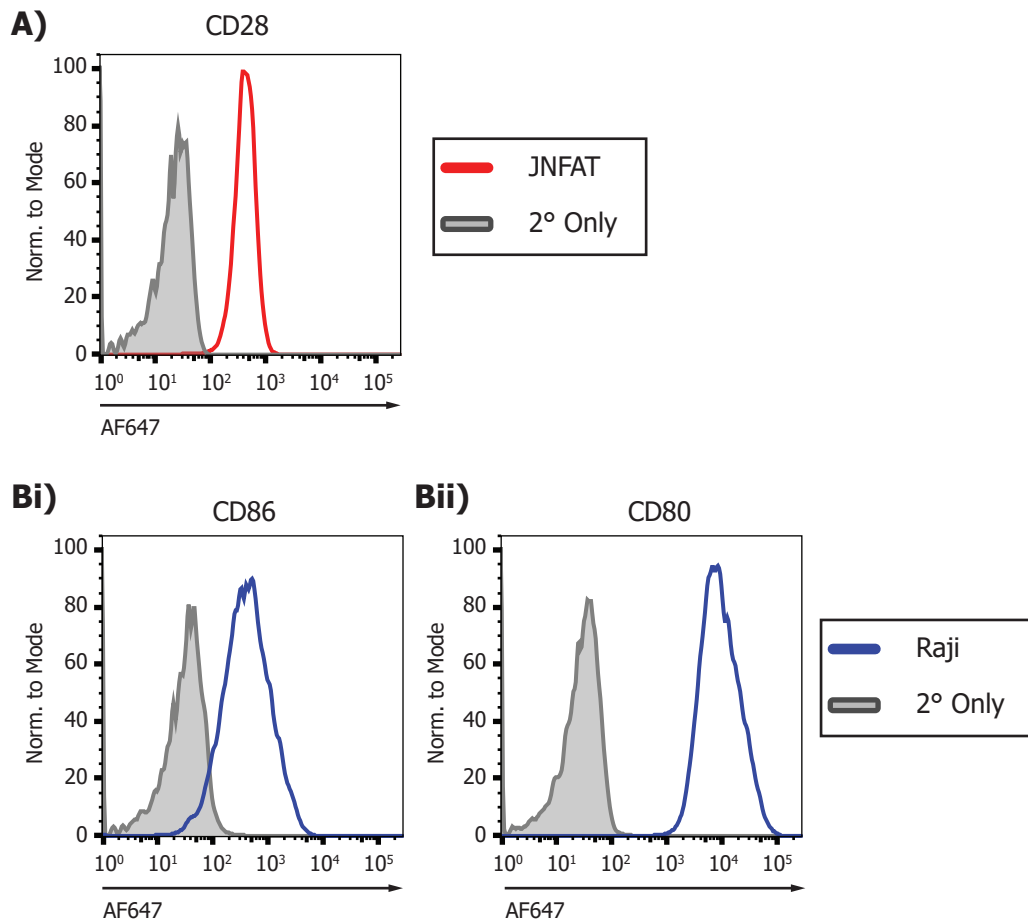


Figure 5.4 Expression of TCR co-stimulatory receptors (A) JNFAT cells highly express the TCR co-stimulatory receptor, CD28. Raji B cells express the ligands for CD28, **(Bi)** CD80 and **(Bii)** CD86.

(CD54) (Y. Kim et al. 2007). These data indicate that the JNFAT OptoCAR cell lines, when conjugated with Raji B cells expressing the complementary receptor, represent a physiologically-relevant model system for the interrogation of T-cell signalling dynamics.

5.3.2 OptoCARs recapitulate early T cell activation

Having generated five JNFAT cell lines expressing different variants of the optoCAR system (Table 5.1), we next sought to investigate the ability of these receptors to recapitulate TCR-induced signalling. It is well established that engagement of the TCR by its ligand induces a cascade of downstream signalling and phosphorylation. One of the earliest events in T cell activation is the release of intracellular calcium stores and the subsequent triggering of extracellular calcium fluxing (Huse et al. 2007; Balagopalan et al. 2010). This is commonly induced in T cells using α CD3 antibodies and a crosslinking agent, or chemically with phorbol esters and calcium ionophores. These techniques potentially trigger calcium fluxing but are clearly non-physiological. I developed an alternative method, whereby real-time signalling outputs can be measured in live-cell conjugates (Figure 5.5). JNFAT optoCAR cells were preloaded with Indo-1 (Figure 5.5A, left) and then conjugated, in the absence of rapalog, with Raji B Cells expressing the complementary FRB receptor and BFP (Figure 5.5A, right). Using standard flow cytometry, conjugated cells can be identified as events that are double-positive for iRFP and BFP (Figure 5.5B). Addition of rapalog triggers the engagement of the optoCAR and subsequent downstream signalling (Figure 5.5C). Using the FACS light box (Appendix J), this conjugate assay allowed for precise triggering of T cell activation and real-time visualisation of the effect of signal modulation on calcium fluxing.

As with the LAT system, I tested the optoCARs using the photo-nonresponsive version of the receptor (optoCAR_{CLOSED}) and the constitutively open and unbound version of the receptor (OptoCAR_{OPEN}). I sought to compare activation through the optoCAR system with activation through the endogenous TCR. The antigen specificity of the Jurkat TCR is unknown, but T cell-APC conjugates are known to be non-specifically triggered by superantigen (Ohnishi et al. 1995). Staphylococcal Enterotoxin E (SEE) simultaneously binds TCR and MHC resulting in potent, polyclonal T cell activation (Saline et al. 2010). The data presented herein show both the calcium flux signal as measured by the ratio of calcium-bound Indo-1 dye to calcium-unbound Indo-1 dye and the fraction of cells undergoing calcium fluxing. On the addition of rapalog, optoCAR_{Closed}-expressing JNFAT cells began to flux calcium following a short delay period of ~60 seconds (Figure 5.6 & Figure 5.7). This delay in calcium flux triggering is consistent with previous studies

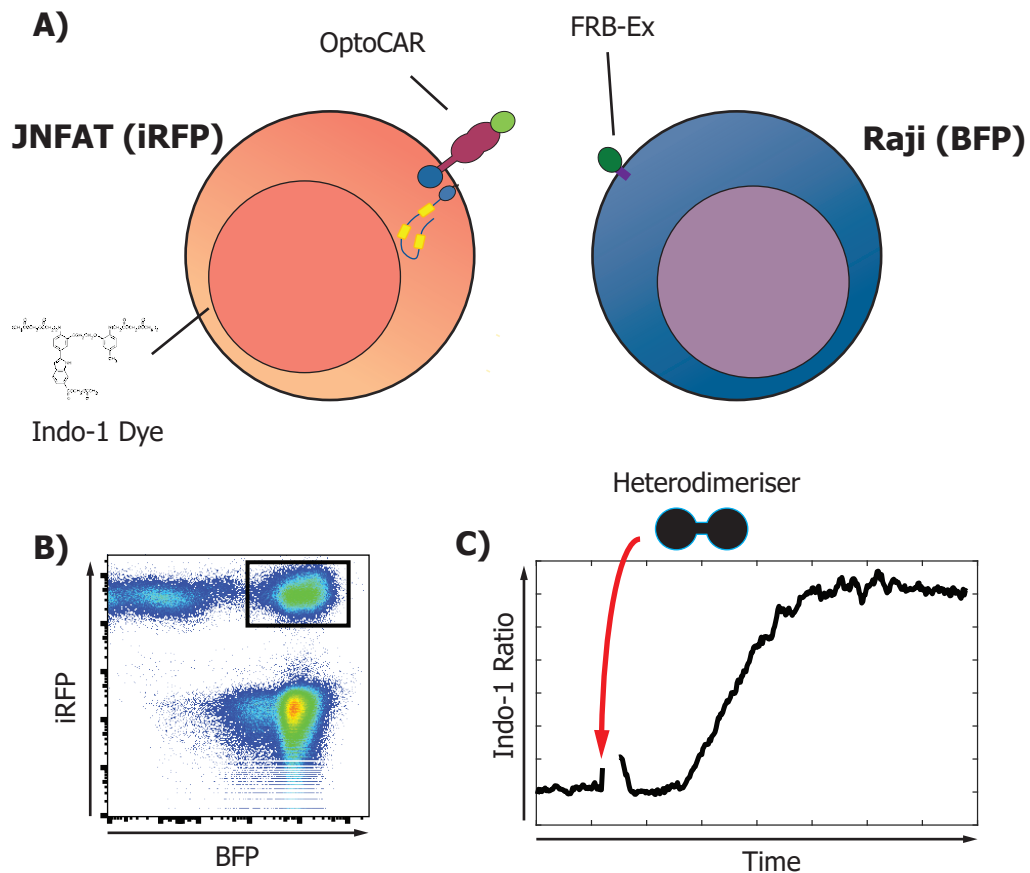


Figure 5.5 Overview of the conjugate flux experiment (A) JNFAT cells expressing the optoCAR receptor are pre-loaded with indo-1 dye, washed and conjugated with Raji B cells expressing the complementary FRB receptor. JNFAT cells are labelled with an iRFP marker and Raji B cells are labelled with a BFP marker. **(B)** During calcium fluxing conjugates are selected on events double-positive for iRFP and BFP. **(C)** Calcium fluxing is triggered on the addition of a heterodimerising drug, which engages the artificial receptors. The FACS light box can then be used to modulate light conditions and the effect on fluxing can be monitored in real-time.

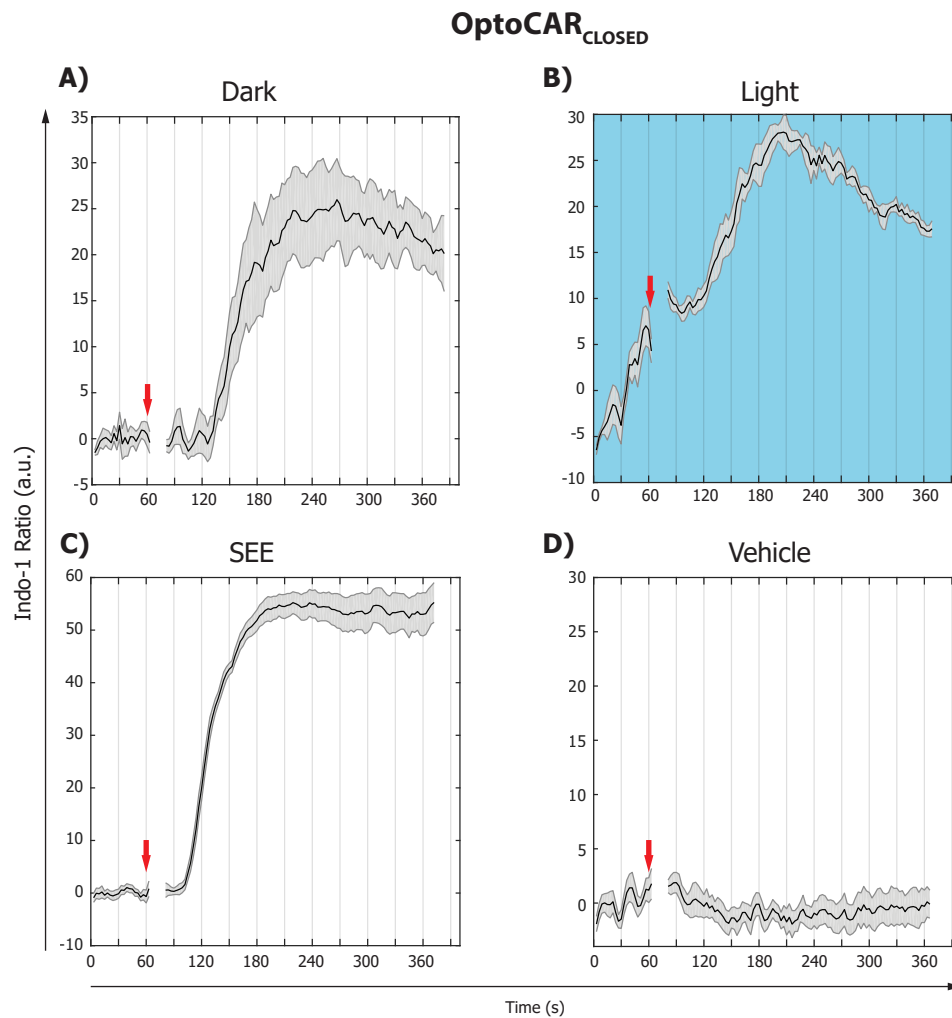


Figure 5.6 Potent calcium fluxing in optoCAR photo-nonresponsive cells
 Pre-gated conjugates were induced to flux calcium via the addition (red arrow) of rapalog **(A-B)**, SEE **(C)**, or vehicle **(D)**. The magnitude of calcium fluxing is presented as the ratio of calcium bound to unbound indo-1 dye. For each flux profile $n=3$, calcium flux is presented as median ratio above the baseline, error bars are given as SEM.

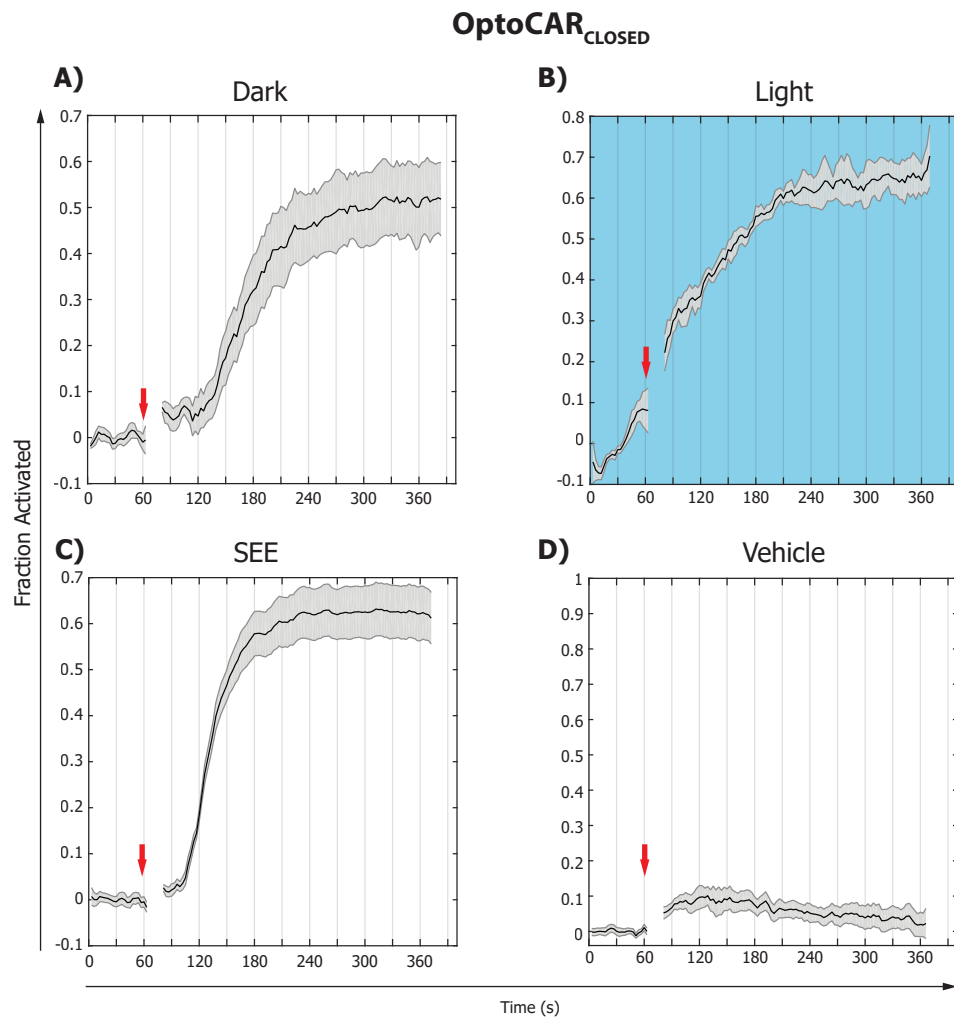


Figure 5.7 Majority of optoCAR photo-nonresponsive cells triggered on addition of rapalog Pre-gated conjgates were induced to flux calcium via the addition (red arrow) of rapalog **(A-B)**, SEE **(C)**, or vehicle **(D)**. The fraction of cells undergoing calcium fluxing was measured for each sample as those whose median flux ratio was higher than the baseline

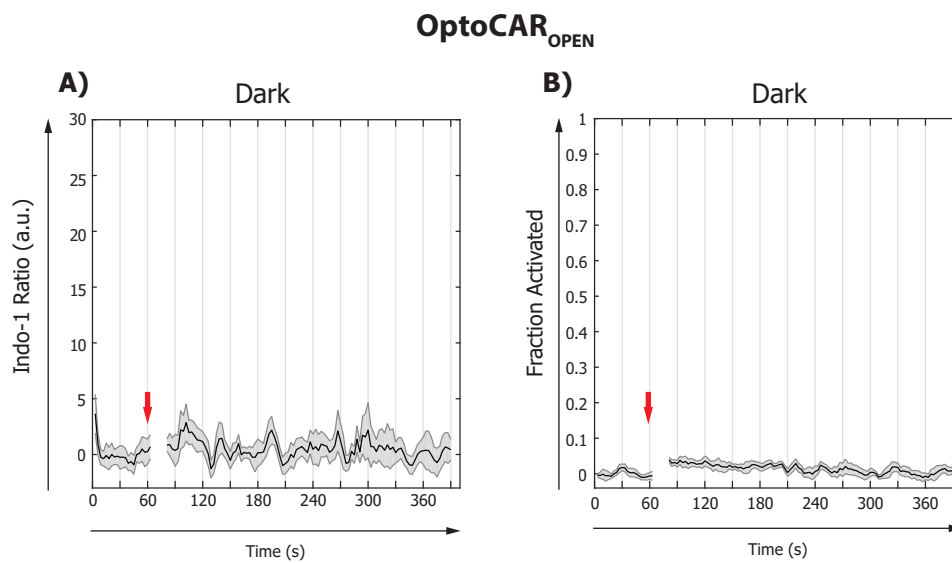


Figure 5.8 OptoCAR_{open} cells do not flux calcium To ensure that the LOVTRAP OptoCAR systems would not flux calcium in the light, the constitutively active I539E variant was used as a negative control. **(A)** There was no increase in intracellular calcium as measure by indo-1 ratio and **(B)** corresponding to no increase in the fraction of cells undergoing fluxing.

(Liu 2014) and is comparable between cells triggered with rapalog or SEE (Figure 5.6A, C; Figure 5.7A, C). As expected, this response was unchanged by blue light irradiation (Figure 5.6B, Figure 5.7B). Cells treated with vehicle did not flux calcium (Figure 5.6D, Figure 5.7D). Of note, the magnitude of calcium fluxing in the SEE-treated cells was double that of the rapalog-treated cells (Figure 5.6A, C). This observation is likely due to ligand availability and receptor expression (Au-Yeung BB et al. 2014; Keck et al. 2014). Furthermore the optoCARs are endowed with only 3 ITAM motifs, whereas the endogenous TCR contains 10 ITAMs. This large difference in the number of ITAMs likely accounts for the differences in flux magnitude between the rapalog-induced cells and the SEE-induced cells (Mukhopadhyay et al. 2016; Guy et al. 2013). Interestingly, the fraction of cells responding was only 10% higher in the SEE sample compared with the rapalog cells (Figure 5.7A, C). This is consistent with previous studies (Au-Yeung BB et al. 2014).

As a negative control we also tested JNFAT cells with a constitutively active LOV2 mutation, optoCAR_{OPEN} (Figure 5.2B, C [red]). In these cells Zdk is unable to bind LOV2 and thus the signalling domains remain disassociated from the CAR. Predictably, optoCAR_{OPEN}-expressing JNFAT cells treated with rapalog did not become activated (Figure 5.8). Taken together these findings indicate that the optoCAR system, in the presence of rapalog and the complementary FRB receptor, recapitulates proximal TCR signalling events. Disengagement of the CD3 ζ signalling domain from the transmembrane component of the OptoCAR prevents downstream signalling (Figure 5.6, 5.7, 5.8).

5.3.3 T cells exhibit tight negative regulation of early signalling events

Having shown that the optoCAR functioned in a manner analogous to the endogenous TCR, I next sought to show that light could be used to modulate input signals to the system. It should be noted that due to the method of quantification, the datasets displaying the fraction of responding cells exhibit slightly delayed kinetics relative to the Indo-1 flux datasets. This is because I count cells as active if they lie above an Indo-1 ratio value determined by the initial baseline reading in the first minute of each sample. Therefore, as the cells begin to decrease calcium influx they are still counted as active until they reach the baseline value causing a slight delay relative to the ratiometric Indo-1 measurements.

I began my analysis by testing the wildtype LOV2 version of the receptor (Table 5.1). On engagement of the receptor with rapalog under continuous dark condition, it was found that optoCAR-expressing JNFAT cells began to flux calcium following a ~60 second delay (Figure 5.9A, Figure 5.10A). This response was effectively identical to optoCAR_{CLOSED}-expressing cells,

both in terms of flux magnitude and the number of responding cells (Figure 5.6A, Figure 5.7A). Strikingly, continuous light treatment, beginning one minute prior to the start of the experiment resulted in complete ablation of the calcium flux response (Figure 5.9B, Figure 5.10B). This flux profile was identical to rapalog-treated optoCAR_{OPEN}-expressing cells (Figure 5.8). This level of signal control represents a significant improvement on the LAT-based LOVTRAP system (Figure 4.15). Interestingly, calcium fluxing could be rapidly attenuated by 1 mW/cm² blue light irradiation, indicating tight negative control of proximal T-cell signalling (Figure 5.9C, D). The response to light treatment was synchronous across the entire population of cells. (Figure 5.10C, D). Importantly, this attenuation in calcium signalling was reversible. Following a 30 second pulse of blue light irradiation there was a rapid drop in calcium fluxing observed across the entire population of activated cells (Figure 5.9E, Figure 5.10E). Calcium fluxing continued to drop post light treatment (Figure 5.9E), reflecting the rate of reversion of the LOV2 domain to the ground-state (Table 5.1). Once the indo-1 value reached baseline, there was an approximately 30 second delay before calcium fluxing was reinitiated. The magnitude of the second flux peak was equivalent to the initial peak showing a complete return to signalling (Figure 5.9E). As mentioned in 5.3.1 receptor expression tended to drop over time (Appendix L). This is reflected in the dropping magnitude of calcium fluxing between samples, though the response to light was still comparable. Pre-treatment with light followed by termination of irradiation was able to delay the signalling response (Figure 5.9F, Figure 5.10F).

To show that my observations were consistent across different variants of the receptor I tested the same light-modulation parameters with optoCAR_{FAST}-expressing JNFAT cells, the LOV2 domain of which returns to the ground-state ~40x as quickly as the wildtype receptor (Table 5.1). Again, the calcium flux profile of cells triggered in the dark was comparable to the photo-nonresponsive mutant (Figure 5.11A, Figure 5.12A & Figure 5.6). Following a 60 second delay there was an increase in calcium fluxing. This fluxing response was attenuated by continuous blue light treatment, but the optoCAR_{FAST}-expressing JNFAT cells did seem to show a gradual increase in cytoplasmic calcium over time (Figure 5.11B). This background signal may be attributed to photocycle kinetics of the LOV2 domain. The V416T mutation makes it energetically more favourable for the domain to be in the dark state. The more rapid return to the ground state increases the probability of a rebinding event between Zdk-CD3ζ-Ruby and LOV2. This idea is discussed in more detail in Chapter 4. Regardless, the fraction of responding cells in the lit state remained low (Figure 5.12B). As with the wildtype receptor, light treatment was able to rapidly attenuate calcium signalling (Figure 5.11C, D) and was synchronous across the activated population of cells (Figure 5.12C, D). A gradual increase in background calcium signalling was also

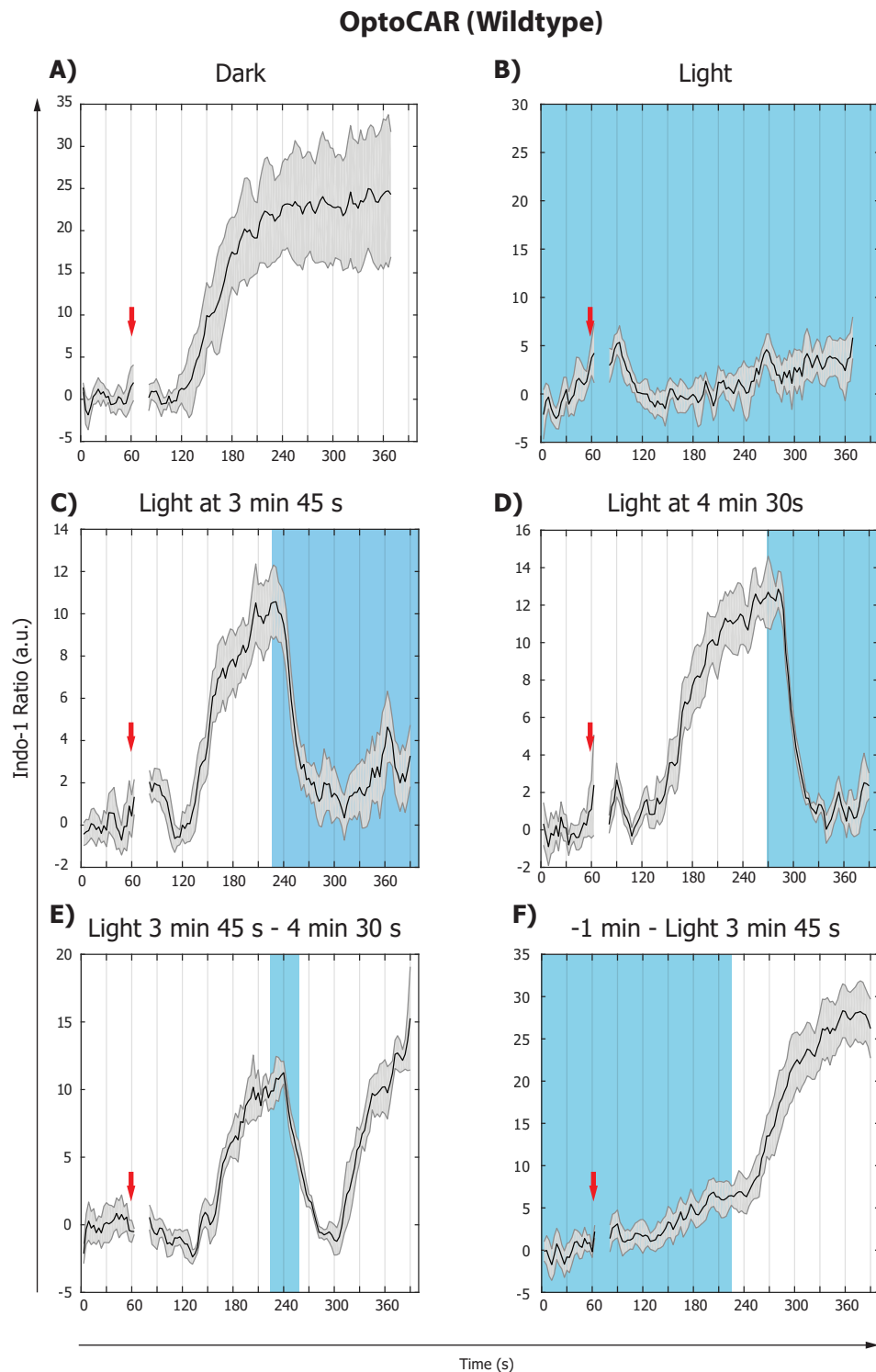


Figure 5.9 Wildtype OptoCAR cells show light-controllable calcium fluxing The median calcium flux ratio above baseline was measured under **(A)** continuous dark, **(B)** continuous light (with 1 minute pre-treatment), **(C)** light at 225 s, **(D)** light at 255 s, **(E)** a 30 s pulse of light at 225 s, or **(F)** 1 minute pre-treatment with cessation of blue light at 225 s. For each experiment $n=3$ (biological replicates), error is given as SEM. Fluxing was triggered by the addition of rapalog (1 μ m) at 1 minute (red arrow).

OptoCAR (Wildtype)

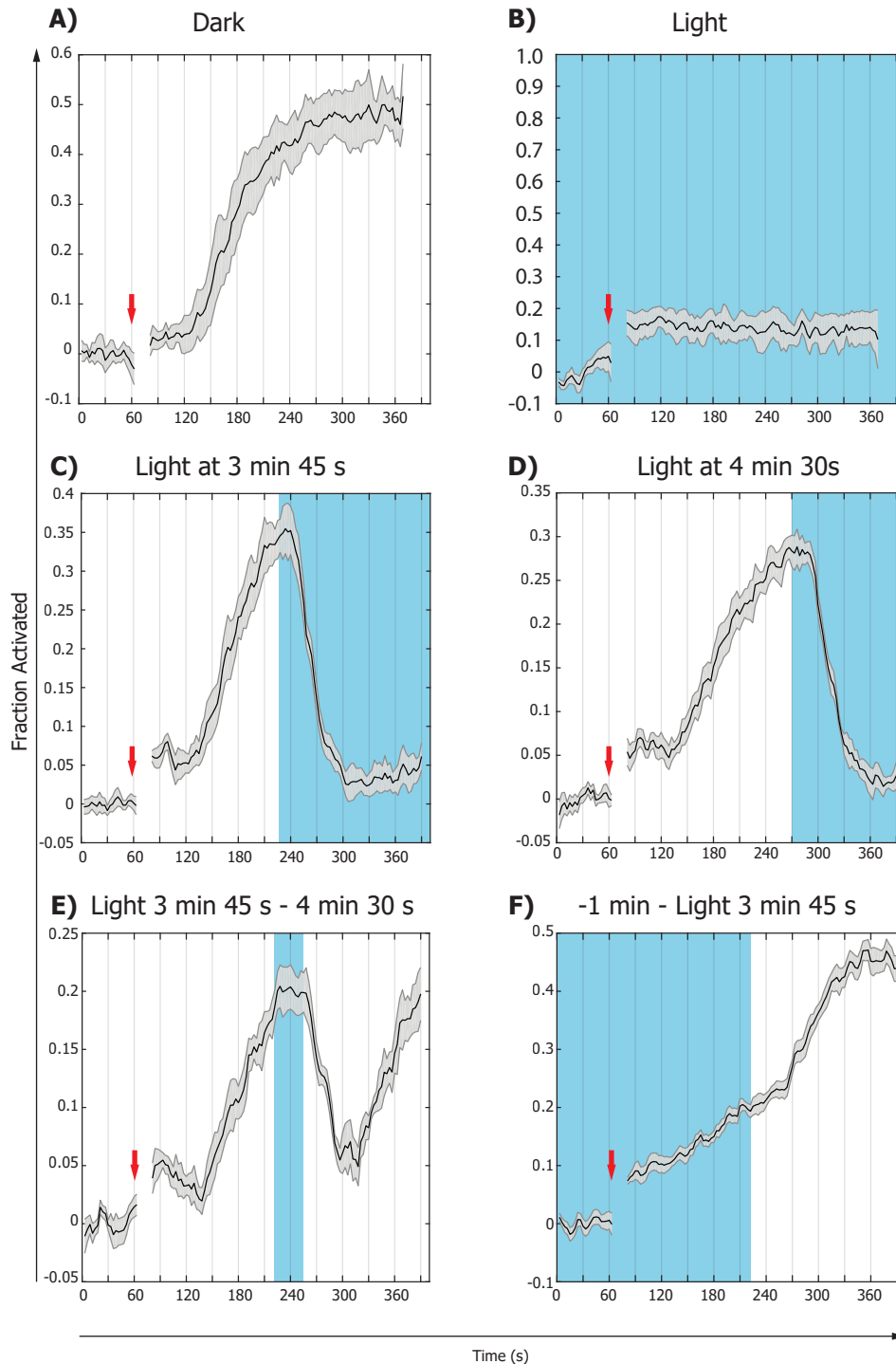


Figure 5.10 Wildtype OptoCAR cells show variation in number of responding cells The fraction of cells responding, as measured by those cells with a median greater than the baseline, were observed under (A) continuous dark, (B) continuous light (with 1 minute pre-treatment), (C) light at 225 s, (D) light at 255 s, (E) a 30 s pulse of light at 225 s, or (F) 1 minute pre-treatment with cessation of blue light at 225 s. For each experiment $n=3$ (biological replicates), error is given as SEM. Fluxing was triggered by the addition of rapalog (1 μ m) at 1 minute (red arrow).

observed in Figure 5.12C. It was noted that although the rate of signal termination was the same between optoCAR and optoCAR_{FAST}, reflecting the rate at which the LOV2 domain switches from the ground state to the active state, the optoCAR_{FAST}-expressing cells returned to calcium signalling more quickly than the wildtype receptor-expressing cells (Figure 5.9E, Figure 5.11E). This is most apparent when looking at the fraction of activated cells, which dips following light exposure, but does not return to baseline in the optoCAR_{FAST} system (Figure 5.12E). This finding lends support to the kinetic proofreading with limited signalling model of T cell activation, whereby activated receptors retain signalling capacity for a limited duration following disengagement from pMHC, increasing the probability of a productive re-binding event (Lever M et al. 2014). Further evidence for background signalling in the fast-cycling system is presented in Figure 5.11F. Unlike the wildtype system, pre-treatment with light followed by termination of irradiation results in the rapid initiation of calcium signalling in the optoCAR_{FAST}-expressing cells (Figure 5.11F, Figure 5.9F). This response was reflected on the population level (Figure 5.12F). With the optoCAR_{FAST} system, mild dark-state phosphorylation of the receptor ITAMs may prime the JNFAT cells for rapid activation. This idea is somewhat akin to the concept of tonic signalling.

Finally, I looked at calcium fluxing in the slow-cycling variant of the optoCAR system (Table 5.1). The rate of return of the LOV2(V416L) mutant is ~12x slower than the wildtype domain. Although the trends I observed were the same, the fraction of responding cells was somewhat lower with optoCAR_{SLOW}-expressing cells than either the wildtype or the fast-cycling variants (Figure 5.14). On engagement of the receptor in the dark, the delay to activation (~90 s) was slightly longer than either of the other two variants (Figure 5.13A, Figure 5.11A & Figure 5.9A). Light treatment resulted in ablation of calcium fluxing (Figure 5.13B, Figure 5.14B). Although Figure 5.13C shows an uptick in intracellular calcium following blue light irradiation, this is likely a result of a skewed median calculation from the small fraction of activated cells (Figure 5.14C). As would be expected, on the timescale examined, optoCAR_{SLOW}-expressing JNFAT cells did not return to signalling following a 30 second pulse of blue light irradiation (Figure 5.13D, Figure 5.14D). A delay in signalling following light pre-treatment was not observed with the optoCAR_{SLOW} system (Figure 5.13E, Figure 5.14E). However, the increase in cytoplasmic calcium observed was shallow and gradual (Figure 5.13E) and thus is likely to represent ambient noise within the small fraction of activated cells (Figure 5.14E) in the system rather than a bona fide activation signal.

The receptor variants presented above represent a set of tools for the analysis of T-cell signalling dynamics at different stages of the activation pathway. The fast-cycling and wildtype variants provide a unique approach to interrogating early signalling events, whereas the prolonged

OptoCAR_{FAST}

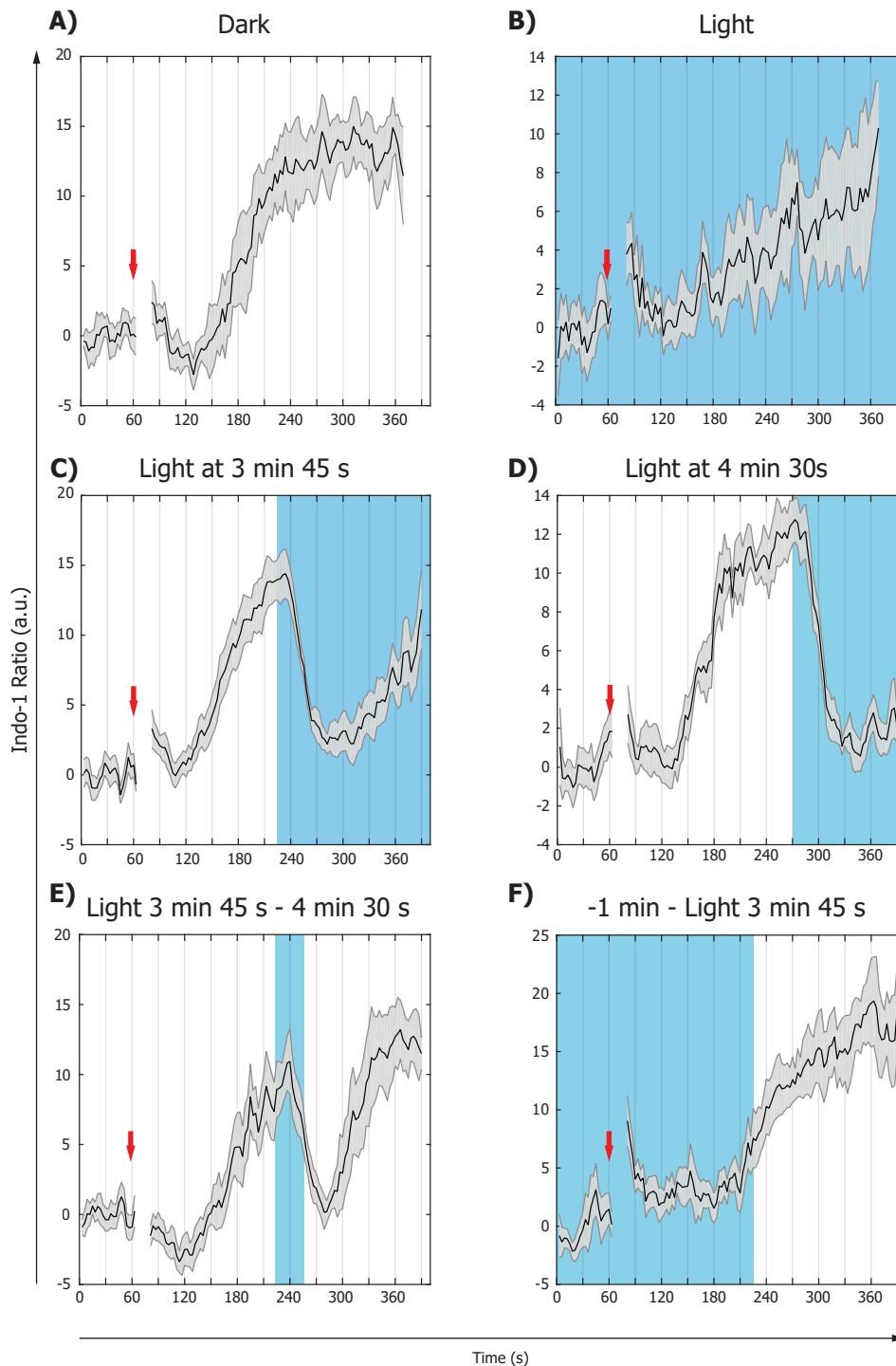


Figure 5.11 OptoCAR_{FAST} cells (V416T) show light-controllable calcium fluxing, but some background signalling The median calcium flux ratio above baseline was measured under **(A)** continuous dark, **(B)** continuous light (with 1 minute pre-treatment), **(C)** light at 225 s, **(D)** light at 255 s, **(E)** a 30 s pulse of light at 225 s, or **(F)** 1 minute pre-treatment with cessation of blue light at 225 s. for each experiment n=3 (biological replicates), error is given as SEM. Fluxing was triggered by the addition of rapalog (1 μ m) at 1 minute (red arrow).

OptoCAR_{FAST}

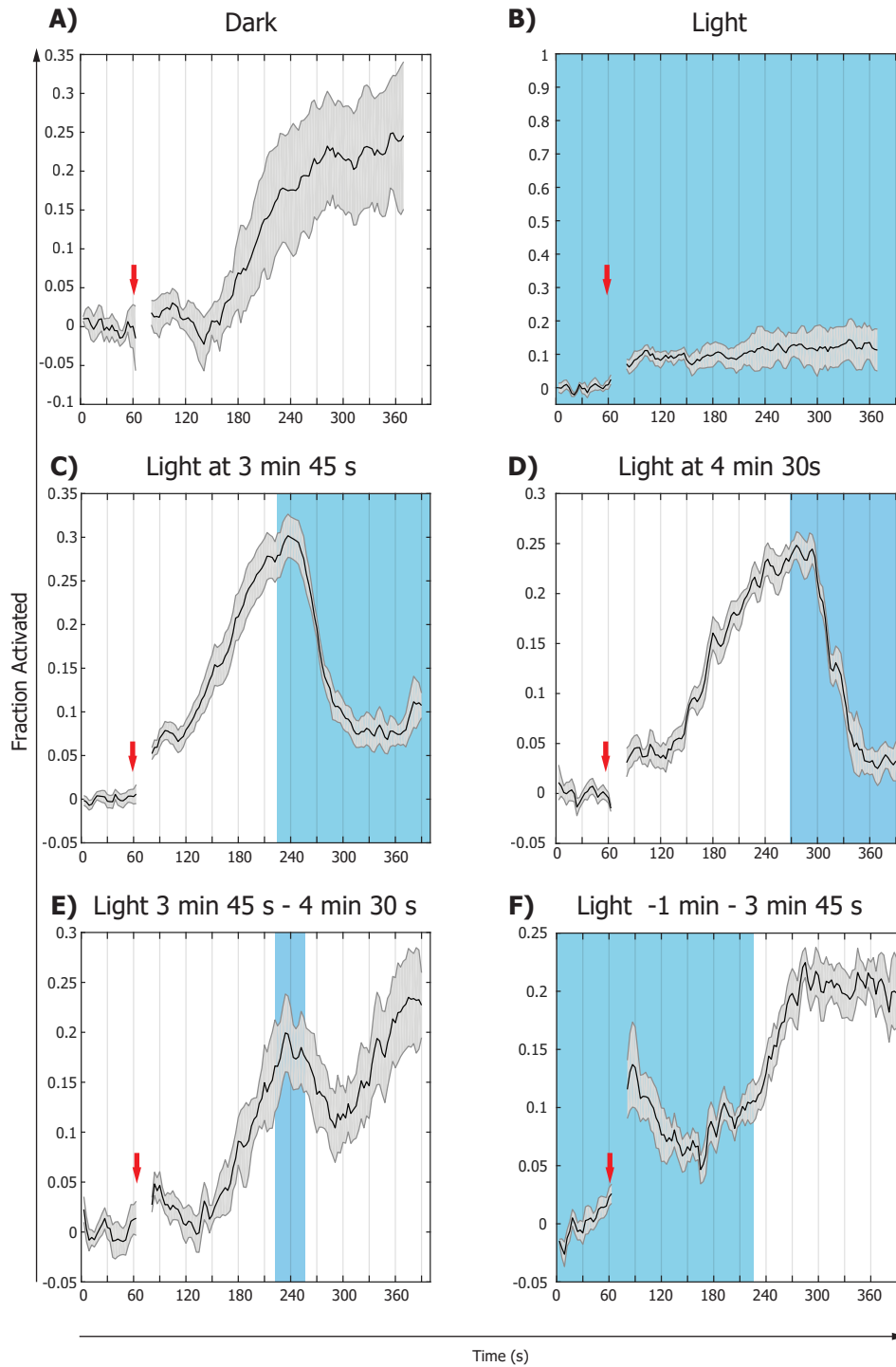


Figure 5.12 OptoCAR_{FAST} cells (V416T) yield low fraction of responding cells The fraction of cells responding, as measured by those cells with a median greater than the baseline, were observed under **(A)** continuous dark, **(B)** continuous light (with 1 minute pre-treatment), **(C)** light at 225 s, **(D)** light at 255 s, **(E)** a 30 s pulse of light at 225 s, or **(F)** 1 minute pre-treatment with cessation of blue light at 225 s. For each experiment $n=3$ (biological replicates), error is given as SEM. Fluxing was triggered by the addition of rapalog (1 μ m) at 1 minute (red arrow).

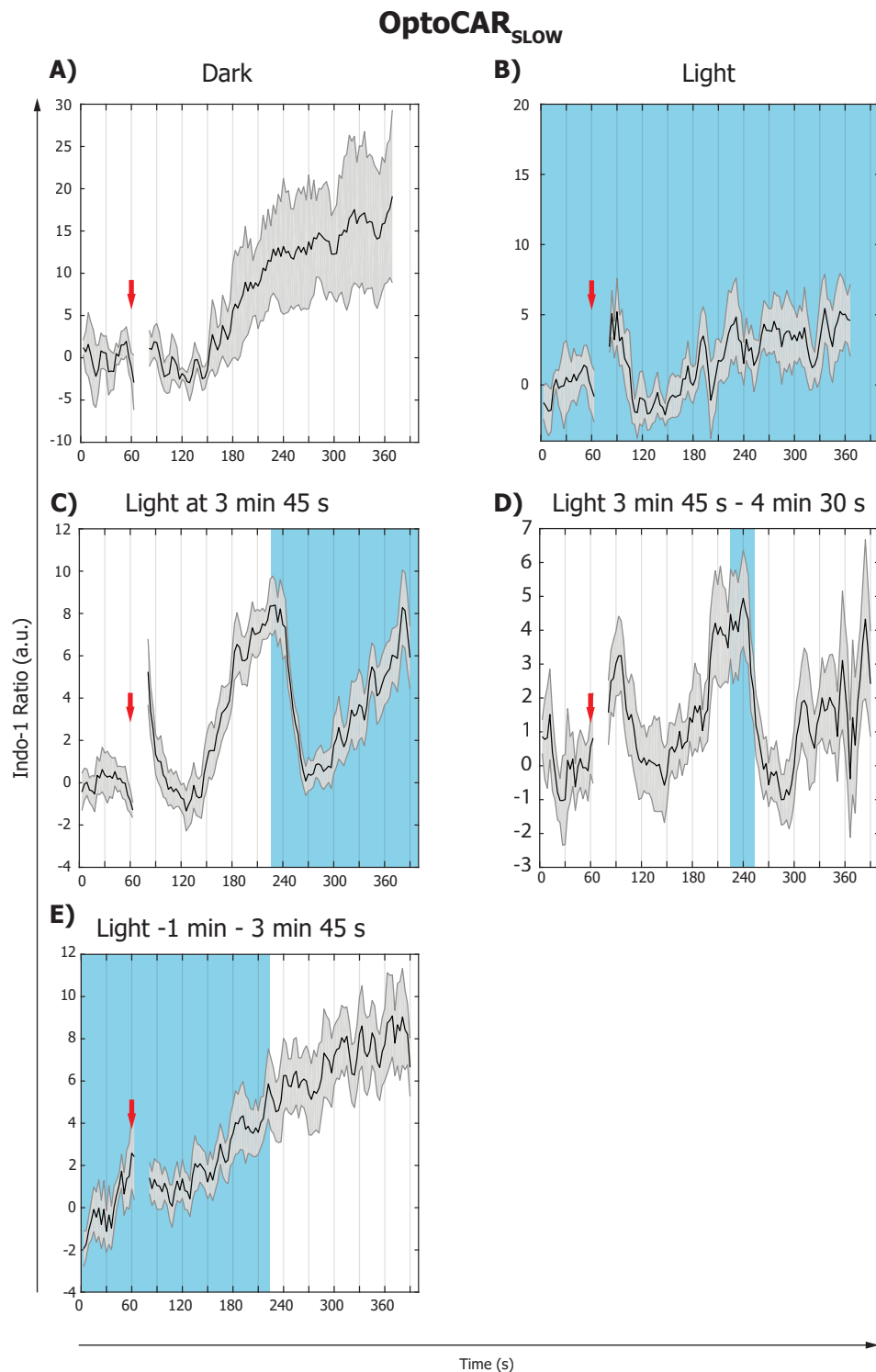


Figure 5.13 OptoCAR_{SLOW} cells (V416L) show light-controllable calcium fluxing
 The median calcium flux ratio above baseline was measured under **(A)** continuous dark, **(B)** continuous light (with 1 minute pre-treatment), **(C)** light at 225 s, **(D)** a 30 s pulse of light at 225 s, or **(E)** 1 minute pre-treatment with cessation of blue light at 225 s. for each experiment $n=3$ (biological replicates), error is given as SEM. Fluxing was triggered by the addition of rapalog ($1\ \mu\text{M}$) at 1 minute (red arrow).

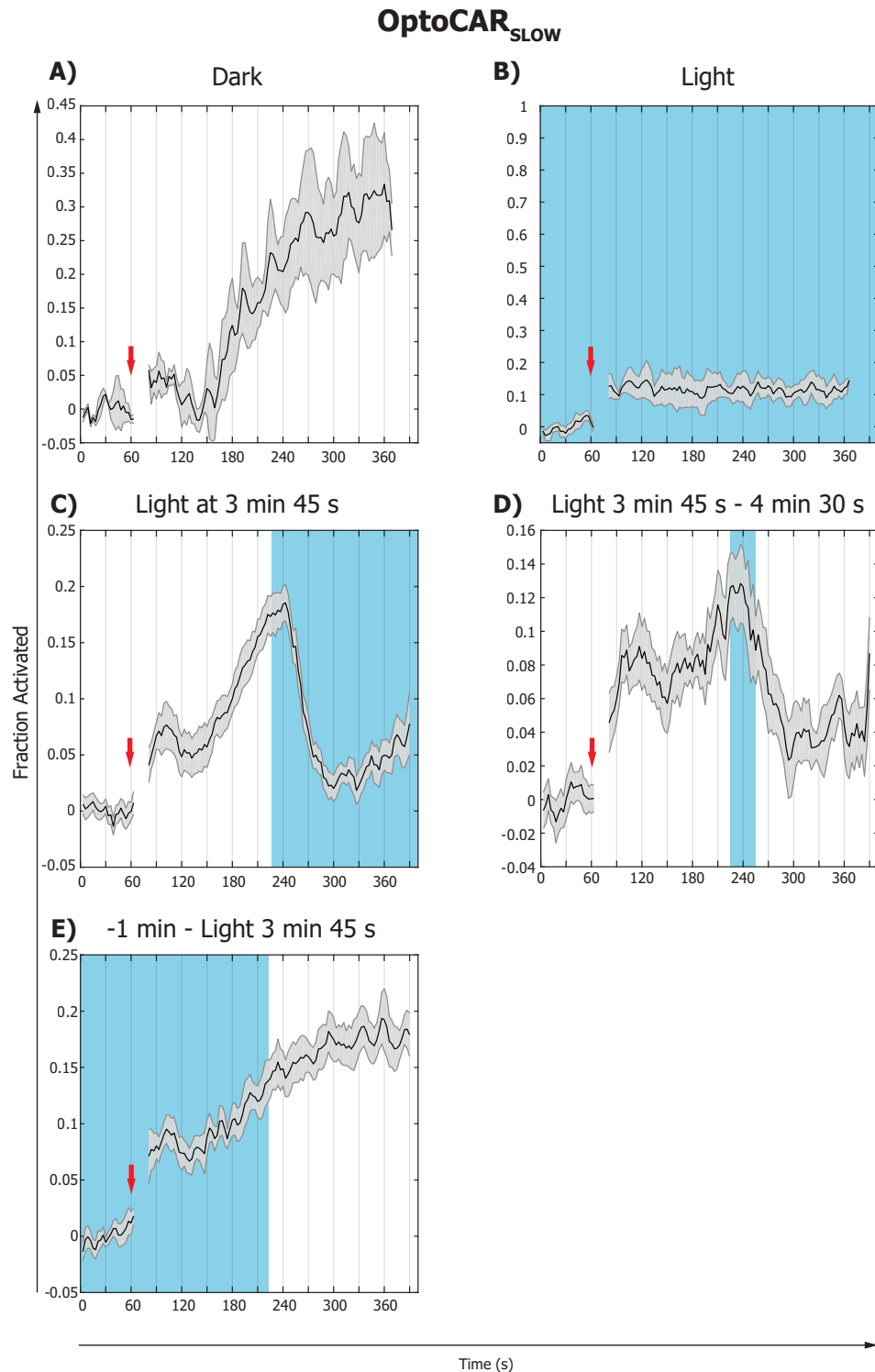


Figure 5.14 OptoCAR_{SLOW} cells (V416L) show delayed return to signalling following blue light exposure The fraction of cells responding, as measure by those cells with a median greater than the baseline, were observed under **(A)** Continuous dark, **(B)** continuous light (with 1 minute pre-treatment), **(C)** light at 225 s, **(D)** a 30 s pulse of light at 225 s, or **(E)** 1 minute pre-treatment with cessation of blue light at 225 s. for each experiment $n=3$, error is given as SEM. Fluxing was triggered by the addition of rapalog at 1 minute (red arrow).

signal attenuation displayed by the slow-cycling variant, optoCAR_{SLOW}, could present a novel approach for looking at downstream activation events.

5.3.4 OptoCARs recapitulate late T cell activation

Engagement of the TCR leads to downstream T cell activation, proliferation, and T cell differentiation into different effector subsets. This process is reported to require sustained signalling over the course of hours to days (Au-Yeung BB et al. 2014; Miskov-Zivanov et al. 2013). On a seconds-to-minutes timescale the optoCARs were able to control receptor-induced calcium signalling. This process was reversible and repeatable with kinetics dependent on the photocycle kinetics of the LOV2 domain. Given that the duration of TCR stimulus is a key determinant of T cell fate I next sought to determine the effect of proximal signal modulation on downstream T-cell activation. To do this, I looked at three separate readouts of T cell activation: upregulation of surface expression of the early activation marker, CD69 (Yamashita et al. 1993; Bartelt et al. 2009); upregulation of GFP expression under control of the NFAT promoter; and the release of the proliferation-inducing cytokine, IL-2 (Bartelt et al. 2009). To perform this assay I needed a means of providing long-term illumination to the cell cultures. In collaboration with the LMB Mechanical and Electronics Workshops, I modified a 3D-printable optogenetic 'Light Plate Apparatus (LPA)', details of which can be found in (Gerhardt et al. 2016). To prevent uneven illumination we developed a solid acrylic diffuser plate, which provided superior diffusive properties than the filter paper suggested by Gerhardt et al. (2016) (Appendix K). The modified LPA allows for modulation of light conditions on a well-by-well basis across a 24-well plate.

For complete T cell activation, antigen stimulation for a period of 24-48 hours has been reported, with longer periods of stimulation driving more rounds of T cell proliferation (Obst 2015; Jenkins and Moon 2012). Although Jurkat T cells are a good model system, they do not respond to proliferative signals in the same way as host-derived peripheral T cells. I therefore focused my analysis on a 24-hour period of stimulation. Over this period I wanted to establish a baseline for the activation kinetics of CD69, NFAT-driven GFP, and IL-2 in the cell-cell conjugate assay. Unfortunately, it was found that the wildtype receptor was unsuitable for long-term activation assays. Pilot experiments looking at a single, 9-hour pulse of activation determined that there was a high degree of background activation (Appendix M). Cells triggered under continuous illumination were indistinguishable from cells triggered under continuous dark. Even at 100% LED intensity (~0.5 mW/cm² on LPA) activation state was unaffected (Appendix M). Instead, I focused my efforts on the optoCAR_{SLOW} system. Data from the calcium flux assay suggested that

these cells would provide a lower level of background signalling than the other two variants (Figure 5.13-14).

The optoCARs are both drug-inducible and light-controllable (Figure 5.1) and as such I tested two means of inactivating the optoCAR system, a chemical method and an optogenetic method. As blue light irradiation rapidly inactivated early signalling events (Figure 5.9-14) one might propose that blue light irradiation should terminate TCR induced downstream signalling on the assumption that continuous signalling from the TCR is required for the mediation of downstream events (Figure 5.15A). However, the effect of proximal signal termination on downstream signalling modules; such as Erk translocation, AP-1/NFAT transcription factor activation, and mRNA transcription and translation, remains somewhat unknown.

To model the activation kinetics of the optoCAR system, conjugated cells were activated with heterodimerising drug and then inactivated by either blue-light irradiation ($\sim 0.2 \text{ mW/cm}^2$) or homodimerising drug after a defined period of activation (Figure 5.15). The homodimerising drug has a higher affinity for the FKBP12 domain ($K_d = 1.8 \text{ nM}$) than the heterodimerising drug, but does not generate a ternary complex with the FRB domain (Clackson et al. 1998). Thus, at low concentrations the homodimeriser outcompetes the heterodimeriser for FRB binding causing disengagement of the OptoCAR. This experiment was run over a 24-hour period (Figure 5.15). The time during which the cells are activated will herein be referred to as 'Signal On' (S^{ON}) and the time during which the cells are inactivated by either homodimeriser or light will be referred to as 'Signal Off' (S^{OFF}).

It was found that drug treatment and light treatment were broadly comparable across the three output markers of T-cell activation. Following S^{ON} of 3 hours ($S^{\text{OFF}} = 21 \text{ hours}$) $\sim 50\%$ of the cells were positive for both CD69 (Figure 5.16A) and GFP (Figure 5.17A). The fraction of activated cells only slightly increased beyond this point. However the MFI of GFP (Figure 5.16B) and CD69 (Figure 5.17B) did not begin to plateau until $S^{\text{ON}} = 6 \text{ hours}$ ($S^{\text{OFF}} = 18 \text{ hours}$). As the half-life of GFP is reported to be $\sim 26 \text{ hours}$ we would expect to see only limited signal decay over this time period (Corish and Tyler-Smith 1999). These findings suggest that at least 3 hours of sustained signalling is needed to initiate gene expression and further sustained signalling is necessary for more robust gene expression. This finding suggests that even downstream TCR signalling events are under tight negative regulation. ELISA analysis of IL-2 cytokine expression confirmed this observation (Figure 5.18). Three hours of signalling was not enough to drive expression of IL-2, but by 6 hours IL-2 expression had begun to plateau (Figure 5.18). IL-2 is

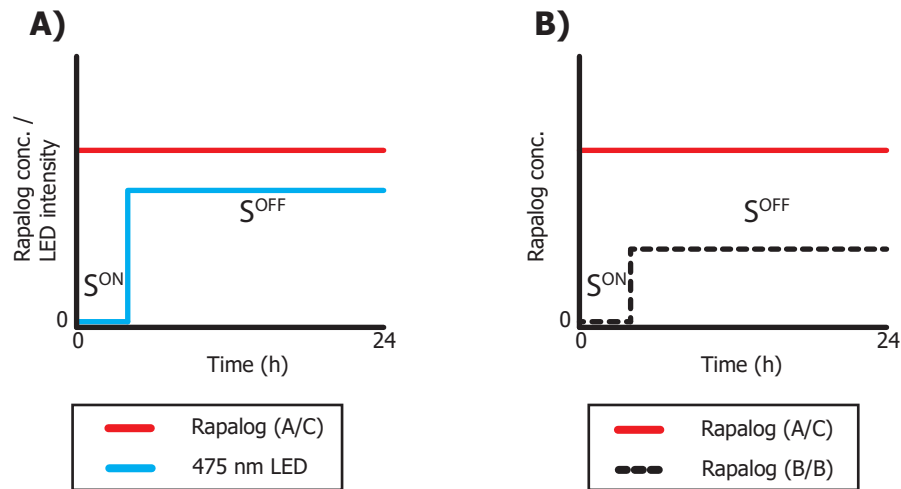


Figure 5.15 Light inactivation and drug washout comparison (A) On the addition of rapalog (red line), after a short delay period the optoCAR systems initiate downstream signalling. Calcium flux experiments show that signalling is rapidly attenuated following blue light irradiation (cyan line). Periods where the receptor is active are referred to as S^{ON} (Signal on) and periods of blue light stimulation, where the receptor is disengaged are referred to as S^{OFF} (Signal off). **(B)** The receptor can also be inactivated on the addition of a homodimerising drug (dotted black line), which binds the Fv domain with higher affinity than the heterodimerising version, but does not engage the FRB domain, thus preventing signalling.

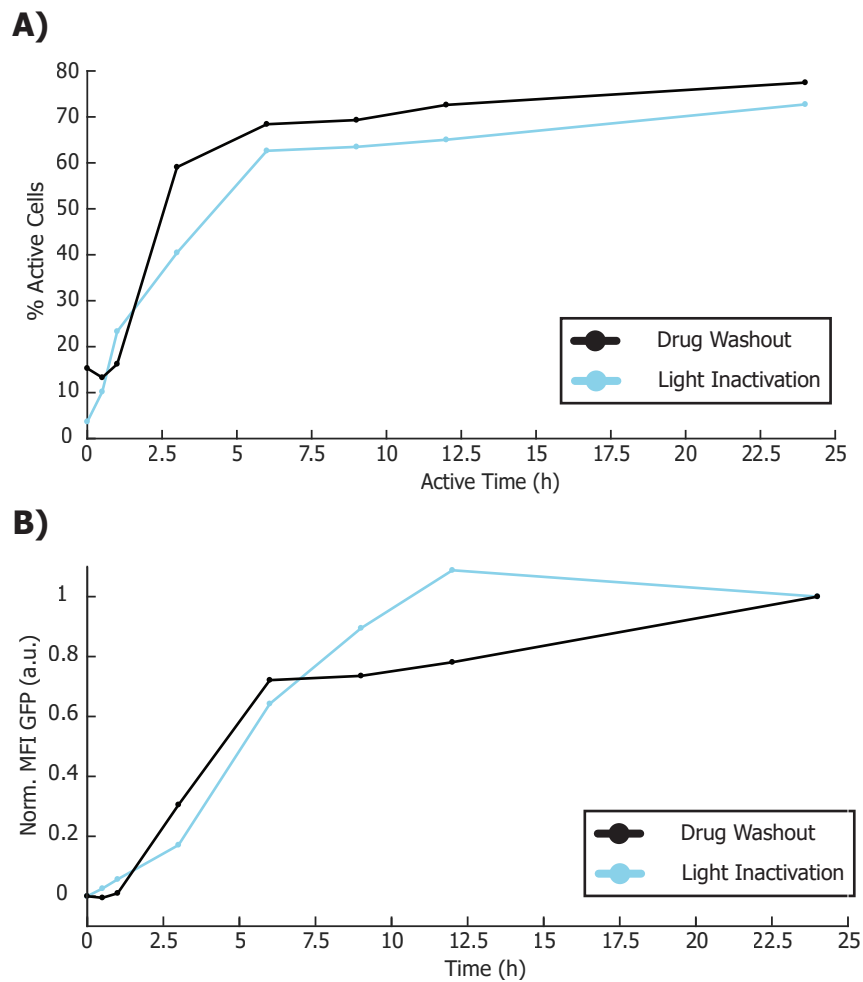


Figure 5.16 OptoCAR-expressing cells upregulate NFAT-driven GFP expression following 3 hours of continuous signalling OptoCAR-expressing JNFAT cells were conjugated with Raji B cells and then triggered by the addition of rapalog (A/C). Signalling was inactivated after 0 hr, 0.5 hr, 1 hr, 3 hr, 6 hr, 9 hr, 12 hr, or 24 hr, either by the addition of rapalog (B/B; black line) or by light (cyan line). All cells were harvest after a 24 hr period. Using a Matlab peak separation script the **(A)** fraction of activated cells was calculated and the **(B)** mean fluorescent intensity of the whole population was calculated. MFI was normalised to the 0 hr activation and 24 hr activation samples. For each sample n=2.

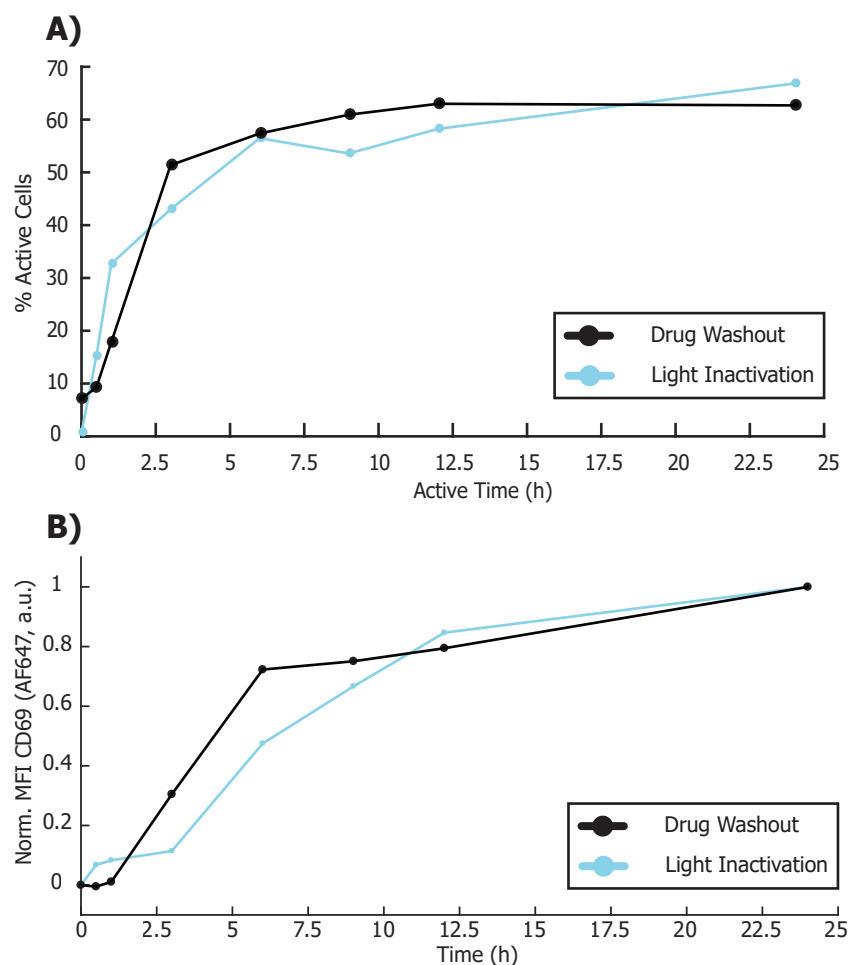


Figure 5.17 OptoCAR-expressing cells upregulate CD69 expression following 3 hours of continuous signalling OptoCAR-expressing JNFAT cells were conjugated with Raji B cells and then triggered by the addition of rapalog (A/C). Signalling was inactivated after 0 hr, 0.5 hr, 1 hr, 3 hr, 6 hr, 9 hr, 12 hr, or 24 hr, either by the addition of rapalog (B/B; black line) or by light (cyan line). All cells were harvest after a 24 hr period. Using a Matlab peak separation script the **(A)** fraction of activated cells was calculated and the **(B)** mean fluorescent intensity of the whole population was calculated. MFI was normalised to the 0 hr activation and 24 hr activation samples. For each sample n=2.

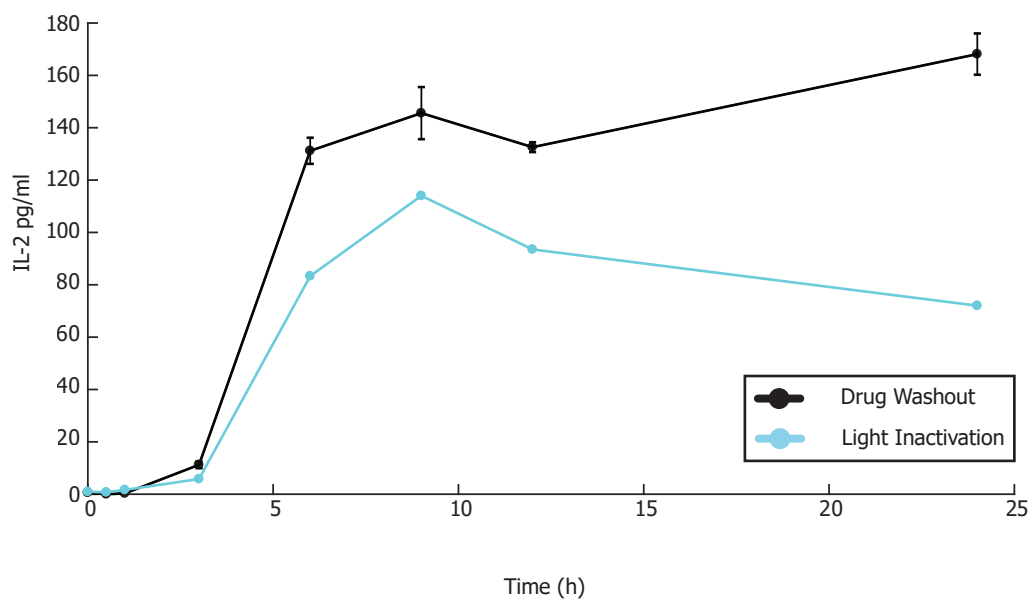


Figure 5.18 IL-2 expression delayed relative to NFAT reporter GFP and CD69
 IL-2 expression in the spent media was assayed by ELISA. JNFAT cells expressing the optoCAR system were inactivated at 0 hr, 0.5 hr, 1 hr, 3 hr, 6 hr, 9 hr, 12 hr, and 24 hr post-stimulation by rapalog (A/C). signalling was terminated either by drug washout with rapalog (B/B; black line) or light (cyan line).

known to be regulated by the NFAT transcription factor and thus this finding is consistent with the NFAT-reporter data (Chow et al. 1997). These findings are also in agreement with the observation that sustained TCR signalling is necessary to drive complete T cell activation (Rachmilewitz, Lanzavecchia, and J. 2002).

A gradual decrease in soluble IL-2 was observed in the light-treated cells (Figure 5.18). It was noted that within the LPA there was an increase in cell death, particularly in the innermost four wells (Appendix K). This was determined using ZombieAqua live-dead cells stain. This increase in cell death would likely affect the amount of cytokine detectable in the assay. Media in wells where cells had died was somewhat more yellow than wells where the majority of cells had lived thus it was determined that the LPA lid was so tight so as to block gas exchange. I have since obtained new lids for the glass-bottom 24-well plates.

5.3.5 TCR signals sharply decay following withdrawal of input signals

The drug washout and light inactivation time course showed that 6 hours ($S^{\text{ON}} = 6$ hours) of continuous signalling was sufficient to drive robust CD69 upregulation and NFAT-driven GFP expression (Figure 5.16-17). With this value in mind, I next sought to interrogate TCR signal integration over time. It has been reported that rapid digitisation of the Ras signalling pathway and the accumulation of downstream signalling intermediates creates bistability within the system allowing T cells to integrate temporally discontinuous signals (Das et al. 2009; Faroudi et al. 2003). By fragmenting S^{ON} into discontinuous pulses, such that the total amount of signalling (S^{TOTAL}) always equalled 6 hours I hypothesised that it should be possible to determine the rate of signal decay downstream of the TCR. Although several signalling intermediates have been proposed, including IRF4 (Man et al. 2013; Huber and Lohoff 2014), Myc (Holst et al. 2008; Guy et al. 2013), and Fos (Faroudi et al. 2003; Locasale 2007), the precise nature of TCR signal integration remains to be fully described. By measuring the rate of signal decay over time I reasoned that it should be possible to build a temporal ‘roadmap’ of T cell activation events.

Shown in Figure 5.19 are three example pulse width modulation (PWM) experiments. A single 6 hour pulse of dark (S^{ON}), in which the system is active was used as the control (Figure 5.19A). This 6 hour pulse of system activation was followed by an 18 hour pulse (18- ΣS^{OFF}) of low-intensity blue light irradiation (~ 0.2 mW/cm²) to inactivate the signalling pathway, such that the total duration of the experiment was always 24 hours. To simplify these experimental conditions I refer to the pulses of dark, during which the signal is active, as S^{ON} and the pulse of light, during which the signal is interrupted, as S^{OFF} . Both S^{ON} and S^{OFF} can be adjusted, but the

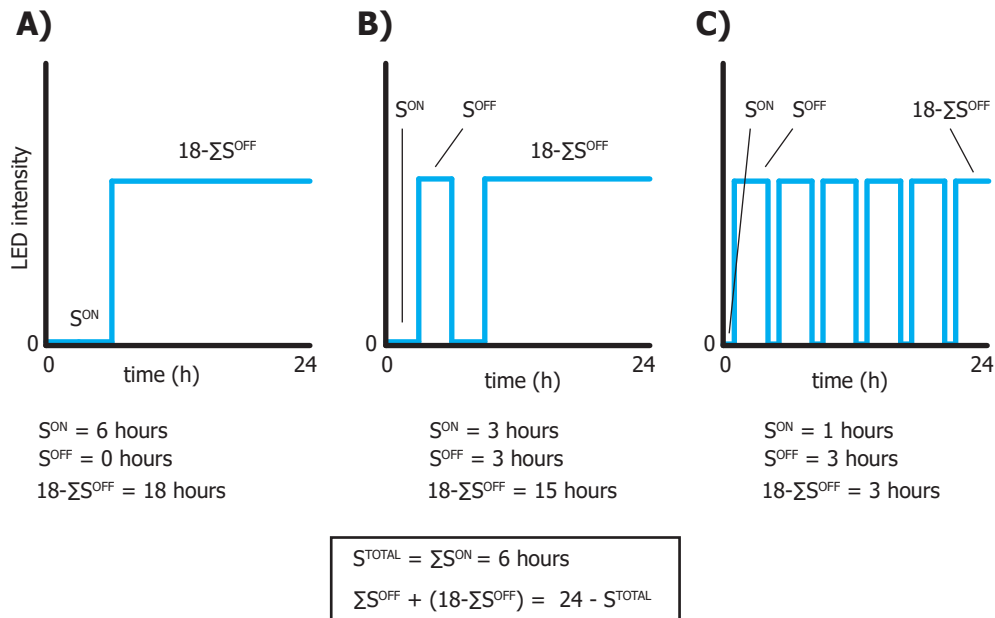


Figure 5.19 Assaying signal integration through pulsed activity The calcium flux assays showed that signalling could be rapidly terminated by blue light, but that the JNFAT cells would return to signalling after a period of time defined by the photocycle kinetics of the LOV2 domain. The signalling time series assay determined that **(A)** 6 hours of continuous signalling was enough to drive GFP NFAT-reporter expression, CD69 upregulation, and secretion of IL-2. Periods of signalling (S^{ON}) were fragmented by pulses of blue light irradiation (S^{OFF}) to assay the temporal integration of signals through the opto-CAR. **(B)** The total amount of signaling was equal to 6 hours (S^{Total}), with two periods of signaling (S^{ON}) of 3 hours each. The two pulses of S^{ON} are divided by a 3 hour pulse of blue light (S^{OFF}). The remaining time until the cells were harvested ($18 - \Sigma S^{OFF}$) was spent under blue light irradiation such that all samples were illuminated for a total of 18 hours. **(C)** Another example of a signal integration experiment. Here, S^{ON} equals 1 hour and S^{OFF} equals 3 hours. S^{TOTAL} remains 6 hours.

total amount of time that the system is in the dark state (S^{TOTAL}) is always equivalent to 6 hours and the total amount of time that the system is in the light is always equivalent to 18 hours ($\Sigma S^{\text{OFF}} + (18 - \Sigma S^{\text{OFF}})$), over the course of a 24 hour experiment (Figure 5.19B, C). In the example in Figure 5.19B, S^{ON} is reduced to 3 hours and S^{OFF} is also 3 hours. Thus, two 3 hour pulses of system activity are separated by a 3 hour pulse of system inactivity. If signalling through the TCR were cumulative, it would be expected that regardless of the duration of S^{ON} , S^{TOTAL} would always be equivalent. That is, NFAT reporter-driven GFP expression, IL-2 expression, or CD69 expression would be expected to be identical regardless of S^{ON} . The previous data show that <3 hours of continuous signalling is insufficient to drive gene expression (Figure 5.16-18) so it is unclear if short, discontinuous TCR signals can be summed toward a cumulative output response.

By pulsing TCR signalling with periods of inactivity, I was able to show that interruption of TCR input signals results in the rapid decay of downstream signalling (Figure 5.20-24). The data suggest that TCR signals are not additive, but are instead tightly negatively controlled. Shown in Figure 5.20 is an example of two different time course experiments, Figure 5.20A and Figure 5.20B represent the type of experiment shown in Figure 5.19C. Here, S^{ON} is 1 hour, thus S^{TOTAL} is divided into six, 1-hour pulses of activity. The topmost histogram is 6-hours of continuous dark and the bottommost is 24-hours of continuous light. Immediately above the bottom histogram is a single pulse S^{ON} control, which in this case is a single 1-hour pulse of darkness followed by 23 hours of light. Between the top and bottom two histograms are increasing pulses of S^{OFF} , given in descending order, with the shortest S^{OFF} increment at the top of the plot and the largest at the bottom. This data shows that increasing the period of inactivity (S^{OFF}) between each pulse of signalling (S^{ON}) decreases the fraction of activated cells and the degree to which those cells are active. This seems to hold true for both GFP expression and CD69 expression (Figure 5.20A and Figure 5.20B, respectively). If S^{ON} is decreased to 30 minutes, this trend becomes more pronounced (Figure 5.20C, D). These plots are representative of just two values of S^{ON} and only a handful of values for S^{OFF} . To build a more complete picture of signal integration in T cells I incremented S^{ON} from 5 minutes to 3 hours and S^{OFF} from 10 seconds to 18 hours.

To visualise T cell activation across the spectrum of pulse width durations I used Matlab to perform peak separation between the positive and negative cells relative to a vehicle treated negative control. By calculating the area under the positive curve relative to the whole population I was able to determine the fraction of activated cells under each condition (Figure 5.21 & Figure 5.23). I looked at the degree to which cells became activated by measuring the mean fluorescent intensity (MFI) of the overall population, which was normalised to the single pulse control samples (Figure 5.22 & Figure 5.24).

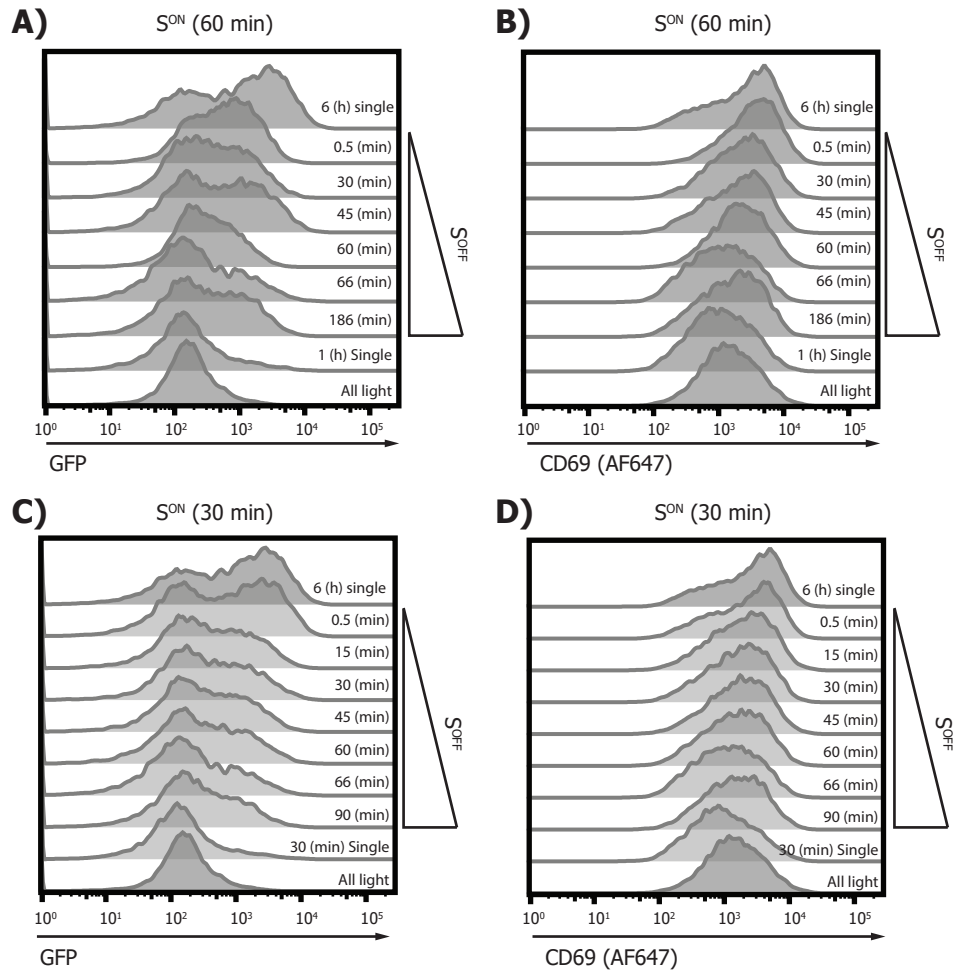


Figure 5.20 TCR signalling is not additive Two example pulse width modulation experiments (**A, B**) S^{ON} equals 1 hour, S^{Total} equals 6 hours. (**C, D**) S^{ON} equals 30 minutes, S^{Total} equals 6 hours. The duration of S^{OFF} is varied from well to well. Each histogram plot is derived from a separate well of the LPA. (**A**) As the pulse of blue light between each pulse of signalling increases, both the fraction of GFP positive cells and the intensity of NFAT-driven GFP expression decreases. (**B**) CD69 upregulation also decreases as the light pulses between S^{ON} increases. (**C**) Each pulse of S^{ON} is reduced to 30 minutes. As the duration of the light pulses between S^{ON} pulses increased NFAT-driven gene expression decreases. (**D**) CD69 expression follows the same trend.

As the duration of S^{ON} was increased, the fraction of cells positive for GFP gradually began to increase. This can be seen in the single pulse controls along the top row of the heat map (Figure 5.21) and is consistent with the finding that <3hrs of continuous signalling is insufficient to drive GFP reporter expression. Interestingly, there was a negative correlation between the percentage of activated cells and the duration of S^{OFF} . That is, as the duration of time between signal pulses increased, the fraction of activated cells decreased (Figure 5.21). This was particularly notable for samples where S^{ON} was below 90 minutes. Where S^{ON} was equal to, 90 minutes, 120 minutes, or 180 minutes, incrementing S^{OFF} did not greatly affect the fraction of activated cells. This finding suggests that T cells are able to integrate discontinuous signals into a cumulative output response. However, quantification of the mean fluorescent intensity (MFI) showed that although T cells were able to integrate discontinuous signals, the output response was not cumulative (Figure 5.22A). By using the Matlab curve fitting function it was possible to measure the rate of exponential decay in TCR-derived signals. In doing this, it was found that increasing the duration of S^{OFF} resulted in a drastic decrease in the MFI of the GFP reporter (Figure 5.22A). This was particularly true where S^{ON} was equal to 5 minutes. As the $t_{1/2}$ of reversion of the LOV2 slow-cycling mutant is ~ 500 s (Table 5.1), the S^{OFF} pulses were cycled more rapidly than the recovery of the LOV2 domain and little signal was able to accumulate (Figure 21, Figure 22A, Appendix [Figure A]).

As the duration of S^{ON} was gradually increased from 5 minutes to 3 hours the rate of signal decay gradually decreased (Figure 22B, Appendix [Figure A]). This finding would be consistent with the hypothesis that continuous T cell signalling results in the accumulation of signalling intermediates. It would be expected that as the duration of TCR signalling were increased, there would be a proportional increase in signalling intermediate, allowing for an increased duration of signal memory between pulses.

Similar findings were observed when looking at CD69 upregulation (Figure 5.23-24). Following only 30 minutes of continuous signalling it was found that the majority of cells were positive for CD69 (Figure 5.23). This result is not surprising and reflects the fact T cells are primed for CD69 upregulation. CD69 is an early response gene and is rapidly transcribed with only low levels of signalling necessary to drive its expression (Yamashita et al., 1993). The ability of T cells to rapidly upregulate CD69 expression is apparent in the single pulse control data, where prior to samples <30 minutes show no CD69 expression, but 30 minutes of continuous activation is enough to drive CD69 expression (Figure 5.23, Top row). This trend is reflected across the heat map, as beyond 30 minutes (S^{ON}) the majority of cells were CD69 positive. This was invariant to

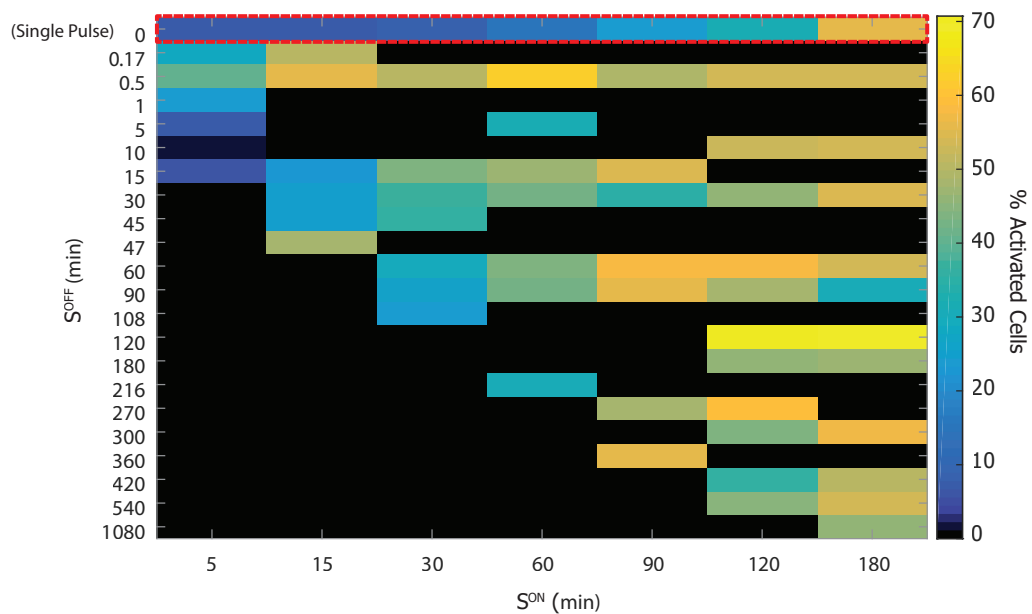


Figure 5.21 NFAT-driven GFP expression and S^{OFF} duration are inversely correlated Using matlab peak separation, the fraction of activated cells in each well were calculated. The duration of each signal pulse (S^{ON}) is varied along the x-axis and the duration of each light pulse is varied along the y-axis (S^{OFF}). The top row, outlined in red, represents a single continuous pulse of signalling equivalent to the value given for S^{ON} along the x-axis. For each unit on the heat map $n = 1 < x < 4$

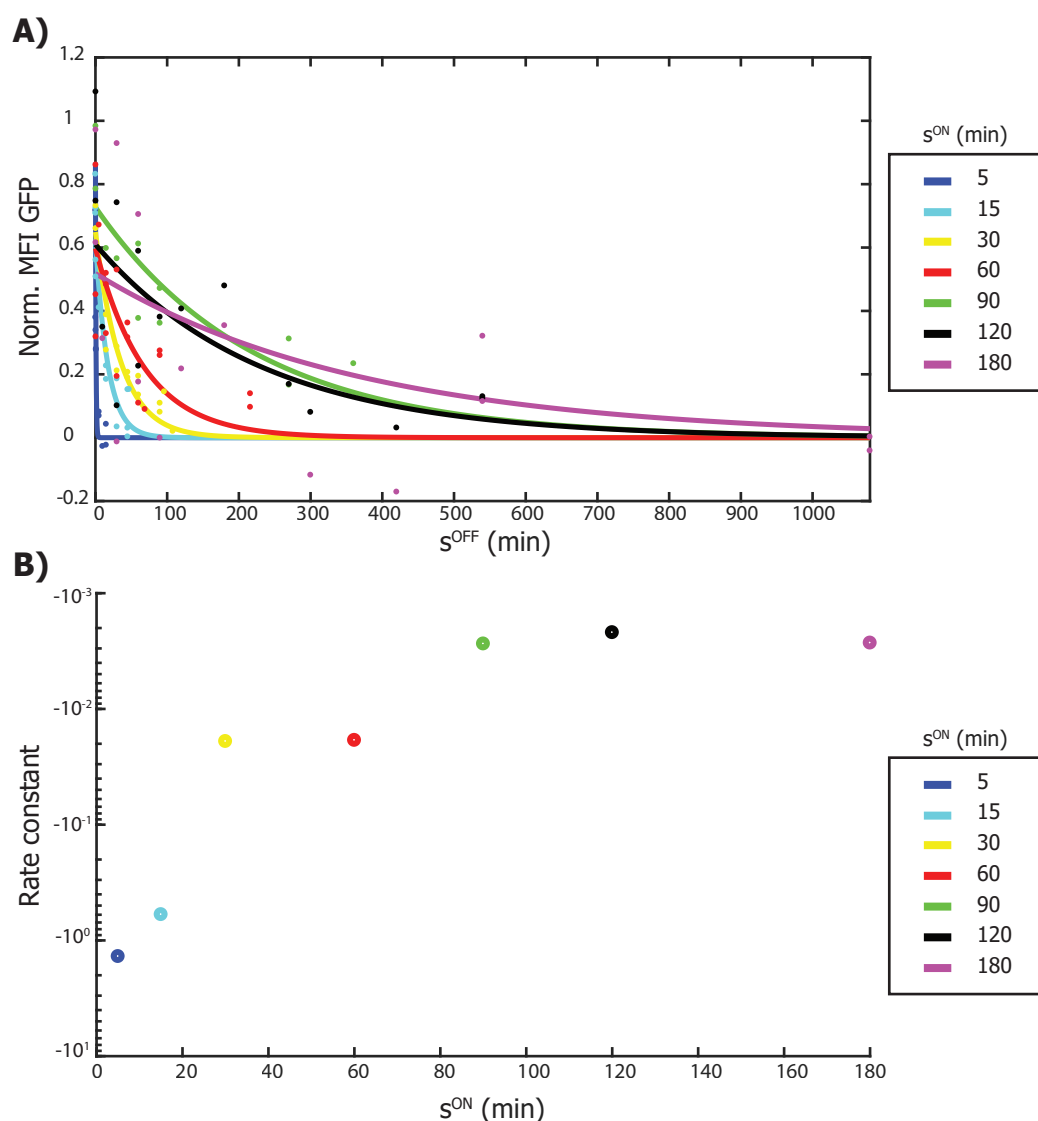


Figure 5.22 NFAT-driven GFP signal exhibits rapid decay (A) Mean fluorescent intensity of the population of cells in each well of the LPA was calculated and normalised to the 6 hour single pulse control and the s^{ON} single pulse control. Each point represents a single sample. Curves were generated using the Matlab exponential curve fitting function. Each curve is representative of a single s^{ON} value. The duration of the s^{OFF} pulses are given along the x-axis. Each point is a single biological replicate. **(B)** The Matlab curve fitting function was used to calculate the rate constant for each s^{ON} curve.

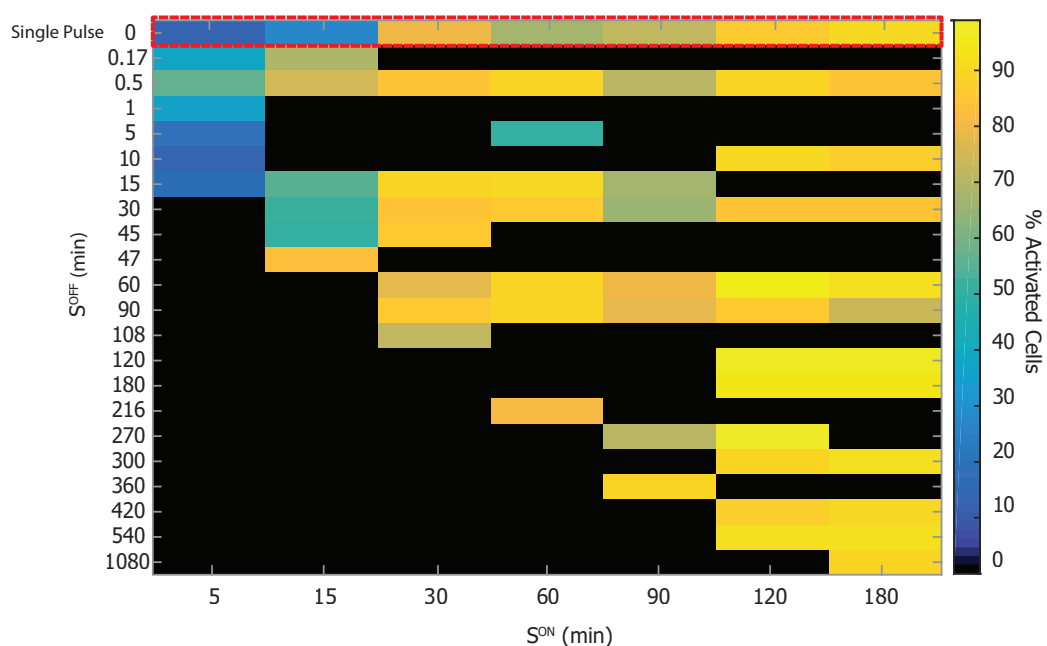


Figure 5.23 CD69 is rapidly expressed on optoCAR stimulation Using matlab peak separation, the fraction of activated cells in each well were calculated. The duration of each signal pulse (S^{ON}) is varied along the x-axis and the duration of each light pulse is varied along the y-axis (S^{OFF}). The top row, outlined in red, represents a single continuous pulse of signalling equivalent to the value given for S^{ON} along the x-axis. For each unit on the heat map $n = 2$ or 3 (Biological replicates)

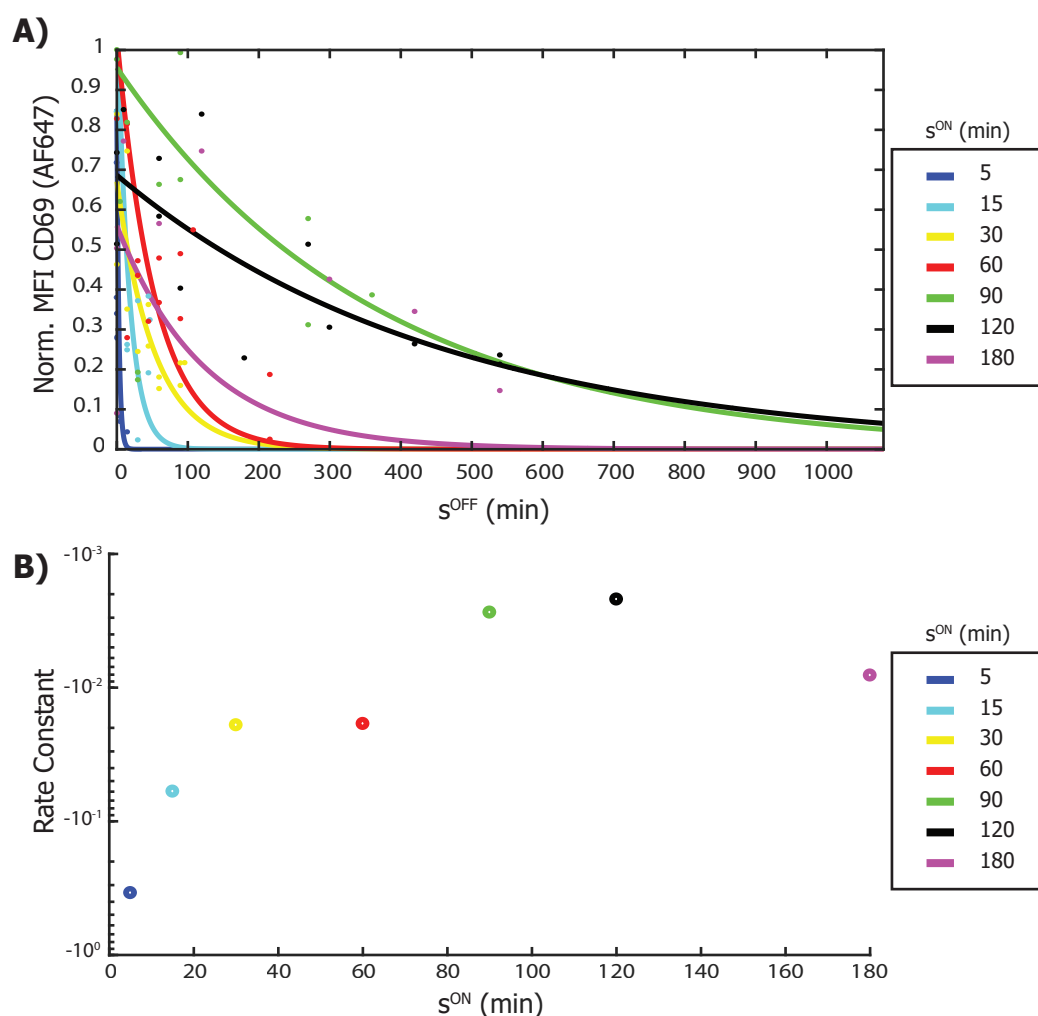


Figure 5.24 CD69 signal exhibits rapid decay (A) Mean fluorescent intensity of the population of cells in each well of the LPA was calculated and normalised to the 6 hour single pulse control and the s^{ON} single pulse control. Each point represents a single sample. Curves were generated using the Matlab exponential curve fitting function. Each curve is representative of a single s^{ON} value. The duration of the s^{OFF} pulses are given along the x-axis. **(B)** The Matlab curve fitting function was used to calculate the decay constant for each s^{ON} curve.

the duration of S^{OFF} . Given the speed of CD69 upregulation and the long $t_{1/2}$ of the receptor reversion rate, it is difficult to discern from this data if signals regulating CD69 expression are summative.

As with the NFAT reporter system, it was found that TCR signals governing CD69 upregulation are tightly negatively controlled (Figure 5.24). Increasing the duration of S^{OFF} caused a rapid decrease in CD69 expression. Once again this effect was most pronounced where S^{ON} was 5 minutes (Figure 5.24A). Interestingly, it was noted that increasing the duration of S^{ON} decreased the rate of signal decay (Figure 5.24B). Again, this finding is consistent with the hypothesis that the accumulation of short term signalling intermediates provides T cells with short-term ‘memory’ of their previous interactions (Locasale 2007; Faroudi et al. 2003). Increasing the duration of signal results in a corresponding increase in downstream signalling intermediates.

The data obtained from the 3 hour S^{ON} datasets should be interpreted with the caveat that as the duration of S^{OFF} is increased the second 3 hour activation pulse is shifted closer to the end of the experiment (24 hours total). Transcription of mRNA and protein translation create an intrinsic time lag within the system, therefore it might be expected that the second pulse of activation would contribute somewhat less to the overall output response (GFP or CD69 expression). This is mitigated by the fact that as S^{ON} is decreased as each individual pulse would now be expected to contribute less to the final output. Thus it is plausible that in the datasets where S^{ON} equals 90 minutes or 120 minutes, the MFI signal of GFP or CD69 could be more than the signal generated from two, 3-hour pulses of signalling. Indeed this does seem to be the case (Figure 22A, Figure 24A).

5.4 Discussion

5.4.1 A physiologically-relevant system for studying T cell activation

Unlike other models of T cell activation, which rely on antibody stimulation or treatment with PMA to activate T cells, the optoCARs provide a system that closely recapitulates the endogenous TCR signalling pathway (Figure 5.1-5.2). As with previous studies we found that increasing the amount of ‘antigen’ (rapalog) did not affect the degree of activation (Au-Yeung BB et al. 2014), but rather the fraction of cells activated. However, in the long-term and short-term activation assay it was found that increasing drug concentration increased the amount of background activation. The calcium flux assays also confirmed that ITAM number affects the potency of the response. As our artificial receptors have only three ITAM signalling motifs, it was observed that the peak

amplitude of the calcium flux triggered through the optoCARs was lower than that seen in the cells triggered through SEE (Figure 5.6-5.7). As with clinically tested CARs, we might seek to address the potency of activation in the future by using a naturally dimerising receptor protein, such as CD28, for the foundation of the optoCAR. Nonetheless, the kinetics of the response including the delay in signalling and the fraction of activated cells remained comparable regardless of the receptor. This is in agreement with theoretical models of T cell activation (Mukhopadhyay et al. 2016). Ultimately, these findings show unprecedented temporal control over T cell signalling dynamics in a physiologically-relevant setting.

5.4.2 *A 'temporal roadmap' for T-cell activation*

By using the optoCAR systems I have approached the T cell as a 'black box' system (Figure 5.25). That is, this system allows for precise, tunable modulation of the input stimulus – light intensity/duration and rapalog concentration – and a set of quantifiable activation markers – CD69, NFAT-driven GFP expression, or IL-2 secretion. Without knowing anything more about T cell biology our data clearly shows that input signals along the TCR signalling axis are tightly regulated (Figure 5.25). Fortunately, extensive research into the basic biology of T cells allows us a framework in which to apply these findings. Contextually this finding makes sense. Conventional T cells play an important role in driving the overall immune response to infection, inappropriate activation of T cells can result in autoimmunity and severe inflammation. It is therefore in the best interest of an organism that relies on adaptive immunity to tightly regulate the activation of T cells.

The data presented in this chapter also highlight key features of T cell signal integration. Several studies have proposed the accumulation of unstable signalling intermediates in T-cell activation. One well-proven signalling intermediate involved in TCR-signal transduction is the accumulation of post-translational protein modifications. Engagement of the TCR results in phosphorylation of ITAM signalling motifs by the associated CD3 chains. These serve as docking sites for the kinase ZAP70, which phosphorylates other signalling molecules further downstream, including LAT and SLP76 (Smith-Garvin et al. 2009). These phosphorylated proteins represent early signalling intermediates in the T-cell activation process. Their accumulation is translated into downstream activation in a manner that is still incompletely resolved. The accumulation of post-translational modifications provides very short-term memory of previous signals (Taylor et al. 2017). Indeed, this is the foundation for the kinetic proofreading model of activation (Hopfield 1974; McKeithan 1995). However, this phosphorylation is counteracted by phosphatases, such as

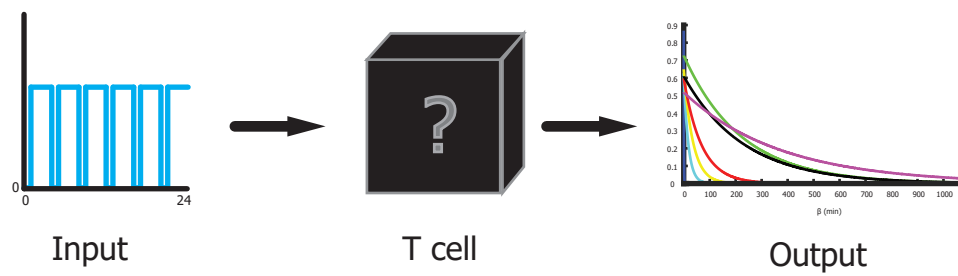


Figure 5.25 T cells as a black box system By controlling the signal inputs through the optoCAR receptor and measuring the signalling outputs one can begin to understand the underlying signalling mechanisms of the system

CD45 and SHP-1/-2 that act to dampen TCR signalling (Schoenborn et al. 2011; Hui et al. 2017). This strong negative feedback mechanisms provides tight control over T-cell activation and is reflected in my results (Figure 5.21-24). The data presented here show that early signals are very quickly cleared from the signalling network on the cessation of optoCAR stimulation. This is seen in the rapid decrease in calcium fluxing observed on blue light irradiation. Interestingly, this effect was at least partially dependent on the photocycle kinetics of the LOV2 domain, as the fast-cycling receptor was able to reinitiate signalling more quickly than the other two. This suggests that the phosphorylation modifications on CD3 ζ last for at least a few seconds. This provides support for the kinetic proofreading with limited signalling model of activation, which allows the system to ‘recall’ past engagements and rapidly reinitiate subsequent phosphorylation of the TCR (Lever et al. 2014). This effect is enhanced by TCR-pMHC interactions with a longer dwell time, which promotes TCR clustering (Taylor et al. 2017).

Further downstream the data support a different mechanism for signal integration. As the duration of the signalling pulse was increased I observed a corresponding decrease in the rate of signal decay (Figure 5.22, 5.24). This process occurred gradually as the duration of S^{ON} was increased. One possible explanation for this is the upregulation of immediate early gene (IEG) expression. IEGs are important in the cellular response to environmental stimuli and are expressed early during activation. The rapid expression of IEGs means that they do not rely on the upregulation of other transcription factors but instead rely on the existing cellular machinery (Abraham, Dragunow, and Tate 1991; Wilson et al. 2017). Indeed, Myc and Fos, two well-characterised IEGs have been proposed as intermediates in the T cell activation process (Y. Wang et al. 2012; Macian 2005). Given that the switch in the rate of signal decay occurs around the time that these genes would be expressed, this presents a tantalising target for future analysis. Other optogenetic studies have identified IEGs as important integrators of signalling downstream of the platelet-derived growth factor receptor (Wilson et al. 2017). It will be interesting to see how these results compare in T cells as it has been suggested that the previous activation events that occur during T cell development shape the genetic and epigenetic landscape of future activation events (Locasale 2007; Ohkura et al. 2012). Taken together our findings can be used to piece together a ‘temporal roadmap’ for T cell signalling. The optoCARs can be used to examine the temporal sequence of events leading to complete T cell activation as well as the broad mechanistic implications for these events.

5.4.3 Co-stimulatory/-inhibitory receptors in TCR signal transduction

T cells express a number of different co-receptors, which act as both positive and negative regulators of T cell activation. Although the activities of these molecules in activating or inhibiting T cells are broadly understood, their mechanistic influence on signal integration remains poorly understood. We confirmed expression of the costimulatory receptor CD28 on the JNFAT cell line. A potential future line of enquiry would be the interrogation of the involvement of CD28 mediated signalling in downstream activation. CD28 is reported to enhance activity of the Phosphoinositide 3-kinase (PI3K) signalling pathway (Garcon et al. 2007). Signalling along the PI3K axis has been shown to be involved in mediating TCR-induced signalling (Okkenhaug and Vanhaesebroeck 2003). In the absence of costimulatory signals T cells are directed toward anergy (Gimmi et al. 1993; Linterman et al. 2014). It might be expected that reducing CD28 signalling could sharpen the signal decay curve observed in NFAT-driven GFP and CD69 assays. Blocking α CD28 antibodies have been used clinically (Jang et al. 2008) and thus antibody blocking of the CD28 receptor interaction with its ligands, CD80 and CD86 on the surface of APCs, could prove useful in determining the involvement of this co- stimulatory receptor in TCR signalling. Alternatively, CTLA-4 (Cytotoxic T-lymphocyte-associated protein 4), an inhibitory receptor expressed on the surface of T cells, has also been shown to interact with CD80 and CD86 (Greene et al. 1996). CTLA-4 has a higher affinity and avidity for CD80 and CD86 than CD28 and thus is able to outcompete CD28 for their binding even at low expression levels (McCoy and Gros 1999). Intracellularly CTLA-4 interacts with PP2A and SHP-2, which dephosphorylate the TCR signalling complex (Teft, Chau, and Madrenas 2009; Schneider and Rudd 2000). It would thus be expected that CTLA-4 would also increase the decay rate of TCR signalling. In enacting these experiments it is important to recognize that Jurkat T cells are reported to exhibit high basal levels of PI3K expression (Astoul et al. 2001). However, even with this in mind, many basic concepts in T cell biology were initially discovered in Jurkat cells and then confirmed in host-derived T cells (Bartelt et al. 2009). CD28 and CTLA-4 represent on two of the many co-receptors expressed on T cells, others have been well reviewed elsewhere (Chen and Flies 2013). Traditional genetic manipulation combined with our optoCAR system could yield new insights into the signal integration and translation of co-receptor-derived inputs. The fact that these sorts of experiments are possible is one of the key attributes of our cell-cell signalling system.

5.4.4 Conclusions

We have applied an engineering perspective to T cell biology by looking at the T cell as a black box system, but this terminology is not necessarily strictly applicable to the T cell. A truly black box system implies that the inner workings are unknown, but decades of research into the fundamental biology of T cells has provided us with a comprehensive understanding of the underlying signalling components. Our optogenetics approach into the interrogation of T cell signal integration has confirmed that proximal TCR signalling events are tightly negatively regulated and exhibit a rapid rate of signal decay. The results presented in this chapter outline the foundations for a precise temporal roadmap of TCR signalling events and their contribution to overall signal integration. Moving forward it will be important to further characterize the underlying biochemistry of the system and understand how manipulating the activation pathway affects T cell fate and function.

Chapter 6 – Structural features of T cell-dependent bispecific antibody epitope affect T-cell activation and therapeutic potential

The work presented herein was done in collaboration Ji Li, Nicola J. Stagg*, Jennifer Johnston*, Sam Menzies, Danielle DiCara*, Vanessa Clark*, Maria Hrisopoulos*, Ryan Cook*, Dionysos Slaga*, Rin Nakamura*, Luke McCarty*, Siddharth Sukumaran*, Elizabeth Luis*, Zhenmao Ye*, Thomas D. Wu*, Tieko Sumiyoshi*, Dmitry Danilenko*, Genee Y. Lee*, Klara Totpal*, Diego Ellerman*, Isidro Hötzel*, John R. James, and Teemu Junttila*. This work is published in: “Membrane-Proximal Epitope Facilitates Efficient T Cell Synapse Formation by Anti-FcRH5/CD3 and is a Requirement for Myeloma Cell Killing”, Cancer Cell 31, 383-395, March 13 2017.*

**Genentech, Inc. 1 DNA Way, South San Francisco, CA 94080, USA*

6.1 Introduction

6.1.1 Multiple Myeloma

Multiple myeloma (MM) is one of the most common haematological malignancies (Siegel, Miller, and Jemal 2016). MM is characterised by the malignant outgrowth of plasma cells in the bone marrow and overproduction of monoclonal immunoglobulin protein (M protein), though this clinical feature varies within the patient population (Drayson et al. 2001; Kyle et al. 2003). Clinical manifestations include anaemia, renal failure, bone disease, and hypercalcaemia (Rajkumar et al. 2014). Current pharmacological treatment of MM relies on proteasome inhibitors, immunomodulatory drugs, monoclonal antibodies and Alkylating agents (Kyle and Rajkumar 2009). Where patients are eligible, autologous haematopoietic stem cell transplantation is also used to treat MM. Unfortunately MM is still incurable and most patients treated for this malignancy will go on to relapse. Even with the most effect therapeutic regimes currently in use, median overall survival is only ~3 years (Kumar et al. 2017). As such, there is a need for new treatment options.

6.1.2 FcRH5 as a clinical target

One limiting factor in the development of cancer therapies is the availability of cancer-specific biomarkers. Fc receptor homolog 5 (FcRH5) – also referred to as FcRL5, IRTA2 or CD307—is a surface-expressed protein found on B cells, including pre-B cells and plasma cells. There are 5 proteins in the FcRH family, each with Ig-like extracellular domains (Polson et al. 2006). The genes expressing the FcRH family proteins are tightly clustered in the human 1q21

region amongst previously identified FcR genes (R. Davis et al. 2001). Genomic instability surrounding the FcRH5 locus frequently results in B cell malignancies with unbalanced translocations causing partial trisomy or tetrasomy of the *IRTA1* and *IRTA2* genes (Hatzivassiliou et al. 2001). As such, it was found that FcRH5 is expressed in MM as well as Burkitt's Lymphoma and B-chronic lymphocytic leukaemia (Polson et al. 2006; Miller et al. 2015), suggesting broad applicability as a biomarker for multiple B cell cancer subtypes.

6.1.2 Immunotherapy and T cell-dependent bispecific antibodies

Bispecific antibodies (bsAb) are a novel class of biopharmaceutical. There are currently around 50 different bsAb formats available, but they can be broadly categorised into two major groups: those containing an Fc region and those lacking an Fc region (Kontermann and Brinkmann 2015). Although the latter is generally smaller, the presence of an Fc region may be desirable in a pharmaceutical context because it allows for the mediation of further effector functions (Kontermann and Brinkmann 2015). Coloma & Morrison (1997) conceived of the idea of bsAbs twenty years ago, but it was not until recently that bsAbs have been applied in a clinical context. Importantly, bsAbs can be administered to patients “off-the-shelf” without the fear of latent reactivation. This is in contrast to chimeric antigen receptor T cell therapy, which requires genetic modification of patient T cells and may eventually result in latent reactivation (Chesi and Fonseca 2017).

The first bsAb to receive market approval was catumaxomab (Removab®) (Linke, Klein, and Seimetz 2010). Catumaxomab is a trifunctional, bispecific antibody that combines anti-epithelial cell adhesion molecule (EpCAM) with anti-CD3ε binding specificities. This bispecific reactivity allows for T cell activation toward tumour cells positive for EpCAM. The presence of the Fc region further serves to activate monocytes, macrophages, dendritic cells, and NK cells via Fcγ-receptor binding (Smith and Clatworthy 2014). Several other types of bispecific antibody are currently under development or are in clinical trials. These are well reviewed by Kontermann & Brinkmann (2015).

We tested the efficacy of bsAbs toward FcRH5-expressing MM cells. Our T cell-dependent bispecific antibody (TDB) combines anti-CD3ε binding specificity with specificity toward varying structural epitopes on FcRH5. CAR T cell therapies and bsAbs have previously been successfully tested against B cell leukaemias and lymphomas (Bargou et al. 2008; Sadelain, Brentjens, and Rivière 2013). Furthermore, clinical trials have shown that full-length TDBs represent an appropriate therapeutic format as they have a long serum half-life and low risk for forming anti-

drug antibodies (Junttila et al. 2014; L. L. Sun et al. 2015). Despite these earlier findings, the molecular mechanism of T-cell activation by TDBs remains to be fully described.

6.1.3 The kinetic segregation model of T-cell activation

The exact details of T-cell activation are still the focus of ongoing research, but it is well-accepted that the process of TCR triggering is characterised by increased phosphorylation of the TCR complex and downstream signalling molecules, including ZAP70, LAT and SLP76 (Smith-Garvin et al. 2009). The kinetic segregation model of T-cell activation states that phosphatases, such as CD45, are passively excluded from regions of close membrane proximity caused by the interaction of the TCR with pMHC, due to their large, rigid extracellular domains. This exclusion of phosphatases from the regions of tight membrane apposition allows Lck to unrestrictedly phosphorylate the ITAMs in the TCR complex, resulting in the recruitment of ZAP70 and a further bias toward downstream phosphorylation (James and Vale 2012). This exclusion of CD45 is critical in the formation of a functional immune synapse (IS). The exclusion of proteins with large extracellular domains from regions where cell membranes are tightly juxtaposed appears to be a fundamental biophysical signalling mechanism (Schmid et al. 2016).

Previous studies of bsAbs have pointed toward the exclusion of CD45 from regions on the plasma membrane when the therapeutic is bound (Offner et al. 2006). It therefore follows that bsAbs may function to activate T cells in a manner analogous to the endogenous TCR-pMHC interaction. We sought to confirm this hypothesis using a reductionist T cell system and a series of FcRH5-binding bsAbs.

6.2 Materials & Methods

6.2.1 TDB labelling

For microscopy, TDBs were first dialysed into PBS, pH 7.2 and then labelled with Alexa Fluor 647 using an antibody labelling kit (Thermo Fisher Scientific) according to the manufacturer's protocol. Following labelling, a dye:protein ratio of ~4 was routinely achieved.

6.2.2 Transient transfection

To prepare HEK-T cells and FcRH5-expressing target cells for microscopy, cells were transiently transfected according to the protocol outlined in chapter 2, section 2.5.1. However, cells were

seeded into 6-well plates rather than MatTek imaging dishes. HEK293Ts were transiently transfected with 1 µg total of pHRSV-FcRH5-Ruby using 3 µl of GeneJuice reagent (Millipore). HEK T-cell expressing the 1G4 TCR (James and Vale 2012) were transiently transfected with ZAP70-BFP, Lck, CD43:45-qGFP, and CBP/Csk to a total of 1.5 µg of DNA with 4.5 µl of GeneJuice. Ratio of DNA between constructs was 1:1:2:1.5, ZAP70:Lck:CD45:CBP/Csk.

6.2.3 Confocal microscopy

For confocal imaging, cells were trypsinised with 500 µl of 0.25% Trypsin, which was then inactivated with 1.5 ml of complete media. Cells were then mixed 1:1 in DBPS at high density with TDB antibody and conjugated at 37°C for 30 minutes. Cells were gently resuspended by pipetting and transferred into imaging dishes with DMEM^{gfp} (Clontech) to reduce photo-bleaching.

6.2.4 Image Analysis

Analysis of microscopy images was performed using Fiji (ImageJ). Channels were separated, background subtracted by 100 pixel rolling ball method, and images enhanced by exponential fitting. Pixel intensity for each channel was calculated to measure CD45 exclusion, FcRH5 clustering, TDB clustering, and ZAP70 recruitment.

6.3 Results

6.3.1 TDBs activate T cells through the kinetic segregation of CD45

During IS formation, the tight apposition of the T cell and APC, caused by the interaction of the TCR with pMHC and by integrin receptors, results in the exclusions of the phosphatase CD45 from the cell-cell interface (Chang et al. 2016; S. Davis and van der Merwe 2006). In this kinetic segregation model of T cell activation CD45 is excluded from TCR-pMHC clusters because of its large, rigid extracellular domain (Figure 6.1) (James and Vale 2012; Schmid et al. 2016). Using HEK293T cells expressing the minimal machinery necessary for T cell activation, we were able to show that TDBs drive T cell activation through the exclusion of CD45 and clustering of the target molecule.

As has been discussed in previous chapters, early T cell activation is characterised by the phosphorylation of CD3 ITAMs by the Src family kinase, Lck. These phosphorylated ITAMs serve as a docking site for the SH2 domain of ZAP70 (Smith-Garvin et al. 2009). As ZAP70 is cytosolic

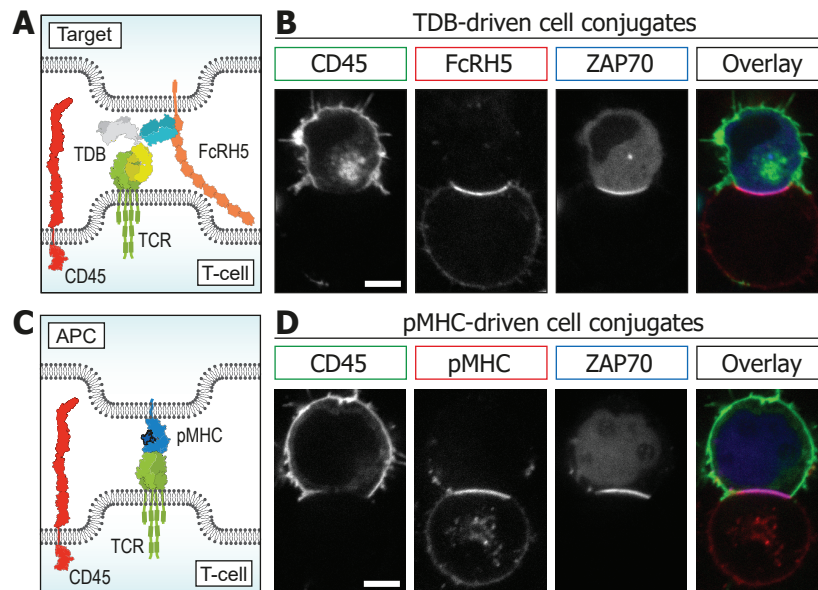


Figure 6.1 Anti-FcRH5/CD3 TDB conjugated cells mimic pMHC/TCR cell-cell junction **(A)** A schematic overview of the cell-cell interface with proteins represented approximately to scale. **(B)** representative image of TDB (1G7)-mediated conjugate between HEK293T cell expressing FcRH5-Ruby and HEK T cell. CD45 segregation and ZAP70 recruitment are clearly shown. **(C)** Schematic overview of TCR-pMHC interaction with proteins shown approximately to scale. **(D)** Conjugate is between pMHC-expressing Raji B cell and HEK T cell. Conjugate shows CD45 segregation from cell-cell interface and clustering of pMHC and ZAP70 recruitment. Cartoon schematics **(A, C)** were prepared by John James. Microscopy was performed and images prepared by Michael Harris **(B,D)**.

in non-activated T cells, the recruitment of ZAP70 to the phosphorylated ITAMs can be used as a visual readout of T cell activation (Figure 6.1) (James and Vale 2012). We transiently expressed Lck, CBP/Csk, CD45 and Zap70 in HEK cells stably expressing the 1G4 TCR (HEK-T cells) (James and Vale 2012). HEK-T cells were conjugated with HEK293T cells transiently expressing FcRH5 in the presence of a TDB antibody with a membrane proximal binding epitope (Figure 6.1A). This resulted in strong recruitment of ZAP70 to the cell-cell interface as well as clustering of the target molecule and exclusions of CD45 (Figure 6.1B). We found that this mimicked the synapse formation between HEK-T cells and Raji B cells expressing pMHC (Figure 6.1C, D). Close membrane apposition driven by the TCR-pMHC interaction resulted in the exclusion of CD45, clustering of pMHC at the membrane interface, and recruitment of ZAP70 to region of cell-cell contact (Figure 6.1D).

The formation of an immunological synapse between a CD8⁺ T cell and its target is essential for the directed secretion of cytolytic granules and target cell killing. To visualise the interface between the HEK-T cell and the target cell, a 3D, Z-stack image was taken of the TDB conjugated cells. This 3D confocal imaging was performed by Sam Menzies. As is consistent with the formation of an IS, these images show the formation of an IS-like structure with CD45 excluded to the distal region of the contact area and FcRH5, and by extension the TCR, clustered within the centre (Figure 6.2A). Regions enriched for FcRH5 and CD45 were mutually exclusive. A line profile of the cell-cell interface confirmed the colocalisation of FcH5 with the TDB and exclusion of CD45 (Figure 6.2B). Taken together, these results indicate that TDBs drive T cell activation through the same molecular mechanism as the intrinsic TCR-pMHC interaction. Both mechanisms of triggering show increased exclusion of CD45 and target clustering at the cell-cell interface. Interestingly, the EpCAM-specific BiTE (Bi-specific T cell Engager) was also reported to drive the same exclusion of CD45 (Offner et al. 2006), indicating that this mechanisms may be intrinsic to bsAbs.

6.3.2 Membrane proximity of TDB epitope enhances T-cell activation and target killing

FcRH5 is a type I membrane protein with a large extracellular domain (Polson et al. 2006). It is known that the interaction of the TCR and pMHC brings the membranes of the T cell and the APC to within approximately 14 nm of each other (James and Vale 2012). The close apposition of the cell membranes is what drives the exclusion of CD45 (James and Vale 2012; Schmid et al. 2016). To test the effect of epitope structural features on T-cell activation and tumour cell killing

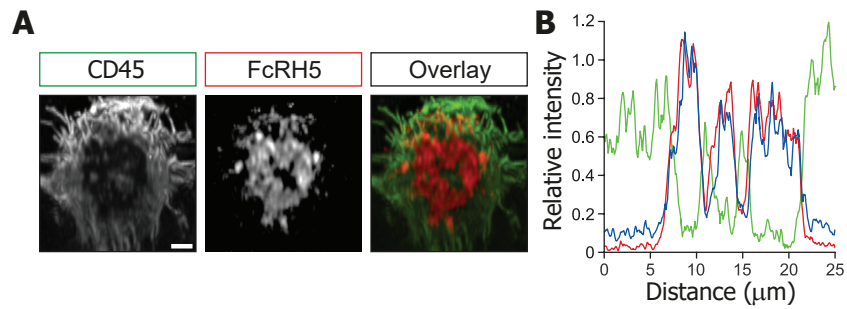


Figure 6.2 FcRH5 clustering and CD45 exclusion at the cell-cell interface (A)

An en face view of the cell-cell interface between a HEK T cell and a HEK expressing FcRH5-Ruby. **(B)** Line profile of the en face junction showing exclusion of CD45 (green) and concomitant clustering of FcRH5 (red) and TDB (blue). Microscopy **(A)** was performed by Sam Menzies and quantification **(B)** was performed by John James

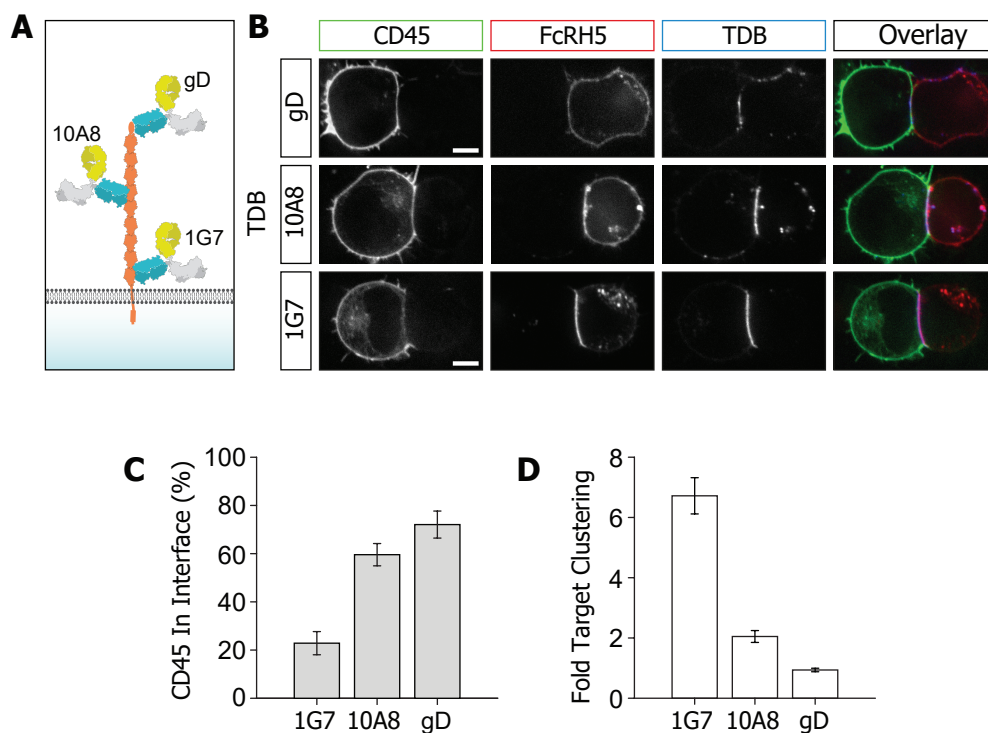


Figure 6.3 Membrane-proximity of TDB FcRH5 epitope drives increased CD45 segregation (A) Schematic overview of the TDB binding sites on FcRH5. **(B)** Representative images of the TDB-mediated conjugates between HEK T cells and HEK293T cells expressing FcRH5. Conjugation was induced using the AF647-labelled TDB specified. **(C)** CD45 segregation and **(D)** FcRH5 clustering were measured by quantifying the intensity along the TDB labelled membrane section, relative to the total membrane. Cartoon schematic **(A)** was prepared by John James, Microscopy and quantification **(B-D)** was performed by Michael Harris.

we generated a series of TDBs with binding sites on FcRH5 increasingly proximal to the plasma membrane (Figure 6.3A).

We generated and tested three different TDBs with epitopes at varying membrane proximities (Figure 6.3A). We found that target clustering and CD45 exclusion correlated with membrane proximity of the epitope (Figure 6.3B). TDB binding to the most membrane proximal Ig domain of FcRH5 (1G7), showed increased exclusion of CD45 when compared to TDBs targeting the central region (10A8) or the distal region (gD) of FcRH5 (Figure 6.3C). Conjugation with TDB-1G7 also resulted in increased clustering of FcRH5 at the cell-cell interface (Figure 6.3D). The representative microscopy images in Figure 6.3 were taken by myself and the quantification of target clustering and CD45 exclusion (Figure 6.3C, D) was performed on data from image-sets created by myself (1G7-TDB and 10A8-TDB) and Sam Menzies (gD).

We next tested the efficiency of the TDB variants to induce T cell activation and target cell killing. CD8⁺ T cells were acquired from healthy donors and stimulated with the TDBs in the presence of FOXP3⁺ cells expressing human FcRH5. This work was performed at Genentech in the lab of Teemu Junttila. It was found that 1G7-TDB triggered more robust T cell activation, as measured by SLP76 phosphorylation, than either the 10A8-TDB or the gD-TDB (Figure 6.4). Indeed, there was almost no observable phosphorylation of SLP76 in CD8⁺ T cells treated with gD-TDB (Figure 6.4). The inability of the gD-TDB to activate T cells was made obvious in a cell-killing assay. Even high concentrations of the gD-TDB were unable to affect target cell killing (Figure 6.5). In contrast, CD8⁺ T cells treated with the 1G7-TDB demonstrated efficient target killing (Figure 6.5; $EC_{50} = 0.5 \text{ nM}$). Finally, to confirm that these effects were driven by the location of the epitope we generated a truncated version of the FcRH5 protein in which the gD epitope was expressed directly above the 1G7 epitope (Figure 6.6A). It was found that in removing most of the extracellular domain, the efficiency of target cell killing was increased 25-fold ($EC_{50} = 20 \text{ pM}$) in CD8⁺ T cells stimulated with 1G7-TDB and that gD-TDB was now able to affect target cell killing (Figure 6.6B; $EC_{50} = 0.19 \text{ nM}$).

Of Note, the differences in binding affinity of the 1G7-TDB and the 10A8-TDB (12 nM and 3 nM, respectively) do not account for their differences in ability to activate T cells (Figure 6.4) (J. Li et al. 2017). Differences in expression of the truncated versus the non-truncated FcRH5 constructs also do not account for the differences in killing (J. Li et al. 2017). These results indicate the structural characteristics of the TDB target epitope can alter the efficiency of T-cell activation and subsequent target cell killing.

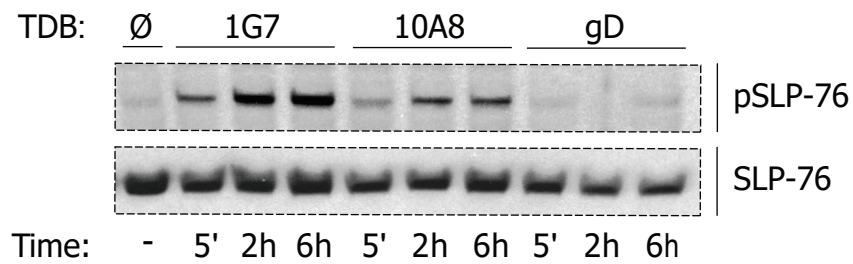


Figure 6.4 Increased phosphorylation of downstream signalling proteins with membrane proximal epitope Peripheral CD8⁺ T cells from healthy donors were stimulated with FoxNY cells expressing human FcRH5 and 1µg/ml TDB. SLP76 phosphorylation was measured by phospho-Western with total SLP76 as the input control. This experiment was performed in the lab of Teemu Junttila.

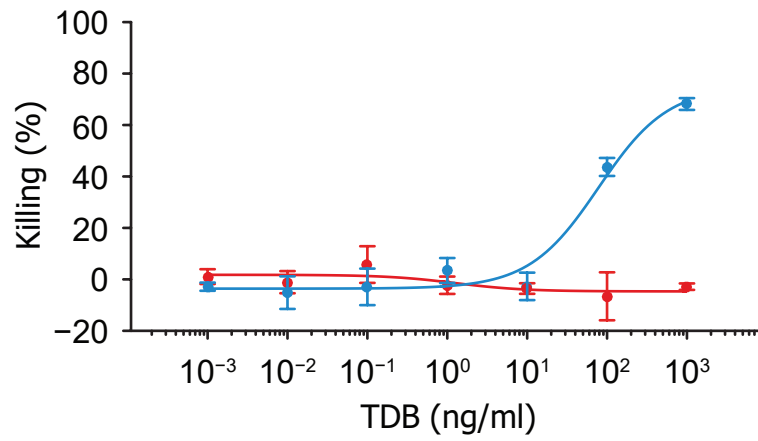


Figure 6.5 Membrane proximal epitope facilitates target cell killing FoxNY cells expressing human FcRH5 were killed by CD8+ T cells using either the 1G7-TDB (blue) or gD-TDB (red).

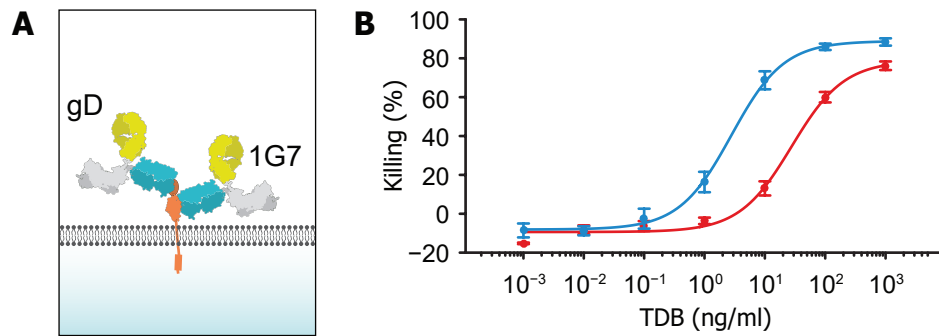


Figure 6.6 Truncation of FcRH5 improves CD8⁺ killing efficiency (A) The FcRH5 construct was truncated such that the gD tag was immediately proximal to the 1G7-TDB binding epitope. **(B)** CD8⁺-mediated target cell killing of FoxNY cells expressing the truncated FcRH5 variant. Target cell killing was induced using either 1G7-TDB (blue) or gD-TDB (red). All killing assays were performed in the lab of Teemu Junttila.

6.4 Discussion

6.4.1 Epitope structural features affect therapeutic potential of bsAbs

The results presented above indicate that along with serum half-life, complement fixation, antibody-dependent cellular cytotoxicity, binding affinity and stability, among other characteristics of bsAbs, the structural features of the target epitope should be considered in therapeutic design. We have shown that the membrane proximity of the bsAb target epitope strongly influences T-cell activation. Epitopes proximal to the membrane showed enhanced capacity to activate T cells compared with membrane distal epitopes. To drive exclusion of CD45, the membrane of the T cell and the target cell must be tightly juxtaposed; a membrane proximal binding epitope facilitates this tight apposition. It was shown as well that optimal T-cell activation was driven by the bsAb target molecule itself. Truncation of FcRH5 resulted in target cell killing by 1G7-TDB at a considerably lower concentration than was required for the full length FcRH5 protein (Figure 6.6). This finding suggests that screens for future immunotherapeutic targets could rank the molecules based on their structural features, facilitating therapeutic design and efficiency.

6.4.2 Combination Immunotherapy

As discussed in chapter 5, T-cell activation is dependent on the integration of multiple signalling pathways. Co-receptors serve to both positively and negatively regulate T-cell activation. Two inhibitory receptors, commonly referred to as ‘checkpoint receptors’ are CTLA-4 and PD-1 (Programmed Cell Death Protein-1) (Osada et al. 2015; McCoy and Gros 1999). Clinical trials have shown that blocking these receptor pathways can serve to enhance T-cell activation and tumour killing capacity (Callahan, Postow, and Wolchok 2015). It has been shown that myeloma cells upregulate the PD-1 binding partner, PD-L1 (programmed cell death protein ligand 1) (Gorgun et al. 2015), to circumvent killing by T cells. In this study it was shown that treatment of cynomolgus monkeys with the TDB resulted in an increase in PD-1 expression on CD8+ and CD4+ T cells (J. Li et al. 2017). T cells in which PD-1 was upregulated showed a reduced capacity for target cell killing, but antibody blockade of PD-L1 resulted in significantly improved target cell killing (J. Li et al. 2017). This finding lends support to the idea that TDBs can be used in combination with checkpoint inhibitors for improved treatment of MM patients, particularly in later disease stages.

6.4.3 Stratification of patient populations

Genetic abnormalities of the 1q21 region, which contains the FcRH gene loci, are a common feature of B cell malignancies including MM (Polson et al. 2006). Duplications of the *IRT42* gene can result in the overexpression of FcRH5. This research suggest that MM cells overexpressing FcRH5 are exquisitely sensitive to TDB treatment (J. Li et al. 2017). There is a current lack of prognostic biomarkers for patients with MM. Genetic testing of the 1q21 locus for the identification of duplication or deletion events may serves as a useful prognostic indicator for the success of treatment with the FcRH5-TDB. In conclusion, these TDBs provide another weapon in the armament against a form of B cell malignancy that currently has limited treatment options.

Chapter 7 – Final Discussion

7.1 Overview of Results

In this thesis I present the development and application of several optogenetic and chemically-controllable tools for the interrogation of T-cell activation events (Figure 3.2, 3.3, 3.9 & 5.1). I began this work by attempting to develop a set of LAT-based optogenetic switches for the analysis of microcluster formation. Although this work did provide novel insights into the understanding of early T cell signalling events, it was ultimately hampered by the intrinsic biological properties of the LOV2 domain. However, using the insights gained from this approach, I was able to reapply this LOV2 optogenetic technology toward the development of a set of optogenetic chimeric antigen receptors, ‘optoCARs’.

Using both the LAT-based LOVTRAP system and the optoCARs I was able to show that early T-cell signalling events are under extremely tight negative regulation. On blue light irradiation of Jurkat T cells expressing either the LOVTRAP-LAT system or the optoCAR, I observed an almost immediate cessation of calcium signalling (Figure 4.16, 5.6-5.14). This results shows that early T cell activation is under tight negative regulation and that this effect is immediately transmitted through the TCR proximal signalling network within a matter of seconds. This feature of T cell signalling probably exists to set a sharp activation threshold between activating pMHC ligands and non-activating pMHC ligands. As the T cell must be able to distinguish between activatory and non-activatory signals with a high degree of selectivity and specificity (McKeithan 1995; François et al. 2013), tight negative regulation of the TCR-proximal signalling components would serve to rapidly extinguish off-target activation. Although such a threshold has been proposed through modelling studies (François et al. 2013; Lever M et al. 2014), it has been difficult to experimentally show with the existing methods of T cell activation.

I have also used the optoCAR system to begin to interrogate the temporal integration of discontinuous TCR signals. It has been proposed that the accumulation of unstable signalling intermediates leads to a summative signalling outputs. This concept is well reviewed by Mayya and Dustin (2016). When viewed in the context of adaptive immune priming this hypothesis makes sense. T cell are reported to interact with multiple DCs on their transit through the secondary lymphoid organs (Qi, Kastenmüller, and Germain 2014). Although the data outlined above indicate that proximal signalling events are rapidly terminated on disengagement of the TCR, this finding does not negate the idea that more sustained interactions may lead to the development of downstream signal intermediates that provide the T cell with a form of ‘short-term’ memory of past signalling events. However, the time scale on which these intermediates accumulate and the

rate at which they decay remain almost completely unknown. To address this outstanding question I used the optoCAR system to fragment pulses of TCR-like signalling with pulses of system inactivity. In doing this I was able to determine that signals received through the optoCAR, and by extension the TCR, decay rapidly (Figure 5.21-24). Again, this finding suggests that TCR signalling is under tight negative regulation. However, it was observed that as the duration of each signalling pulse was increased, the rate of TCR signalling decay gradually decreased (Figure 5.22, 5.23). This finding points to the accumulation of signalling intermediates. As the quantity of these intermediates increases, the longer the duration of short-term memory of past signalling events will be.

Finally, in this thesis I also define the mechanism of action of bispecific antibodies using a reductionist model of the T-cell signalling apparatus. Using HEK293T cells expressing the TCR (HEK T cells), CBP/Lck, CD45, and ZAP70 conjugated with cells expressing the Multiple Myeloma target FcRH5, I was able to show that α CD3/ α FcRH5 bispecific antibodies activate T cells in a manner analogous to the endogenous TCR-pMHC interaction (Figure 6.1). That is, TDBs mediate the formation of a tight juxtaposition between the T cell and target cell membranes. This narrow cell-cell junction causes the exclusion of the phosphatase CD45 due to its large extracellular domain (Figure 6.3) (James and Vale 2012; Schmid et al. 2016). Interestingly, TDBs also mediate the clustering of the target molecule (J. Li et al. 2017). It was found as well that more membrane proximal epitopes drove this process more robustly, causing greater segregation of CD45 and increased target cluster and improved CD8⁺ T cell-mediated killing. This finding may have important implications for future therapeutic design both of antibody therapies and chimeric antigen receptors.

7.2 Defining the limitations of the LOV2 optogenetic system

The results presented in Chapter 4 highlight the current limitations of optogenetic tools. It was found that neither the LOVTRAP- nor the TULIPs-based LAT optogenetics tools were able to sustain downstream T cell signalling. Protein complexes are in a constant state of equilibrium between the associated state and the dissociated state. The propensity of these complexes to dissociate is measured as the dissociation constant (K_d). The effect of this intrinsic biochemical property was observed in both the TULIPs and the LOVTRAP system, but was more apparent during the Calcium flux assays with the TULIPs system. Both the constitutively active variant of the LOVpep system and a truncated version of the system where the PDZ binding sequence was fused directly to the TM domain of LAT showed identical calcium flux profiles, indicating that the

unsustained calcium flux was caused by an intrinsic property of the LOVpep-PDZ interaction. Indeed, experiments with the low affinity PDZ domain, which has a higher K_d , showed that calcium fluxing decreased more quickly in this version of the system than the high affinity (ePDZb1) version (Figure 4.22). Steric effects were ruled out by creating a fusion protein in which the high affinity PDZ domain was inserted between the TM domain and the signalling domain of LAT. Simply by anchoring the signalling domains at plasma membrane I was able to completely resolve the unsustained calcium fluxing phenotype.

As well as this, a high degree of background signalling was also detected in the LAT-based systems. This was determined to be due to the equilibrium state of the LOV2 domain itself, which oscillates between the active and inactive states. Blue light and darkness simply bias the equilibrium toward one state of the other, but regardless of the state of illumination a proportion of the protein will always exist in both states. Rational engineering and careful design of optogenetic systems in the future will likely help overcome this problem (Strickland et al. 2010; Yao, Rosen, and Gardner 2008).

7.3 Learning from past LOVs

In developing the optoCARs, I implemented lessons from the LAT-based optogenetic systems. Namely, the addition of a CID domain to trigger the receptors. This second degree of control seemed to buffer the systems more against background binding of the Zdk domain to LOV2 and provided a cleaner ‘off’ state (Figure 5.6-5.14). This finding has important implications for the implementation of optogenetics systems. It may be that to overcome background binding in the ‘off state’ a second degree of drug-inducible control may help reduce off-target effects.

7.4 Future directions for the optoCAR system

In Chapter 5, I show that the TCR signalling pathway is under tight negative control, but is still able to integrate temporally discontinuous signals. Das et al. (2009) showed that positive feedback in the Ras signalling pathway leads to hysteresis, which could provide a mechanism for short-term signalling memory. Although this may be true for more long term signals, the experiments presented in chapter 4 and 5 show that TCR signalling is under tight negative control and ceases almost immediately on interruption of proximal signalling events. The mechanistic implication for this remain to be fully described, though modelling studies have suggested the involvement of negative and positive feedback loops in regulating TCR signalling (Lever et al. 2016; Dushek et al.

2011; Honda et al. 2014; Altan-Bonnet and Germain 2005). To further characterise the mechanistic underpinnings of T cell activation it will be necessary to better characterise the dynamics of other signalling events. The optoCAR systems can be used to selectively 'break' the TCR signalling pathway to gain insight into the fundamental mechanisms of signalling.

Activation of the Ras pathway on TCR ligation, leads to phosphorylation and translocation of the canonical Erk protein. In unstimulated T cells Erk is present in the cytoplasm, but phosphorylation of Erk causes it to relocate to the nucleus. Once in the nucleus Erk alters the active state of early-acting transcription factors and initiates changes in gene transcription. It would be interesting to understand the dynamics of this process as the initiation of transcription and translation create an intrinsic lag in the signalling system (Mayya and Dustin 2016). Such a delay could create a degree of short-term memory. As with the calcium flux assay and the NFAT-GFP reporter, combining the optoCARs with fluorescent Erk reporters would allow us to visualise the effects of proximal signals on proteins much further down the signalling pathway. Others have used fluorescently tagged Erk constructs to visualise Erk dynamics in response to receptor activation (Fujioka et al. 2006), but by combining optogenetics with this system we can precisely measure the effects of signal modulation of Erk dynamics in real time.

For completeness, a fluorescently labelled Erk reporter, could be combined with a red-fluorescent calcium indicator (Oheim et al. 2014) to observe both calcium signalling and Erk mobilisation. Both could be observed via confocal microscopy in conjunction with the LOV2 optogenetic system. Assuming an appropriate panel of fluorescent markers were selected for the receptor components and Erk.

With regards to signal intermediates it would be interesting to begin to quantify the accumulation IEG products during the activation process and their rate of decay. Excitingly this approach was recently applied by Wilson et al. (2017) to investigate signal transmission along the Erk signalling axis. The authors investigated the expression dynamics of five IEG products: c-fos, btg2, rhob, klf2, and dusp4. These products were selected from a list of candidate genes upregulated following PDGF receptor stimulation (Wilson et al. 2017). Although this approach is more comprehensive, a number of candidates have been proposed to fulfil this role in T cell, including c-fos, IRF4, and BATF (Man et al. 2013; Nayar et al. 2014; Locasale 2007). Additionally, data mining the Gene Expression Omnibus (GEO) datasets may provide the transcription level data necessary to identify further candidate genes. Once a panel of candidates has been selected it should be possible to measure the accumulation and degradation of mRNA by qPCR and the protein by immunoblot. By comparing this data with the signal integration data presented in Figure

5.20-5.24, it should be possible to build a more complete picture of the mechanism by which T cells are able to decipher temporally encoded signals.

7.5 Fine-scale adjustment of TCR signalling

TCR signalling has been reported to occur digitally by a number of groups (Au-Yeung BB et al. 2014; Kingeter et al. 2010; Das et al. 2009), but the presence of specific costimulatory or co-inhibitory receptors is known to influence the ultimate state of T cell activation – this concept is well review by Chen & Flies (2013) . One important costimulatory receptor is CD28, which is expressed on the surface of T cells and interacts with both CD80 and CD86 expressed on the surface of CD86. CD28 is reported to interact intracellularly with PI3K. Antibody blockade of CD28 could yield insights into the nature costimulatory signals on T cell activation. Specifically, it would be interesting to measure the capacity for T cells integrate signals in the absence of these costimulatory signals. Would the rate of signal decay increase or remain the same? How are readouts of T cell activation changed including CD69, the NFAT-GFP reporter and IL-2 production?

7.6 Reapplying the optogenetic signalling approach to other immune receptors

Finally, the optogenetic approach to signalling presented in this thesis could be useful in interrogating the signalling dynamics of other immune receptors. For example the BCR is also known to signal through a set of ITAMs on CD79. One could envision a reasonably easy substitution between the CD3 ζ chain and CD79 for the interrogation of BCR signalling dynamics. Another interesting future target could be the FcRs, which function through the interplay of ITAM and ITIM motifs. Optogenetic tools provide a powerful mechanism for spatially restricting and precisely activating or inhibiting FcR signalling pathways. By redesigning the optoCAR system to function more like an FcR, it may be possible to investigate the mechanisms of signal integration along competing FcR signalling pathways. Such questions have remained difficult to address with the existing molecular toolkit, but optogenetics is opening up the field of molecular biology with a new set of tools that better reflect the dynamic nature of cell biology.

Bibliography of References

- Abraham, W C, M Dragunow, and W P Tate. 1991. "The Role of Immediate Early Genes in the Stabilization of Long-Term Potentiation." *Molecular Neurobiology* 5 (2–4): 297–314. <http://www.ncbi.nlm.nih.gov/pubmed/1688055>.
- Aguado, E., Sylvie Richelme, Selene Nuñez-Cruz, Arkadiusz Miazek, Anne-Marie Mura, Mireille Richelme, Xiao-Jun Guo, et al. 2002. "Induction of T Helper Type 2 Immunity by a Point Mutation in the LAT Adaptor." *Science* 296 (5575): 2036–40. doi:10.1126/science.1069057.
- Akira, Shizuo, and Kiyoshi Takeda. 2004. "Toll-like Receptor Signalling." *Nature Reviews Immunology* 4 (7): 499–511. doi:10.1038/nri1391.
- Altan-Bonnet, G, and R N Germain. 2005. "Modeling T Cell Antigen Discrimination Based on Feedback Control of Digital ERK Responses." *PLoS.Biol.*
- Altman, Amnon, and Martin Villalba. 2002. "Protein Kinase C-Theta (PKC Theta): A Key Enzyme in T Cell Life and Death." *Journal of Biochemistry* 132 (6): 841–46. <http://www.ncbi.nlm.nih.gov/pubmed/12473184>.
- Anderson, M. S. 2002. "Projection of an Immunological Self Shadow Within the Thymus by the Aire Protein." *Science* 298 (5597): 1395–1401. doi:10.1126/science.1075958.
- Anthony, Robert M., Laura I. Rutitzky, Joseph F. Urban, Miguel J. Stadecker, and William C. Gause. 2007. "Protective Immune Mechanisms in Helminth Infection." *Nature Reviews. Immunology* 7 (12). Nature Publishing Group: 975–87. doi:10.1038/nri2199.
- Astoul, E, C Edmunds, D A Cantrell, and S G Ward. 2001. "PI 3-K and T-Cell Activation: Limitations of T-Leukemic Cell Lines as Signaling Models." *Trends in Immunology* 22 (9). Elsevier: 490–96. doi:10.1016/S1471-4906(01)01973-1.
- Au-Yeung BB, Zikherman J, Mueller JL, Ashouri JF, Matloubian M, Cheng DA, Chen Y, et al. 2014. "A Sharp T-Cell Antigen Receptor Signaling Threshold for T-Cell Proliferation." *Proceedings of the National Academy of Sciences* 111 (25): E3679-88. doi:10.1073/pnas.1413726111.
- Baarlink, C., H. Wang, and R. Grosse. 2013. "Nuclear Actin Network Assembly by Formins Regulates the SRF Coactivator MAL." *Science* 340 (6134): 864–67. doi:10.1126/science.1235038.
- Bacchelli, Chiara, Federico A Moretti, Marlene Carmo, Stuart Adams, Horia C Stanescu, Kerra Pearce, Manisha Madkaikar, et al. 2017. "Mutations in Linker for Activation of T Cells (LAT) Lead to a Novel Form of Severe Combined Immunodeficiency." *The Journal of Allergy and Clinical Immunology* 139 (2): 634–642.e5. doi:10.1016/j.jaci.2016.05.036.
- Badovinac, Vladimir P., Brandon B. Porter, and John T. Harty. 2002. "Programmed Contraction of CD8+ T Cells after Infection." *Nature Immunology* 3 (7): 619–26. doi:10.1038/ni804.
- Bahrami, Shahram, and Finn Drabløs. 2016. "Gene Regulation in the Immediate-Early Response Process." *Advances in Biological Regulation* 62 (7491). Elsevier Ltd: 37–49. doi:10.1016/j.jbior.2016.05.001.
- Balogopalan, Lakshmi, Benjamin A Ashwell, Kelsie M Bernot, Ito O Akpan, Naeha Quasba, Valarie A Barr, and Lawrence E Samelson. 2011. "Enhanced T-Cell Signaling in Cells Bearing Linker for Activation of T-Cell (LAT) Molecules Resistant to Ubiquitylation." *Proceedings of the National Academy of Sciences of the United States of America* 108 (7). National Academy of Sciences: 2885–90. doi:10.1073/pnas.1007098108.
- Balogopalan, Lakshmi, Valarie a Barr, Robert L Kortum, Anna K Park, and Lawrence E Samelson. 2013. "Cutting Edge: Cell Surface Linker for Activation of T Cells Is Recruited to Microclusters and Is Active in Signaling." *Journal of Immunology (Baltimore, Md. : 1950)* 190 (8): 3849–53. doi:10.4049/jimmunol.1202760.
- Balogopalan, Lakshmi, Valarie A Barr, Connie L Sommers, Mira Barda-Saad, Amrita Goyal, Matthew S Isakowitz, and Lawrence E Samelson. 2007. "C-Cbl-Mediated Regulation of LAT-Nucleated Signaling Complexes." *Molecular and Cellular Biology* 27 (24). American Society for Microbiology: 8622–36. doi:10.1128/MCB.00467-07.
- Balogopalan, Lakshmi, Nathan P. Coussens, Eilon Sherman, Lawrence E. Samelson, and Connie L. Sommers. 2010. "The LAT Story: A Tale of Cooperativity, Coordination, and Choreography." *Cold Spring Harbor Perspectives in Biology* 2 (8). doi:10.1101/cshperspect.a005512.
- Banaszynski, Laura a., Corey W. Liu, and Thomas J. Wandless. 2005. "Characterization of the FKBP-Rapamycin-FRB Ternary Complex." *Journal of the American Chemical Society* 127 (13): 4715–21. doi:10.1021/ja043277y.
- Barda-Saad, Mira, Alex Braiman, Rachel Titerence, Stephen C Bunnell, Valarie a Barr, and Lawrence E Samelson. 2005. "Dynamic Molecular Interactions Linking the T Cell Antigen Receptor to the Actin Cytoskeleton." *Nature Immunology* 6 (1): 80–89. doi:10.1038/ni1143.
- Bargou, Ralf, Eugen Leo, Gerhard Zugmaier, Matthias Klinger, Mariele Goebeler, Stefan Knop, Richard Noppeney,

- et al. 2008. "Tumor Regression in Cancer Patients by Very Low Doses of a T Cell-Engaging Antibody." *Science (New York, N.Y.)* 321 (5891). American Association for the Advancement of Science: 974–77. doi:10.1126/science.1158545.
- Barral, Duarte C., and Michael B. Brenner. 2007. "CD1 Antigen Presentation: How It Works." *Nature Reviews Immunology* 7 (12). Nature Publishing Group: 929–41. doi:10.1038/nri2191.
- Barrat-Boyes, Simon, Michael I Zimmer, Larry Harshyne, Michael Meyer, Simon C Watkins, Saverio Capuano III, Michael Murphey-Corn, Louis Falo, and Albert Donnenberg. 2000. "Maturation and Trafficking of Monocyte-Derived Dendritic Cells in Monkeys: Implications for Dendritic Cell-Based Vaccines." *J Immunol The Journal of Immunology by Guest on* 164: 2487–95. doi:10.4049/jimmunol.164.5.2487.
- Bartelt, Rebekah R., Noemi Cruz-Orcutt, Michaela Collins, and Jon C D Houtman. 2009. "Comparison of T Cell Receptor-Induced Proximal Signaling and Downstream Functions in Immortalized and Primary T Cells." *PLoS ONE* 4 (5). doi:10.1371/journal.pone.0005430.
- Bayle, J. Henri, Joshua S. Grimley, Kryn Stankunas, Jason E. Gestwicki, Thomas J. Wandless, and Gerald R. Crabtree. 2006. "Rapamycin Analogs with Differential Binding Specificity Permit Orthogonal Control of Protein Activity." *Chemistry and Biology* 13 (1): 99–107. doi:10.1016/j.chembiol.2005.10.017.
- Beemiller, Peter, Jordan Jacobelli, and Matthew F Krummel. 2012. "Integration of the Movement of Signaling Microclusters with Cellular Motility in Immunological Synapses." *Nature Immunology* 13 (8): 787–95. doi:10.1038/ni.2364.
- Beemiller, Peter, and Matthew F Krummel. 2010. "Mediation of T-Cell Activation by Actin Meshworks." *Cold Spring Harbor Perspectives in Biology* 2 (9): a002444. doi:10.1101/cshperspect.a002444.
- Belshaw, P J, S N Ho, G R Crabtree, and S L Schreiber. 1996. "Controlling Protein Association and Subcellular Localization with a Synthetic Ligand That Induces Heterodimerization of Proteins." *Proceedings of the National Academy of Sciences of the United States of America* 93 (10): 4604–7. doi:10.1073/pnas.93.10.4604.
- Billadeau, Daniel D., Jeffrey C. Nolz, and Timothy S. Gomez. 2007. "Regulation of T-Cell Activation by the Cytoskeleton." *Nature Reviews Immunology* 7 (2): 131–43. doi:10.1038/nri2021.
- Blander, J. Magarian, and Leif E. Sander. 2012. "Beyond Pattern Recognition: Five Immune Checkpoints for Scaling the Microbial Threat." *Nature Reviews Immunology* 12 (3). Nature Publishing Group: 215–25. doi:10.1038/nri3167.
- Borrego, Francisco. 2006. "The First Molecular Basis of the Missing Self Hypothesis." *The Journal of Immunology* 177: 5759–60. doi:10.4049/jimmunol.177.9.5759.
- Bounab, Yacine, Anne-Marie Hesse, Bruno Iannascoli, Luca Grieco, Yohann Couté, Anna Niarakis, Romain Roncagalli, et al. 2013. "Proteomic Analysis of the SH2 Domain-Containing Leukocyte Protein of 76 kDa (SLP76) Interactome in Resting and Activated Primary Mast Cells [Corrected]." *Molecular & Cellular Proteomics : MCP* 12 (10): 2874–89. doi:10.1074/mcp.M112.025908.
- Bouneaud, Cécile, Zacarias Garcia, Philippe Kourilsky, and Christophe Pannetier. 2005. "Lineage Relationships, Homeostasis, and Recall Capacities of Central- and Effector-Memory CD8 T Cells in Vivo." *The Journal of Experimental Medicine* 201 (4). The Rockefeller University Press: 579–90. doi:10.1084/jem.20040876.
- Boussso, Philippe, and Ellen Robey. 2003. "Dynamics of CD8+ T Cell Priming by Dendritic Cells in Intact Lymph Nodes." *Nature Immunology* 4 (6): 579–85. doi:10.1038/ni928.
- Boyden, Edward S, Feng Zhang, Ernst Bamberg, Georg Nagel, and Karl Deisseroth. 2005. "Millisecond-Timescale, Genetically Targeted Optical Control of Neural Activity." *Nature Neuroscience* 8 (9): 1263–68. doi:10.1038/nn1525.
- Boyer, Claude, Nathalie Auphan, Frédéric Luton, Jean-Marc Malburet, Marc Barad, Jean-Pierre Bizozzero, Hubert Reggio, and Anne-Marie Schmitt-Verhulst. 1991. "T Cell receptor/CD3 Complex Internalization Following Activation of a Cytolytic T Cell Clone: Evidence for a Protein Kinase C-Independent Staurosporine-Sensitive Step." *European Journal of Immunology* 21 (7): 1623–34. doi:10.1002/eji.1830210707.
- Boyman, Onur, Sven Létourneau, Carsten Krieg, and Jonathan Sprent. 2009. "Homeostatic Proliferation and Survival of Naïve and Memory T Cells." *European Journal of Immunology* 39 (8): 2088–94. doi:10.1002/eji.200939444.
- Breuning, Johannes, and Marion H Brown. 2017. "T Cell Costimulation by CD6 Is Dependent on Bivalent Binding of a GADS/SLP-76 Complex." *Molecular and Cellular Biology* 37 (11). American Society for Microbiology: e00071-17. doi:10.1128/MCB.00071-17.
- Briggs, Winslow R, and John M Christie. 2002. "Phototropins 1 and 2: Versatile Plant Blue-Light Receptors." *Trends in Plant Science* 7 (5): 204–10. <http://www.ncbi.nlm.nih.gov/pubmed/11992825>.
- Brignatz, C., a. Restouin, G. Bonello, D. Olive, and Y. Collette. 2005. "Evidences for Ubiquitination and Intracellular Trafficking of LAT, the Linker of Activated T Cells." *Biochimica et Biophysica Acta - Molecular*

- Cell Research* 1746 (2): 108–15. doi:10.1016/j.bbamcr.2005.08.009.
- Brossard, Cédric, Vincent Feuillet, Alain Schmitt, Clotilde Randriamampita, Maryse Romao, Graça Raposo, and Alain Trautmann. 2005. "Multifocal Structure of the T Cell - Dendritic Cell Synapse." *European Journal of Immunology* 35 (6): 1741–53. doi:10.1002/eji.200425857.
- Bubeník, Jan. 2004. "MHC Class I down-Regulations: Tumour Escape from Immune Surveillance?" *International Journal of Oncology* 25 (2). University of Crete, Faculty of Medicine, Laboratory of Clinical Virology: 487–91. <https://www.spandidos-publications.com/ijo/25/2/487>.
- Buchholz, Veit R., Ton N.M. Schumacher, and Dirk H. Busch. 2016. "T Cell Fate at the Single-Cell Level." *Annual Review of Immunology* 34 (1): 65–92. doi:10.1146/annurev-immunol-032414-112014.
- Buday, L, S E Egan, P Rodriguez Vician, D A Cantrell, and J Downward. 1994. "A Complex of Grb2 Adaptor Protein, Sos Exchange Factor, and a 36-kDa Membrane-Bound Tyrosine Phosphoprotein Is Implicated in Ras Activation in T Cells." *The Journal of Biological Chemistry* 269 (12): 9019–23. <http://www.ncbi.nlm.nih.gov/pubmed/7510700>.
- Bujdoso, R, J Hopkins, B M Dutia, P Young, and I McConnell. 1989. "Characterization of Sheep Afferent Lymph Dendritic Cells and Their Role in Antigen Carriage." *The Journal of Experimental Medicine* 170 (4). Rockefeller University Press: 1285–1301. doi:10.1084/JEM.170.4.1285.
- Bunnell, Stephen C., David I. Hong, Julia R. Kardon, Tetsuo Yamazaki, C. Jane McGlade, Valerie A. Barr, and Lawrence E. Samelson. 2002. "T Cell Receptor Ligation Induces the Formation of Dynamically Regulated Signaling Assemblies." *Journal of Cell Biology* 158 (7): 1263–75. doi:10.1083/jcb.200203043.
- Bunnell, Stephen C, Veena Kapoor, Ronald P Tribble, Weiguo Zhang, Lawrence E Samelson, North Carolina, J Pik, and Ras-gef Sos. 2001. "T Cell Receptor – Induced Spreading : A Role for the Signal Transduction Adaptor LAT" 14: 315–29.
- Cahalan, Michael D., and Ian Parker. 2008. "Choreography of Cell Motility and Interaction Dynamics Imaged by Two-Photon Microscopy in Lymphoid Organs." *Annual Review of Immunology* 26 (1): 585–626. doi:10.1146/annurev.immunol.24.021605.090620.
- Callahan, Margaret K., Michael A. Postow, and Jedd D. Wolchok. 2015. "CTLA-4 and PD-1 Pathway Blockade: Combinations in the Clinic." *Frontiers in Oncology* 4 (January): 385. doi:10.3389/fonc.2014.00385.
- Campbell, Daniel J., and Eugene C. Butcher. 2002. "Rapid Acquisition of Tissue-Specific Homing Phenotypes by CD4⁺ T Cells Activated in Cutaneous or Mucosal Lymphoid Tissues." *The Journal of Experimental Medicine* 195 (1): 135–41. doi:10.1084/jem.20011502.
- Castro, Mario, Hisse M van Santen, María Férez, Balbino Alarcón, Grant Lythe, and Carmen Molina-París. 2014. "Receptor Pre-Clustering and T Cell Responses: Insights into Molecular Mechanisms." *Frontiers in Immunology* 5. Frontiers Media SA: 132. doi:10.3389/fimmu.2014.00132.
- Čemerski, Sašo, Jayajit Das, Emanuele Giurisato, Mary A. Markiewicz, Paul M. Allen, Arup K. Chakraborty, and Andrey S. Shaw. 2008. "The Balance between T Cell Receptor Signaling and Degradation at the Center of the Immunological Synapse Is Determined by Antigen Quality." *Immunity* 29 (3): 414–22. doi:10.1016/j.immuni.2008.06.014.
- Chang, Veronica T, Ricardo A Fernandes, Kristina A Ganzinger, Steven F Lee, Christian Siebold, James McColl, Peter Jönsson, et al. 2016. "Initiation of T Cell Signaling by CD45 Segregation at 'Close Contacts.'" *Nature Immunology* 17 (5). Nature Research: 574–82. doi:10.1038/ni.3392.
- Chaplin, David D. 2010. "Overview of the Immune Response." *The Journal of Allergy and Clinical Immunology* 125 (2 Suppl 2). Elsevier Ltd: S3-23. doi:10.1016/j.jaci.2009.12.980.
- Che, Daphne L., Liting Duan, Kai Zhang, and Bianxiao Cui. 2015. "The Dual Characteristics of Light-Induced Cryptochrome 2, Homo-Oligomerization and Heterodimerization, for Optogenetic Manipulation in Mammalian Cells." *ACS Synthetic Biology* 4 (10): 1124–35. doi:10.1021/acssynbio.5b00048.
- Chen, Lieping, and Dallas B. Flies. 2013. "Molecular Mechanisms of T Cell Co-Stimulation and Co-Inhibition." *Nature Reviews Immunology* 13 (4): 227–42. doi:10.1038/nri3405.
- Chesi, Marta, and Rafael Fonseca. 2017. "Antibodies Create Killer Bonds in Myeloma." *Cancer Cell* 31 (3). Elsevier Inc.: 305–7. doi:10.1016/j.ccell.2017.02.011.
- Cho, Yi Li, Michael Flossdorf, Lorenz Kretschmer, Thomas Höfer, Dirk H. Busch, and Veit R. Buchholz. 2017. "TCR Signal Quality Modulates Fate Decisions of Single CD4⁺ T Cells in a Probabilistic Manner." *Cell Reports* 20 (4): 806–18. doi:10.1016/j.celrep.2017.07.005.
- Chow, C W, M Rincón, J Cavanagh, M Dickens, and R J Davis. 1997. "Nuclear Accumulation of NFAT4 Opposed by the JNK Signal Transduction Pathway." *Science* 278 (5343). American Association for the Advancement of Science: 1638–41. doi:10.1126/SCIENCE.278.5343.1638.
- Christie, J M, M Salomon, K Nozue, M Wada, and W R Briggs. 1999. "LOV (Light, Oxygen, or Voltage) Domains of the Blue-Light Photoreceptor Phototropin (nph1): Binding Sites for the Chromophore Flavin

- Mononucleotide." *Proceedings of the National Academy of Sciences of the United States of America* 96 (15): 8779–83. <http://www.pubmedcentral.nih.gov/articlerender.fcgi?artid=17593&tool=pmcentrez&rendertype=abstract>.
- Chu, P G, and D A Arber. 2001. "CD79: A Review." *Applied Immunohistochemistry & Molecular Morphology : A IMM* 9 (2): 97–106. <http://www.ncbi.nlm.nih.gov/pubmed/11396639>.
- Clackson, T., W. Yang, L. W. Rozamus, M. Hatada, J. F. Amara, C. T. Rollins, L. F. Stevenson, et al. 1998. "Redesigning an FKBP-Ligand Interface to Generate Chemical Dimerizers with Novel Specificity." *Proceedings of the National Academy of Sciences* 95 (18): 10437–42. doi:10.1073/pnas.95.18.10437.
- Clistone, N A, and G R Crabtree. 1992. "Identification of Calcineurin as a Key Signalling Enzyme in T-Lymphocyte Activation." *Nature* 357 (6380): 695–97. doi:10.1038/357695a0.
- Coloma, M. Josefina, and Sherie L. Morrison. 1997. "Design and Production of Novel Tetravalent Bispecific Antibodies." *Nature Biotechnology* 15 (2): 159–63. doi:10.1038/nbt0297-159.
- Comrie, W. a., a. Babich, and J. K. Burkhardt. 2015. "F-Actin Flow Drives Affinity Maturation and Spatial Organization of LFA-1 at the Immunological Synapse." *The Journal of Cell Biology*, February. doi:10.1083/jcb.201406121.
- Comrie, W. a., S. Li, S. Boyle, and J. K. Burkhardt. 2015. "The Dendritic Cell Cytoskeleton Promotes T Cell Adhesion and Activation by Constraining ICAM-1 Mobility." *The Journal of Cell Biology*, February. doi:10.1083/jcb.201406120.
- Cong, L., F. A. Ran, D. Cox, S. Lin, R. Barretto, N. Habib, P. D. Hsu, et al. 2013. "Multiplex Genome Engineering Using CRISPR/Cas Systems." *Science* 339 (6121): 819–23. doi:10.1126/science.1231143.
- Conrad, Daniel H, Jaime R Carlos, and Shaun Ruddy. 1978. "Interaction of [beta]31H Globulin with Cell-Bound C3b: Quantitative Analysis of Binding and Influence of Alternative Pathway Components on Binding*." *Journal of Experimental Medicine* 147: 1792–1805. <http://europemc.org/backend/ptpmcrender.fcgi?accid=PMC2184316&blobtype=pdf>.
- Corbin, Gail A, and John T Harty. 2004. "Duration of Infection and Antigen Display Have Minimal Influence on the Kinetics of the CD4+ T Cell Response to Listeria Monocytogenes Infection." *Journal of Immunology* 173 (9). American Association of Immunologists: 5679–87. doi:10.4049/JIMMUNOL.173.9.5679.
- Cordoba, Shaun-Paul, Kaushik Choudhuri, Hao Zhang, Marcus Bridge, Alp Bugra Basat, Michael L Dustin, and P Anton van der Merwe. 2013. "The Large Ectodomains of CD45 and CD148 Regulate Their Segregation from and Inhibition of Ligated T-Cell Receptor." *Blood* 121 (21). American Society of Hematology: 4295–4302. doi:10.1182/blood-2012-07-442251.
- Corish, P, and C Tyler-Smith. 1999. "Attenuation of Green Fluorescent Protein Half-Life in Mammalian Cells." *Protein Engineering* 12 (12): 1035–40. <http://www.ncbi.nlm.nih.gov/pubmed/10611396>.
- Cornall, R J, A M Cheng, T Pawson, and C C Goodnow. 2000. "Role of Syk in B-Cell Development and Antigen-Receptor Signaling." *Proceedings of the National Academy of Sciences of the United States of America* 97 (4). National Academy of Sciences: 1713–18. doi:10.1073/PNAS.97.4.1713.
- Cotta-de-Almeida, V., L. Westerberg, M. H. Maillard, D. Onaldi, H. Wachtel, P. Meelu, U.-i. Chung, R. Xavier, F. W. Alt, and S. B. Snapper. 2007. "Wiskott Aldrich Syndrome Protein (WASP) and N-WASP Are Critical for T Cell Development." *Proceedings of the National Academy of Sciences* 104 (39): 15424–29. doi:10.1073/pnas.0706881104.
- Crites, Travis J, Kartika Padhan, James Muller, Michelle Krogsgaard, Prabhakar R Gudla, Stephen J Lockett, and Rajat Varma. 2014. "TCR Microclusters Pre-Exist and Contain Molecules Necessary for TCR Signal Transduction." *Journal of Immunology (Baltimore, Md. : 1950)* 193 (1): 56–67. doi:10.4049/jimmunol.1400315.
- Crosson, Sean, and K. Moffat. 2001. "Structure of a Flavin-Binding Plant Photoreceptor Domain: Insights into Light-Mediated Signal Transduction." *Proceedings of the National Academy of Sciences* 98 (6): 2995–3000. doi:10.1073/pnas.051520298.
- Crosson, Sean, Sudarshan Rajagopal, and Keith Moffat. 2003. "The LOV Domain Family: Photoresponsive Signaling Modules Coupled to Diverse Output Domains." *Biochemistry* 42 (1): 2–10. doi:10.1021/bi026978l.
- Dagliyan, Onur, Mirosław Tarnawski, Pei-Hsuan Chu, David Shirvanyants, Ilme Schlichting, Nikolay V. Dokholyan, and Klaus M. Hahn. 2016. "Engineering Extrinsic Disorder to Control Protein Activity in Living Cells." *Science* 354 (6318). <http://science.sciencemag.org/content/354/6318/1441.full>.
- Dang, Chi V. 2013. "MYC, Metabolism, Cell Growth, and Tumorigenesis." *Cold Spring Harbor Perspectives in Medicine* 3 (8). Cold Spring Harbor Laboratory Press. doi:10.1101/cshperspect.a014217.
- Das, Jayajit, Mary Ho, Julie Zikherman, Christopher Govern, Ming Yang, Arthur Weiss, Arup K. Chakraborty, and

- Jeroen P. Roose. 2009. "Digital Signaling and Hysteresis Characterize Ras Activation in Lymphoid Cells." *Cell* 136 (2). Elsevier Inc.: 337–51. doi:10.1016/j.cell.2008.11.051.
- Davis, R S, Y H Wang, H Kubagawa, and M D Cooper. 2001. "Identification of a Family of Fc Receptor Homologs with Preferential B Cell Expression." *Proceedings of the National Academy of Sciences of the United States of America* 98 (17): 9772–77. doi:10.1073/pnas.171308498.
- Davis, Simon J, and P Anton van der Merwe. 2006. "The Kinetic-Segregation Model: TCR Triggering and beyond." *Nature Immunology* 7 (8): 803–9. doi:10.1038/ni1369.
- De Silva, Nilushi S., and Ulf Klein. 2015. "Dynamics of B Cells in Germinal Centres." *Nature Reviews Immunology* 15 (3). Nature Publishing Group: 137–48. doi:10.1038/nri3804.
- DeMond, Andrew L, Kaspar D Mossman, Toby Starr, Michael L Dustin, and Jay T Groves. 2008. "T Cell Receptor Microcluster Transport through Molecular Mazes Reveals Mechanism of Translocation." *Biophysical Journal* 94 (8). Elsevier: 3286–92. doi:10.1529/biophysj.107.119099.
- DeRose, Robert, Takafumi Miyamoto, and Takanari Inoue. 2013. "Manipulating Signaling at Will: Chemically-Inducible Dimerization (CID) Techniques Resolve Problems in Cell Biology." *European Journal of Physiology* 465 (3): 409–17. doi:10.1007/s00424-012-1208-6.
- Devlin, P F, and S A Kay. 2000. "Cryptochromes Are Required for Phytochrome Signaling to the Circadian Clock but Not for Rhythmicity." *The Plant Cell* 12 (12). American Society of Plant Biologists: 2499–2510. <http://www.ncbi.nlm.nih.gov/pubmed/11148293>.
- Drayson, Mark, Lian X Tang, Roger Drew, Graham P Mead, Hugh Carr-Smith, and Arthur R Bradwell. 2001. "Serum Free Light-Chain Measurements for Identifying and Monitoring Patients with Nonsecretory Multiple Myeloma." *Blood* 97 (9): 2900–2902. <http://www.bloodjournal.org/content/bloodjournal/97/9/2900.full.pdf?sso-checked=true>.
- Duan, Liting, Daphne Che, Kai Zhang, Qunxiang Ong, Shunling Guo, and Bianxiao Cui. 2015. "Optogenetic Control of Molecular Motors and Organelle Distributions in Cells." *Chemistry and Biology* 22 (5). Elsevier Ltd: 671–82. doi:10.1016/j.chembiol.2015.04.014.
- DuBridge, R B, P Tang, H C Hsia, P M Leong, J H Miller, and M P Calos. 1987. "Analysis of Mutation in Human Cells by Using an Epstein-Barr Virus Shuttle System." *Molecular and Cellular Biology* 7 (1): 379–87. <http://www.ncbi.nlm.nih.gov/pubmed/3031469>.
- Dudley, M. E. 2002. "Cancer Regression and Autoimmunity in Patients After Clonal Repopulation with Antitumor Lymphocytes." *Science* 298 (5594): 850–54. doi:10.1126/science.1076514.
- Dushek, Omer, Milos Aleksic, Richard J Wheeler, Hao Zhang, Shaun-Paul Cordoba, Yan-Chun Peng, Ji-Li Chen, et al. 2011. "Antigen Potency and Maximal Efficacy Reveal a Mechanism of Efficient T Cell Activation." *Science Signaling* 4 (176). American Association for the Advancement of Science: ra39. doi:10.1126/scisignal.2001430.
- Dustin, M L, J M Miller, S Ranganath, D A Vignali, N J Viner, C A Nelson, and E R Unanue. 1996. "TCR-Mediated Adhesion of T Cell Hybridomas to Planar Bilayers Containing Purified MHC Class II/peptide Complexes and Receptor Shedding during Detachment." *Journal of Immunology (Baltimore, Md. : 1950)* 157 (5): 2014–21. <http://www.ncbi.nlm.nih.gov/pubmed/8757322>.
- Dustin, Michael L. 2004. "Stop and Go Traffic to Tune T Cell Responses." *Immunity* 21 (3): 305–14. doi:10.1016/j.immuni.2004.08.016.
- Elhanati, Yuval, Anand Murugan, Curtis G Callan, Thierry Mora, and Aleksandra M Walczak. 2014. "Quantifying Selection in Immune Receptor Repertoires." *Proceedings of the National Academy of Sciences of the United States of America* 111 (27). National Academy of Sciences: 9875–80. doi:10.1073/pnas.1409572111.
- Epstein, M A, G Henle, B G Achong, and Y M Barr. 1965. "Morphology and Biological Studies on a Virus in Cultured Lymphoblasts from Burkitt's Lymphoma." *The Journal of Experimental Medicine* 121 (5). The Rockefeller University Press: 761–70. doi:10.1084/jem.121.5.761.
- Erhart, Dominik, Mirjam Zimmermann, Olivier Jacques, Matthias B. Wittwer, Beat Ernst, Edwin Constable, Marketa Zvelebil, Florent Beauflis, and Matthias P. Wymann. 2013. "Chemical Development of Intracellular Protein Heterodimerizers." *Chemistry and Biology* 20 (4). Elsevier Ltd: 549–57. doi:10.1016/j.chembiol.2013.03.010.
- Eyerich, Stefanie, Kilian Eyerich, Davide Pennino, Teresa Carbone, Francesca Nasorri, Sabatino Pallotta, Francesca Cianfarani, et al. 2009. "Th22 Cells Represent a Distinct Human T Cell Subset Involved in Epidermal Immunity and Remodeling." *Journal of Clinical Investigation* 119 (12): 3573–85. doi:10.1172/JCI40202.
- Faroudi, Mustapha, Rossana Zaru, Pierre Paulet, Sabina Müller, and Salvatore Valitutti. 2003. "Cutting Edge: T Lymphocyte Activation by Repeated Immunological Synapse Formation and Intermittent Signaling." *Journal of Immunology* 171 (3): 1128–32. <http://www.ncbi.nlm.nih.gov/pubmed/12874197>.

- Favory, Jean-Jacques, Agnieszka Stec, Henriette Gruber, Luca Rizzini, Attila Oravecz, Markus Funk, Andreas Albert, et al. 2009. "Interaction of COP1 and UVR8 Regulates UV-B-Induced Photomorphogenesis and Stress Acclimation in Arabidopsis." *The EMBO Journal* 28 (5): 591–601. doi:10.1038/emboj.2009.4.
- Fazilleau, Nicolas, Linda Mark, Louise J. McHeyzer-Williams, and Michael G. McHeyzer-Williams. 2009. "Follicular Helper T Cells: Lineage and Location." *Immunity* 30 (3). Elsevier Inc.: 324–35. doi:10.1016/j.immuni.2009.03.003.
- Feinerman, O., J. Veiga, J. R. Dorfman, R. N. Germain, and G. Altan-Bonnet. 2008. "Variability and Robustness in T Cell Activation from Regulated Heterogeneity in Protein Levels." *Science* 321 (5892): 1081–84. doi:10.1126/science.1158013.
- Fenno, Lief, Ofer Yizhar, and Karl Deisseroth. 2011. "The Development and Application of Optogenetics." *Annual Review of Neuroscience* 34 (January): 389–412. doi:10.1146/annurev-neuro-061010-113817.
- Ferrer, Marc, Jim Maiolo, Patricia Kratz, Jessica L. Jackowski, Dennis J. Murphy, Simon Delagrave, and James Inglese. 2005. "Directed Evolution of PDZ Variants to Generate High-Affinity Detection Reagents." *Protein Engineering, Design and Selection* 18 (4): 165–73. doi:10.1093/protein/gzi018.
- Finco, Timothy S, Theresa Kadlecik, Weiguo Zhang, Lawrence E Samelson, and Arthur Weiss. 1998. "LAT Is Required for TCR-Mediated Activation of PLCgamma1 and the Ras Pathway." *Immunity* 9 (5): 617–26. <http://www.ncbi.nlm.nih.gov/pubmed/9846483>.
- Flock, Tilman, Robert Weatheritt, Natasha Latysheva, and M Madan Babu. 2014. "Controlling Entropy to Tune the Functions of Intrinsically Disordered Regions." *Current Opinion in Structural Biology* 26 (June). Elsevier Current Trends: 62–72. doi:10.1016/J.SBI.2014.05.007.
- François, Paul, Guillaume Voisinne, Eric D Siggia, Grégoire Altan-bonnet, and Massimo Vergassola. 2013. "Phenotypic Model for Early T-Cell Activation Displaying Sensitivity , Speci Fi City , and Antagonism." *Proceedings of the National Academy of Sciences of the United States of America* 110 (10): E888–97. doi:10.1073/pnas.1300752110/-/DCSupplemental.www.pnas.org/cgi/doi/10.1073/pnas.1300752110.
- Fu, Guoping, Yuhong Chen, Mei Yu, Andy Podd, James Schuman, Yinghong He, Lie Di, et al. 2010. "Phospholipase Cγ1 Is Essential for T Cell Development, Activation, and Tolerance." *The Journal of Experimental Medicine* 207 (2): 309–18. doi:10.1084/jem.20090880.
- Fujioka, Aki, Kenta Terai, Reina E. Itoh, Kazuhiro Aoki, Takeshi Nakamura, Shinya Kuroda, Eisuke Nishida, and Michiyuki Matsuda. 2006. "Dynamics of the Ras/ERK MAPK Cascade as Monitored by Fluorescent Probes." *Journal of Biological Chemistry* 281 (13): 8917–26. doi:10.1074/jbc.M509344200.
- Ganz, Tomas. 2003. "Defensins: Antimicrobial Peptides of Innate Immunity." *Nature Reviews Immunology* 3 (9): 710–20. doi:10.1038/nri1180.
- Gao, Xiang, and Michael Wehr. 2015. "A Coding Transformation for Temporally Structured Sounds within Auditory Cortical Neurons." *Neuron* 86 (1). Cell Press: 292–303. doi:10.1016/J.NEURON.2015.03.004.
- Garcon, F., D. T. Patton, J. L. Emery, E. Hirsch, R. Rottapel, T. Sasaki, and K. Okkenhaug. 2007. "CD28 Provides T-Cell Costimulation and Enhances PI3K Activity at the Immune Synapse Independently of Its Capacity to Interact with the p85/p110 Heterodimer." *Blood* 111 (3): 1464–71. doi:10.1182/blood-2007-08-108050.
- Geisler, C, J Kuhlmann, and B Rubin. 1989. "Assembly, Intracellular Processing, and Expression at the Cell Surface of the Human Alpha Beta T Cell receptor/CD3 Complex. Function of the CD3-Zeta Chain." *Journal of Immunology (Baltimore, Md. : 1950)* 143 (12): 4069–77. <http://www.ncbi.nlm.nih.gov/pubmed/2531776>.
- Gerhardt, Karl P., Evan J. Olson, Sebastian M. Castillo-Hair, Lucas A. Hartsough, Brian P. Landry, Felix Ekness, Rayka Yokoo, et al. 2016. "An Open-Hardware Platform for Optogenetics and Photobiology." *Scientific Reports* 6 (November). Nature Publishing Group: 35363. doi:10.1038/srep35363.
- Germain, Ronald N. 2002. "T-Cell Development and the CD4–CD8 Lineage Decision." *Nature Reviews Immunology* 2 (5): 309–22. doi:10.1038/nri798.
- Gimmi, C D, G J Freeman, J G Gribben, G Gray, and L M Nadler. 1993. "Human T-Cell Clonal Anergy Is Induced by Antigen Presentation in the Absence of B7 Costimulation." *Proceedings of the National Academy of Sciences of the United States of America* 90 (14): 6586–90. <http://www.ncbi.nlm.nih.gov/pubmed/7688125>.
- Globerson-Levin, Anat, Tova Waks, and Zelig Eshhar. 2014. "Elimination of Progressive Mammary Cancer by Repeated Administrations of Chimeric Antigen Receptor-Modified T Cells." *Molecular Therapy* 22 (5). American Society of Gene & Cell Therapy: 1029–38. doi:10.1038/mt.2014.28.
- Gorgun, G., M. K. Samur, K. B. Cowens, S. Paula, G. Bianchi, J. E. Anderson, R. E. White, et al. 2015. "Lenalidomide Enhances Immune Checkpoint Blockade-Induced Immune Response in Multiple Myeloma." *Clinical Cancer Research* 21 (20): 4607–18. doi:10.1158/1078-0432.CCR-15-0200.
- Graef, Isabella a., Leslie J. Holsinger, Steve Diver, Stuart L. Schreiber, and Gerald R. Crabtree. 1997. "Proximity and Orientation Underlie Signaling by the Non-Receptor Tyrosine Kinase ZAP70." *EMBO Journal* 16 (18): 5451–61.

- 5618–28. doi:10.1093/emboj/16.18.5618.
- Graf, Beth, Timothy Bushnell, and J Miller. 2007. "LFA-1-Mediated T Cell Costimulation through Increased Localization of TCR/Class II Complexes to the Central Supramolecular Activation Cluster and Exclusion of CD45 from the Immunological Synapse." *Journal of Immunology* 179 (3). American Association of Immunologists: 1616–24. doi:10.4049/jimmunol.179.3.1616.
- Green, H, and M Meuth. 1974. "An Established Pre-Adipose Cell Line and Its Differentiation in Culture." *Cell* 3 (2): 127–33. <http://www.ncbi.nlm.nih.gov/pubmed/4426090>.
- Greene, JoAnne L., Gina M. Leytze, John Emswiler, Robert Peach, Jürgen Bajorath, Wesley Cosand, and Peter S. Linsley. 1996. "Covalent Dimerization of CD28/CTLA-4 and Oligomerization of CD80/CD86 Regulate T Cell Costimulatory Interactions." *Journal of Biological Chemistry* 271 (43): 26762–71. doi:10.1074/jbc.271.43.26762.
- Griffiths, Gillian M., Andy Tsun, and Jane C. Stinchcombe. 2010. "The Immunological Synapse: A Focal Point for Endocytosis and Exocytosis." *The Journal of Cell Biology* 189 (3): 399–406. doi:10.1083/jcb.201002027.
- Gringhuis, S I, A Leow, E A Papendrecht-Van Der Voort, P H Remans, F C Breedveld, and C L Verweij. 2000. "Displacement of Linker for Activation of T Cells from the Plasma Membrane due to Redox Balance Alterations Results in Hyporesponsiveness of Synovial Fluid T Lymphocytes in Rheumatoid Arthritis." *Journal of Immunology (Baltimore, Md. : 1950)* 164 (4): 2170–79. <http://www.ncbi.nlm.nih.gov/pubmed/10657671>.
- Gross, G, T Waks, and Z Eshhar. 1989. "Expression of Immunoglobulin-T-Cell Receptor Chimeric Molecules as Functional Receptors with Antibody-Type Specificity." *Proceedings of the National Academy of Sciences of the United States of America* 86 (24). National Academy of Sciences: 10024–28. <http://www.ncbi.nlm.nih.gov/pubmed/2513569>.
- Grynkiewicz, G, M Poenie, and R Y Tsien. 1985. "A New Generation of Ca²⁺ Indicators with Greatly Improved Fluorescence Properties." *The Journal of Biological Chemistry* 260 (6): 3440–50. <http://www.ncbi.nlm.nih.gov/pubmed/3838314>.
- Guy, Clifford S, Kate M Vignali, Jamshid Temirov, Matthew L Bettini, Abigail E Overacre, Matthew Smeltzer, Hui Zhang, et al. 2013. "Distinct TCR Signaling Pathways Drive Proliferation and Cytokine Production in T Cells." *Nature Immunology* 14 (3): 262–70. doi:10.1038/ni.2538.
- Hammarlund, Erika, Matthew W Lewis, Scott G Hansen, Lisa I Strelow, Jay A Nelson, Gary J Sexton, Jon M Hanifin, and Mark K Slifka. 2003. "Duration of Antiviral Immunity after Smallpox Vaccination." *Nature Medicine* 9 (9): 1131–37. doi:10.1038/nm917.
- Hamon, Mélanie, Hélène Bierne, and Pascale Cossart. 2006. "Listeria Monocytogenes: A Multifaceted Model." *Nature Reviews Microbiology* 4 (6): 423–34. doi:10.1038/nrmicro1413.
- Harkiolaki, Maria, Marc Lewitzky, Robert J C Gilbert, E Yvonne Jones, Roland P Bourette, Guy Mouchiroud, Holger Sondermann, Ismail Moarefi, and Stephan M Feller. 2003. "Structural Basis for SH3 Domain-Mediated High-Affinity Binding between Mona/Gads and SLP-76." *The EMBO Journal* 22 (11). European Molecular Biology Organization: 2571–82. doi:10.1093/emboj/cdg258.
- Harper, Shannon M., Lori C. Neil, and Kevin H. Gardner. 2003. "Structural Basis of a Phototropin Light Switch." *Science (New York, N.Y.)* 301 (5639): 1541–44. doi:10.1126/science.1086810.
- Haruki, Hirohito, Junichi Nishikawa, and Ulrich K Laemmli. 2008. "The Anchor-Away Technique: Rapid, Conditional Establishment of Yeast Mutant Phenotypes." *Molecular Cell* 31 (6): 925–32. doi:10.1016/j.molcel.2008.07.020.
- Hashimoto-Tane, Akiko, Tadashi Yokosuka, Chitose Ishihara, Machie Sakuma, Wakana Kobayashi, and Takashi Saito. 2010. "T-Cell Receptor Microclusters Critical for T-Cell Activation Are Formed Independently of Lipid Raft Clustering." *Molecular and Cellular Biology* 30 (14). American Society for Microbiology: 3421–29. doi:10.1128/MCB.00160-10.
- Hashimoto-Tane, Akiko, Tadashi Yokosuka, Kumiko Sakata-Sogawa, Machie Sakuma, Chitose Ishihara, Makio Tokunaga, and Takashi Saito. 2011. "Dynamin-Driven Transport of T Cell Receptor Microclusters Regulates Immune Synapse Formation and T Cell Activation." *Immunity* 34 (6). Elsevier Inc.: 919–31. doi:10.1016/j.immuni.2011.05.012.
- Hataye, Jason, James J Moon, Alexander Khoruts, Cavan Reilly, and Marc K Jenkins. 2006. "Naive and Memory CD4⁺ T Cell Survival Controlled by Clonal Abundance." *Science (New York, N.Y.)* 312 (5770). American Association for the Advancement of Science: 114–16. doi:10.1126/science.1124228.
- Hatzivassiliou, Georgia, Ira Miller, Jun Takizawa, Nallasivam Palanisamy, Pulivarthi H. Rao, Shinsuke Iida, Shinichi Tagawa, et al. 2001. "IRTA1 and IRTA2, Novel Immunoglobulin Superfamily Receptors Expressed in B Cells and Involved in Chromosome 1q21 Abnormalities in B Cell Malignancy." *Immunity* 14 (3): 277–89. doi:10.1016/S1074-7613(01)00109-1.

- Häusser, Michael. 2014. "Optogenetics: The Age of Light." *Nature Methods* 11 (10). Nature Publishing Group: 1012–14. doi:10.1038/nmeth.3111.
- Henrickson, Sarah E, Thorsten R Mempel, Irina B Mazo, Bai Liu, Maxim N Artyomov, Huan Zheng, Antonio Peixoto, et al. 2008. "T Cell Sensing of Antigen Dose Governs Interactive Behavior with Dendritic Cells and Sets a Threshold for T Cell Activation." *Nature Immunology* 9 (3): 282–91. doi:10.1038/ni1559.
- Holers, V. Michael. 2014. "Complement and Its Receptors: New Insights into Human Disease." *Annual Review of Immunology* 32 (1): 433–59. doi:10.1146/annurev-immunol-032713-120154.
- Holst, Jeff, Haopeng Wang, Kelly Durick Eder, Creg J Workman, Kelli L Boyd, Zachary Baquet, Harvir Singh, et al. 2008. "Scalable Signaling Mediated by T Cell Antigen receptor–CD3 ITAMs Ensures Effective Negative Selection and Prevents Autoimmunity." *Nature Immunology* 9 (6): 658–66. doi:10.1038/ni.1611.
- Honda, Tetsuya, Jackson G. G. Egen, Tim Lämmermann, Wolfgang Kastenmüller, Parizad Torabi-Parizi, and Ronald N. N. Germain. 2014. "Tuning of Antigen Sensitivity by T Cell Receptor-Dependent Negative Feedback Controls T Cell Effector Function in Inflamed Tissues." *Immunity* 40 (2): 235–47. doi:10.1016/j.immuni.2013.11.017.
- Hopfield, J J. 1974. "Kinetic Proofreading: A New Mechanism for Reducing Errors in Biosynthetic Processes Requiring High Specificity." *Proceedings of the National Academy of Sciences of The United States of America* 71 (10): 4135–39. <http://www.pnas.org/content/71/10/4135.full.pdf>.
- Horejsí, Václav, Weiguo Zhang, Burkhardt Schraven, Václav Hořejší, Weiguo Zhang, and Burkhardt Schraven. 2004. "Transmembrane Adaptor Proteins: Organizers of Immunoreceptor Signalling." *Nature Reviews. Immunology* 4 (8): 603–16. doi:10.1038/nri1455.
- Hori, Shohei, Shohei Hori, Takashi Nomura, Takashi Nomura, Shimon Sakaguchi, and Shimon Sakaguchi. 2009. "Control of Regulatory T Cell Development by the Transcription Factor Foxp3." *Science (New York, N.Y.)* 329 (5609): 1057–61. doi:10.1126/science.1079490.
- Houtman, Jon C D, Hiroshi Yamaguchi, Mira Barda-Saad, Alex Braiman, Brent Bowden, Ettore Appella, Peter Schuck, and Lawrence E Samelson. 2006. "Oligomerization of Signaling Complexes by the Multipoint Binding of GRB2 to Both LAT and SOS1." *Nature Structural & Molecular Biology* 13 (9): 798–805. doi:10.1038/nsmb1133.
- Huang, J., Akiko Koide, Koki Makabe, and Shohei Koide. 2008. "Design of Protein Function Leaps by Directed Domain Interface Evolution." *Proceedings of the National Academy of Sciences of the United States of America* 105 (18): 6578–83. doi:10.1073/pnas.0801097105.
- Huang, Jin, Koki Makabe, Matthew Biancalana, Akiko Koide, and Shohei Koide. 2009. "Structural Basis for Exquisite Specificity of Affinity Clamps, Synthetic Binding Proteins Generated through Directed Domain-Interface Evolution." *Journal of Molecular Biology* 392 (5): 1221–31. doi:10.1016/j.jmb.2009.07.067.
- Huang, Jin, Stanislav S. Nagy, Akiko Koide, Ronald S. Rock, and Shohei Koide. 2009. "A Peptide Tag System for Facile Purification and Single-Molecule Immobilization." *Biochemistry* 48 (50): 11834–36. doi:10.1021/bi901756n.
- Huang, Weishan, Sabrina Solouki, Nicholas Koylass, Song-Guo Zheng, and Avery August. 2017. "ITK Signalling via the Ras/IRF4 Pathway Regulates the Development and Function of Tr1 Cells." *Nature Communications* 8 (June): 15871. doi:10.1038/ncomms15871.
- Huber, Magdalena, and Michael Lohoff. 2014. "IRF4 at the Crossroads of Effector T-Cell Fate Decision." *European Journal of Immunology* 44 (7): 1886–95. doi:10.1002/eji.201344279.
- Hui, Enfu, Jeanne Cheung, Jing Zhu, Xiaolei Su, Marcus J. Taylor, Heidi A. Wallweber, Dibyendu K. Sasmal, et al. 2017. "T Cell Costimulatory Receptor CD28 Is a Primary Target for PD-1–mediated Inhibition." *Science* 355 (6332). <http://science.sciencemag.org/content/355/6332/1428.full>.
- Hundt, M., Y. Harada, L. De Giorgio, N. Tanimura, W. Zhang, and A. Altman. 2009. "Palmitoylation-Dependent Plasma Membrane Transport but Lipid Raft-Independent Signaling by Linker for Activation of T Cells." *The Journal of Immunology* 183 (3): 1685–94. doi:10.4049/jimmunol.0803921.
- Hundt, Matthias, Hiroki Tabata, Myung Shin Jeon, Keitaro Hayashi, Yoshihiko Tanaka, Roma Krishna, Lauren De Giorgio, Yun Cai Liu, Masaki Fukata, and Amnon Altman. 2006. "Impaired Activation and Localization of LAT in Anergic T Cells as a Consequence of a Selective Palmitoylation Defect." *Immunity* 24 (5): 513–22. doi:10.1016/j.immuni.2006.03.011.
- Huse, Morgan, Lawrence O Klein, Andrew T Girvin, Joycelyn M Faraj, Qi-Jing Li, Michael S Kuhns, and Mark M Davis. 2007. "Spatial and Temporal Dynamics of T Cell Receptor Signaling with a Photoactivatable Agonist." *Immunity* 27 (1): 76–88. doi:10.1016/j.immuni.2007.05.017.
- James, John R, and Ronald D Vale. 2012. "Biophysical Mechanism of T-Cell Receptor Triggering in a Reconstituted System." *Nature* 487 (7405): 64–69. doi:10.1038/nature11220.
- Jang, Mei-Shiang, Fan Pan, Laurie M. Erickson, Ogert Fisniku, Gladys Crews, Carmen Wynn, In Chul Hong, Kouichi

- Tamura, Masakazu Kobayashi, and Hongsi Jiang. 2008. "A Blocking Anti-CD28-Specific Antibody Induces Long-Term Heart Allograft Survival by Suppression of the PKC Theta-JNK Signal Pathway." *Transplantation* 85 (7): 1051–55. doi:10.1097/TP.0b013e31816846f6.
- Jenkins, M. K., and J. J. Moon. 2012. "The Role of Naive T Cell Precursor Frequency and Recruitment in Dictating Immune Response Magnitude." *The Journal of Immunology* 188 (9): 4135–40. doi:10.4049/jimmunol.1102661.
- Johnson, Heath E., Yogesh Goyal, Nicole L. Pannucci, Trudi Schüpbach, Stanislav Y. Shvartsman, and Jared E. Toettcher. 2017. "The Spatiotemporal Limits of Developmental Erk Signaling." *Developmental Cell* 40 (2). Elsevier: 185–92. doi:10.1016/j.devcel.2016.12.002.
- Joung, J. Keith, and Jeffry D. Sander. 2012. "TALENs: A Widely Applicable Technology for Targeted Genome Editing." *Nature Reviews Molecular Cell Biology* 14 (1). Nature Publishing Group: 49–55. doi:10.1038/nrm3486.
- Judd, Barbi A, Peggy S Myung, Achim Oberfell, Erin E Myers, Alec M Cheng, Stephen P Watson, Warren S Pear, David Allman, Sanford J Shattil, and Gary A Koretzky. 2002. "Differential Requirement for LAT and SLP-76 in GPVI versus T Cell Receptor Signaling." *The Journal of Experimental Medicine* 195 (6). The Rockefeller University Press: 705–17. doi:10.1084/JEM.20011583.
- Junttila, T. T., J. Li, J. Johnston, M. Hristopoulos, R. Clark, D. Ellerman, B.-E. Wang, et al. 2014. "Antitumor Efficacy of a Bispecific Antibody That Targets HER2 and Activates T Cells." *Cancer Research* 74 (19): 5561–71. doi:10.1158/0008-5472.CAN-13-3622-T.
- Kaberniuk, Andrii A, Anton A Shemetov, and Vladislav V Verkhusha. 2016. "A Bacterial Phytochrome-Based Optogenetic System Controllable with near-Infrared Light." *Nature Methods* 13 (7). doi:10.1038/nmeth.3864.
- Kanhere, Aditi, Arnulf Hertweck, Urvashi Bhatia, M. Refik Gökmen, Esperanza Perucha, Ian Jackson, Graham M. Lord, and Richard G. Jenner. 2012. "T-Bet and GATA3 Orchestrate Th1 and Th2 Differentiation through Lineage-Specific Targeting of Distal Regulatory Elements." *Nature Communications* 3. doi:10.1038/ncomms2260.
- Kaplan, Mark H. 2013. "Th9 Cells: Differentiation and Disease." *Immunological Reviews* 252 (1): 104–15. doi:10.1111/imr.12028.
- Karasuyama, H, T Nakamura, K Nagata, T Kuramochi, F Kitamura, and K Kuida. 1997. "The Roles of preB Cell Receptor in Early B Cell Development and Its Signal Transduction." *Immunology and Cell Biology* 75 (2): 209–16. doi:10.1038/icb.1997.32.
- Kato, Takuma, Katsuhisa Kawai, Youhei Egami, Yoshiyuki Kakehi, and Nobukazu Araki. 2014. "Rac1-Dependent Lamellipodial Motility in Prostate Cancer PC-3 Cells Revealed by Optogenetic Control of Rac1 Activity." Edited by Daotai Nie. *PLoS ONE* 9 (5). Public Library of Science: e97749. doi:10.1371/journal.pone.0097749.
- Kawano, Fuun, Yuki Aono, Hideyuki Suzuki, Moritoshi Sato, and KM Hahn. 2013. "Fluorescence Imaging-Based High-Throughput Screening of Fast- and Slow-Cycling LOV Proteins." Edited by Andrew J. Roe. *PLoS One* 8 (12). Public Library of Science: e82693. doi:10.1371/journal.pone.0082693.
- Kawano, Fuun, Hideyuki Suzuki, Akihiro Furuya, and Moritoshi Sato. 2015. "Engineered Pairs of Distinct Photoswitches for Optogenetic Control of Cellular Proteins." *Nature Communications* 6. Nature Publishing Group: 6256. doi:10.1038/ncomms7256.
- Keck, Simone, Mathias Schmalzer, Stefan Ganter, Lena Wyss, Susanne Oberle, Eric S. Huseby, Dietmar Zehn, et al. 2014. "Antigen Affinity and Antigen Dose Exert Distinct Influences on CD4 T-Cell Differentiation." *Proceedings of the National Academy of Sciences* 111 (41): 14852–57. doi:10.1073/pnas.1403271111.
- Keller, Baerbel, Irina Zaidman, O. Sascha Yousefi, Dov HersHKovitz, Jerry Stein, Susanne Unger, Kristina Schachtrup, et al. 2016. "Early Onset Combined Immunodeficiency and Autoimmunity in Patients with Loss-of-Function Mutation in LAT." *The Journal of Experimental Medicine* 213 (7): 1185–99. doi:10.1084/jem.20151110.
- Kennedy, Matthew J, Robert M Hughes, Leslie a Peteya, Joel W Schwartz, Michael D Ehlers, and Chandra L Tucker. 2010. "Rapid Blue-Light-Mediated Induction of Protein Interactions in Living Cells." *Nature Methods* 7 (12): 973–75. doi:10.1038/nmeth.1524.
- Kim, Chulwoo, Theodore Wilson, Kael F. Fischer, and Matthew A. Williams. 2013. "Sustained Interactions between T Cell Receptors and Antigens Promote the Differentiation of CD4+ Memory T Cells." *Immunity* 39 (3). Elsevier Inc.: 508–20. doi:10.1016/j.immuni.2013.08.033.
- Kim, Yeong Seok, Ga Bin Park, Hyun Keun Song, Indo Hur, Hyun-Kyung Lee, Jae Seung Kang, Eunsil Hahm, Wang Jae Lee, and Dae Young Hur. 2007. "Cross-Linking of CD54 on Burkitt Lymphoma Cell Line Raji and Ramos Induces FasL Expression by Reactive Oxygen Species and Apoptosis of Adjacent Cells in Fas/FasL

- Interaction." *Journal of Immunotherapy* (Hagerstown, Md.: 1997) 30 (7): 727–39. doi:10.1097/CJI.0b013e31814a69fa.
- King, Carolyn G., Sabrina Koehli, Barbara Hausmann, Mathias Schmalzer, Dietmar Zehn, and Ed Palmer. 2012. "T Cell Affinity Regulates Asymmetric Division, Effector Cell Differentiation, and Tissue Pathology." *Immunity* 37 (4): 709–20. doi:10.1016/j.immuni.2012.06.021.
- Kingeter, L. M., S. Paul, S. K. Maynard, N. G. Cartwright, and B. C. Schaefer. 2010. "Cutting Edge: TCR Ligation Triggers Digital Activation of NF- κ B." *The Journal of Immunology* 185 (8): 4520–24. doi:10.4049/jimmunol.1001051.
- Kinjo, Yuki, Douglass Wu, Gisen Kim, Guo-Wen Xing, Michael A. Poles, David D. Ho, Moriya Tsuji, Kazuyoshi Kawahara, Chi-Huey Wong, and Mitchell Kronenberg. 2005. "Recognition of Bacterial Glycosphingolipids by Natural Killer T Cells." *Nature* 434 (7032). Nature Publishing Group: 520–25. doi:10.1038/nature03407.
- Klein, Ludger, Bruno Kyewski, Paul M. Allen, and Kristin A. Hogquist. 2014. "Positive and Negative Selection of the T Cell Repertoire: What Thymocytes See (and Don't See)." *Nature Reviews Immunology* 14 (6). Nature Publishing Group: 377–91. doi:10.1038/nri3667.
- Kleinstiver, Benjamin P, Michelle S Prew, Shengdar Q Tsai, Nhu T Nguyen, Ved V Topkar, Zongli Zheng, and J Keith Joung. 2015. "Broadening the Targeting Range of Staphylococcus Aureus CRISPR-Cas9 by Modifying PAM Recognition." *Nature Biotechnology* 33 (12). Nature Publishing Group: 1293–98. doi:10.1038/nbt.3404.
- Knyazhitsky, M., E. Moas, E. Shaginov, A. Luria, and A. Braiman. 2012. "Vav1 Oncogenic Mutation Inhibits T Cell Receptor-Induced Calcium Mobilization through Inhibition of Phospholipase C 1 Activation." *Journal of Biological Chemistry*. doi:10.1074/jbc.M111.309799.
- Kollmann, Tobias R, Ofer Levy, Ruth R Montgomery, and Stanislas Goriely. 2012. "Innate Immune Function by Toll-like Receptors: Distinct Responses in Newborns and the Elderly." *Immunity* 37 (5). Elsevier Inc.: 771–83. doi:10.1016/j.immuni.2012.10.014.
- Kontermann, Roland E., and Ulrich Brinkmann. 2015. "Bispecific Antibodies." *Drug Discovery Today* 20 (7). Elsevier Ltd: 838–47. doi:10.1016/j.drudis.2015.02.008.
- Kredel, Simone, Franz Oswald, Karin Nienhaus, Karen Deuschle, Carlheinz Röcker, Michael Wolff, Ralf Heilker, G. Ulrich Nienhaus, and Jörg Wiedenmann. 2009. "mRuby, a Bright Monomeric Red Fluorescent Protein for Labeling of Subcellular Structures." Edited by Amy S. Gladfelter. *PLoS ONE* 4 (2). Public Library of Science: e4391. doi:10.1371/journal.pone.0004391.
- Krishnamoorthy, Veena, Sunil Kannanganat, Mark Maienschein-Cline, Sarah L Cook, Jianjun Chen, Neil Bahroos, Evelyn Sievert, Emily Corse, Anita Chong, and Roger Sciammas. 2017. "The IRF4 Gene Regulatory Module Functions as a Read-Write Integrator to Dynamically Coordinate T Helper Cell Fate." *Immunity* 47 (3). Elsevier Inc.: 481–497.e7. doi:10.1016/j.immuni.2017.09.001.
- Kumar, Shaji K., Vincent Rajkumar, Robert A. Kyle, Mark van Duin, Pieter Sonneveld, María-Victoria Mateos, Francesca Gay, and Kenneth C. Anderson. 2017. "Multiple Myeloma." *Nature Reviews Disease Primers* 3. Macmillan Publishers Limited: 17046. doi:10.1038/nrdp.2017.46.
- Kumari, Sudha, David Depoil, Roberta Martinelli, Edward Judokusumo, Guillaume Carmona, Frank B Gertler, Lance C Kam, et al. 2015. "Actin Foci Facilitate Activation of the Phospholipase C- γ in Primary T Lymphocytes via the WASP Pathway." *eLife* 4 (March). eLife Sciences Publications Limited: 775–87. doi:10.7554/eLife.04953.
- Kumari, Sudha, Santosha Vardhana, Michael Cammer, Silvia Curado, Luis Santos, Michael P. Sheetz, and Michael L. Dustin. 2012. "T Lymphocyte Myosin IIA Is Required for Maturation of the Immunological Synapse." *Frontiers in Immunology* 3 (AUG): 1–13. doi:10.3389/fimmu.2012.00230.
- Kunii, Naoki, Yangbing Zhao, Shuguang Jiang, Xiaojun Liu, John Scholler, Lakshmi Balagopalan, Lawrence E Samelson, Michael C Milone, and Carl H June. 2012. "Enhanced Function of Redirected Human T Cells Expressing Linker for Activation of T-Cells That Is Resistant to Ubiquitylation." *Human Gene Therapy* 37 (January): 120921123437006. doi:10.1089/hum.2012.130.
- Kurachi, Makoto, R Anthony Barnitz, Nir Yosef, Pamela M Odorizzi, Michael A Dilorio, Madeleine E Lemieux, Kathleen Yates, et al. 2014. "The Transcription Factor BATF Operates as an Essential Differentiation Checkpoint in Early Effector CD8+ T Cells." *Nature Immunology* 15 (4): 373–83. doi:10.1038/ni.2834.
- Kurosaki, Tomohiro, Kohei Kometani, and Wataru Ise. 2015. "Memory B Cells." *Nature Reviews Immunology* 15 (3). Nature Publishing Group: 149–59. doi:10.1038/nri3802.
- Kyle, Robert A., Morie A. Gertz, Thomas E. Witzig, John A. Lust, Martha Q. Lacy, Angela Dispenzieri, Rafael Fonseca, et al. 2003. "Review of 1027 Patients With Newly Diagnosed Multiple Myeloma." *Mayo Clinic Proceedings* 78 (1): 21–33. doi:10.4065/78.1.21.
- Kyle, Robert A., and S. Vincent Rajkumar. 2009. "Treatment of Multiple Myeloma: A Comprehensive Review."

- Clinical Lymphoma and Myeloma* 9 (4): 278–88. doi:10.3816/CLM.2009.n.056.
- Lara-Tejero, M, and Eric G Pamer. 2004. "T Cell Responses to *Listeria Monocytogenes*." *Current Opinion in Microbiology* 7 (1): 45–50. doi:10.1016/j.mib.2003.12.002.
- Lever, Melissa, Hong-Sheng Lim, Philipp Kruger, John Nguyen, Nicola Trendel, Enas Abu-Shah, Philip Kumar Maini, Philip Anton van der Merwe, and Omer Dushek. 2016. "Architecture of a Minimal Signaling Pathway Explains the T-Cell Response to a 1 Million-Fold Variation in Antigen Affinity and Dose." *Proceedings of the National Academy of Sciences of the United States of America* 113 (43). National Academy of Sciences: E6630–38. doi:10.1073/pnas.1608820113.
- Lever, Melissa, Philip K. Maini, P. Anton van der Merwe, Omer Dushek, Lever M, Maini PK, van der Merwe PA, and Dushek O. 2014. "Phenotypic Models of T Cell Activation." *Nature Reviews: Immunology* 14 (9). Nature Publishing Group: 619–29. doi:10.1038/nri3728.
- Lever M, Maini PK, van der Merwe PA, and Dushek O. 2014. "Phenotypic Models of T Cell Activation." *Nature Reviews. Immunology*, August, 619–29. <https://www.pubchase.com/article/25145757>.
- Levine, Andrew G, Aaron Arvey, Wei Jin, Alexander Y Rudensky, Levine AG, Arvey A, Jin W, and Rudensky AY. 2014. "Continuous Requirement for the TCR in Regulatory T Cell Function." *Nature Immunology*, no. September (September). Nature Publishing Group: 1–10. doi:10.1038/ni.3004.
- Levine, Bruce L, James Miskin, Keith Wonnacott, and Christopher Keir. 2017. "Global Manufacturing of CAR T Cell Therapy." doi:10.1016/j.omtm.2016.12.006.
- Levskaya, Anselm, Orion D Weiner, Wendell a Lim, and Christopher a Voigt. 2009. "Spatiotemporal Control of Cell Signalling Using a Light-Switchable Protein Interaction." *Nature* 461 (7266). Nature Publishing Group: 997–1001. doi:10.1038/nature08446.
- Li, Ji, Nicola J Stagg, Jennifer Johnston, Michael J Harris, Sam A Menzies, Danielle DiCara, Vanessa Clark, et al. 2017. "Membrane-Proximal Epitope Facilitates Efficient T Cell Synapse Formation by Anti-FcRH5/CD3 and Is a Requirement for Myeloma Cell Killing." *Cancer Cell* 31 (3): 383–95. doi:10.1016/j.ccell.2017.02.001.
- Li, Ming O., and Alexander Y. Rudensky. 2016. "T Cell Receptor Signalling in the Control of Regulatory T Cell Differentiation and Function." *Nature Reviews Immunology* 16 (4). Nature Publishing Group: 220–33. doi:10.1038/nri.2016.26.
- Li, Ming O, Alexander Y Rudensky, Memorial Sloan, Kettering Cancer, Memorial Sloan, and Kettering Cancer. 2016. "T Cell Receptor Signaling in the Control of Regulatory T Cell Differentiation and Function" 16 (4): 220–33. doi:10.1038/nri.2016.26.T.
- Li, Xu, Qin Wang, Xuhong Yu, H. Liu, Huan Yang, Chenxi Zhao, Xuanming Liu, et al. 2011. "Arabidopsis Cryptochrome 2 (CRY2) Functions by the Photoactivation Mechanism Distinct from the Tryptophan (Trp) Triad-Dependent Photoreduction." *Proceedings of the National Academy of Sciences* 108 (51): 20844–49. doi:10.1073/pnas.1114579108.
- Li, Yan, Nora G Singer, Joy Whitbred, Michael A Bowen, David A Fox, and Feng Lin. 2017. "CD6 as a Potential Target for Treating Multiple Sclerosis." *Proceedings of the National Academy of Sciences of the United States of America* 114 (10). National Academy of Sciences: 2687–92. doi:10.1073/pnas.1615253114.
- Li, Y S, K Hayakawa, and R R Hardy. 1993. "The Regulated Expression of B Lineage Associated Genes during B Cell Differentiation in Bone Marrow and Fetal Liver." *The Journal of Experimental Medicine* 178 (3). Rockefeller University Press: 951–60. doi:10.1084/JEM.178.3.951.
- Liang, Fu-Sen, Wen Q. Qi Ho, and Gerald R. Crabtree. 2011. "Engineering the ABA Plant Stress Pathway for Regulation of Induced Proximity." *Science Signaling* 4 (164). American Association for the Advancement of Science: rs2-rs2. doi:10.1126/scisignal.2001449.
- Liberles, S D, S T Diver, D J Austin, and S L Schreiber. 1997. "Inducible Gene Expression and Protein Translocation Using Nontoxic Ligands Identified by a Mammalian Three-Hybrid Screen." *Proceedings of the National Academy of Sciences of the United States of America* 94 (15): 7825–30. doi:10.1073/pnas.94.15.7825.
- Lillemeier, Björn F, Manuel a Mörtelmaier, Martin B Forstner, Johannes B Huppa, Jay T Groves, and Mark M Davis. 2010. "TCR and Lat Are Expressed on Separate Protein Islands on T Cell Membranes and Concatenate during Activation." *Nature Immunology* 11 (1): 90–96. doi:10.1038/ni.1832.
- Lim, Wendell a. 2010. "Designing Customized Cell Signalling Circuits." *Nature Reviews. Molecular Cell Biology* 11 (6). Nature Publishing Group: 393–403. doi:10.1038/nrm2904.
- Lin, Chentao. 2002. "Blue Light Receptors and Signal Transduction." *The Plant Cell* 14 Suppl (Suppl). American Society of Plant Biologists: S207-25. doi:10.1105/TPC.000646.
- Lin, Chentao, and Takeshi Todo. 2005. "The Cryptochromes." *Genome Biology* 6 (5): 220. doi:10.1186/gb-2005-6-5-220.
- Lin, Joseph, Arthur Weiss, S Timothy, and Timothy S Finco. 1999. "Localization of LAT in for T Cell Activation *."
- Linke, Rolf, Anke Klein, and Diane Seimetz. 2010. "Catumaxomab: Clinical Development and Future Directions."

- mAbs* 2 (2): 129–36. <http://www.ncbi.nlm.nih.gov/pubmed/20190561>.
- Linterman, Michelle A, Alice E Denton, Devina P Divekar, Ilona Zvetkova, Leanne Kane, Marc Veldhoen, Simon Clare, Gordon Dougan, Marion Espéli, and Kenneth G C Smith. 2014. "CD28 Expression Is Required after T Cell Priming for Helper T Cell Responses and Protective Immunity to Infection."
- Liu, H., X. Yu, K. Li, J. Klejnot, H. Yang, D. Lisiero, and C. Lin. 2008. "Photoexcited CRY2 Interacts with CIB1 to Regulate Transcription and Floral Initiation in Arabidopsis." *Science* 322 (5907): 1535–39. doi:10.1126/science.1163927.
- Locasale, Jason W. 2007. "Computational Investigations into the Origins of Short-Term Biochemical Memory in T Cell Activation." *PLoS ONE* 2 (7). doi:10.1371/journal.pone.0000627.
- Lungu, Oana I., Ryan a. Hallett, Eun Jung Choi, Mary J. Aiken, Klaus M. Hahn, and Brian Kuhlman. 2012. "Designing Photoswitchable Peptides Using the AsLOV2 Domain." *Chemistry and Biology* 19 (4). Elsevier Ltd: 507–17. doi:10.1016/j.chembiol.2012.02.006.
- Macian, Fernando. 2005. "NFAT Proteins: Key Regulators of T-Cell Development and Function." *Nature Reviews. Immunology* 5 (6): 472–84. doi:10.1038/nri1632.
- Malissen, Bernard, Claude Grégoire, Marie Malissen, and Romain Roncagalli. 2014. "Integrative Biology of T Cell Activation." *Nature Immunology* 15 (9): 790–97. doi:10.1038/ni.2959.
- Malissen, Bernard, and Didier Marguet. 2011. "La(s)t but Not Least." *Nature Immunology* 12 (7): 592–93. doi:10.1038/ni.2054.
- Man, Kevin, Maria Miasari, Wei Shi, Annie Xin, Darren C Henstridge, Simon Preston, Marc Pellegrini, et al. 2013. "The Transcription Factor IRF4 Is Essential for TCR Affinity-mediated Metabolic Programming and Clonal Expansion of T Cells." *Nature Immunology* 14 (11): 1155–65. doi:10.1038/ni.2710.
- Mandal, Arundhati, and Chandra Viswanathan. 2015. "Natural Killer Cells: In Health and Disease." *Hematology/Oncology and Stem Cell Therapy* 8 (2). King Faisal Specialist Hospital & Research Centre: 47–55. doi:10.1016/j.hemonc.2014.11.006.
- Martínez-Martín, Nuria, Elena Fernández-Arenas, Saso Cemerski, Pilar Delgado, Martin Turner, John Heuser, Darrell J. Irvine, et al. 2011. "T Cell Receptor Internalization from the Immunological Synapse Is Mediated by TC21 and RhoG GTPase-Dependent Phagocytosis." *Immunity* 35 (2): 208–22. doi:10.1016/j.immuni.2011.06.003.
- Maul, Robert W, Zheng Cao, Lakshmi Venkataraman, Carol A Giorgetti, Joan L Press, Yves Denizot, Hansen Du, Ranjan Sen, and Patricia J Gearhart. 2014. "Spt5 Accumulation at Variable Genes Distinguishes Somatic Hypermutation in Germinal Center B Cells from Ex Vivo-Activated Cells." *The Journal of Experimental Medicine* 211 (11). Rockefeller University Press: 2297–2306. doi:10.1084/jem.20131512.
- Maul, Robert W, and Patricia J Gearhart. 2010. "Controlling Somatic Hypermutation in Immunoglobulin Variable and Switch Regions." *Immunologic Research* 47 (1–3). NIH Public Access: 113–22. doi:10.1007/s12026-009-8142-5.
- Mayya, Viveka, and Michael L Dustin. 2016. "What Scales the T Cell Response?" *Trends in Immunology* 37 (8): 513–22. doi:10.1016/j.it.2016.06.005.
- McCoy, Kathy D, and Graham Le Gros. 1999. "The Role of CTLA-4 in the Regulation of T Cell Immune Responses." *Immunology and Cell Biology* 77 (1): 1–10. doi:10.1046/j.1440-1711.1999.00795.x.
- McIntosh, Brian E., John B. Hogenesch, and Christopher A. Bradfield. 2010. "Mammalian Per-Arnt-Sim Proteins in Environmental Adaptation." *Annual Review of Physiology* 72 (1): 625–45. doi:10.1146/annurev-physiol-021909-135922.
- McKeithan, T W. 1995. "Kinetic Proofreading in T-Cell Receptor Signal Transduction." *Proceedings of the National Academy of Sciences of the United States of America* 92 (11): 5042–46. <http://www.pubmedcentral.nih.gov/articlerender.fcgi?artid=41844&tool=pmcentrez&rendertype=abstract>.
- Medzhitov, Ruslan, Paula Preston-Hurlburt, and Charles A. Janeway. 1997. "A Human Homologue of the Drosophila Toll Protein Signals Activation of Adaptive Immunity." *Nature* 388 (6640). Nature Publishing Group: 394–97. doi:10.1038/41131.
- Mempel, Thorsten R., Sarah E. Henrickson, and Ulrich H. von Andrian. 2004. "T-Cell Priming by Dendritic Cells in Lymph Nodes Occurs in Three Distinct Phases." *Nature* 427 (6970): 154–59. doi:10.1038/nature02238.
- Miletic, Ana V., Daniel B. Graham, Kumiko Sakata-Sogawa, Michio Hiroshima, Michael J. Hamann, Saso Cemerski, Tracie Kloeppel, et al. 2009. "Vav Links the T Cell Antigen Receptor to the Actin Cytoskeleton and T Cell Activation Independently of Intrinsic Guanine Nucleotide Exchange Activity." Edited by Derya Unutmaz. *PLoS ONE* 4 (8): e6599. doi:10.1371/journal.pone.0006599.
- Millard, T H, S J Sharp, and L M Machesky. 2004. "Signalling to Actin Assembly via the WASP (Wiskott-Aldrich Syndrome Protein)-Family Proteins and the Arp2/3 Complex." *Biochem J* 380 (Pt 1): 1–17.

doi:10.1042/BJ20040176.

- Miller, Ira, Georgia Hatzivassiliou, Giorgio Cattoretti, Cathy Mendelsohn, and Riccardo Dalla-favera. 2015. "Plenary Paper IRTAs : A New Family of Immunoglobulinlike Receptors Differentially Expressed in B Cells" 99 (8): 2662–70.
- Miskov-Zivanov, Natasa, Michael S. Turner, Lawrence P. Kane, Penelope a. Morel, James R. Faeder, James R. Faeder November, and James R. Faeder. 2013. "The Duration of T Cell Stimulation Is a Critical Determinant of Cell Fate and Plasticity." *Science Signaling* 6 (300): ra97-ra97. doi:10.1126/scisignal.2004217.
- Miyamoto, Takafumi, Robert DeRose, Allison Suarez, Tasuku Ueno, Melinda Chen, Tai-ping Sun, Michael J Wolfgang, Chandrani Mukherjee, David J Meyers, and Takanari Inoue. 2012. "Rapid and Orthogonal Logic Gating with a Gibberellin-Induced Dimerization System." *Nature Chemical Biology* 8 (5). Nature Publishing Group: 465–70. doi:10.1038/nchembio.922.
- Möglich, Andreas, and Keith Moffat. 2010. "Engineered Photoreceptors as Novel Optogenetic Tools." *Photochemical & Photobiological Sciences* 9 (10): 1286. doi:10.1039/c0pp00167h.
- Mombaerts, P, J Iacomini, R S Johnson, K Herrup, S Tonegawa, and V E Papaioannou. 1992. "RAG-1-Deficient Mice Have No Mature B and T Lymphocytes." *Cell* 68 (5): 869–77. <http://www.ncbi.nlm.nih.gov/pubmed/1547488>.
- Monks, Colin R. F., Benjamin a Freiberg, Hannah Kupfer, Noah Sciaky, and Abraham Kupfer. 1998. "Three-Dimensional Segregation of supramolecular Activation clusters in T cells." *Nature* 395 (6697): 82–86. doi:10.1038/25764.
- Moran, Amy E., Keli L. Holzapfel, Yan Xing, Nicole R. Cunningham, Jonathan S. Maltzman, Jennifer Punt, and Kristin A. Hogquist. 2011. "T Cell Receptor Signal Strength in T_{reg} and iNKT Cell Development Demonstrated by a Novel Fluorescent Reporter Mouse." *The Journal of Experimental Medicine* 208 (6): 1279–89. doi:10.1084/jem.20110308.
- Moran, Oscar, Manfred W. Roessle, Roy A. Mariuzza, and Nazzareno Dimasi. 2008. "Structural Features of the Full-Length Adaptor Protein GADS in Solution Determined Using Small-Angle X-Ray Scattering." *Biophysical Journal* 94 (5). Elsevier: 1766–72. doi:10.1529/biophysj.107.116590.
- Motta-Mena, Laura B, Anna Reade, Michael J Mallory, Spencer Glantz, Orion D Weiner, Kristen W Lynch, and Kevin H Gardner. 2014. "An Optogenetic Gene Expression System with Rapid Activation and Deactivation Kinetics." *Nature Chemical Biology* 10 (3). Nature Publishing Group: 196–202. doi:10.1038/nchembio.1430.
- Mueller, Daniel L. 2010. "Mechanisms Maintaining Peripheral Tolerance." *Nature Immunology* 11 (1). Nature Publishing Group: 21–27. doi:10.1038/ni.1817.
- Mukhopadhyay, Himadri, Ben De Wet, Lara Clemens, Philip K. Maini, Jun Allard, P. Anton Van Der Merwe, and Omer Dushek. 2016. "Multisite Phosphorylation Modulates the T Cell Receptor ζ -Chain Potency but Not the Switchlike Response." *Biophysical Journal* 110 (8). The Authors: 1896–1906. doi:10.1016/j.bpj.2016.03.024.
- Myers, Darienne R., Julie Zikherman, and Jeroen P. Roose. 2017. "Tonic Signals: Why Do Lymphocytes Bother?" *Trends in Immunology* xx. Elsevier Ltd: 1–14. doi:10.1016/j.it.2017.06.010.
- Nagaleekar, Viswas K, Sean A Diehl, Ignacio Juncadella, Colette Charland, Natarajan Muthusamy, Sheri Eaton, Laura Haynes, Lee Ann Garrett-Sinha, Juan Anguita, and Mercedes Rincón. 2008. "IP3 Receptor-Mediated Ca²⁺ Release in Naive CD4 T Cells Dictates Their Cytokine Program." *Journal of Immunology* 181 (12). NIH Public Access: 8315–22. <http://www.ncbi.nlm.nih.gov/pubmed/19050248>.
- Nagel, G., Doris Ollig, Markus Fuhrmann, Suneel Kateriya, Anna Maria Musti, Ernst Bamberg, and Peter Hegemann. 2002. "Channelrhodopsin-1: A Light-Gated Proton Channel in Green Algae." *Science* 296 (5577): 2395–98. doi:10.1126/science.1072068.
- Nagel, G., T. Szellas, W. Huhn, S. Kateriya, N. Adeishvili, P. Berthold, D. Ollig, P. Hegemann, and E. Bamberg. 2003. "Channelrhodopsin-2, a Directly Light-Gated Cation-Selective Membrane Channel." *Proceedings of the National Academy of Sciences* 100 (24): 13940–45. doi:10.1073/pnas.1936192100.
- Napolitani, Giorgio, Andrea Rinaldi, Francesco Bertoni, Federica Sallusto, and Antonio Lanzavecchia. 2005. "Selected Toll-like Receptor Agonist Combinations Synergistically Trigger a T Helper Type 1–polarizing Program in Dendritic Cells." *Nature Immunology* 6 (8): 769–76. doi:10.1038/ni1223.
- Nayar, Ribhu, Elizabeth Schutten, Bianca Bautista, Keith Daniels, Amanda L. Prince, Megan Enos, Michael A. Brehm, Susan L. Swain, Raymond M. Welsh, and Leslie J. Berg. 2014. "Graded Levels of IRF4 Regulate CD8⁺ T Cell Differentiation and Expansion, but Not Attrition, in Response to Acute Virus Infection." *The Journal of Immunology* 192 (12): 5881–93. doi:10.4049/jimmunol.1303187.
- Negulescu, P A, T B Krasieva, A Khan, H H Kerschbaum, and M D Cahalan. 1996. "Polarity of T Cell Shape, Motility, and Sensitivity to Antigen." *Immunity* 4 (5): 421–30. <http://www.ncbi.nlm.nih.gov/pubmed/8630728>.

- Nemazee, D, and M Weigert. 2000. "Revising B Cell Receptors." *The Journal of Experimental Medicine* 191 (11). Rockefeller University Press: 1813–17. doi:10.1084/JEM.191.11.1813.
- Netea, Mihai G, Eicke Latz, Kingston H G Mills, and Luke A J O'Neill. 2015. "Innate Immune Memory: A Paradigm Shift in Understanding Host Defense." *Nature Immunology* 16 (7). Nature Publishing Group: 675–79. doi:10.1038/ni.3178.
- Niopek, Dominik, Dirk Benzinger, Julia Roensch, Thomas Draebing, Pierre Wehler, Roland Eils, and Barbara Di Ventura. 2014. "Engineering Light-Inducible Nuclear Localization Signals for Precise Spatiotemporal Control of Protein Dynamics in Living Cells." *Nature Communications* 5 (January). Nature Publishing Group: 4404. doi:10.1038/ncomms5404.
- Niopek, Dominik, Pierre Wehler, Julia Roensch, Roland Eils, and Barbara Di Ventura. 2016. "Optogenetic Control of Nuclear Protein Export." *Nature Communications* 7 (February): 10624. doi:10.1038/ncomms10624.
- Notarangelo, Luigi D, Carol H Miao, and Hans D Ochs. 2008. "Wiskott-Aldrich Syndrome." *Current Opinion in Hematology* 15 (1): 30–36. doi:10.1097/MOH.0b013e3282f30448.
- Nouroz, Faisal, Farzana Bibi, Shumaila Noreen, and Nosheen Masood. 2016. "Natural Killer Cells Enhance the Immune Surveillance of Cancer." *Egyptian Journal of Medical Human Genetics* 17 (2). Ain Shams University: 149–54. doi:10.1016/j.ejmhg.2015.08.006.
- Nunes, J A, M Battifora, J R Woodgett, A Truneh, D Olive, and D A Cantrell. 1996. "CD28 Signal Transduction Pathways. A Comparison of B7-1 and B7-2 Regulation of the Map Kinases: ERK2 and Jun Kinases." *Molecular Immunology* 33 (1): 63–70. <http://www.ncbi.nlm.nih.gov/pubmed/8604225>.
- Núñez-Cruz, Selene, Enrique Aguado, Sylvie Richelme, Bruno Chetaille, Anne-Marie Mura, Mireille Richelme, Laurent Pouyet, et al. 2003. "LAT Regulates Gammadelta T Cell Homeostasis and Differentiation." *Nature Immunology* 4 (10): 999–1008. doi:10.1038/ni977.
- Obst, Reinhard. 2015. "The Timing of T Cell Priming and Cycling." *Frontiers in Immunology* 6 (NOV): 1–10. doi:10.3389/fimmu.2015.00563.
- Offner, Sonja, Robert Hofmeister, Andrea Romaniuk, Peter Kufer, and Patrick A. Baeuerle. 2006. "Induction of Regular Cytolytic T Cell Synapses by Bispecific Single-Chain Antibody Constructs on MHC Class I-Negative Tumor Cells." *Molecular Immunology* 43 (6): 763–71. doi:10.1016/j.molimm.2005.03.007.
- Oh-hora, Masatsugu. 2009. "Calcium Signaling in the Development and Function of T-Lineage Cells." *Immunological Reviews* 231 (1): 210–24. doi:10.1111/j.1600-065X.2009.00819.x.
- Oheim, Martin, Marcel van 't Hoff, Anne Feltz, Alsu Zamaleeva, Jean-Maurice Mallet, and Mayeul Collot. 2014. "New Red-Fluorescent Calcium Indicators for Optogenetics, Photoactivation and Multi-Color Imaging." *Biochimica et Biophysica Acta (BBA) - Molecular Cell Research* 1843 (10): 2284–2306. doi:10.1016/j.bbamcr.2014.03.010.
- Ohkura, Naganari, Masahide Hamaguchi, Hiromasa Morikawa, Kyoko Sugimura, Atsushi Tanaka, Yoshinaga Ito, Motonao Osaki, et al. 2012. "T Cell Receptor Stimulation-Induced Epigenetic Changes and Foxp3 Expression Are Independent and Complementary Events Required for Treg Cell Development." *Immunity* 37 (5). Elsevier Inc.: 785–99. doi:10.1016/j.immuni.2012.09.010.
- Ohnishi, H, J a Ledbetter, S B Kanner, P S Linsley, T Tanaka, a M Geller, and M Kotb. 1995. "CD28 Cross-Linking Augments TCR-Mediated Signals and Costimulates Superantigen Responses." *Journal of Immunology (Baltimore, Md. : 1950)* 154 (7): 3180–93.
- Ohtsuka, T, Y Kaziro, and T Satoh. 1996. "Analysis of the T-Cell Activation Signaling Pathway Mediated by Tyrosine Kinases, Protein Kinase C, and Ras Protein, Which Is Modulated by Intracellular Cyclic AMP." *Biochimica et Biophysica Acta* 1310 (2): 223–32. <http://www.ncbi.nlm.nih.gov/pubmed/8611637>.
- Okkenhaug, Klaus, and Bart Vanhaesebroeck. 2003. "PI3K in Lymphocyte Development, Differentiation and Activation." *Nature Reviews Immunology* 3 (4): 317–30. doi:10.1038/nri1056.
- Osada, Takuya, Sandip P. Patel, Scott A. Hammond, Koya Osada, Michael A. Morse, and H. Kim Lyster. 2015. "CEA/CD3-Bispecific T Cell-Engaging (BiTE) Antibody-Mediated T Lymphocyte Cytotoxicity Maximized by Inhibition of Both PD1 and PD-L1." *Cancer Immunology, Immunotherapy* 64 (6): 677–88. doi:10.1007/s00262-015-1671-y.
- Osorio, Fabiola, and Caetano Reis e Sousa. 2011. "Myeloid C-Type Lectin Receptors in Pathogen Recognition and Host Defense." *Immunity* 34 (5). Cell Press: 651–64. doi:10.1016/J.IMMUNI.2011.05.001.
- Otipoby, Kevin L, Ari Waisman, Emmanuel Derudder, Lakshmi Srinivasan, and Andrew Franklin. 2015. "The B-Cell Antigen Receptor Integrates Adaptive and Innate Immune Signals" 112 (39): 1–6. doi:10.1073/pnas.1516428112.
- Pageon, Sophie V, Thibault Tabarin, Yui Yamamoto, Yuanqing Ma, John S Bridgeman, André Cohnen, Carola Benzing, et al. 2016. "Functional Role of T-Cell Receptor Nanoclusters in Signal Initiation and Antigen Discrimination." *Proceedings of the National Academy of Sciences of the United States of America* 113 (37): 1–6. doi:10.1073/pnas.1516428112.

- 5454–63. doi:10.1073/pnas.1607436113.
- Palomares, O, M Martín-Fontecha, R Lauener, C Traidl-Hoffmann, O Cavkaytar, M Akdis, and C a Akdis. 2014. "Regulatory T Cells and Immune Regulation of Allergic Diseases: Roles of IL-10 and TGF- β ." *Genes and Immunity*, no. April (July): 511–20. doi:10.1038/gene.2014.45.
- Parham, Peter. 2005. "MHC Class I Molecules and Kirs in Human History, Health and Survival." *Nature Reviews Immunology* 5 (3): 201–14. doi:10.1038/nri1570.
- Park, Hyerim, Na Yeon Kim, Sangkyu Lee, Nury Kim, Jihoon Kim, and Won Do Heo. 2017. "Optogenetic Protein Clustering through Fluorescent Protein Tagging and Extension of CRY2." *Nature Communications* 8 (1). Nature Publishing Group: 30. doi:10.1038/s41467-017-00060-2.
- Pasquet, J M, B Gross, L Quek, N Asazuma, W Zhang, C L Sommers, E Schweighoffer, et al. 1999. "LAT Is Required for Tyrosine Phosphorylation of Phospholipase cgamma2 and Platelet Activation by the Collagen Receptor GPVI." *Molecular and Cellular Biology* 19 (12): 8326–34.
- Paster, W., C. Brockmeyer, G. Fu, P. C. Simister, B. de Wet, A. Martinez-Riano, J. A. H. Hoerter, et al. 2013. "GRB2-Mediated Recruitment of THEMIS to LAT Is Essential for Thymocyte Development." *The Journal of Immunology* 190 (7): 3749–56. doi:10.4049/jimmunol.1203389.
- Pathak, Gopal P., Devin Strickland, Justin D. Vrana, and Chandra L. Tucker. 2014. "Benchmarking of Optical Dimerizer Systems." *ACS Synthetic Biology* 3 (11): 832–38. doi:10.1021/sb500291r.
- Paz, P E, S Wang, H Clarke, X Lu, D Stokoe, and A Abo. 2001. "Mapping the Zap-70 Phosphorylation Sites on LAT (Linker for Activation of T Cells) Required for Recruitment and Activation of Signalling Proteins in T Cells." *The Biochemical Journal* 356 (Pt 2). Portland Press Ltd: 461–71. <http://www.ncbi.nlm.nih.gov/pubmed/11368773>.
- Pedmale, Ullas V., Shao-shan Carol Huang, Mark Zander, Benjamin J. Cole, Jonathan Hetzel, Karin Ljung, Pedro A.B. Reis, et al. 2016. "Cryptochromes Interact Directly with PIFs to Control Plant Growth in Limiting Blue Light." *Cell* 164 (1–2): 233–45. doi:10.1016/j.cell.2015.12.018.
- Peter, Emanuel, Bernhard Dick, and Stephan a Baeurle. 2010. "Mechanism of Signal Transduction of the LOV2-Ja Photosensor from Avena Sativa." *Nature Communications* 1 (8). Nature Publishing Group: 122. doi:10.1038/ncomms1121.
- Philpott, Dana J., Matthew T. Sorbara, Susan J. Robertson, Kenneth Croitoru, and Stephen E. Girardin. 2013. "NOD Proteins: Regulators of Inflammation in Health and Disease." *Nature Reviews Immunology* 14 (1): 9–23. doi:10.1038/nri3565.
- Podtschaske, Miriam, Uwe Benary, Sandra Zwinger, Thomas Höfer, Andreas Radbruch, and Ria Baumgrass. 2007. "Digital NFATc2 Activation per Cell Transforms Graded T Cell Receptor Activation into an All-or-None IL-2 Expression." Edited by Jean Kanellopoulos. *PLoS ONE* 2 (9): e935. doi:10.1371/journal.pone.0000935.
- Polic, B., D. Kunkel, A. Scheffold, and K. Rajewsky. 2001. "How Alpha Beta T Cells Deal with Induced TCR Ablation." *Proceedings of the National Academy of Sciences* 98 (15): 8744–49. doi:10.1073/pnas.141218898.
- Polson, Andrew G., Bing Zheng, Kristi Elkins, Wesley Chang, Changchun Du, Patrick Dowd, Lulu Yen, et al. 2006. "Expression Pattern of the Human FcRH/IRTA Receptors in Normal Tissue and in B-Chronic Lymphocytic Leukemia." *International Immunology* 18 (9): 1363–73. doi:10.1093/intimm/dx1069.
- Posey, Avery D., Robert D. Schwab, Alina C. Boesteanu, Catharina Steentoft, Ulla Mandel, Boris Engels, Jennifer D. Stone, et al. 2016. "Engineered CAR T Cells Targeting the Cancer-Associated Tn-Glycoform of the Membrane Mucin MUC1 Control Adenocarcinoma." *Immunity* 44 (6). Elsevier Inc.: 1444–54. doi:10.1016/j.immuni.2016.05.014.
- Prlic, Martin, Gabriela Hernandez-Hoyos, and Michael J Bevan. 2006. "Duration of the Initial TCR Stimulus Controls the Magnitude but Not Functionality of the CD8+ T Cell Response." *The Journal of Experimental Medicine* 203 (9). The Rockefeller University Press: 2135–43. doi:10.1084/jem.20060928.
- Pulvertart, J V. 1964. "Cytology of Burkitt's Tumour (African Lymphoma)." *Lancet* 1 (7327): 238–40. <http://www.ncbi.nlm.nih.gov/pubmed/14086209>.
- Putyrski, Mateusz, and Carsten Schultz. 2012. "Protein Translocation as a Tool: The Current Rapamycin Story." *FEBS Letters* 586 (15). Federation of European Biochemical Societies: 2097–2105. doi:10.1016/j.febslet.2012.04.061.
- Qi, Hai, Wolfgang Kastenmüller, and Ronald N. Germain. 2014. "Spatiotemporal Basis of Innate and Adaptive Immunity in Secondary Lymphoid Tissue." *Annual Review of Cell and Developmental Biology* 30 (1): 141–67. doi:10.1146/annurev-cellbio-100913-013254.
- Qi Q, Liu Y, Cheng Y, Glanville J, Zhang D, Lee JY, Olshen RA, et al. 2014. "Diversity and Clonal Selection in the Human T-Cell Repertoire." *Proceedings of the National Academy of Sciences of the United States of America* 111 (36). National Academy of Sciences: 13139–44. doi:10.1073/pnas.1409155111.

- Rachmilewitz, Jacob, Antonio Lanzavecchia, and Rachmilewitz J. 2002. "A Temporal and Spatial Summation Model for T-Cell Activation: Signal Integration and Antigen Decoding." *Trends in Immunology* 23 (12): 592–95.
<http://ovidsp.ovid.com/ovidweb.cgi?T=JS&PAGE=reference&D=emed5&NEWS=N&AN=2002451442%5Cnhttp://ovidsp.ovid.com/ovidweb.cgi?T=JS&PAGE=reference&D=med4&NEWS=N&AN=12464571>.
- Rajkumar, S Vincent, Meletios A Dimopoulos, Antonio Palumbo, Joan Blade, Giampaolo Merlini, María-Victoria Mateos, Shaji Kumar, et al. 2014. "International Myeloma Working Group Updated Criteria for the Diagnosis of Multiple Myeloma." *The Lancet. Oncology* 15 (12). Elsevier: e538-48. doi:10.1016/S1470-2045(14)70442-5.
- Regner, Matthias. 2001. "Cross-Reactivity in T-Cell Antigen Recognition." *Immunology and Cell Biology* 79 (2). Nature Publishing Group: 91–100. doi:10.1046/j.1440-1711.2001.00994.x.
- Reina, Jose, Emmanuel Lacroix, Scott D. Hobson, Gregorio Fernandez-Ballester, Vladimir Rybin, Markus S. Schwab, Luis Serrano, and Cayetano Gonzalez. 2002. "Computer-Aided Design of a PDZ Domain to Recognize New Target Sequences." *Nature Structural Biology* 9 (8). Nature Publishing Group: nsb815. doi:10.1038/nsb815.
- Repina, Nicole A., Alyssa Rosenbloom, Abhirup Mukherjee, David V. Schaffer, and Ravi S. Kane. 2017. "At Light Speed: Advances in Optogenetic Systems for Regulating Cell Signaling and Behavior." *Annual Review of Chemical and Biomolecular Engineering* 8 (1). Annual Reviews : 13–39. doi:10.1146/annurev-chembioeng-060816-101254.
- Reth, Michael G., Patrizia Ammirati, Sharon Jackson, and Frederick W. Alt. 1985. "Regulated Progression of a Cultured Pre-B-Cell Line to the B-Cell Stage." *Nature* 317 (6035): 353–55. doi:10.1038/317353a0.
- Robinson, Margaret S, Daniela a Sahlender, and Samuel D Foster. 2010. "Rapid Inactivation of Proteins by Rapamycin-Induced Rerouting to Mitochondria." *Developmental Cell* 18 (2). Elsevier: 324–31. doi:10.1016/j.devcel.2009.12.015.
- Roncagalli, Romain, Simon Hauri, Frédéric Fiore, Yinming Liang, Zhi Chen, Amandine Sansoni, Kartiek Kanduri, et al. 2014. "Quantitative Proteomics Analysis of Signalosome Dynamics in Primary T Cells Identifies the Surface Receptor CD6 as a Lat Adaptor-Independent TCR Signaling Hub." *Nature Immunology* 15 (4): 384–92. doi:10.1038/ni.2843.
- Roose, J. P., M. Mollenauer, M. Ho, T. Kurosaki, and A. Weiss. 2007. "Unusual Interplay of Two Types of Ras Activators, RasGRP and SOS, Establishes Sensitive and Robust Ras Activation in Lymphocytes." *Molecular and Cellular Biology* 27 (7): 2732–45. doi:10.1128/MCB.01882-06.
- Roose, Jeroen P, Marianne Mollenauer, Vikas A Gupta, James Stone, and Arthur Weiss. 2005. "A Diacylglycerol-Protein Kinase C-RasGRP1 Pathway Directs Ras Activation upon Antigen Receptor Stimulation of T Cells A Diacylglycerol-Protein Kinase C-RasGRP1 Pathway Directs Ras Activation upon Antigen Receptor Stimulation of T Cells." *Society* 25 (11): 4426–41. doi:10.1128/MCB.25.11.4426.
- Sadelain, Michel, Renier Brentjens, and Isabelle Rivière. 2013. "The Basic Principles of Chimeric Antigen Receptor Design." *Cancer Discovery* 3 (4). NIH Public Access: 388–98. doi:10.1158/2159-8290.CD-12-0548.
- Saito, Takashi, and Tadashi Yokosuka. 2006. "Immunological Synapse and Microclusters: The Site for Recognition and Activation of T Cells." *Current Opinion in Immunology* 18 (3): 305–13. doi:10.1016/j.coi.2006.03.014.
- Saito, Takashi, Tadashi Yokosuka, and Akiko Hashimoto-Tane. 2010. "Dynamic Regulation of T Cell Activation and Co-Stimulation through TCR-Microclusters." *FEBS Letters* 584 (24): 4865–71. doi:10.1016/j.febslet.2010.11.036.
- Sakaguchi, Noriko, Takeshi Takahashi, Hiroshi Hata, Takashi Nomura, Tomoyuki Tagami, Sayuri Yamazaki, Toshiko Sakihama, et al. 2003. "Altered Thymic T-Cell Selection due to a Mutation of the ZAP-70 Gene Causes Autoimmune Arthritis in Mice." *Nature* 426 (6965): 454–60. doi:10.1038/nature02119.
- Saleiro, Diana, and Leonidas C. Plataniias. 2014. "Intersection of mTOR and STAT Signaling in Immunity." *Trends in Immunology*, November. Elsevier Ltd, 1–9. doi:10.1016/j.it.2014.10.006.
- Salek, Mogjiborahman, Simon McGowan, David C. Trudgian, Omer Dushek, Ben de Wet, Georgios Efstathiou, and Oreste Acuto. 2013. "Quantitative Phosphoproteome Analysis Unveils LAT as a Modulator of CD3ζ and ZAP-70 Tyrosine Phosphorylation." Edited by Laszlo Buday. *PLoS ONE* 8 (10). Public Library of Science: e77423. doi:10.1371/journal.pone.0077423.
- Saline, Maria, Karin E J Rödström, Gerhard Fischer, Vladislav Yu Orekhov, B Göran Karlsson, and Karin Lindkvist-Petersson. 2010. "The Structure of Superantigen Complexed with TCR and MHC Reveals Novel Insights into Superantigenic T Cell Activation." *Nature Communications* 1 (May): 119. doi:10.1038/ncomms1117.
- Sallusto, F, B Palermo, D Lenig, M Miettinen, S Matikainen, I Julkunen, R Forster, R Burgstahler, M Lipp, and A Lanzavecchia. 1999. "Distinct Patterns and Kinetics of Chemokine Production Regulate Dendritic Cell Function." *European Journal of Immunology* 29 (5): 1617–25. doi:10.1002/(SICI)1521-

- 4141(199905)29:05<1617::AID-IMMU1617>3.0.CO;2-3.
- Salomon, M, W Eisenreich, H Dürr, E Schleicher, E Knieb, V Massey, W Rüdiger, F Müller, a Bacher, and G Richter. 2001. "An Optomechanical Transducer in the Blue Light Receptor Phototropin from *Avena Sativa*." *Proceedings of the National Academy of Sciences of the United States of America* 98 (22): 12357–61. doi:10.1073/pnas.221455298.
- Sanchez-Lockhart, Mariano, Beth Graf, and Jim Miller. 2008. "Signals and Sequences That Control CD28 Localization to the Central Region of the Immunological Synapse." *Journal of Immunology* 181 (11): 7639–48. <http://www.ncbi.nlm.nih.gov/pubmed/19017952>.
- Sanchez-Lockhart, Mariano, and Jim Miller. 2006. "Engagement of CD28 outside of the Immunological Synapse Results in up-Regulation of IL-2 mRNA Stability but Not IL-2 Transcription." *Journal of Immunology* 176 (8): 4778–84. <http://www.ncbi.nlm.nih.gov/pubmed/16585571>.
- Sancho, J, T Chatila, R C Wong, C Hall, R Blumberg, B Alarcon, R S Geha, and C Terhorst. 1989. "T-Cell Antigen Receptor (TCR)-Alpha/beta Heterodimer Formation Is a Prerequisite for Association of CD3-Zeta 2 into Functionally Competent TCR.CD3 Complexes." *The Journal of Biological Chemistry* 264 (34): 20760–69. <http://www.ncbi.nlm.nih.gov/pubmed/2531145>.
- Sander, Jeffry D, and J Keith Joung. 2014. "CRISPR-Cas Systems for Editing, Regulating and Targeting Genomes." *Nature Biotechnology* 32 (4). Nature Publishing Group: 347–55. doi:10.1038/nbt.2842.
- Sarma, Vidya J, and Peter A Ward. 2011. "The Complement System." *Cell & Tissue Research* 343: 227–35. doi:10.1007/s00441-010-1034-0.
- Schamel, W. W a. 2007. "The Stoichiometry of the T Cell Antigen Receptor and Its Implications for the Signal Transduction Mechanism." *Signal Transduction* 7 (4): 311–19. doi:10.1002/sita.200600123.
- Schamel, Wolfgang W. A., and Balbino Alarcón. 2013. *Organization of the Resting TCR in Nanoscale Oligomers. Immunological Reviews*. Vol. 251. doi:10.1111/imr.12019.
- Schmid, Eva M., Matthew H. Bakalar, Kaushik Choudhuri, Julian Weichsel, Hyoung Sook Ann, Phillip L. Geissler, Michael L. Dustin, and Daniel A. Fletcher. 2016. "Size-Dependent Protein Segregation at Membrane Interfaces." *Nature Physics* 12 (7). doi:10.1038/nphys3678.
- Schmidt, Daniel, and Yong Ku Cho. 2015. "Natural Photoreceptors and Their Application to Synthetic Biology." *Trends in Biotechnology* 33 (2). Elsevier Ltd: 80–91. doi:10.1016/j.tibtech.2014.10.007.
- Schneider, Helga, and Christopher E. Rudd. 2000. "Tyrosine Phosphatase SHP-2 Binding to CTLA-4: Absence of Direct YVKM/YFIP Motif Recognition." *Biochemical and Biophysical Research Communications* 269 (1): 279–83. doi:10.1006/bbrc.2000.2234.
- Schoenborn, Jamie R, Ying Xim Tan, Chao Zhang, Kevan M Shokat, and Arthur Weiss. 2011. "Feedback Circuits Monitor and Adjust Basal Lck-Dependent Events in T Cell Receptor Signaling." *Science Signaling* 4 (190): ra59. doi:10.1126/scisignal.2001893.
- Shah, D. K., and J. C. Zuniga-Pflucker. 2014. "An Overview of the Intrathymic Intricacies of T Cell Development." *The Journal of Immunology* 192 (9): 4017–23. doi:10.4049/jimmunol.1302259.
- Shen, Shudan, Minghua Zhu, Jasmine Lau, Mariana Chuck, and Weiguo Zhang. 2009. "The Essential Role of LAT in Thymocyte Development during Transition from the Double-Positive to Single-Positive Stage." *Journal of Immunology (Baltimore, Md. : 1950)* 182 (9): 5596–5604. doi:10.4049/jimmunol.0803170.
- Sheng, Weiwei, Chunyan Liu, Rong Fu, Huaquan Wang, Wen Qu, Erbao Ruan, Guojin Wang, et al. 2014. "Abnormalities of Quantities and Functions of Linker for Activations of T Cells in Severe Aplastic Anemia." *European Journal of Haematology* 93 (3): 214–23. doi:10.1111/ejh.12327.
- Shi, Jianguo, Richard S McIntosh, and Richard J Pleass. 2006. "Antibody- and Fc-Receptor-Based Therapeutics for Malaria." *Clinical Science (London, England : 1979)* 110 (1): 11–19. doi:10.1042/CS20050136.
- Shin, Haina, and Akiko Iwasaki. 2013. "Tissue-Resident Memory T Cells." *Immunological Reviews* 255 (1): 165–81. doi:10.1111/imr.12087.
- Siegel, Rebecca L., Kimberly D. Miller, and Ahmedin Jemal. 2016. "Cancer Statistics, 2016." *CA: A Cancer Journal for Clinicians* 66 (1): 7–30. doi:10.3322/caac.21332.
- Siggs, Owen M, Lisa A Miosge, Adèle L Yates, Edyta M Kucharska, Daniel Sheahan, Tomas Brdicka, Arthur Weiss, Adrian Liston, and Christopher C Goodnow. 2007. "Opposing Functions of the T Cell Receptor Kinase ZAP-70 in Immunity and Tolerance Differentially Titrate in Response to Nucleotide Substitutions." *Immunity* 27 (6): 912–26. doi:10.1016/j.immuni.2007.11.013.
- Smith-Garvin, Jennifer E, Gary a Koretzky, Martha S Jordan, and 1 Gary A Koretzky. 2009. "T Cell Activation." *Annual Review of Immunology* 27 (1): 591–619. doi:10.1146/annurev.immunol.021908.132706.
- Smith, Kenneth G. C., and Menna R. Clatworthy. 2010. "FcγRIIB in Autoimmunity and Infection: Evolutionary and Therapeutic Implications." *Nature Reviews Immunology* 10 (5). Nature Publishing Group: 328–43. doi:10.1038/nri2762.

- Sommers, Connie L, Cheung-Seog Park, Jan Lee, Chiguang Feng, Claudette L Fuller, Alexander Grinberg, Jay a Hildebrand, et al. 2002. "A LAT Mutation That Inhibits T Cell Development yet Induces Lymphoproliferation." *Science (New York, N.Y.)* 296 (5575): 2040–43. doi:10.1126/science.1069066.
- Sommers, Connie L, Lawrence E Samelson, and Paul E Love. 2004. "LAT: A T Lymphocyte Adapter Protein That Couples the Antigen Receptor to Downstream Signaling Pathways." *BioEssays : News and Reviews in Molecular, Cellular and Developmental Biology* 26 (1): 61–67. doi:10.1002/bies.10384.
- Speiser, Daniel E, Daniel T Utzschneider, Susanne G Oberle, Christian Münz, Pedro Romero, and Dietmar Zehn. 2014. "T Cell Differentiation in Chronic Infection and Cancer: Functional Adaptation or Exhaustion?" *Nature Reviews. Immunology*, no. September (September). Nature Publishing Group: 1–7. doi:10.1038/nri3740.
- Spencer, D M, T J Wandless, S L Schreiber, and G R Crabtree. 1993. "Controlling Signal Transduction with Synthetic Ligands." *Science* 262 (5136): 1019–24. doi:10.1126/science.7694365.
- Spiltoir, Jessica I., Devin Strickland, Michael Glotzer, and Chandra L. Tucker. 2016. "Optical Control of Peroxisomal Trafficking." *ACS Synthetic Biology* 5 (7): 554–60. doi:10.1021/acssynbio.5b00144.
- Starbeck-Miller, Gabriel R., Hai-Hui Xue, and John T. Harty. 2014. "IL-12 and Type I Interferon Prolong the Division of Activated CD8 T Cells by Maintaining High-Affinity IL-2 Signaling in Vivo." *The Journal of Experimental Medicine* 211 (1): 105–20. doi:10.1084/jem.20130901.
- Štefanová, Irena, Bernhard Hemmer, Marco Vergelli, Roland Martin, William E. Biddison, and Ronald N. Germain. 2003. "TCR Ligand Discrimination Is Enforced by Competing ERK Positive and SHP-1 Negative Feedback Pathways." *Nature Immunology* 4 (3): 248–54. doi:10.1038/ni895.
- Stein, Viktor, and Kirill Alexandrov. 2014. "Synthetic Protein Switches : Design Principles and Applications." *Trends in Biotechnology* 33 (2). Elsevier Ltd: 101–10. doi:10.1016/j.tibtech.2014.11.010.
- Stinchcombe, Jane C., Endre Majorovits, Giovanna Bossi, Stephen Fuller, and Gillian M. Griffiths. 2006. "Centrosome Polarization Delivers Secretory Granules to the Immunological Synapse." *Nature* 443 (7110): 462–65. doi:10.1038/nature05071.
- Stockley, John H., Kimberley Evans, Moritz Matthey, Katrin Volbracht, Sylvia Agathou, Jana Mukanowa, Juan Burrone, and Ragnhildur T. Káradóttir. 2017. "Surpassing Light-Induced Cell Damage in Vitro with Novel Cell Culture Media." *Scientific Reports* 7 (1). Nature Publishing Group: 849. doi:10.1038/s41598-017-00829-x.
- Stratiievska, Anastasiia, and Sharona E. Gordon. 2016. "Light-Controlled PI3K Activation Mimics TRPV1 Potentiation by NGF." *Biophysical Journal* 110 (3). Cell Press: 285a. doi:10.1016/J.BJP.2015.11.1542.
- Strickland, Devin, Yuan Lin, Elizabeth Wagner, C Hope, Josiah Zayner, Chloe Antoniou, Tobin Sosnick, Eric Weiss, and Michael Glotzer. 2012. "TULIPs: Tunable, Light-Controlled Interacting Protein Tags for Cell Biology." *Nature Methods* 9 (4): 379–84.
- Strickland, Devin, Xiaolan Yao, Grzegorz Gawlak, Michael K Rosen, Kevin H Gardner, and Tobin R Sosnick. 2010. "Rationally Improving LOV Domain–based Photoswitches." *Nature Methods* 7 (8). Nature Research: 623–26. doi:10.1038/nmeth.1473.
- Su, Authors Xiaolei, Jonathon A Ditlev, Enfu Hui, Sudeep Banjade, and Julia Okrut. 2016. "Phase Separation of Signaling Molecules Promotes T Cell Receptor Signal Transduction" 9964. doi:10.1126/science.aad9964.
- Sun, L. L., D. Ellerman, M. Mathieu, M. Hristopoulos, X. Chen, Y. Li, X. Yan, et al. 2015. "Anti-CD20/CD3 T Cell-Dependent Bispecific Antibody for the Treatment of B Cell Malignancies." *Science Translational Medicine* 7 (287): 287ra70–287ra70. doi:10.1126/scitranslmed.aaa4802.
- Sun, Meili, Huan Shi, Chuanyong Liu, Jie Liu, Xianqiang Liu, and Yuping Sun. 2014. "Construction and Evaluation of a Novel Humanized HER2-Specific Chimeric Receptor." *Breast Cancer Research* 16 (3). BioMed Central: R61. doi:10.1186/bcr3674.
- Surh, C D, and J Sprent. 2000. "Homeostatic T Cell Proliferation: How Far Can T Cells Be Activated to Self-Ligands?" *The Journal of Experimental Medicine* 192 (4). Rockefeller University Press: F9–14. doi:10.1084/JEM.192.4.F9.
- Szalay, G, C H Ladel, and S H Kaufmann. 1995. "Stimulation of Protective CD8+ T Lymphocytes by Vaccination with Nonliving Bacteria." *Proceedings of the National Academy of Sciences of the United States of America* 92 (26): 12389–92. <http://www.ncbi.nlm.nih.gov/pubmed/8618907>.
- Taslimi, Amir, Justin D Vrana, Daniel Chen, Sofya Borinskaya, Bruce J Mayer, Matthew J Kennedy, and Chandra L Tucker. 2014. "An Optimized Optogenetic Clustering Tool for Probing Protein Interaction and Function." *Nature Communications* 5. Nature Publishing Group: 4925. doi:10.1038/ncomms5925.
- Taslimi, Amir, Brian Zoltowski, Jose G Miranda, Gopal P Pathak, Robert M Hughes, and Chandra L Tucker. 2016. "Optimized Second-Generation CRY2–CIB Dimerizers and Photoactivatable Cre Recombinase." *Nature Chemical Biology*, no. April. Nature Publishing Group: 1–8. doi:10.1038/nchembio.2063.

- Taylor, Marcus J., Kabir Husain, Zev J. Gartner, Satyajit Mayor, and Ronald D. Vale. 2017. "A DNA-Based T Cell Receptor Reveals a Role for Receptor Clustering in Ligand Discrimination." *Cell* 169 (1): 108–119.e20. doi:10.1016/j.cell.2017.03.006.
- Teft, Wendy A, Thu A Chau, and Joaquín Madrenas. 2009. "Structure-Function Analysis of the CTLA-4 Interaction with PP2A." *BMC Immunology* 10 (1): 23. doi:10.1186/1471-2172-10-23.
- Tesmer, L A, S K Lundy, S Sarkar, and D A Fox. 2008. "Th17 Cells in Human Disease." *Immunol Rev* 223: 87–113. doi:10.1111/j.1600-065X.2008.00628.x.
- Tischer, Doug, and Orion D. Weiner. 2014. "Illuminating Cell Signalling with Optogenetics Tools." *Nature Reviews Molecular Cell Biology* 15 (August): 551–58.
- Tkach, Karen, and Grégoire Altan-Bonnet. 2013. "T Cell Responses to Antigen: Hasty Proposals Resolved through Long Engagements." *Current Opinion in Immunology* 25 (1): 120–25. doi:10.1016/j.coi.2012.12.001.
- Tkach, Karen E, Debashis Barik, Guillaume Voisinne, Nicole Malandro, Matthew M Hathorn, Jesse W Cotari, Robert Vogel, et al. 2014. "T Cells Translate Individual , Quantal Activation into Collective , Analog Cytokine Responses via Time-Integrated Feedbacks," 1–30. doi:10.7554/eLife.01944.
- Toettcher, Jared E., Orion D. Weiner, and Wendell A. Lim. 2013. "Using Optogenetics to Interrogate the Dynamic Control of Signal Transmission by the Ras/Erk Module." *Cell* 155 (6). Elsevier Inc.: 1422–34. doi:10.1016/j.cell.2013.11.004.
- Toettcher, Jared E, Christopher A Voigt, Orion D Weiner, and Wendell A Lim. 2011. "The Promise of Optogenetics in Cell Biology: Interrogating Molecular Circuits in Space and Time." *Nature Methods* 8: 35–38. doi:10.1038/nmeth.f.326.
- Trombetta, E Sergio, Melanie Ebersold, Wendy Garrett, Marc Pypaert, and Ira Mellman. 2003. "Activation of Lysosomal Function during Dendritic Cell Maturation." *Science (New York, N.Y.)* 299 (5611). American Association for the Advancement of Science: 1400–1403. doi:10.1126/science.1080106.
- Tscharke, David C., Nathan P. Croft, Peter C. Doherty, and Nicole L. La Gruta. 2015. "Sizing up the Key Determinants of the CD8+ T Cell Response." *Nature Reviews Immunology* 15 (11): 705–16. doi:10.1038/nri3905.
- Tube, Noah J., and Marc K. Jenkins. 2014. "TCR Signal Quantity and Quality in CD4+ T Cell Differentiation." *Trends in Immunology* 35 (12). Elsevier Ltd: 591–96. doi:10.1016/j.it.2014.09.008.
- Tube, Noah J., Antonio J. Pagán, Justin J. Taylor, Ryan W. Nelson, Jonathan L. Linehan, James M. Ertelt, Eric S. Huseby, Sing Sing Way, and Marc K. Jenkins. 2013. "Single Naive CD4+ T Cells from a Diverse Repertoire Produce Different Effector Cell Types during Infection." *Cell* 153 (4): 785–96. doi:10.1016/j.cell.2013.04.007.
- Tucker, Chandra L, Justin D Vrana, and Matthew J Kennedy. 2014. "Tools for Controlling Protein Interactions Using Light." *Current Protocols in Cell Biology / Editorial Board, Juan S. Bonifacino ... [et Al.]* 64: 17.16.1-17.16.20. doi:10.1002/0471143030.cb1716s64.
- Turley, S J, K Inaba, W S Garrett, M Ebersold, J Untermaehrer, R M Steinman, and I Mellman. 2000. "Transport of Peptide-MHC Class II Complexes in Developing Dendritic Cells." *Science (New York, N.Y.)* 288 (5465). American Association for the Advancement of Science: 522–27. doi:10.1126/SCIENCE.288.5465.522.
- Tyler, Christopher J., Derek G. Doherty, Bernhard Moser, and Matthias Eberl. 2015. "Human Vγ9/Vδ2 T Cells: Innate Adaptors of the Immune System." *Cellular Immunology* 296 (1). Elsevier Inc.: 10–21. doi:10.1016/j.cellimm.2015.01.008.
- van Panhuys, Nicholas, Frederick Klauschen, and Ronald N. Germain. 2014. "T-Cell-Receptor-Dependent Signal Intensity Dominantly Controls CD4+ T Cell Polarization In Vivo." *Immunity* 41 (1). Elsevier Inc.: 63–74. doi:10.1016/j.immuni.2014.06.003.
- van Bergeijk, Petra, Max Adrian, Casper C Hoogenraad, and Lukas C Kapitein. 2015. "Optogenetic Control of Organelle Transport and Positioning." *Nature*, January. Nature Publishing Group. doi:10.1038/nature14128.
- van der Lee, Robin, Marija Buljan, Benjamin Lang, Robert J. Weatheritt, Gary W. Daughdrill, A. Keith Dunker, Monika Fuxreiter, et al. 2014. "Classification of Intrinsically Disordered Regions and Proteins." *Chemical Reviews* 114 (13). American Chemical Society: 6589–6631. doi:10.1021/cr400525m.
- van Heijst, J, C Gerlach, E Swart, D Sie, C Nunes-Alves, R Kerkhoven, R Arens, M Correia-Neves, K Schepers, and T Schumacher. 2009. "Recruitment of Antigen-Specific CD8+ T Cells in Response O Infection Is Markedly Efficient." *Science* 325 (September): 1265–70.
- Van Roey, Kim, and Norman E Davey. 2015. "Motif Co-Regulation and Co-Operativity Are Common Mechanisms in Transcriptional, Post-Transcriptional and Post-Translational Regulation." *Cell Communication and Signaling : CCS* 13 (December). BioMed Central: 45. doi:10.1186/s12964-015-0123-9.
- Varma, Rajat, Gabriele Campi, Tadashi Yokosuka, Takashi Saito, and Michael L. Dustin. 2006. "T Cell Receptor-

- Proximal Signals Are Sustained in Peripheral Microclusters and Terminated in the Central Supramolecular Activation Cluster." *Immunity* 25 (1): 117–27. doi:10.1016/j.immuni.2006.04.010.
- Varnai, Peter, Baskaran Thyagarajan, Tibor Rohacs, and Tamas Balla. 2006. "Rapidly Inducible Changes in Phosphatidylinositol 4,5-Bisphosphate Levels Influence Multiple Regulatory Functions of the Lipid in Intact Living Cells." *The Journal of Cell Biology* 175 (3): 377–82. doi:10.1083/jcb.200607116.
- Vaz, Winchil L C, Federico Goodsaid-Zalduondo, and Ken Jacobson. 1984. "Lateral Diffusion of Lipids and Proteins in Bilayer Membranes." *FEBS Letters* 174 (2): 199–207. doi:10.1016/0014-5793(84)81157-6.
- Vogt, Julia H M, and Jos H M Schippers. 2015. "Setting the PAS, the Role of Circadian PAS Domain Proteins during Environmental Adaptation in Plants." *Frontiers in Plant Science* 6. Frontiers Media SA: 513. doi:10.3389/fpls.2015.00513.
- Voisinne, Guillaume, Briana G. Nixon, Anna Melbinger, Georg Gasteiger, Massimo Vergassola, and Gr??goire Altan-Bonnet. 2015. "T Cells Integrate Local and Global Cues to Discriminate between Structurally Similar Antigens." *Cell Reports* 11 (8): 1208–19. doi:10.1016/j.celrep.2015.04.051.
- Wang, Hui, Marco Vilela, Andreas Winkler, Mirosław Tarnawski, Ilme Schlichting, Hayretin Yumerefendi, Brian Kuhlman, Rihe Liu, Gaudenz Danuser, and Klaus M Hahn. 2016. "LOVTRAP: An Optogenetic System for Photoinduced Protein Dissociation." *Nature Methods* 13 (9): 755–58. doi:10.1038/nmeth.3926.
- Wang, Yunjiao, Pawel Paszek, Caroline A. Horton, Hong Yue, Michael R.H. White, Douglas B. Kell, Mark R. Muldoon, and David S. Broomhead. 2012. "A Systematic Survey of the Response of a Model NF- κ B Signalling Pathway to TNF α Stimulation." *Journal of Theoretical Biology* 297: 137–47. doi:10.1016/j.jtbi.2011.12.014.
- Wange, R L, S N Malek, S Desiderio, and L E Samelson. 1993. "Tandem SH2 Domains of ZAP-70 Bind to T Cell Antigen Receptor Zeta and CD3 Epsilon from Activated Jurkat T Cells." *The Journal of Biological Chemistry* 268 (26): 19797–801.
- Wardemann, Hedda, Sergey Yurasov, Anne Schaefer, James W Young, Eric Meffre, and Michel C Nussenzweig. 2003. "Predominant Autoantibody Production by Early Human B Cell Precursors." *Science (New York, N.Y.)* 301 (5638). American Association for the Advancement of Science: 1374–77. doi:10.1126/science.1086907.
- Weber, J R, S Orstavik, K M Torgersen, N C Danbolt, S F Berg, J C Ryan, K Taskén, J B Imboden, and J T Vaage. 1998. "Molecular Cloning of the cDNA Encoding pp36, a Tyrosine-Phosphorylated Adaptor Protein Selectively Expressed by T Cells and Natural Killer Cells." *The Journal of Experimental Medicine* 187 (7): 1157–61. <http://www.ncbi.nlm.nih.gov/pubmed/9529333>.
- Weiss, A, J Imboden, D Shoback, and J Stobo. 1984. "Role of T3 Surface Molecules in Human T-Cell Activation: T3-Dependent Activation Results in an Increase in Cytoplasmic Free Calcium." *Proceedings of the National Academy of Sciences of the United States of America* 81 (13): 4169–73. <http://www.ncbi.nlm.nih.gov/pubmed/6234599>.
- Williams, Matthew A, and Michael J Bevan. 2004. "Shortening the Infectious Period Does Not Alter Expansion of CD8 T Cells but Diminishes Their Capacity to Differentiate into Memory Cells." *Journal of Immunology* 173 (11): 6694–702. <http://www.ncbi.nlm.nih.gov/pubmed/15557161>.
- Williamson, David J, Dylan M Owen, Jérémie Rossy, Astrid Magenau, Matthias Wehrmann, J Justin Gooding, and Katharina Gaus. 2011. "Pre-Existing Clusters of the Adaptor Lat Do Not Participate in Early T Cell Signaling Events." *Nature Immunology* 12 (7). Nature Publishing Group: 655–62. doi:10.1038/ni.2049.
- Wilson, Maxwell Z, Pavithran T Ravindran, Wendell A Lim, and Jared E Toettcher. 2017. "Tracing Information Flow from Erk to Target Gene Induction Reveals Mechanisms of Dynamic and Combinatorial Control." *Molecular Cell* 67 (5). Elsevier: 757–769.e5. doi:10.1016/j.molcel.2017.07.016.
- Wonerow, Peter, and Steve P Watson. 2001. "The Transmembrane Adapter LAT Plays a Central Role in Immune Receptor Signalling." *Oncogene* 20 (44). Nature Publishing Group: 6273–83. doi:10.1038/sj.onc.1204770.
- Wu, Yi I, Daniel Frey, Oana I Lungu, Angelika Jaehrig, Ilme Schlichting, Brian Kuhlman, and Klaus M Hahn. 2009. "A Genetically Encoded Photoactivatable Rac Controls the Motility of Living Cells." *Nature* 461 (7260): 104–8. doi:10.1038/nature08241.
- Yamashita, I, T Nagata, T Tada, and T Nakayama. 1993. "CD69 Cell Surface Expression Identifies Developing Thymocytes Which Audition for T Cell Antigen Receptor-Mediated Positive Selection." *International Immunology* 5 (9): 1139–50. <http://www.ncbi.nlm.nih.gov/pubmed/7902130>.
- Yanagihara, Shigehiro, Emiko Komura, Jun Nagafune, Hiroshi Watarai, and Yasunori Yamaguchi. 1998. "EBI1/CCR7 Is a New Member of Dendritic Cell Chemokine Receptor That Is Up-Regulated upon Maturation." *J Immunol The Journal of Immunology by Guest on* 161: 3096–3102. <http://www.jimmunol.org/content/161/6/3096>.
- Yao, Xiaolan, Michael K Rosen, and Kevin H Gardner. 2008. "Estimation of the Available Free Energy in a LOV2-J

- Alpha Photoswitch." *Nature Chemical Biology* 4 (8): 491–97. doi:10.1038/nchembio.99.
- Yazawa, Masayuki, Amir M Sadaghiani, Brian Hsueh, and Ricardo E Dolmetsch. 2009. "Induction of Protein-Protein Interactions in Live Cells Using Light." *Nature Biotechnology* 27 (10): 941–45. doi:10.1038/nbt.1569.
- Yi, J., X. S. Wu, T. Crites, and J. A. Hammer. 2012. "Actin Retrograde Flow and Actomyosin II Arc Contraction Drive Receptor Cluster Dynamics at the Immunological Synapse in Jurkat T Cells." *Molecular Biology of the Cell* 23 (5): 834–52. doi:10.1091/mbc.E11-08-0731.
- Yoder, J., C Pham, Y M Iizuka, O Kanagawa, S K Liu, J McGlade, and A M Cheng. 2001. "Requirement for the SLP-76 Adaptor GADS in T Cell Development." *Science* 291 (5510): 1987–91. doi:10.1126/science.1057176.
- Yokosuka, Tadashi, Kumiko Sakata-Sogawa, Wakana Kobayashi, Michio Hiroshima, Akiko Hashimoto-Tane, Makio Tokunaga, Michael L Dustin, and Takashi Saito. 2005. "Newly Generated T Cell Receptor Microclusters Initiate and Sustain T Cell Activation by Recruitment of Zap70 and SLP-76." *Nature Immunology* 6 (12): 1253–62. doi:10.1038/ni1272.
- Yoneyama, Mitsutoshi, and Takashi Fujita. 2007. "Function of RIG-I-like Receptors in Antiviral Innate Immunity." *The Journal of Biological Chemistry* 282 (21). American Society for Biochemistry and Molecular Biology: 15315–18. doi:10.1074/jbc.R700007200.
- Yoneyama, Mitsutoshi, Mika Kikuchi, Takashi Natsukawa, Noriaki Shinobu, Tadaatsu Imaizumi, Makoto Miyagishi, Kazunari Taira, Shizuo Akira, and Takashi Fujita. 2004. "The RNA Helicase RIG-I Has an Essential Function in Double-Stranded RNA-Induced Innate Antiviral Responses." *Nature Immunology* 5 (7). Nature Publishing Group: 730–37. doi:10.1038/ni1087.
- Yu, Cheng-han, Hung-jen Wu, Yoshihisa Kaizuka, Ronald D Vale, and Jay T Groves. 2010. "Altered Actin Centripetal Retrograde Flow in Physically Restricted Immunological Synapses." *PloS One* 5 (7). Public Library of Science: e11878. doi:10.1371/journal.pone.0011878.
- Yu, Xuhong, Hongtao Liu, John Klejnot, and Chentao Lin. 2010. *The Cryptochrome Blue Light Receptors. The Arabidopsis Book*. Vol. 8. American Society of Plant Biologists. doi:10.1199/TAB.0135.
- Yu, Yan, Alexander a Smoligovets, and Jay T Groves. 2013. "Modulation of T Cell Signaling by the Actin Cytoskeleton." *Journal of Cell Science* 126 (Pt 5): 1049–58. doi:10.1242/jcs.098210.
- Zayner, Josiah P., Chloe Antoniou, Alexander R. French, Ronald J. Hause, Tobin R. Sosnick, Ronald J Hause Jr, and Tobin R. Sosnick. 2013. "Investigating Models of Protein Function and Allostery with a Widespread Mutational Analysis of a Light-Activated Protein." *Biophysical Journal* 105 (4). Elsevier: 1027–36. doi:10.1016/j.bpj.2013.07.010.
- Zayner, Josiah P., Chloe Antoniou, and Tobin R. Sosnick. 2012. "The Amino-Terminal Helix Modulates Light-Activated Conformational Changes in AsLOV2." *Journal of Molecular Biology* 419 (1–2). Elsevier Ltd: 61–74. doi:10.1016/j.jmb.2012.02.037.
- Zayner, Josiah P., and Tobin R. Sosnick. 2014. "Factors That Control the Chemistry of the LOV Domain Photocycle." *Plos One* 9 (1): 1–9. doi:10.1371/journal.pone.0087074.
- Zehn, Dietmar, Sarah Y. Lee, and Michael J. Bevan. 2009. "Complete but Curtailed T-Cell Response to Very Low-Affinity Antigen." *Nature* 458 (7235): 211–14. doi:10.1038/nature07657.
- Zeng, Rong, Judy L Cannon, Robert T Abraham, Michael Way, Daniel D Billadeau, Julie Bubeck-Wardenberg, and Janis K Burkhardt. 2003. "SLP-76 Coordinates Nck-Dependent Wiskott-Aldrich Syndrome Protein Recruitment with Vav-1/Cdc42-Dependent Wiskott-Aldrich Syndrome Protein Activation at the T Cell-APC Contact Site." *J Immunol* 171 (3): 1360–68. doi:10.4049/jimmunol.171.3.1360.
- Zhang, Nu, and Michael J. Bevan. 2011. "CD8+ T Cells: Foot Soldiers of the Immune System." *Immunity* 35 (2): 161–68. doi:10.1016/j.immuni.2011.07.010.
- Zhang, W, C L Sommers, D N Burshtyn, C C Stebbins, J B DeJarnette, R P Tribble, A Grinberg, et al. 1999. "Essential Role of LAT in T Cell Development." *Immunity* 10: 323–32. doi:S1074-7613(00)80032-1 [pii].
- Zhang, W, R P Tribble, and L E Samelson. 1998. "LAT Palmitoylation: Its Essential Role in Membrane Microdomain Targeting and Tyrosine Phosphorylation during T Cell Activation." *Immunity* 9: 239–46. doi:S1074-7613(00)80606-8 [pii].
- Zhang, Weiguo, Brenda J. Irvin, Ronald P. Tribble, Robert T. Abraham, and Lawrence E. Samelson. 1999. "Functional Analysis of LAT in TCR-Mediated Signaling Pathways Using a LAT-Deficient Jurkat Cell Line." *International Immunology* 11 (6): 943–50. doi:10.1093/intimm/11.6.943.
- Zhang, Weiguo, Joanne Sloan-Lancaster, Jason Kitchen, Ronald P. Tribble, and Lawrence E. Samelson. 1998. "LAT: The ZAP-70 Tyrosine Kinase Substrate That Links T Cell Receptor to Cellular Activation." *Cell* 92 (1): 83–92. doi:10.1016/S0092-8674(00)80901-0.
- Zheng, B, S Han, and G Kelsoe. 1996. "T Helper Cells in Murine Germinal Centers Are Antigen-Specific Emigrants That Downregulate Thy-1." *The Journal of Experimental Medicine* 184 (3). Rockefeller University Press:

- 1083–91. doi:10.1084/JEM.184.3.1083.
- Zheng, Biao, Shuhua Han, Qing Zhu, Richard Goldsby, and Garnett Kelsoe. 1996. "Alternative Pathways for the Selection of Antigen-Specific Peripheral T Cells." , *Published Online: 21 November 1996*; / doi:10.1038/384263a0 384 (6606). Nature Publishing Group: 263. doi:10.1038/384263a0.
- Zhou, Xinyuan, Shuyang Yu, Dong-Mei Zhao, John T Harty, Vladimir P Badovinac, and Hai-Hui Xue. 2010. "Differentiation and Persistence of Memory CD8(+) T Cells Depend on T Cell Factor 1." *Immunity* 33 (2). NIH Public Access: 229–40. doi:10.1016/j.immuni.2010.08.002.
- Zhou, Yubin, Paul Meraner, Hyoung T Kwon, Danya Machnes, Masatsugu Oh-hora, Jochen Zimmer, Yun Huang, Antonio Stura, Anjana Rao, and Patrick G Hogan. 2010. "STIM1 Gates the Store-Operated Calcium Channel ORAI1 in Vitro." *Nature Structural & Molecular Biology* 17 (1). Nature Publishing Group: 112–16. doi:10.1038/nsmb.1724.
- Zhu, Minghua, Shudan Shen, Yan Liu, Olivia Granillo, and Weiguo Zhang. 2005. "Cutting Edge: Localization of Linker for Activation of T Cells to Lipid Rafts Is Not Essential in T Cell Activation and Development." *Journal of Immunology* 174 (1): 31–35. <http://www.ncbi.nlm.nih.gov/pubmed/15611224>.
- Zikherman, Julie, Ramya Parameswaran, and Arthur Weiss. 2012. "Endogenous Antigen Tunes the Responsiveness of Naive B Cells but Not T Cells." *Nature* 489 (7414). NIH Public Access: 160–64. doi:10.1038/nature11311.
- Zimmerman, S.P., B. Kuhlman, and H. Yumerefendi. 2016. *Engineering and Application of LOV2-Based Photoswitches. Peptide, Protein and Enzyme Design*. 1sted. Elsevier Inc. doi:10.1016/bs.mie.2016.05.058.

Appendix A

Name	Sequence	Tm (°C)	Notes
LATint'-SpeI_Fwd	5'- tagtagactagtcaggcaggttacgacagcacatcctcag	-3' 65.7	CRISPR PAM Knockout
IRES-NTOM20_Fwd	5'- cacgatgataatatggccacaacccatgggtgggcccgaacagcgcg	-3' 70.0	Overlap extension IRES-NTOM
NTOM20-IRES_Rev	5'- cgcgctgttgccggcccaccatgggtgtggccatattatcatcgtg	-3' 55.0	Overlap extension IRES-NTOM
NTOM20-IFP2_Fwd	5'- cgatccgaacttttaaatctagagctcgggacccctcaacctttc	-3' 57.6	NTOM-tag IFP2
IFP2-NTOM20_Rev	5'- gaaaggttgagggtcccagctctagatttaaagtccgcatcg	-3' 54.5	NTOM-tag IFP2
LOV-IFP2_Rev	5'- gtagtagccaaggaaaccacttccagaaccggcttctttcctctgcacctg	-3' 63.2	IFP2 – LOV2 fusion
IFP2-LOV-Fwd	5'- caggtgcagaggaaagaagccgggtctctggaagtgggttccttggtactac	-3' 59.8	IFP2 – LOV2 fusion
NTOM20_Fwd	5'- atggtgggcccgaacagc	-3' 62.0	NTOM20 sequence cloning
NTOM20_Rev	5'- tctagatttaaagttcggatcgctgcg	-3' 58.6	NTOM20 sequence cloning
LATmut1_Fwd	5'- tagtcacgcgtgccaccatggaggaggccattttgggtgccttgtgtccttggggctcctgctgctg	-3' 70.0	CRISPR gRNA mutation
LATdblmut-LOV_fwd	5'- gccacagactgccaggcagtggaagtcctagggttggtactactacattg	-3' 70.6	LAT-TM cloning
LATdblmut-LOV_Rev	5'- caagtgtagtagccaacccataggacttccACTgcctggcagctctgtggc	-3' 70.6	LAT-TM cloning
IRES-LATmut_fwd	5'- cacgatgataatatggccacaacccatggaggaggccattttgggtg	-3' 68.5	IRES LAT cloning
IRES-Latmut_Rev	5'- caccaaaatggcctcctccatgggtgtggccatattatcatcgtg	-3' 68.5	IRES LAT cloning
Cherry 3'_Fwd-seq	5'- cccacaacgaggactacaccatcg	-3' 61.2	3' sequencing primer
IFP2-LOV_fwd2	5'- caggtgcagaggaaagaagccggctccggaagtcctaggttggtactac	-3' 61.2	IFP2 - LOV2 fusion
LOV-IFP2_Rev2	5'- gtagtagccaacccataggacttccggagccggcttctttcctctgcacctg	-3' 64.2	IFP2 - LOV2 fusion
IFP2stitch_fwd	5'- tccctcctctgtatctcggaggaccagaga	-3' 65.2	IFP2 overlap extension
IFP2stitch_Rev	5'- tctctgggtcctccgagatacagaggaggga	-3' 65.2	IFP2 overlap extension
PDZ-Bgl_For	5'- tagtagagatctgatgccagaacttggatttagcatatcaggt	-3' 62.7	BglII site insertion
FN3-Bam_Rev	5'- ctactaggatcccggtagttaatcgagattgggctagagtag	-3' 63.5	BamHI site insertion
cpPDZ-Bam_Rev	5'- ctactaggatccgagtccttttcaaccctcactcgaatctcttgggt	-3' 64.8	BamHI site insertion
AsiSI_LATtm_fwd	5'- tagtaggcgatcgccaccatggaggaggccattttgggtgc	-3' 70.4	AsiSI site insertion
LOVp_SpeI_Rev	5'- ctactaactagttcacaccaggtatccaccgc	-3' 63.3	SpeI site insertion LOVp
LOV2_SpeI_Rev	5'- ctactaactagttcaaagttcttttgccgcctcatc	-3' 60.7	SpeI insertion LOV2
MluI_LAT(AGT)_fwd	5'- tagtagacgcgtgccaccatgggcagttacgacagcacatcctc	-3' 71.6	MluI insertion LAT
Ruby-PDZ_fwd	5'- gtgggatggacgagctgtacaaggcagtgccatgccagaacttggatttagcatatcag	-3' 59.6	Ruby-PDZ fusion
PDZ-Ruby_Rev	5'- ctgatatgctaaatccaagttctggcatgccactgccctgtacagctcgtccatcccac	-3' 66.6	Ruby-PDZ fusion
FN3-StopNotI_Rev	5'- ctactagcggccgctcaacggtagttaatcgagattgggctagag	-3' 68.4	FN3 Ruby fusion STOP
Ruby-zdk_fwd	5'- gtgggatggacgagctgtacaaggcagtgccatgggtggataacaaattcaataaagaaaaag	-3' 53.4	ZDK – Ruby fusion
Zdk-Ruby_rev	5'- cttttctttattgaatttggatccaccatgccactgccctgtacagctcgtccatcccac	-3' 66.6	ZDK – Ruby fusion
zdk-StopNotI_rev	5'- ctactagcggccgctcattttggggcctgggcatcg	-3' 72.7	ZDK – Ruby fusion
LAT-3'_seq	5'- gaactgcacccctggagcggctaag	-3' 61.7	LAT sequencing primer
iRFP670-NoATG-Mul_For	5'- tagtagacgcgtgcccgttaaggtcgatctcacc	-3' 67.5	
iRFP670-Bam_Rev	5'- ctactaggatcccgttgggtgggtggcggcggtg	-3' 68.5	
cpPDZ-StopNotI_Rev	5'- ctactagcggccgctcagtccttttcaaccctcactcgaatctcttgggt	-3' 63.0	for Ruby-cpPDZ stitch
IRES-3'_seq_For	5'- ccacggggacgtggttttcc	-3' 61.0	Forward sequencing primer for 3' end of IRES sequence

LOV-5'_seq_Rev	5'-	actatcggacgcgaatataatggg	-3'	58.0	Reverse primer from 5' end of LOV
P1_CRISPR_LAT_fwd	5'-	cacagtcagctggacgcacactcagc	-3'	65.0	LAT CRISPR
P2_CRISPR_LAT_Rev	5'-	ctggcacccaaggtaggggacc	-3'	64.0	LAT CRISPR
P3_CRISPR_LAT_fwd	5'-	ctggcacctggtgcctacctgc	-3'	65.0	LAT CRISPR
P4_CRISPR_LAT_Rev	5'-	ggttcacgctcactcccacaccagg	-3'	66.0	LAT CRISPR
P1_CRISPR_Mlu_fwd	5'-	tagtagacgctgccaccacagtcagctggacgcacactcagc	-3'	73.9	LAT gDNA cloning
P2_CRISPR_LAT_Not_Rev	5'-	ctactagcggcgcctggcacccaaggtaggggacc	-3'	75.0	LAT gDNA cloning
LATtm-pep_STOP_Not_Rev	5'-	taggcggccgctcacaccaggtatcgatgctgcctctacttccactgcctggcagtcctgtgg	-3'	69.4	LAT-TMpep cloning
BglII_nMag_Fwd	5'-	tagagatctggcgaagcggaggtagtggac	-3'	64.1	Magnets cloning
BglII_FKBP_Fwd	5'-	tagagatctggcgaagcggaggtagtggcgtccaagtcgaaaccattagtc	-3'	61.4	CID cloning
MluI_ATGpMag_Fwd	5'-	tagacgcgtgccaccatgcacactctttacgccctg	-3'	66.6	Magnets cloning
MluI_ATG_FRB	5'-	TAGacgcgtGCCACCATGatcctctggcatgagatgtggcatg	-3'	67.2	CID cloning
FRB_Spe_Rev	5'-	ctaactagtctttgagattcgtcggaacacatg	-3'	59.7	CID cloning
pMag3X_Spe_Rev	5'-	ctaactagtctcagtcctgcactgaaaccccatgc	-3'	63.3	Magnets cloning
pMag_Spe_Rev	5'-	ctaactagtctcggttcgcactggaatcc	-3'	60.5	Magnets cloning
Bam_FRB_Fwd	5'-	tagggatccggaagtatcctctggcatgagatgtggcatg	-3'	63.0	CID cloning
FRB-pep_Not_Rev	5'-	ctagcggccgctcacaccaggtatcgcatgctgcctctacttccggagcccttgagattcgtcggaacac	-3'	57.0	FRB spacer
Bam_qGFP_Fwd	5'-	tagggatccggaagtgtgagcaagggcgaggagctg	-3'	62.8	GFP spacer
qGFP-pep_Not_Rev	5'-	ctagcggccgctcacaccaggtatcGATGCTGCCTCTacttccggagcccttgtagactcgtccatgccgag	-3'	63.0	GFP spacer
Spe_Ruby_fwd	5'-	tagtagactagtgtgtctaagggcgaagagctgac	-3'	59.1	Ruby for CRISPR vector
CD6_CRISPR1_Fwd	5'-	CACCGCTCCGTTTGTGTCAGACGGAC	-3'	N/A	CRISPR oligo
CD6_CRISPR1_Rev	5'-	AAACGTCCGTCTGACAAACGGGAGC	-3'	N/A	CRISPR oligo
CD6_CRISPR2_Fwd	5'-	CACCGAGTGGCATTAGCTGCTACGC	-3'	N/A	CRISPR oligo
CD6_CRISPR2_Rev	5'-	AAACGCGTAGCAGCTAATGCCACTC	-3'	N/A	CRISPR oligo
LATtm-PDZ_Fwd	5'-	gccacagactgccaggatccggaagtccagaacttgatttagcatatcagg	-3'	58.0	LAT-PDZ fusion
LATtm-PDZ_Rev	5'-	cctgatatgctaaatccaagtcttggaacttccggatcctggcagtcctgtggc	-3'	63.0	LAT-PDZ fusion
LATint	5'-	ttgaactggatgcccttggatac	-3'	60.0	
HA-Liker_Rev	5'-	ccgtacgacgtaccagactacgcaGGCTCCGGGAGCGGAAGC	-3'	64.4	Overlap extension HA to the Zdk
ZDK-Linker_fwd	5'-	ggctccggagcgggaagcgtggataacaaattcaataaagaaaagacacg	-3'	55.6	Overlap extension HA to the Zdk
LOV2_C450G_fwd	5'-	gggaagaaacggcaggtttctacaagg	-3'	58.0	C/G mutation LOV2
LOV2_C450G_Rev	5'-	ccttgtagaaacctgccgtttcttccc	-3'	58.0	C/G mutation LOV2
QC_C450G_Rev	5'-	aaatttcttcacggctatatctgtcaactgc	-3'	58.0	QuikChange Q5
LOV2_C450S_Fwd	5'-	gggaagaaactccaggtttctacaagg	-3'	58.0	C/S mutation LOV2
LOV2_C450S_Rev	5'-	ccttgtagaaacctggagtttcttccc	-3'	58.0	C/S mutation LOV2
AsiSI-NTOM_fwd	5'-	tagtaggcgatcgccaccatggtgggccgaacagc	-3'	62.0	AsiSI NTOM instert
LATint_Mlu_Fwd	5'-	tagtagacgcgtccaggcagttacgacagcacatcc	-3'	60.0	Mlu instert LATint
NTOM-LAT_Fwd	5'-	cgccgcagcgatccgaacttttaaaggtagtcaggcagttacgacagcacatcctcag	-3'	63.0	NTOM-LATint fusion
NTOM-LAT_Rev	5'-	ctgaggatgtgctgtcgtaactgcctggactacctttaaagttcggatcgctgcggcg	-3'	63.0	NTOM-LATint fusion
MluI-NTOM_fwd	5'-	tagtagacgcgtgccaccatggtgggccgaacagc	-3'	67.7	
Spe-NTOM_Rev	5'-	tagtagactagttttaaagttcggatcgctgcggcg	-3'	65.0	
CRY2-Mlu_fwd	5'-	Tagacgcgtgccaccatgaagatggacaaaagactatagtttgg	-3'	59.0	CRY2 cloning
CRY2PHR-Spe_Rev	5'-	ctactaactagtgtgctccgatcatgatctgtgc	-3'	61.4	CRY2 cloning

CRY2FL-Spe_Rev	5'-	ctactaactagttttgcaaccattttttcccaaactttag	-3'	57.3	CRY2 cloning
CRY2(535)-Spe_Rev	5'-	ctactaactagtaacagccgaaggtagcttgggtc	-3'	59.3	CRY2 cloning
CRY2(515)-Spe_Rev	5'-	ctactaactagtaatggattagcccctaaggcctcg	-3'	60.0	CRY2 cloning
CRY2(W349R)_Fwd	5'-	ggaatgagagagcttcgggctaccggatgg	-3'	62.0	W/R overlap extension
CRY2(W349R)_Rev	5'-	ccatccggtagcccgaagctctctcattcc	-3'	62.0	W/R overlap extension
CRY2(L348F)_Fwd	5'-	ggaatgagagagttttgggtaccggatgg	-3'	62.0	L/F overlap extension
CRY2(L348F)_Rev	5'-	ccatccggtagcccaaaactctctcattcc	-3'	62.0	L/F overlap extension
CRY2(G337E)_Fwd	5'-	gacaaggcaggaccgagtagtccgttggtggatg	-3'	68.0	G/E overlap extension
CRY2(G337E)_Rev	5'-	catccaccaacggatactcggtcctgccttgtc	-3'	68.0	G/E overlap extension
CRY2-W734R_Fwd	5'-	gaagtttcttctcctccagccaaatggggaatgaagtatttc	-3'	57.0	W/R overlap extension
CRY2-W734R_Rev	5'-	gaaatacttcattccccatttggtcggaaggagaagaaacttc	-3'	57.0	W/R overlap extension
CD6-3_fwd	5'-	caccgttgcaacttcacgcccgccg	-3'	68.0	CD6 cloning
CD6-3_Rev	5'-	aaaccggccggcggtgaagtgaac	-3'	68.0	CD6 cloning
LATint-YtoF-Spe_Fwd	5'-	tagtagactagtcaggcagtttccgacagcacatcctcag	-3'	65	LAT Y-to-F cloning
CD6_SpeI_fwd	5'-	tagtagactagtgccaccatgtggctcttcttcgggatcactgg	-3'	64.0	CD6 cloning
CD6_MluI_fwd	5'-	tagtagacgcgtgcccaccatgtggctcttcttcgggatcactgg	-3'	64.0	CD6 cloning
CD6_MluKO_Fwd	5'-	gggtggagcacgcctgccgcagcg	-3'	65.0	CD6 MluI knockout
CD6_MluKO_Rev	5'-	cgctgcggcaggcgtgctccacc	-3'	63.0	CD6 MluI Knockout
CD6_STOP-Not	5'-	ctactagcggccgcctaggtgcgctgatgtcatcgtagtc	-3'	64.0	CD6 cloning
CD6_Bam-STOP_Rev(DP)	5'-	tcacaggatccccggctgcgctgatgtcatcgtagtc	-3'	63.0	CD6 cloning
CD6_AsiSI_Fwd	5'-	tagtaggcgatcgccaccatgtggctcttcttcgggatcactgg	-3'	64.0	CD6 cloning
Zeta_Ex1_1CRISPR_Fwd	5'-	caccgggtgaaaggcgcttttcaccg	-3'	N/A	Zeta CRISPR gRNA oligo
Zeta_Ex1_1CRISPR_Rev	5'-	aaaccgggtgaaaagcgccttcacC	-3'	N/A	Zeta CRISPR gRNA oligo
Zeta_Ex1_2CRISPR_Fwd	5'-	caccgtaatcggaactgtgcctgc	-3'	N/A	Zeta CRISPR gRNA oligo
Zeta_Ex1_2CRISPR_Rev	5'-	aaacgcaggcacagttgccgattac	-3'	N/A	Zeta CRISPR gRNA oligo
Mlu_BFP_Fwd	5'-	tagtagacgcgtgccaccatgagcgagctgattaaggagaacatgc	-3'	61.0	BFP into CRISPR construct
BFP_BamSTOP_REV	5'-	tcacaggatccattaagcttgtgccccagtttgctaggg	-3'	65.0	
CD3zeta_gDNA_MluFwd	5'-	acgcgtcaaaggccccacagtcctcc	-3'	59.0	
CD3zeta_gDNA_NotRev	5'-	gcggccgcgaggaggaggtattgaagg	-3'	59.0	
Foxo_BamSTOP_Rev	5'-	caccgtaatcggcaactgtgcctgc	-3'	70.0	Foxo1 reporter cloning
Foxo_MluKO_fwd	5'-	cgtcccgccgcaacgcctggggcaacc	-3'	72.0	Foxo1 MluI knockout
Foxo_MluKO_Rev	5'-	ggttgccccaggcgttgccggcggaagc	-3'	72.0	Foxo1 MluI knockout
Foxo1_AsiSI_fwd	5'-	tagtaggcgatcgccaccatggccgaggcgccctcaggtgg	-3'	71.0	Foxo1 cloning
Foxo_IF_Fwd	5'-	gagaattctcacgcggccaccatggccgaggcgccctcaggtgg	-3'	70.0	Foxo1 InFusion
Foxo_IF_Rev	5'-	ggcgaccggtggatcggatccccgggccccgc	-3'	70.0	Foxo1 InFusion
FoxoGib_Fwd	5'-	gctctcgagaattctcacgcgtatggccgaggcgccctcag	-3'	72.0	Foxo1 Gibson
FoxoGib_Rev	5'-	ccatgggtggcgaccgggtggatccggggcccgcggtaccgtcg	-3'	72.0	Foxo1 Gibson
CD6_Gib_Fwd	5'-	ggagctctcgagaattctcacgcgtatgtggctcttcttcggg	-3'	75.0	CD6 Gibson
CD6_Gib_Rev	5'-	caggctgactctagagtcgcccgcgtaggtgcgctgatgtc	-3'	75.0	CD6 Gibson
Foxo-3'_seq	5'-	tgccccacacctcgggtatgaacc	-3'	64.0	Foxo sequencing oligo
1166-SFFV_5'seq	5'-	cttctgttcgcgcgttctctgttc	-3'	65.0	Sequencing from pHR promoter
1167-WPRE_3'seq	5'-	ccagaggttgattatcgataagc	-3'	65.0	Sequencing from WPRE sequence

Appendix B

Construct	Notes
pHR-LATdblmut-Ruby	CRISPR-proof LAT
pHR-LATmut-Ruby	gRNA site mutant LAT
pHR-LAT(AGT)-Ruby	LAT ser mutant
pHR-LAT-Ruby	Wildtype LAT
pHR-LAT-TM-LOVpep	LAT transmembrane LOVpep fusion Bam KO
pHR-LAT-TM-LOVpep (No AGT)	LAT transmembrane LOVpep fusion Bam site intact
pHR-LAT-TM-LOV2	LAT transmembrane LOV2 fusion
pHR-LATmutTM-LOV2	LAT transmembrane LOV2fusion Bam KO
pHR-LATmutTM-LOV2 (No AGT)	LAT transmembrane LOV2fusion BamHI site intact
pHR-LAT-LOVpCA	Constitutively active LOVpep
pHR-LATmutTM-LOVpCA	Constitutively active LOVpep CRISPR proof
pHR-Zdk-LATint-Ruby	Zdk-LAT fusion protein
pHR-ePDZb1-LATint-Ruby	High affinity PDZ LAT fusion protein
pHR-ePDZb-LATint-Ruby	Mid affinity fusion protein
cpPDZ-LATint-Ruby	Low affinity PDZ fusion protein
pHR-ZDK-LATint-Ruby-IRES-LATtmLOV2	LOVTRAP IRES construct
pHR-ePDZb1-LATint-Ruby-IRES-LATtmLOVpep	High affinity TULIPs IRES construct
pHR-ePDZb-LATint-Ruby-IRES-LAT-TM-LOVpep	Mid affinity TULIPs IRES construct
pHR-cpPDZ-LATint-Ruby-IRES-LAT-TM-LOVpep	Low affinity TULIPs IRES construct
pHR-ePDZb1-LATint-Ruby-IRES-LATtmLOVpCA	Constitutively active IRES TULIPs construct
pHR-ZDK-LAT(AGT)int-Ruby-IRES-LATtmLOV2	LOVTRAP IRES construct PAM KO
pHR-ePDZb1-LAT(AGT)int-Ruby-IRES-LATtmLOVpep	High affinity TULIPs IRES construct PAM KO
pHR-ePDZb-LAT(AGT)int-Ruby-IRES-LAT-TM-LOVpep	Mid affinity TULIPs IRES construct PAM KO
pHR-cpPDZ-LAT(AGT)int-Ruby-IRES-LAT-TM-LOVpep	Low affinity TULIPs IRES construct PAM KO
pHR-ePDZb1-LAT(AGT)int-Ruby-IRES-LATtmLOVpCA	Constitutively active IRES TULIPs construct PAM KO
pHR-ZDK-LAT(AGT)int-Ruby-IRES-LATmutTMLOV2	LOVTRAP IRES construct CRISPR proof
pHR-ePDZb1-LAT(AGT)int-Ruby-IRES-LATmutTMLOVpep	High affinity TULIPs IRES construct CRISPR proof
pHR-ePDZb-LAT(AGT)int-Ruby-IRES-LAT-mutTM-LOVpep	Mid affinity TULIPs IRES construct CRISPR proof
pHR-cpPDZ-LAT(AGT)int-Ruby-IRES-LAT-mutTM-LOVpep	Low affinity TULIPs IRES construct CRISPR proof
pHR-ePDZb1-LAT(AGT)int-Ruby-IRES-LATmutTmLOVpCA	Constitutively active IRES TULIPs construct CRISPR proof
pHCr[LAT1]-GFP	LAT CRISPR construct
pHCr[LAT1]-GFP	LAT CRISPR construct
pHR-mTagBFP	BFP
pHRSV-IFP2-Erk2	Mid Erk expression reporter
pHR-IFP2-Erk2	High Erk expression reporter
pHRI-IFP2-Erk2	Low Erk expression reporter
pHR-Lck	
pHR-ICAM-1	
pHR-ZAP70-Ruby	
pHR-CD3	CD3 chains
pHR-(1G4)-TCR	1G4 TCR subunits
pHR-Zdk-LAT(AGT)int-ePDZb1-Ruby	LOVTRAP-TULIPs fusion high affinity
pHR-Zdk-LAT(AGT)int-ePDZb-Ruby	LOVTRAP-TULIPs fusion mid affinity
pHR-Zdk-LAT(AGT)int-cpPDZ-Ruby	LOVTRAP-TULIPs fusion low affinity
pHR-cpPDZ-LAT(AGT)int-Zdk-Ruby	LOVTRAP-TULIPs fusion low affinity
pHR-ePDZb-LAT(AGT)int-Zdk-Ruby	LOVTRAP-TULIPs fusion mid affinity
pHR-ePDZb1-LAT(AGT)int-Zdk-Ruby	LOVTRAP-TULIPs fusion high affinity
pHR-cpPDZ-LAT(AGT)int-Ruby-Zdk	LOVTRAP-TULIPs fusion low affinity

pHR-ePDZb-LAT(AGT)int-Ruby-Zdk	LOVTRAP-TULIPs fusion mid affinity
pHR-ePDZb1-LAT(AGT)int-Ruby-Zdk	LOVTRAP-TULIPs fusion high affinity
pHR-LAT(AGT)-Zdk-Ruby	
pHR-LAT(AGT)-ePDZb1-Ruby	
pHR-Zdk-LAT(AGT)int-Ruby-cpPDZ	LOVTRAP-TULIPs fusion low affinity
pHR-Zdk-LAT(AGT)int-Ruby-ePDZb	LOVTRAP-TULIPs fusion mid affinity
pHR-Zdk-LAT(AGT)int-Ruby-ePDZb1	LOVTRAP-TULIPs fusion high affinity
pHCM-CD43:45cyto-qGFP	
pHR-Junk-NTOM-LOV2F	Intermediate NTOM cloning vector
pHR-Junk-NTOM-LOVpF	Intermediate NTOM cloning vector
pHR-LATmutTM-LOV2-IRES-NTOM20-IFP2-LOVpF	
pHR-LATmutTM-LOV2-IRES-NTOM20-IFP2-LOVpep	
pHR-LATmutTM-LOVpep-IRES-NTOM20-iRFP670-LOV2	
pHR-LATmutTM-LOVpep-IRES-NTOM20-IFP2-LOV2	
pHR-LATmutTM-LOVpep-IRES-NTOM20-iRFP670-LOV2	
pHR-LATmutTM-LOVpF-IRES-NTOM20-IFP2-LOV2	
pHR-LATmutTM-LOV2-IRES-NTOM20-iRFP670-LOVpep	
pHR-LATmutTM-LOV2F-IRES-NTOM20-IFP2-LOVpF	
pHR-FcRH5-Ruby	TDB target
pHR-CaaX-IFP2	Membrane marker
pHR-Clover	Clover
pHR-CD86tm-Fv	Fv membrane tag
pHR-LATmutTM-ePDZb1-LAT(AGT)-Ruby	ePDZb1 LAT fusion protein
pHR-pMagFast2-LAT(AGT)-Ruby	Magnets LAT construct
pHR-LATmutTM-nMagHigh1	Magnets LAT transmembrane constructs
pHR-FRB-ZAP70-Citrine	CID ZAP70
pHR-CBP-P2A-Csk	
pHR-ePDZb1-LAT(AGT)-Ruby-IRES-LATmutTM-FRBpep	
pHR-ePDZb1-LAT(AGT)-Ruby-IRES-LATmutTM-pep	Truncated TULIPs constructs
pHR-LATmutTM-FKBP(Fv)	
pHR-LATmutTM-FRBpep	
pHR-IRES-LATmutTM-LOVpepCA	
pHR-IRES-LATmutTM-LOVpep	
pHR-IRES-LATmutTM-LOV2	
pHR-LATmutTM-qGFPpep	
pHR-FRB-LAT(AGT)-Ruby	
pHR-FRB-LAT(AGT)-Ruby-IRES-LATmutTM-FKBP	CID LAT system
pHR-pMagFast2-LAT(AGT)-Ruby-IRES-LATmutTM-nMagHigh1	Magnets LAT system
pHCr[x]	CRISPR
pHCr[x]-Ruby	CRISPR
pHCr[x]-eGFP	CRISPR
pHCr[x]-mTagBFP	CRISPR
pHCr[CD6-1]-Ruby	CD6 CRISPR
pHCr[CD6-2]-Ruby	CD6 CRISPR
pHCr[CD6-1.1]-Ruby	CD6 CRISPR
pHCr[CD6-1.2]-Ruby	CD6 CRISPR
pHCr[CD6-2.1]-Ruby	CD6 CRISPR
pHCr[CD6-2.2]-Ruby	CD6 CRISPR
pHR-myrZDK-LAT(AGT)-Ruby	Myristoylated ZDK
pHR-LATmutTM-LOV(C450G)	Photo-nonresponsive LOV2 domain
pHR-HA-Zdk-LAT(AGT)-Ruby	HA-tagged Zdk

pHR-LATmut TM -LOV2(V416T)	Fast-cycling LOV2
pHR-GFP-Erk2	
pHRI-myrZdk-LAT(AGT)-Ruby	Low expression myrZdk construct
pHR-Zdk-LAT(AGT)-Ruby-IRES-LATmut TM -LOV2(C450G)	
p8.91	
pMD2.G	
pHR-LATmut TM -LOV2(C450S)	
pHR-TCR G10 $\alpha\beta$ -qGFP	
pHR-TCR 1G4 $\alpha\beta$ -qGFP	
pHRI-LATdblmut-Ruby	Low expression LAT construct
pHRI-cPDZb1-LAT(AGT)-Ruby	Low expression, high affinity PDZ construct
pHRSV-Zdk-LAT(AGT)-Ruby	Mid expression Zdk construct
pHR ZAP70-BFP	
pHRSV-LATdblmut-Ruby	Mid expression LAT vector
pHRSV-cPDZb1-LAT(AGT)-Ruby	Mid expression, high affinity construct
pHR-ZAP70-qGFP (K369R)	
pHR-ZAP70-Ruby (K369R)	
pHCM-CD45(cyto)-qGFP	
pHR-ZAP70-BFP-K369R	
pHRI-ZDK-LAT(AGT)-Ruby	Low expression Zdk construct
pHR-mRuby2	RFP
pHR-NTOM-IFP2-LOV _{pep}	
pHR-NTOM-IFP2-LOV2	
pHR-NTOM-LOV2	pHR-NTOM-LAT-Ruby
pHR-Cherry-CaaX	Cherry membrane label
pCRY2 Δ NLS-FL-mCherry	Full length CRY2 construct
pCRY2PHR-Cherry	CRY2PHR
pCIBN-pmGFP	CaaX GFP CIBN
pHR-CIBN-pmGFP	Same as above, but pHR vector
pHR-CRY2PHR-LAT(AGT)-Ruby	CRY2 LAT system
pHR-CRY2PHR(L348F)-LAT(AGT)-Ruby	Slow cycling
pHR-CRY2PHR(W349R)-LAT(AGT)-Ruby	Fast cycling
pHR-CRY2(515)-LAT(AGT)-Ruby	Truncated CRY2
pHR-CRY2(535)-LAT(AGT)-Ruby	Truncated CRY2
pHR-CRY2 Δ NLS)-LAT(AGT)-Ruby	Full length CRY2
pHR-CRY2PHR(W374A)-LAT(AGT)-Ruby	Constitutive
pHR-CRY2PHR(G337E)-LAT(AGT)-Ruby	Dead CRY2
pHR-CRY2(535;G337E)-LAT(AGT)-Ruby	Dead, truncated CRY2
pHR-CRY2(535;W374A)-LAT(AGT)-Ruby	Constitutive, truncated CRY2
pHu[LAT]R-TagBFP	LAT siRNA
pHu[LAT]R-mCherry	LAT siRNA
pHCr[CD6-1]-BFP	CD6 CRISPR
pHCr[CD6-1]-GFP	CD6 CRISPR
pHR-HAFv86-LOV2	OptoCAR transmembrane
pHR-myrZDK-Zeta-Ruby	OptoCAR signalling
pBJneo	CD6
pHCr[CD6-3]-BFP	CD6 CRISPR
pHCr[CD6-3]-GFP	CD6 CRISPR
pHR-Zdk-LAT(YtoF)-Ruby	Non-functional Zdk LAT fusion
pHR-LAT (YtoF)-Ruby	Non-functional full length LAT
pHR-HAFv86-LOV _{pep}	TULIPs optoCAR

pHEFI-HAfv86-LOV2	Intron promoter OptoCAR
pHEFI-HAfv86-LOV2(C450G)	Intron promoter OptoCAR photo-nonresponsive
pHRI-LATmutTM-LOV2	Low expression LAT transmembrane
pHRSV-LATmutTM-LOV2	Mid expression LAT transmembrane
pHR-LATmutTM-LOV2(I539E)	Constitutively active LOV2
pHR-LATmutTM-LOV2(V416L)	Slow cycling LOV2
pHR-LATmutTM-LOVpep (C450G)	Photo-nonresponsive LOVpep
pHEFI-HAFv86-LOV2(I539E)	Intron promoter OptoCAR constitutively active
pHCr[ZetaEx1.1]	CD3 zeta CRISPR
pHCr[ZetaEx1.2]	CD3 zeta CRISPR
pHCr[ZetaEx1.1]-GFP	CD3 zeta CRISPR
pHCr[ZetaEx1.2]-GFP	CD3 zeta CRISPR
CIBN-CaaX	Membrane-bound CIBN
mCherry-CRY2-iSH2	
ePDZb1-Cherry-Caax	
pcDNA3.1 myc-p110a	P110alpha subunit myc tag
Zeta-LOV2 NO CRISPR	CD3 transmembrane LOV2, CRISPR proof
pHR-ZetaShort	CD3 zeta transmembrane domain
pHR-Zeta-LOV2	CD3zeta- LOV2 fusion
pHR-Zeta-LOV2(V416L)	CD3zeta- LOV2 fusion (slow)
pHR-Zeta-LOV2(I539E)	CD3zeta- LOV2 fusion (constitutively active)
pHR-Zeta-LOV2(C450G)	CD3zeta- LOV2 fusion (photo-nonresponsive)
Foxo1-wt-EGFP	
Foxo1-mut-EGFP	Does not translocate
pHR-NFAT-GFP:iRFP	
pHRI-BFP-Erk2	Low expression Erk reporter
pHRSV-BFP-Erk2	Mid expression Erk reporter

Appendix C

The script below was written in BeanShell and run on MicroManager1.4. It was used to automate the confocal imaging process. Annotations are denoted in the script by “//”.

```
//Place to save the image data
String acqName = "FileName";
String saveDir = "FilePath";

//Number of frames to capture
int numFramesPre = 5;
int numFramesDuring = 20;
int numFramesPost = 35;

//Length of time to expose LED source
int LEDExposure = 2; //seconds

//Name of Channels to use for the imaging
String[] channels = {"568Ex - 607Em", "640Ex - 708Em"};
Color[] colors = {Color.RED, Color.GREEN};
channelGroup = "BlueChannels";
//the channel strings

//Exposure Times for each channel required (in ms)
int[] exposures = {200, 200};

//Time between frames
int FrameDelay=1000;

//Whether to show the acquired data, and whether to save it or not
boolean shouldShow = true;
boolean shouldSave = true;

//***DONT CHANGE BEYOND HERE!***

//Make new channelgroup with blue filter
channelGroup = "BlueChannels";
if (mmc.isGroupDefined(channelGroup)) {
    mmc.deleteConfigGroup(channelGroup);}
mmc.defineConfigGroup(channelGroup);
//Make the 568 Channel
mmc.defineConfig(channelGroup,channels[0],"TICondenserCassette","State", "2"); //This moves condenser to 450nm
mmc.defineConfig(channelGroup,channels[0],"RotrWheel","State", "3");
mmc.defineConfig(channelGroup,channels[0],"Laser_568nm_TTL","State", "1"); //Laser 568nm On
mmc.defineConfig(channelGroup,channels[0],"Laser_640nm_TTL","State", "0"); //Laser 640nm off
//mmc.defineConfig(channelGroup,channels[0],"ESIOShutter","OnOff", "1");
mmc.defineConfig(channelGroup,channels[0],"Core","AutoShutter", "0");
mmc.defineConfig(channelGroup,channels[0],"Core","Shutter", "ALC");
//Make the 640 Channel
mmc.defineConfig(channelGroup,channels[1],"TICondenserCassette","State", "2"); //This moves condenser to 450nm
mmc.defineConfig(channelGroup,channels[1],"RotrWheel","State", "5");
mmc.defineConfig(channelGroup,channels[1],"Laser_640nm_TTL","State", "1"); //Laser 640nm On
mmc.defineConfig(channelGroup,channels[1],"Laser_568nm_TTL","State", "0"); //Laser 568nm Off
//mmc.defineConfig(channelGroup,channels[1],"ESIOShutter","OnOff", "1");
mmc.defineConfig(channelGroup,channels[1],"Core","AutoShutter", "0");
mmc.defineConfig(channelGroup,channels[1],"Core","Shutter", "ALC");

//Number of times/positions/slices to repeat the assay on same position
int numRepetitions=1;
int numSlices = 1;
int numPositions = 1;

//stop any acquisitions and refresh
gui.closeAllAcquisitions();
gui.refreshGUI();

//Create acquisition with defined values
int numFrames=numFramesPre + numFramesDuring + numFramesPost;
gui.openAcquisition(acqName, saveDir, numFrames, channels.length, numSlices, numPositions, shouldShow, shouldSave);

//Set the data for the channels in the defined acquisition
for (int i=0; i<colors.length; i++)
    gui.setChannelColor(acqName, i, colors[i]);
```

```

for (int i=0; i<channels.length; i++)
    gui.setChannelName(acqName, i, channels[i]);

//Make sure LED light is off before starting
mmc.setProperty("CoolLED_TTL", "State", "0");

gui.clearMessageWindow();

int i = 0; //Which channels to use
mmc.setConfig(channelGroup, channels[i]);
mmc.waitForConfig(channelGroup, channels[i]);

//Start the loop for imaging
start=System.currentTimeMillis(); //time from begin of acquisition

for (int k=0; k< numRepetitions; k++){
    mmc.setExposure(exposures[i]);
        for (int j=0; j<numFrames; j++) {
            for (int i=0; i<channels.length; i++) {
                mmc.setConfig(channelGroup, channels[i]);
                mmc.waitForConfig(channelGroup, channels[i]);

                //gui.snapAndAddImage(acqName,      frame_number,      channel_number,      slice_number,
position_number);

                gui.message("About to snap image: Frame " + (j+1) + ", Channel " + (channels[i]) + "
now");

                gui.snapAndAddImage(acqName, j, i, 0, 0); //Have removed variable for repetitions and
position as never likely to be used

            }
            //gui.sleep(2000); //Interval between frames
            if (j==numFramesPre-1){ //counter j starts from 0, so have minus 1 from value
                //Turn the light on and off using simple commands
                mmc.setProperty("TICCondenserCassette", "Label", "3-450nm");
                mmc.setProperty("CoolLED_TTL", "State", "1");
                gui.message("Turning blue light on now!");
                //gui.sleep(LEDExposure*1000); //Has to be in ms
                //mmc.setProperty("CoolLED Shutter", "State", 0);
            }
            if (j==numFramesPre+numFramesDuring-1){
                mmc.setProperty("CoolLED_TTL", "State", "0"); //turn off the LED
                gui.message("Turning blue light off now!");
            }
            while ((System.currentTimeMillis() - start) < FrameDelay*(j+1)) {gui.sleep(1);} //time already in ms

        }
    }

}

//To end the acquisition
mmc.setProperty("CoolLED_TTL", "State", "0");
mmc.deleteConfigGroup(channelGroup);
gui.closeAcquisition(acqName);
gui.refreshGUI();

```

Appendix D

The following script was used to interpret calcium flux data from the conjugate fluxing assay (Chapter 5). This script is written for use in Matlab. Annotations are denoted in green by “%”

```
clearvars -except BigDataMedian BigDataFraction;
clc;
%First get the CSV files to import...
[FileNames, PathName]=uigetfile({'*.csv'}, 'Select The CSV Files To Import...', 'MultiSelect',
'on');
if isequal(FileNames,0),
    clear;
    return;
else
    FileNames = cellstr(FileNames);
    NumFiles=length(FileNames);
end
%% Now get the default settings from user...
clearvars -except FileNames PathName NumFiles BigDataMedian BigDataFraction

qValues=doInputBox; %This opens dialog with all default values
drawnow;

% For 2500nM, time = 0:1:600, flux = 0:120 with 50 bins
% For 500nM, time = 0:1:600, flux = 0:180 with 75 bins

%Now assign the user inputted values to variables:
StartTime = qValues.StartTime;
EndTime = qValues.EndTime;
TimeWindow = qValues.TimeWindow;
MinFlux = qValues.MinFlux;
MaxFlux = qValues.MaxFlux;
NumHistSlices = qValues.NumHistSlices;
IndoBG = qValues.IndoBG;
IndoLObg = qValues.IndoLObg;
IndoHIbg = qValues.IndoHIbg;
IndoLOcol = qValues.IndoLOcol;
IndoHicol = qValues.IndoHicol;
Timecol = qValues.Timecol;
PreDrugTime = qValues.PreDrugTime;
InjectionTime = qValues.InjectionTime;
ThresholdVal = qValues.ThresholdVal;
ShowSurfPlots = qValues.ShowSurfPlots;
ShowIndFits = qValues.ShowIndFits;
ShowMeanPlots = qValues.ShowMeanPlots;

%% Retrieve data and derive parameters
close all;
for ii = 1:NumFiles,
    ThisFile = regexprep(FileNames{ii}, '\W', ''); % Get rid of any characters
    that violate Matlab code
    ThisFile = ['r' ThisFile(1:end-3)]; % Remove the csv tag
    from end of filename
    ThisFileFull=char(strcat(PathName,FileNames{ii})); % Make complete FilePath
    RawData.(ThisFile) =csvread(ThisFileFull,1); % Import the selected file,
    removing header row
end

h1=fields(RawData); % Get the names of files from
RawData structure
for ii = 1:length(h1),
    ThisFile=char(h1{ii}); % The file to work on
    DerivedData.(ThisFile)=(100*(RawData.(ThisFile) (:,IndoLOcol)-
IndoLObg)./(RawData.(ThisFile) (:,IndoHicol)-IndoHIbg)) - IndoBG; %Calculation of Derived
parameter in single column
    TimeData.(ThisFile)=RawData.(ThisFile) (:,Timecol); % Puts time data in separate
structure
end

NumTimeSlices=fix((EndTime-StartTime)/TimeWindow); % Calculate appropriate bounds
for time axis
histedges=linspace(MinFlux,MaxFlux,NumHistSlices+1); % Create bins for Indo-1 ratio
timeedges=linspace(StartTime,EndTime,NumTimeSlices+1); % Create bins for Time
```

```

for ii = 1:length(h1),
    ThisFile=char(h1(ii));
    [~,~,TimeBins.(ThisFile)]=histcounts(TimeData.(ThisFile),timeedges); % The file to work on
    % Parse time values
    into required bins
    Data.(ThisFile)=zeros(NumHistSlices+1,NumTimeSlices+1); % Create Data structure and
    add zero padding so surface displays all data
    NormData.(ThisFile)=zeros(NumHistSlices+1,NumTimeSlices+1); % Create Normalised Data
    structure and add zero padding so surface displays all data

    for i=1:NumTimeSlices,
        [N,~] = histcounts(DerivedData.(ThisFile)(TimeBins.(ThisFile)==i),histedges);
    % Bin the Indo-1 data into
        Data.(ThisFile)(1:NumHistSlices,i)=N';
        NormData.(ThisFile)(:,i)=100*(Data.(ThisFile)(:,i)/norm(Data.(ThisFile)(:,i)));
        NormData.(ThisFile)(isnan(NormData.(ThisFile)))=0;

        if timeedges(i) >= PreDrugTime && timeedges(i) < (PreDrugTime + InjectionTime),
            NormData.(ThisFile)(:,i)=0;
        end
    end
end

%% Get Median Values above Threshold
% User sets a defined value (could do by percentile?) and we use this to
% index data so only values above it are used to determine median value.
% Should be able to use the Derived data rather than histogram data

h1=fields(DerivedData);

fig1=figure;
hold on;
fig2=figure;
hold on;

for j=1:length(h1),
    ThisFile=char(h1(j));
    ThisName=ThisFile;

    AllFits.(ThisFile)=zeros(NumTimeSlices,6);
    for i=1:NumTimeSlices,
        TestY=NormData.(ThisFile)(:,i);
        ThisFit=createFit(histedges',TestY,ThresholdVal);
        ThisCoeffs=coeffvalues(ThisFit);
        AllFits.(ThisFile)(i,:)=ThisCoeffs;
        if timeedges(i) >= PreDrugTime && timeedges(i) < (PreDrugTime + InjectionTime),
            AllFits.(ThisFile)(i,:)=NaN;
        end
    end

    BGOffset=nanmean(AllFits.(ThisFile)(:,6));
    Threshold.(ThisFile)=smooth(AllFits.(ThisFile)(:,5),21) + BGOffset;
    PreBins=round(PreDrugTime/TimeWindow);

    for i=1:NumTimeSlices
        ThisThreshold(i)=Threshold.(ThisFile)(i)+BGOffset;
        ThisData=DerivedData.(ThisFile)(TimeBins.(ThisFile)==i);
        ThisThreshData = ThisData(ThisData > ThisThreshold(i));
        MedianData.(ThisFile)(i)=median(ThisThreshData) - Threshold.(ThisFile)(i); % Correct
    for baseline drift
        FractionData.(ThisFile)(i)=length(ThisThreshData)/length(ThisData); %%% This is
    wrong, do count not sum!!!!
        if timeedges(i) >= PreDrugTime && timeedges(i) < (PreDrugTime + InjectionTime),
            MedianData.(ThisFile)(i)=NaN;
            FractionData.(ThisFile)(i)=NaN;
        end
    end

    % Remove background values
    PreMedian=nanmean(MedianData.(ThisFile)(1:PreBins));
    PreFraction=nanmean(FractionData.(ThisFile)(1:PreBins));

    MedianDataCorr.(ThisFile)=MedianData.(ThisFile)-PreMedian;
    FractionDataCorr.(ThisFile)=FractionData.(ThisFile)-PreFraction;

```

```

disp([ThisFile]); drawnow;
figure(fig1);
plot(timeedges(2:end),MedianDataCorr.(ThisFile),'DisplayName', [ThisFile ' - Median' ]);
xlim([0 EndTime]);
set(gca,'XTick',0:30:510)
figure(fig2);
plot(timeedges(2:end),FractionDataCorr.(ThisFile),'DisplayName', [ThisFile ' - Median' ]);
xlim([0 EndTime]);
set(gca,'XTick',0:30:510)
%ylim([0 1]);
end

%% Show Surface Plots, if required
ShowSurfPlots = true;
if ShowSurfPlots == true,

    %load('HeatColourMap.mat');

    h1=fields(DerivedData);
    for ii = 1:length(h1),
        ThisFile=char(h1(ii));
        figure;
        %surf(timeedges,histedges,NormData.(ThisFile));
        imagesc(timeedges,histedges,NormData.(ThisFile));
        set(gca,'YDir','normal');
        title(ThisFile,'interpreter','none');
        %axis square;
        xlim([0 EndTime]);
        ylim([0 MaxFlux]);
        %mycmap=HeatCMap;
        %colormap(mycmap);
        xlabel('Time (s)');
        ylabel('Indo-1 Ratio');
        set(gca,'YDir','normal')
        set(gca,'XTick',0:30:510)
        %caxis([0 25]);
        view([0 90]);
        hold on;

    plot3(timeedges(2:end),Threshold.(ThisFile),repmat(MaxFlux,1,NumTimeSlices),'LineWidth',1,'Color','k','LineStyle','--');
    end
end

%% Average Data plots
h2=fields(MedianDataCorr);
fig3=figure;
hold on;
fig4=figure;
hold on;
fig5=figure;
hold on;

sumMedian=0;
sumFraction=0;
sumSTDEV = 0;
for i=1:length(h2),

    tempMedian(i,:) = MedianDataCorr.(h2{i});
    tempFraction(i,:) = FractionDataCorr.(h2{i});
end
MedianDataCorr.Mean = mean(tempMedian());
MedianDataCorr.STDEV = std(tempMedian());
MedianDataCorr.SEM = std(tempMedian()) / sqrt(NumFiles);
FractionDataCorr.Mean = mean(tempFraction());
FractionDataCorr.STDEV = std(tempFraction());
FractionDataCorr.SEM = std(tempFraction()) / sqrt(NumFiles);

figure(fig3);
plot(timeedges(2:end),MedianDataCorr.Mean,'DisplayName', ['Median']);
xlim([0 EndTime]);
ylim([-5 20]);
xlabel('Time (s)');

```

```

ylabel('Indo-1 Ratio');

figure(fig4);
plot(timeedges(2:end),FractionDataCorr.Mean,'DisplayName', ['Fraction']);
xlim([0 EndTime]);
ylim([0 1]);
xlabel('Time (s)');
ylabel('Fraction Activated');

figure(fig5);
plot3(timeedges(2:end),MedianDataCorr.Mean,FractionDataCorr.Mean,'DisplayName', h2{j});
xlim([0 EndTime]);
zlim([0 1]);
xlabel('Time (s)');
ylabel('Indo-1 Ratio');
axis square; grid on;
view([-40 34]);
drawnow;

%%
%Make some plots wiht shaded errors
figure;
shadedErrorBar(timeedges(2:end),MedianDataCorr.Mean,MedianDataCorr.STDEV);
figure;
smoothData = smooth(MedianDataCorr.Mean,3,'moving');
smoothErr=smooth(MedianDataCorr.SEM,3,'moving');
shadedErrorBar(timeedges(2:end),smoothData,smoothErr);
figure;
smoothData2 = smooth(FractionDataCorr.Mean,3,'moving');
smoothErr2=smooth(FractionDataCorr.SEM,3,'moving');
shadedErrorBar(timeedges(2:end),smoothData2,smoothErr2);

%% Make BigData!
%Change Condition...
BigDataFraction.Nada=FractionDataCorr;
BigDataMedian.Nada=MedianDataCorr;

function [ answer ] = doInputBox()
%UNTITLED2 Summary of this function goes here
% Detailed explanation goes here

%Change the box size here
BoxSize=50;

Title = 'User Inputs for Ca Flux Analysis';
Prompt = {};
Formats = {};
DefAns = struct([]);

Prompt(1,:) = {'Start Time','StartTime','s'};
Formats(1,1).required = 'on'; % StartTime
Formats(1,1).type = 'edit';
Formats(1,1).format = 'integer';
Formats(1,1).unitsloc = 'rightmiddle';
Formats(1,1).size = BoxSize; % automatically assign the height
DefAns(1).StartTime=0;

Prompt(2,:) = {'End Time','EndTime','s'};
Formats(1,2).required = 'on'; % EndTime
Formats(1,2).type = 'edit';
Formats(1,2).format = 'integer';
Formats(1,2).unitsloc = 'rightmiddle';
Formats(1,2).size = BoxSize; % automatically assign the height
DefAns.EndTime=390;

Prompt(3,:) = {'Time Window','TimeWindow','s'};
Formats(1,3).required = 'on'; % TimeWindow
Formats(1,3).type = 'edit';
Formats(1,3).format = 'integer';
Formats(1,3).unitsloc = 'rightmiddle';
Formats(1,3).size = BoxSize; % automatically assign the height
DefAns.TimeWindow=3;

Prompt(4,:) = {'Min Flux','MinFlux',''};
Formats(2,1).required = 'on'; % MinFlux
Formats(2,1).type = 'edit';

```

```

Formats(2,1).format = 'integer';
Formats(2,1).size = BoxSize; % automatically assign the height
DefAns.MinFlux=0;

Prompt(5,:) = {'Max Flux'},['MaxFlux'],[''];
Formats(2,2).required = 'on'; % MaxFlux
Formats(2,2).type = 'edit';
Formats(2,2).format = 'integer';
Formats(2,2).size = BoxSize; % automatically assign the height
DefAns.MaxFlux=120;

Prompt(6,:) = {'Flux Bins'},['NumHistSlices'],[''];
Formats(2,3).required = 'on'; % NumHistSlices
Formats(2,3).type = 'edit';
Formats(2,3).format = 'integer';
Formats(2,3).size = BoxSize; % automatically assign the height
DefAns.NumHistSlices=50;

Prompt(7,:) = {'Column numbers for the required parameters'},[],[];
Formats(3,2).type = 'text';
Formats(3,2).span = [1 2];

Prompt(8,:) = {'Indo1 (UV-405)'},['IndoLOcol'],[''];
Formats(4,1).required = 'on'; % IndoLOcol
Formats(4,1).type = 'edit';
Formats(4,1).format = 'integer';
Formats(4,1).size = BoxSize; % automatically assign the height
DefAns.IndoLOcol=1;

Prompt(9,:) = {'Indo1 (UV-485)'},['IndoHicol'],[''];
Formats(4,2).required = 'on'; % IndoLOcol
Formats(4,2).type = 'edit';
Formats(4,2).format = 'integer';
Formats(4,2).size = BoxSize; % automatically assign the height
DefAns.IndoHicol=2;

Prompt(10,:) = {'Time (ms)'},['Timeecol'],[''];
Formats(4,3).required = 'on'; % IndoLOcol
Formats(4,3).type = 'edit';
Formats(4,3).format = 'integer';
Formats(4,3).size = BoxSize; % automatically assign the height
DefAns.Timeecol=3;

Prompt(11,:) = {'Background values for Indo-1 parameters'},[],[];
Formats(5,2).type = 'text';
Formats(5,2).span = [1 2];

Prompt(12,:) = {'Indo1 (UV-405)'},['IndoLObg'],[''];
Formats(6,1).required = 'on'; % IndoLOcol
Formats(6,1).type = 'edit';
Formats(6,1).format = 'integer';
Formats(6,1).size = BoxSize; % automatically assign the height
DefAns.IndoLObg=0;

Prompt(13,:) = {'Indo1 (UV-485)'},['IndoHIbg'],[''];
Formats(6,2).required = 'on'; % IndoLOcol
Formats(6,2).type = 'edit';
Formats(6,2).format = 'integer';
Formats(6,2).size = BoxSize; % automatically assign the height
DefAns.IndoHIbg=0;

Prompt(14,:) = {'Indo-1 Ratio'},['IndoBG'],[''];
Formats(6,3).required = 'on'; % IndoLOcol
Formats(6,3).type = 'edit';
Formats(6,3).format = 'integer';
Formats(6,3).size = BoxSize; % automatically assign the height
DefAns.IndoBG=20;

Prompt(15,:) = {'Other parameters to set'},[],[];
Formats(7,2).type = 'text';
Formats(7,2).span = [1 2];

Prompt(16,:) = {'Time before stimulus'},['PreDrugTime'],['s'];
Formats(8,1).required = 'on'; % IndoLOcol
Formats(8,1).type = 'edit';
Formats(8,1).format = 'integer';
Formats(8,1).unitsloc = 'rightmiddle';

```

```

Formats(8,1).size = BoxSize; % automatically assign the height
DefAns.PreDrugTime=60;

Prompt(17,:) = {'Time needed for Injection'},['InjectionTime'],['s'];
Formats(8,2).required = 'on'; % IndoLOcol
Formats(8,2).type = 'edit';
Formats(8,2).format = 'integer';
Formats(8,2).unitsloc = 'rightmiddle';
Formats(8,2).size = BoxSize; % automatically assign the height
DefAns.InjectionTime=20;

Prompt(18,:) = {'Indo-1 peak separation value'},['ThresholdVal'],[''];
Formats(8,3).required = 'on'; % IndoLOcol
Formats(8,3).type = 'edit';
Formats(8,3).format = 'integer';
Formats(8,3).size = BoxSize; % automatically assign the height
DefAns.ThresholdVal=30;

Prompt(19,:) = {'Show Plots?'},[],[];
Formats(9,2).type = 'text';
Formats(9,2).span = [1 2];

Prompt(20,:) = {'Surface Plots'},['ShowSurfPlots'],[''];
Formats(10,1).required = 'on'; % IndoLOcol
Formats(10,1).type = 'check';
Formats(10,1).format = 'logical';
DefAns.ShowSurfPlots=false;

Prompt(21,:) = {'Individual Fits'},['ShowIndFits'],[''];
Formats(10,2).required = 'on'; % IndoLOcol
Formats(10,2).type = 'check';
Formats(10,2).format = 'logical';
DefAns.ShowIndFits=false;

Prompt(22,:) = {'Mean Plot'},['ShowMeanPlots'],[''];
Formats(10,3).required = 'on'; % IndoLOcol
Formats(10,3).type = 'check';
Formats(10,3).format = 'logical';
DefAns.ShowMeanPlots=true;

Options.AlignControls = 'on';

answer = inputsdlg(Prompt,Title,Formats,DefAns,Options);

end

```

Appendix E

The following script was written in Matlab for the purpose of peak separation from the GFP reporter and CD69 data, Chapter 5. Annotations are denoted by “%”

```
clear;
clc;
close all;
%%Find background variance value from negative control
%First get the CSV files for the background data
[FileNames, PathName]=uigetfile({'*.csv'},'Select The CSV Files To Import...','MultiSelect',
'on');
if isequal(FileNames,0),
    clear;
    return;
else
    FileNames = cellstr(FileNames);
    NumFiles=length(FileNames);
end

clearvars -except FileNames PathName NumFiles

% Retrieve data

close all;
for ii = 1:NumFiles,
    ThisFile = regexprep(FileNames{ii},'\W',''); % Get rid of any characters
    % that violate Matlab code
    ThisFile = ThisFile(1:end-3); % Remove the csv tag from end
    % of filename
    ThisFileFull=char(strcat(PathName,FileNames{ii})); % Make complete FilePath
    RawData.(ThisFile) =csvread(ThisFileFull,1); % Import the selected file,
    % removing header row
    tempData1 = RawData.(ThisFile) (:,1);
    tempData1 = tempData1(tempData1>0);
    tempData2 = RawData.(ThisFile) (:,2);
    tempData2 = tempData2(tempData2>0);
    %LogData.(ThisFile). = zeros(length(:,2));
    LogRawData.(ThisFile).GFP = log10(tempData1);
    LogRawData.(ThisFile).R670 = log10(tempData2);
end

MinFlux=1; %Consider entering these values from the input box in the future.
MaxFlux=100000;
NumHistSlices=1000;

histedges=linspace(log10(MinFlux),log10(MaxFlux),NumHistSlices+1);

h1=fields(LogRawData);
for ii = 1:length(h1),
    ThisFile=char(h1{ii}); % The file to work on
    BinData.(ThisFile).GFP=zeros(NumHistSlices+1,1); % Create Data structure and add zero
    % padding so surface displays all data
    BinData.(ThisFile).R670=zeros(NumHistSlices+1,1); % Create Data structure and add zero
    % padding so surface displays all data
    [N,~] = histcounts(LogRawData.(ThisFile).GFP,histedges); % Bin the Indo-1
    % data into
    BinData.(ThisFile).GFP(1:NumHistSlices)=N';
    [N,~] = histcounts(LogRawData.(ThisFile).R670,histedges); % Bin the Indo-1
    % data into
    BinData.(ThisFile).R670(1:NumHistSlices)=N';
end

%%
%%Define background peak for both variables
fig1=figure;
hold on;
fig2=figure;
hold on;
for j=1:length(h1),
    ThisFile=char(h1{j});
    ThresholdGFP =2.5;
    ThresholdR670 =2.25;
```

```

%Define the background curve for GFP channel (NFAT reporter)
TestYGFP=BinData.(ThisFile).GFP;
%       ThisFit=createFit(histedges',TestYR670,ThresholdR670);
%       ThisFit=createFitNoThresh(histedges',TestYR670);
smoothDataGFP=smooth(TestYGFP,51);

figure(fig1);
plot(histedges',TestYGFP);
hold on;
plot(histedges',smoothDataGFP);
xlim([0 5]);

bgGFP=smoothDataGFP;

%Repeat and find the background curve for the R670 channel (CD69)
TestYR670=BinData.(ThisFile).R670;
%       ThisFit=createFit(histedges',TestYR670,ThresholdR670);
%       ThisFit=createFitNoThresh(histedges',TestYR670);
smoothDataR670=smooth(TestYR670,51);

figure(fig2);
plot(histedges',TestYR670);
hold on;
plot(histedges',smoothDataR670);
xlim([0 5]);

bgR670=smoothDataR670;
hold on;

end
% %%
%can now use this proxy background peak to perform background subtraction
%calculations. Replace this variable by using appropriate controls during
%the FACS run.

%% Now that you have defined the background values proceed to the rest of the data
clearvars -except bgR670 bgGFP pBGR670 pBGGFP offsetR670 offsetGFP
[FileNames, PathName]=uigetfile({'*.csv'}, 'Select The CSV Files To Import...', 'MultiSelect',
'on');
if isequal(FileNames,0),
    clear;
    return;
else
    FileNames = cellstr(FileNames);
    NumFiles=length(FileNames);
end

for ii = 1:NumFiles,
    ThisFile = regexprep(FileNames{ii},'\W',''); % Get rid of any characters
    that violate Matlab code
    ThisFile = ThisFile(1:end-3); % Remove the csv tag from end
    of filename
    ThisFileFull=char(strcat(PathName,FileNames{ii})); % Make complete FilePath
    RawData.(ThisFile) =csvread(ThisFileFull,1); % Import the selected file,
    removing header row
    tempData1 = RawData.(ThisFile) (:,1);
    tempData1 = tempData1(tempData1>0);
    tempData2 = RawData.(ThisFile) (:,2);
    tempData2 = tempData2(tempData2>0);
    %LogData.(ThisFile). = zeros(length(,2);
    LogRawData.(ThisFile).GFP = log10(tempData1);
    LogRawData.(ThisFile).R670 = log10(tempData2);
end

MinFlux=1;
MaxFlux=100000;
NumHistSlices=1000;

histedges=linspace(log10(MinFlux),log10(MaxFlux),NumHistSlices+1); % Create bins
for Indo=1 ratio

h1=fields(LogRawData);
for ii = 1:length(h1),
    ThisFile=char(h1(ii)); % The file to work on

```

```

        BinData.(ThisFile).GFP=zeros(NumHistSlices+1,1);      % Create Data structure and add zero
padding so surface displays all data
        BinData.(ThisFile).R670=zeros(NumHistSlices+1,1);    % Create Data structure and add zero
padding so surface displays all data
        [N,~] = histcounts(LogRawData.(ThisFile).GFP,histedges);      % Bin the Indo-1
data into
        BinData.(ThisFile).GFP(1:NumHistSlices)=N';
        [N,~] = histcounts(LogRawData.(ThisFile).R670,histedges);      % Bin the Indo-1
data into
        BinData.(ThisFile).R670(1:NumHistSlices)=N';
end
%% smooth and plot data
h1=fields(LogRawData);
fig3=figure;
hold on;
fig4=figure;
hold on;
for j=1:length(h1),
    ThisFile=char(h1(j));
    ThresholdGFP =2.5;
    ThresholdR670 =2.7;

    TestYGFP=BinData.(ThisFile).GFP;
    smoothData=smooth(TestYGFP, 51);
    %         ThisFit=createFit(histedges',TestYGFP,ThresholdGFP);
    %         ThisFit=createFitNoThresh(histedges',TestYGFP);
    figure(fig3);
    subplot(4,6,j); %should proably figure out a better way to layout theses figures
    plot(histedges',TestYGFP);
    hold on;
    plot(histedges',smoothData)
    xlim([0 5]);
    allSmooth.(ThisFile).GFP=smoothData;%Think about making the smoothData bit an input
variable that can be changed day to day.

    TestYR670=BinData.(ThisFile).R670;
    smoothData=smooth(TestYR670, 51);
    %         ThisFit=createFit(histedges',TestYR670,ThresholdR670);
    %         ThisFit=createFitNoThresh(histedges',TestYR670);
    figure(fig4);
    subplot(4,6,j);
    plot(histedges',TestYR670);
    hold on;
    plot(histedges',smoothData);
    xlim([0 5]);
    allSmooth.(ThisFile).R670=smoothData;
end
%%
%Calculate the background peak from your data and subtract the background
%Need to make this into a loop for all of the data...
h1=fields(LogRawData);
fig5=figure;
hold on;
fig6=figure;
hold on;

%Calculate shift in amplitude between background and data background peak.
%Plot background data against samples and show background subtracted data.
for j=1:length(h1),
    ThisFile=char(h1(j));
    smoothDataR670=allSmooth.(ThisFile).R670;

    [bgR670max, bgR670idx] = max(bgR670);
    bgR670xval = max(histedges(bgR670max == bgR670));
    %     mask1 = (histedges < bgR670xval-(offsetR670/1000)); %This is if using proxy background
    mask1 = (histedges < bgR670xval);
    z0 = 5;
    tol = 0.0001;
    token=1;
    prevSum = 1e6;
    count = 0;
    while token
        newSum = (z0 * bgR670(mask1)) - smoothDataR670(mask1);
        newSum = sum(sqrt((newSum).^2));

        if newSum > prevSum
            token = 0;

```

```

        else
            prevSum=newSum;
            z0=z0-tol;
        end

        count = count + 1;

    end
    disp(z0);
    disp(count);
    figure(fig5);
    subplot(4,6,j);
    plot(histedges,smoothDataR670);
    hold on
    plot(histedges,bgR670);
    plot(histedges,z0*bgR670);
    %     plot(histedges,pBGR670);
    %     plot(histedges,z0*pBGR670);
    xlim([0 5]);
    bgCorrR670=smoothDataR670-(z0*bgR670);
    %     bgCorrR6702=smoothDataR670-(z0*pBGR670);
    plot(histedges,bgCorrR670);
    %     plot(histedges,bgCorrR6702');
    allCorr.(ThisFile).R670=bgCorrR670;
    %     allCorr2.(ThisFile).R670=bgCorrR6702;
    allBgAdjusted.(ThisFile).R670=z0*bgR670;
    %     allBgAdjusted2.(ThisFile).R670=z0*pBGR670;
end
% z0=0:tol:5;
% newSum = (z0 .* bgR670(mask1)) - smoothDataR670(mask1);
% newSum = sum(sqrt((newSum).^2));
% plot(z0,newSum);

%Repeat for GFP values
for j=1:length(h1),
    ThisFile=char(h1(j));
    smoothDataGFP=allSmooth.(ThisFile).GFP;

    [bgGFPmax, bgGFPidx] = max(bgGFP);
    bgGFPxval = max(histedges(bgGFPmax == bgGFP));
    %     mask1 = (histedges < bgGFPxval-(offsetGFP/1000));
    mask1 = (histedges < bgGFPxval);
    z0 = 5;
    tol = 0.0001;
    token=1;
    prevSum = 1e6;
    count = 0;
    while token
        newSum = (z0 * bgGFP(mask1)) - smoothDataGFP(mask1);
        newSum = sum(sqrt((newSum).^2));

        if newSum > prevSum
            token = 0;
        else
            prevSum=newSum;
            z0=z0-tol;
        end

        count = count + 1;

    end
    disp(z0);
    disp(count);
    figure(fig6);
    subplot(4,6,j);
    plot(histedges,smoothDataGFP);
    hold on;
    plot(histedges,bgGFP);
    plot(histedges,z0*bgGFP);
    %     plot(histedges,pBGGFP);
    %     plot(histedges,z0*pBGGFP);
    xlim([0 5]);
    bgCorrGFP=smoothDataGFP-(z0*bgGFP); %subtract actual background peak from data
    %     bgCorrGFP2=smoothDataGFP-(z0*pBGGFP);%subtract proxy background peak from data
    plot(histedges,bgCorrGFP);
    %     plot(histedges,bgCorrGFP2);
    allCorr.(ThisFile).GFP=bgCorrGFP;

```

```

%     allCorr2.(ThisFile).GFP=bgCorrGFP2;
%     allBgAdjusted.(ThisFile).GFP=z0*bgGFP;
%     allBgAdjusted2.(ThisFile).GFP=z0*pBGGFP;
end

%Will need to create a data mask to specify the actual peak that we are
%interested in. This can then be used to calculate the percentage of
%activated cells.

%This data will probably need to be adjusted to shift the peak left/right
%%
%Plot the postive peaks only.
h1=fields(LogRawData);
fig7=figure;
hold on;
fig8=figure;
hold on;
fig9=figure;
hold on;
fig10=figure;
hold on;
%calculate the area under the positive curve for R670
mask5 = (histedges >= bgR670xval);
mask6 = (histedges >= bgGFPxval);

for j=1:length(h1),
    ThisFile=char(h1(j));

    TempData=allCorr.(ThisFile).R670; %corrected to actual background
%     TempData2=allCorr2.(ThisFile).R670; %corrected to proxy background
    smoothData=allSmooth.(ThisFile).R670;
    BgAdjData=allBgAdjusted.(ThisFile).R670;
%     BgAdjData2=allBgAdjusted2.(ThisFile).R670;

    figure(fig7);
    subplot(4,6,j);
    TempData(TempData<0)=0; %make all subzero values equivalent to zero.
    plot(histedges,TempData);
    hold on;

        plot(histedges,smoothData);
%     plot(histedges,BgAdjData);
    plot(histedges,BgAdjData);
    plot(histedges(mask5),TempData(mask5));
%     plot(histedges(mask4),TempData(mask4));
    xlim([0 5]);

    PosArea=trapz(histedges,TempData);
    totalArea=trapz(histedges,smoothData);
        OutputR670(j,1) = PosArea;
        OutputR670(j,2) = totalArea;
        OutputR670(j,3) = OutputR670(j,1)/OutputR670(j,2);
    figure(fig9);
    hold on
        title('Background Adjusted Areas')
        ylabel('Fraction of Cells Activated w/o Background')
        bar(OutputR670(:,3));
        xlim([0 (length(FileNames)+0.5)]);
        ylim([0 1])
end

for j=1:length(h1),
    ThisFile=char(h1(j));

    TempData=allCorr.(ThisFile).GFP;
%     TempData2=allCorr2.(ThisFile).GFP; %corrected to proxy background
    smoothData=allSmooth.(ThisFile).GFP;
    BgAdjData=allBgAdjusted.(ThisFile).GFP;
%     BgAdjData2=allBgAdjusted2.(ThisFile).GFP;
    figure(fig8);
    subplot(4,6,j);
    hold on;
    TempData(TempData<0)=0;
    plot(histedges,TempData)
    plot(histedges,smoothData);
    hold on;
    plot(histedges,BgAdjData);

```

```

plot(histedges(mask6),TempData(mask6));
xlim([0 5]);

PosArea=trapz(histedges(mask6),TempData(mask6));
totalArea=trapz(histedges,smoothData);
    OutputGFP(j,1) = PosArea;
    OutputGFP(j,2) = totalArea;
    OutputGFP(j,3) = OutputGFP(j,1)/OutputGFP(j,2);
figure(fig10)
hold on
    title('Background Adjusted Areas')
    ylabel('Fraction of Cells Activated w/o Background')
    bar(OutputGFP(:,3));
    xlim([0 (length(FileNames)+0.5)]);
    ylim([0 0.80])
end
%%
%Calculate median of activated cells
mask5 = (histedges > bgR670xval);
mask6 = (histedges > bgGFPxval);
for j=1:length(h1),
    ThisFile=char(h1(j));

    diffdata = allCorr.(ThisFile).R670;
    diffdata(diffdata<0)=0;
    sum1 = sum(histedges(mask5).*diffdata(mask5)); %Mean calculations
    sum2 = sum(diffdata(mask5)); %Mean calculations

    medianR670 = bgR670xval + 0.001;
    maskpre = mask5 & (histedges < medianR670);
    maskpost = (histedges >= medianR670);
    while trapz(histedges(maskpre),diffdata(maskpre)) <
trapz(histedges(maskpost),diffdata(maskpost))
        medianR670 = medianR670 + 0.01;
        maskpre = mask5 & (histedges < medianR670);
        maskpost = (histedges >= medianR670);
    end

    OutputR670(j,4)=medianR670;
    OutputR670(j,5)=sum1/sum2;
end

for j=1:length(h1),
    ThisFile=char(h1(j));

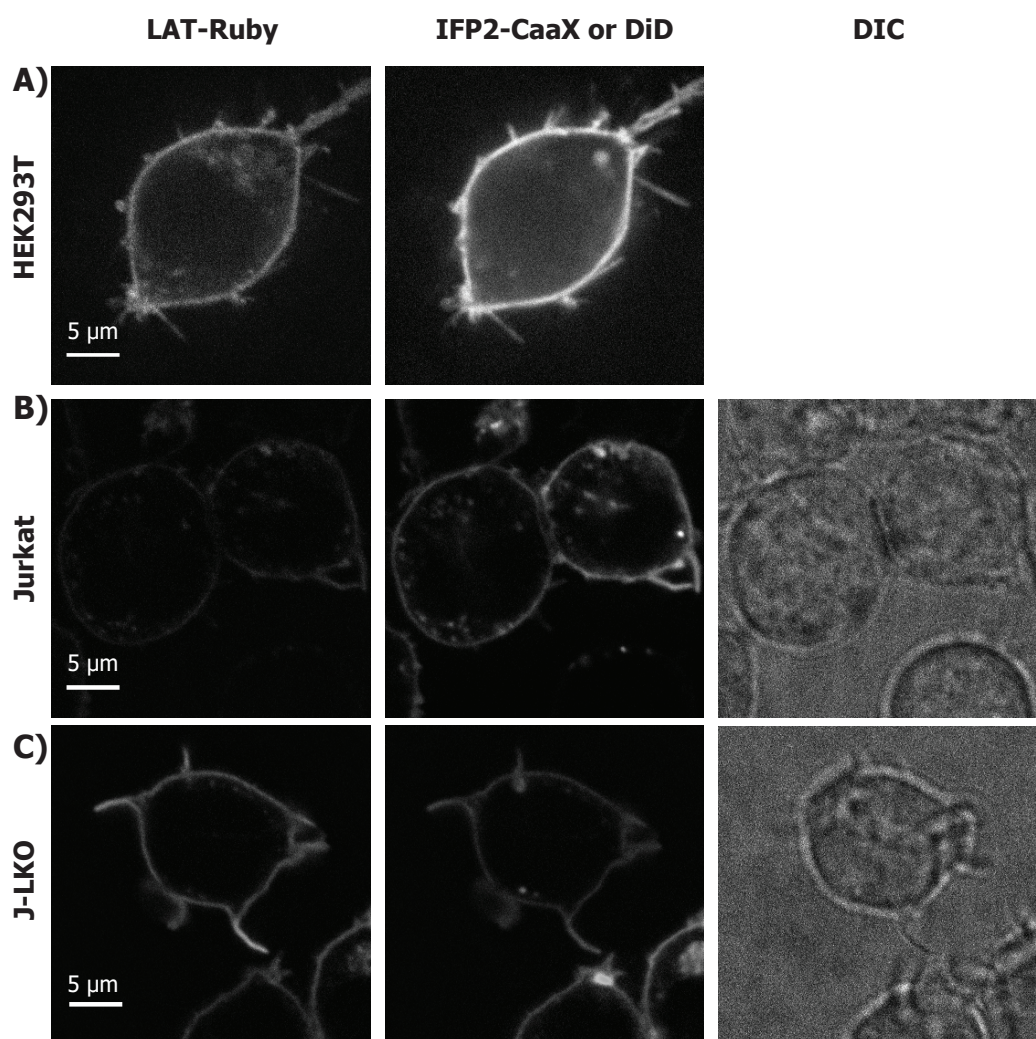
    diffdata = allCorr.(ThisFile).GFP;
    diffdata(diffdata<0)=0;

    sum1 = sum(histedges(mask6).*diffdata(mask6)); %Mean calculations
    sum2 = sum(diffdata(mask6)); %Mean calculations

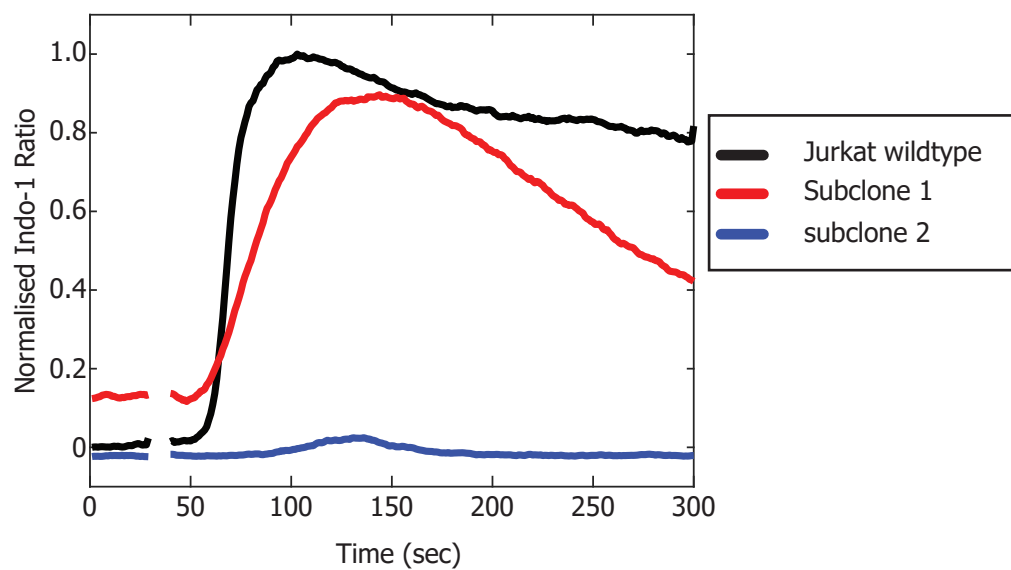
    medianGFP = bgGFPxval + 0.001;
    maskpre = mask6 & (histedges < medianR670);
%    maskpre = (histedges < medianGFP);
    maskpost = histedges >= medianGFP;
    while trapz(histedges(maskpre),diffdata(maskpre)) <
trapz(histedges(maskpost),diffdata(maskpost))
        medianGFP = medianGFP + 0.01;
        maskpre = (histedges < medianR670) & mask6;
%    maskpre = (histedges < medianGFP);
        maskpost = (histedges > medianGFP);
    end

    OutputGFP(j,4)=medianGFP;
    OutputGFP(j,5)=sum1/sum2;
end

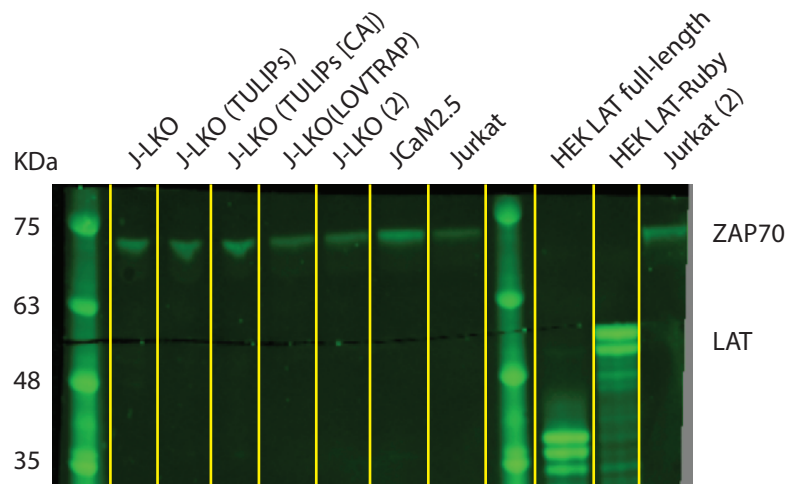
```



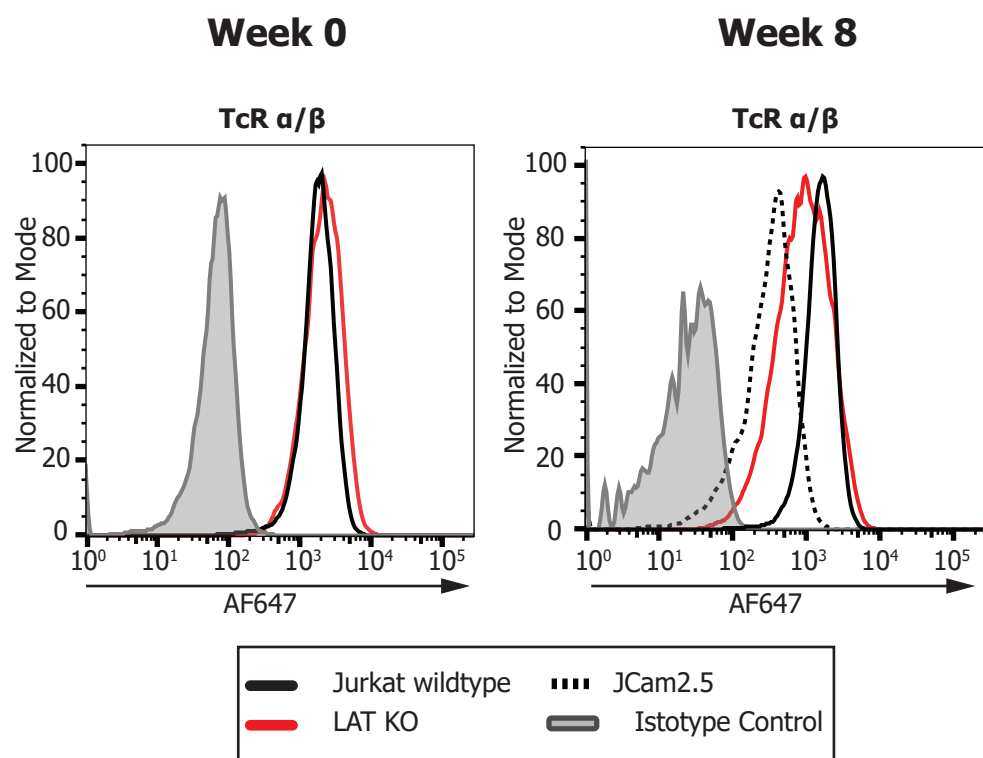
Appendix F (A) HEK293T cells expressing full-length LAT-Ruby **(B)** Jurkat E6.1 Cells expressing full-length LAT-Ruby **(C)** J-LKO cells expressing full-length LAT-Ruby



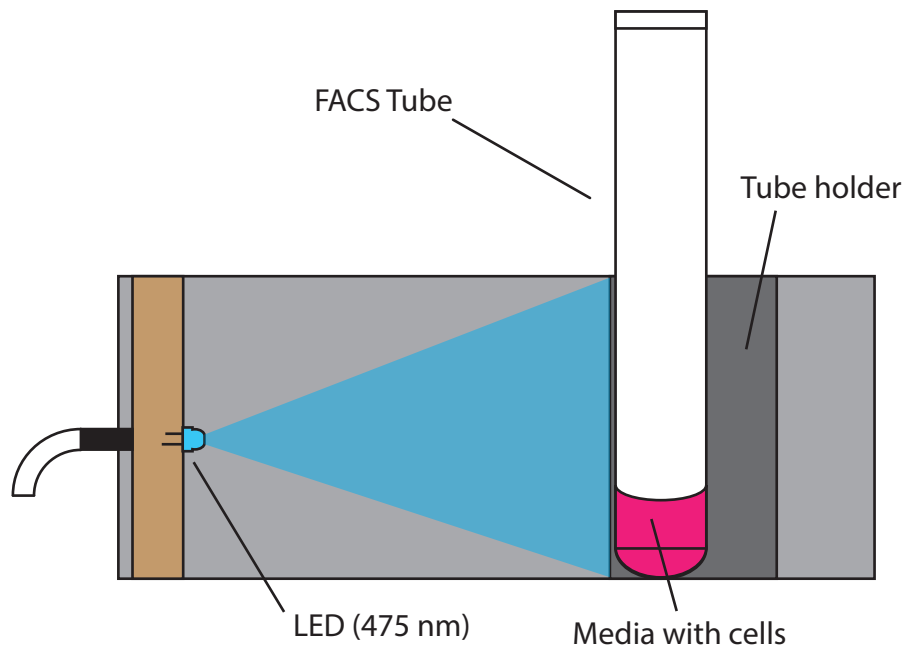
Appendix G Single cell cloning of the Jurkat LAT CRISPR cell lines provided us with a range of different clones. Shown above are the representative flux profiles relative to the Jurkat parental cell line.



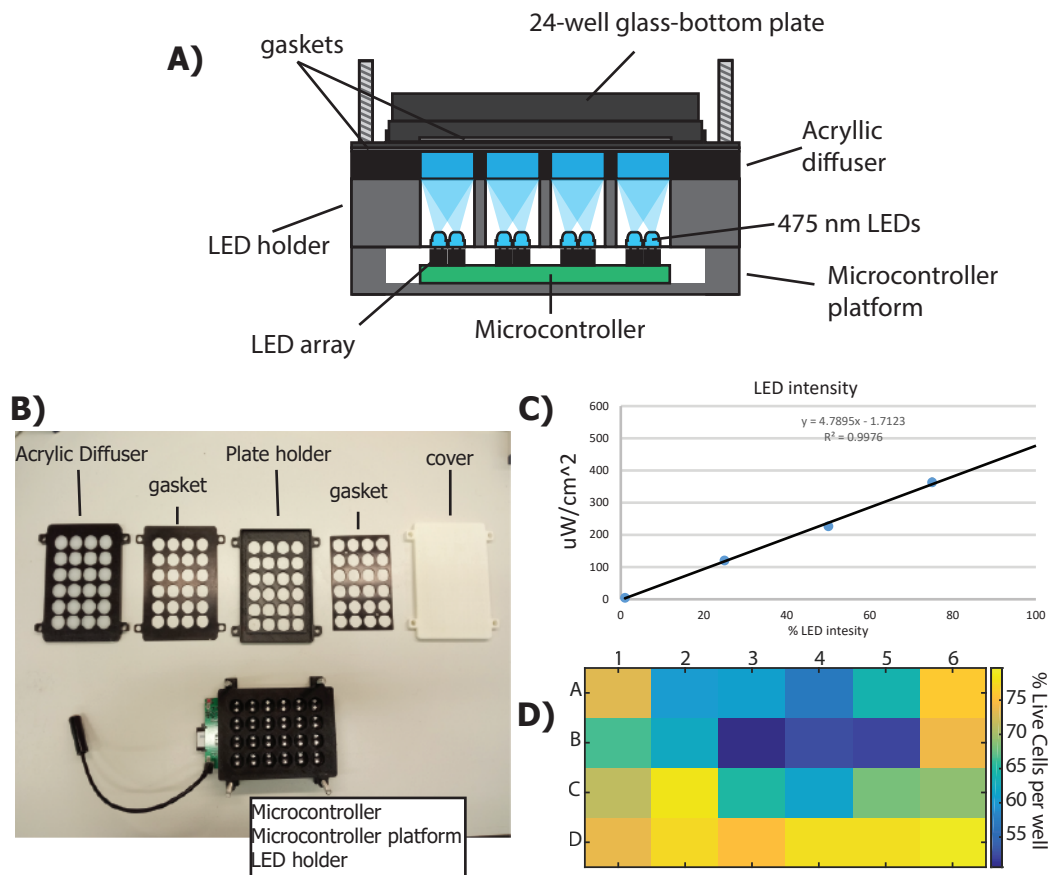
Appendix H Prior to intracellular FACS, I used immunoblotting to interrogate LAT expression. Shown above is the J-LKO cell line transduced with the IRES versions of the TULIPs and LOVTRAP constructs. ZAP70 was used as the input control. HEK293T cells were used as an expression control for LAT.



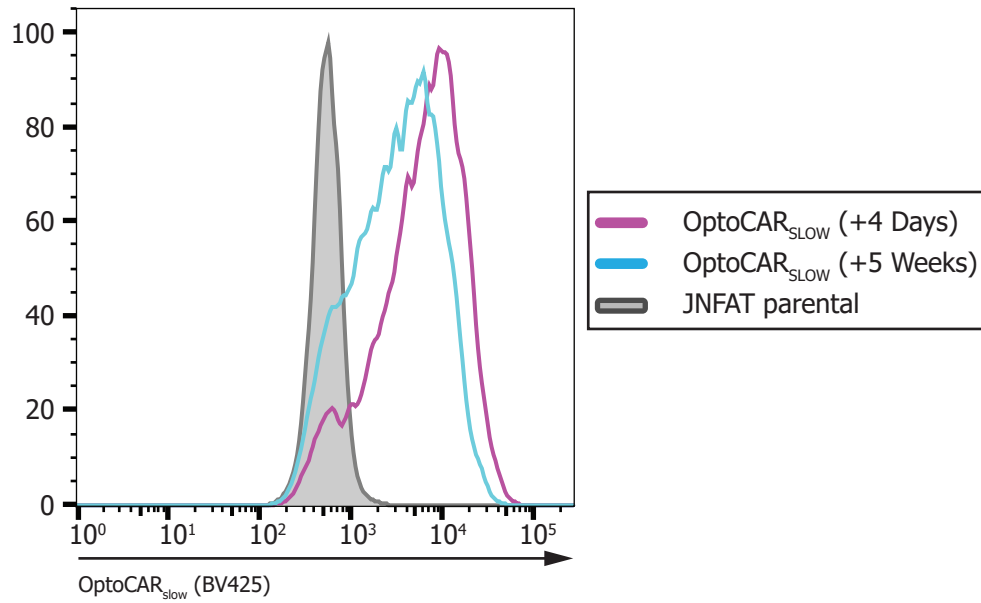
Appendix I Over the course of weeks I observed a drop in TCR expression in the J-LKO cell line.



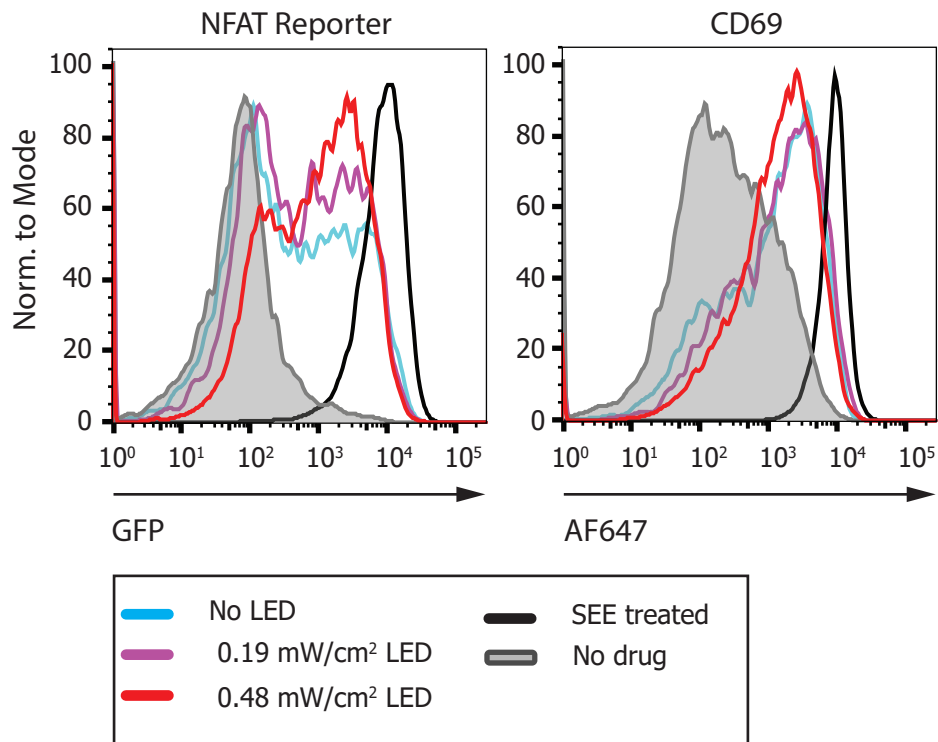
Appendix J To perform real time modulation of calcium signalling we developed a FACS light box. This box can be used to modulate the light conditions for a single FACS tube while running samples on a flow cytometer



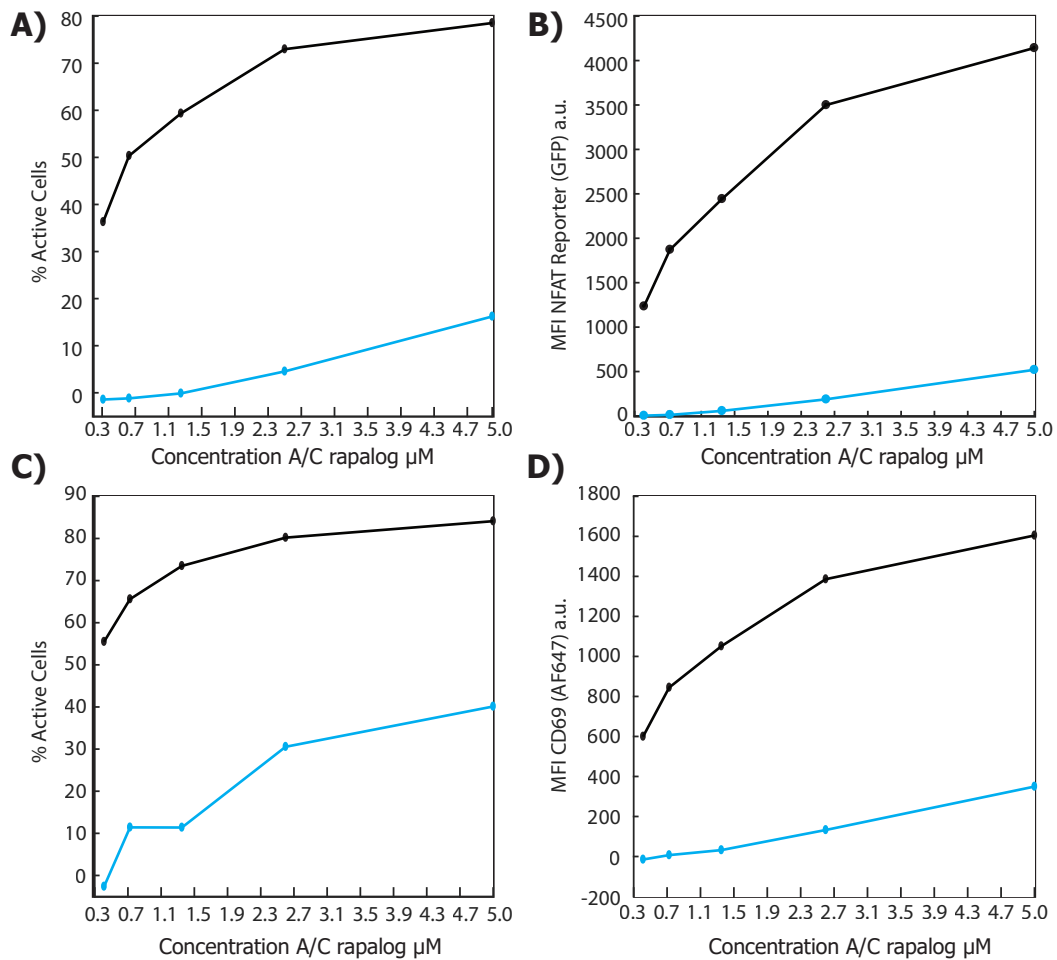
Appendix K (A) Schematic overview of the LPA **(B)** Image of LPA with labelled components **(C)** Calibrated LED intensity calculations. **(D)** Prior to upgrading the LPA lid we consistently observed a large degree of cell death in some wells of the LPA. This is a representative heat map of cell viability.



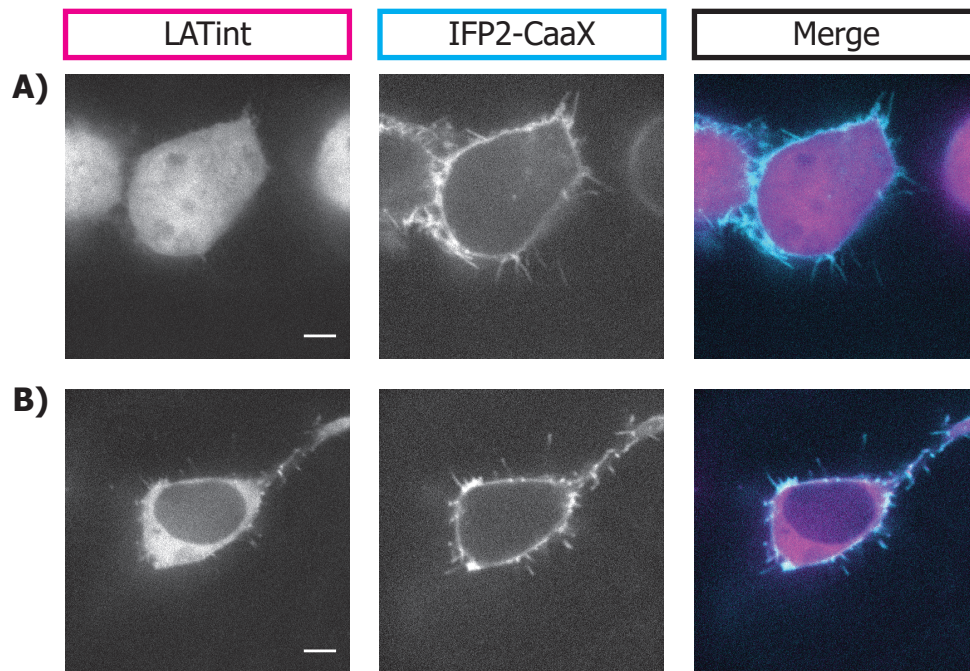
Appendix L OptoCAR_{SLOW} expression was observed to decrease slight over a period of weeks. Here, receptor expression immediately after thawing (magenta) and after 5 weeks of use (cyan)



Appendix M I initially tried long term LPA stimulations with the wildtype optoCAR system. IT was found that blue light irradiation equivalent to the slow-cycling experiment was not sufficient to terminate NFAT-GFP expression or CD69 upregulation. Even when the LED intensity was increased to maximum on the LPA there was still no drop in GFP expression or CD69 upregulation.



Appendix N Using the OptoCAR_{SLOW} system I titrated the concentration of (A/C) heterodimerizer required to inactivate The majority of cells over a 9 hour period of stimulation. As the concentration of drug was increased the fraction of responding cells increased as did the population mean fluorescent intensity (MFI) (A) The fraction of GFP positive cells (B) The MFI of the whole population of reporter cells for GFP (C) The fraction of cells positive for CD69 (D) The MFI of the reporter cell population for CD69.



Appendix O The Zdk-LATint-Ruby and ePDZb1-LATint-Ruby show cytoplasmic localisation in the absence of their LOV2 binding partners (A) HEK293T cells were transfected with pHR-ePDZb1-LATint-Ruby and pHR-IFP2-CaaX. In the absence of the LOVpep domain, the LATint-Ruby construct is localised to the cytoplasm. **(B)** HEK293T cells were transfected with pHR-Zdk-LATint-Ruby and pHR-IFP2-CaaX. In the absence of the LOV2 domain, the LATint-Ruby construct shows cytoplasmic localisation. Images are representative of n=2 (biological replicates).